ASSESSMENT OF INDIVIDUAL PHOTOVOLTAIC MODULE PERFORMANCE AFTER 26 YEARS OF FIELD EXPOSURE AT THE TELONICHER MARINE LAB IN TRINIDAD, CALIFORNIA

By

Jake Rada

A Project Presented to

The Faculty of Humboldt State University

In Partial Fulfillment of the Requirements for the Degree

Master of Science in Environmental Systems: Environmental Resources Engineering

Committee Membership

Dr. Arne Jacobson, Committee Chair

Dr. Charles Chamberlin, Committee Member

Dr. Rick Zechman, Program Graduate Coordinator

May 2017

ABSTRACT

ASSESSMENT OF INDIVIDUAL PHOTOVOLTAIC MODULE PERFORMANCE AFTER 26 YEARS OF FIELD EXPOSURE AT THE TELONICHER MARINE LAB IN TRINIDAD, CALIFORNIA

Jake Rada

In 1990, 192 ARCO M75 photovoltaic (PV) modules were installed as a part of the Schatz Solar Hydrogen Project at the Humboldt State University (HSU) Telonicher Marine Lab in Trinidad, California, within 150 m of the Pacific Ocean. This 9.2 kW-rated PV array was used to power the marine laboratory air compressor and an electrolyzer. Individual current-voltage (IV) curve tests were performed on each of the PV modules prior to the array's construction in 1990 and again in 2001, 2010, and, most recently, in 2016, following decommissioning of the array. After 25.5 years of use, 188 of the original 192 modules were operational, significantly outliving their 10-year warranties.

Based on the previous testing results and the 2016 results, the lifetime decline in the maximum power output, at the normal operating cell temperature (NOCT) testing conditions of 1000 W/m^2 of solar insolation and 47°C module temperature, of the modules averaged 21.6%, or 8.6 W, with 47% of the modules still producing at least 80% of their original (1990) measured maximum power. The average rate of the power output degradation grew from 0.4%/year in the first decade to 1.4%/year in the second decade, and the average degradation rate over the 25.5 years of exposure came to 0.85%/year.

ACKNOWLEDGEMENTS

This project would not have been conceivable without all the great work done by the members of the Schatz Energy Research Center team throughout the years, and I would not have this opportunity without the Environmental Resources Engineering graduate program at Humboldt State University (HSU). Jim Zoellick's work with the solar modules of the Telonicher Marine Lab PV array set the stage for this 26-year analysis, and all the participants in the subsequent analyses of these modules provided the data necessary to map the power output degradation throughout the lifetime of the project. Peter Lehman has been a constant source of knowledge and experience during my time at SERC, and he's all right for a Phillies fan (Go Braves!).

I need to give a big thanks to Arne Jacobson and Charles Chamberlin, the members of my thesis project committee. Arne taught many of the classes I took at HSU and offered great counsel for both my academic and professional endeavors, and Charles never hesitated to offer invaluable advice or answer my endless questions throughout this project. These two have significantly contributed to my project and to my future in the renewable energy engineering field.

I want to thank my family (Joe, Joanne, and Katy) for providing unlimited support of my decision to further my education in California and the pursuit of helping provide the world with clean, renewable energy.

Last, but certainly not least, I want to thank my love, Emily, for always being there for me and selflessly supporting my long nights on campus these last two years.

TABLE OF CONTENTS

LIST OF TABLES

LIST OF FIGURES

LIST OF APPENDICES

ACRONYMS AND SYMBOLS

Acronym of Symbol	Description
%	percent
°C	Celsius
A	surface area; or Amps
AM	air-mass ratio
ASTM	American Society for Testing and Materials
c-Si	crystalline silicon
ekt	degree of IV curve knee curvature
EVA	ethylene vinyl acetate
FF	fill factor
G	solar insolation
GHG	greenhouse gas
HSU	Humboldt State University
I	current, Amps
I_L	light induced module current
I_{mp}	max power current
IR	infrared imaging
I_{sc}	short-circuit current
IV	current-voltage relationship

Acronym of Symbol	Description
k	Boltzmann's constant
LCA	life cycle assessment
LID	light induced degradation
LL	lower limit
m	meter
MC4	connectors used with PV modules
n	ideality factor per cell
NOCT	Normal Operating Cell Temperature
NREL	National Renewable Energy Laboratory
P	power
P_{max}	max power output
PV	photovoltaic
q	electron charge
raw	measurement before normalized
ROI	return on investment
R_p	parallel resistance
R_s	series resistance
se	standard deviation (or error)
SERC	Schatz Energy Research Center
SNL	Sandia National Laboratories

Acronym of Symbol	Description
STC	Standard Testing Conditions
T	temperature
UL	upper limit
UV	ultraviolet
V	voltage, Volts
V_{mp}	max power voltage
V_{oc}	open-circuit voltage
W	Watts
yr	year
η	efficiency
Φ	open circuit voltage temperature correction factor
ω	open circuit voltage irradiance correction factor
Ω	Ohms

INTRODUCTION

The reduction of photovoltaic system equipment and installation costs and policies in key markets supporting installation of grid-connected systems are primarily responsible for the growth of solar photovoltaic (PV) market (Silvestre et al., 2009). As PV-generated power becomes more popular in the electrical grid, accurate projections of power degradation are necessary to predict the return on investments (ROI) that investors use to determine which projects to finance (Jordan and Kurtz, 2011). Historically, PV technologies have been hindered by high up-front capital costs (Bazilian et al., 2013), and the Telonicher Marine Lab array had a total installed cost of $6/W with a module retail cost of $4.80/W (Humboldt State University Foundation, 1989). For reference, these are equivalent to an installed cost $11.61/W and a module cost of $9.29/W in 2016 dollars (U.S. Bureau of Labor Statistics, 2017), both of which are significantly more expensive than those respective costs in the present solar market. Crystalline-silicon (c-Si) solar module retail prices dropped to $4/W by 2008 ($4.46 in 2016 dollars), to $2/W by 2009 ($2.24 in 2016 dollars), and to $1/W as a benchmark price in the 2012 market ($1.05 in 2016 dollars) (Bazilian et al., 2013, U.S. Bureau of Labor Statistics, 2017).

From 2000 to 2010, global PV capacity increased significantly, with an average annual growth rate of 41%, from 0.26 GW to 16.1 GW (Branker et al., 2011). Figure 1 shows the actual and projected growth of installed PV capacity in the world. According to International Energy Agency, solar technology could produce 20% of the total global energy generation by 2050 (Peters et al., 2011). As highlighted in the graph, 85% of the

234 GW installed PV capacity as of 2015 has been operational for five years or less, indicating that field-proven, lifetime, degradation analysis is reliant upon projects constructed more than five years ago when prices were not nearly as competitive as they are today (Meydbray and Dross, 2016).

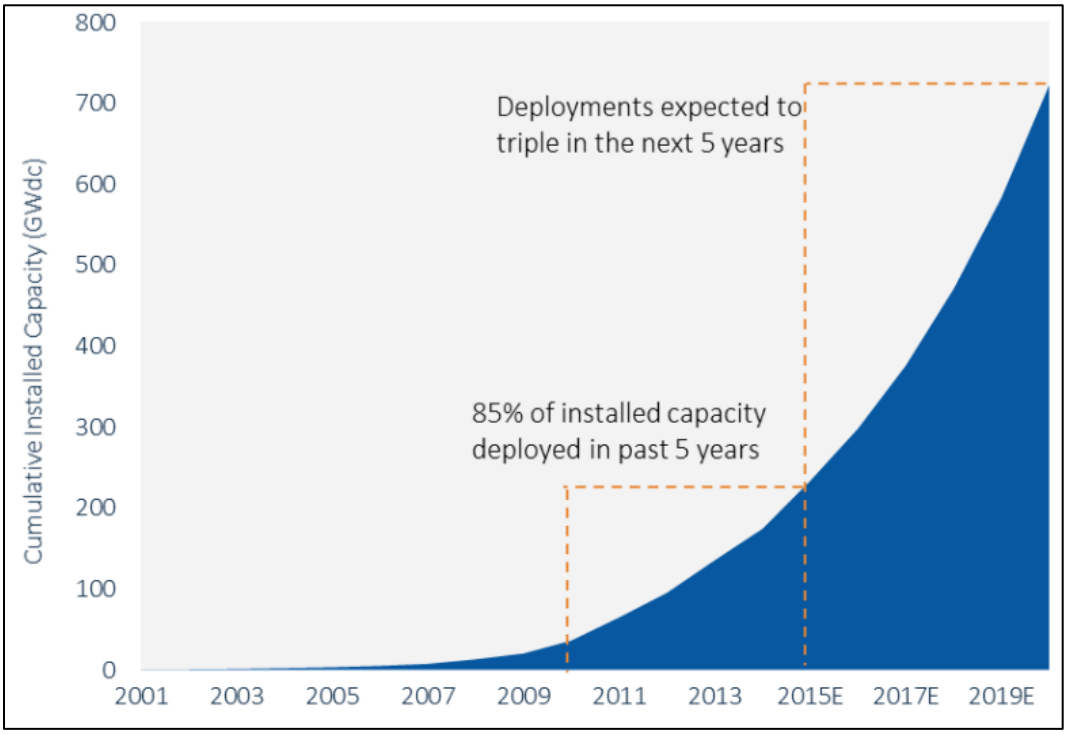

Figure 1: Global PV capacity exponential growth projection (Meydbray and Dross, 2016)

Long-term array field exposure data can help determine expected module lifetimes, failure rates, and failure mechanisms (Wohlgemuth et al., 2006), as well as support reliable and utility-friendly integration of PV generation (Zhang, 2013). The analysis of the 25.5-year-old PV modules from the Telonicher Marine Lab array in Trinidad, California, with the benefit of three previous sets of measurements in 1990, 2001, and 2010 provides a good platform to assess how mono-crystalline PV modules

age physically and perform as they approach and exceed their warranty periods. The fact that the array was positioned only 150 meters inland from the ocean also offers the opportunity to identify any quantifiable affects that a coastal climate, high in humidity, wind, and salinity in the air, has on the aging process of PV modules. Figure 2 helps set the bearings of where this project took place on the Pacific coast of California in northern Humboldt County, and Figure 3 is a view of the ocean from this solar array.

Figure 2: Location of the solar array; Humboldt County, CA (Benbennick, 2006)

Figure 3: View of the Pacific Ocean from the Trinidad solar array (Lehman et al., 2011)

Two important cost drivers for solar PV applications are the efficiency at which solar energy is converted into electricity and how that efficiency changes as the modules and array ages (Jordan and Kurtz, 2011). Warranties for the power production of the solar modules help define the expectations of the operating period, and the typical PV module warranty has grown from 5 years, for modules prior to 1987, to the more currently used warranty of 25 years that arose in 1999. In the near future, PV module warranties could be designated for up to 30 years (Vazquez and Rey-Stolle, 2008). The current standard for a 25-year warranty limits the power loss of modules to 3% in the first year, to account for immediate light induced degradation (LID), and then allows for a linear degradation down to 80% of the original power output (Meydbray and Dross, 2016).

In order to satisfy the warranty commitment of 80% of the original power performance after 25 years, Vazquez and Rey-Stolle (2008) used a reliability function to determine that an average degradation rate of 0.5%/year is required. After testing over

2000 solar modules, Jordan and Kurtz (2011) from the National Renewable Energy Laboratory (NREL) determined that the median and mean degradation rates are 0.5%/year and 0.8%/year, respectively. The economic losses due to degradation at a rate of 0.5%/year are more substantial in large utility-scale projects, as opposed to the much smaller residential arrays, and studies on solar projects such as the Telonicher Marine Lab array can help quantify degradation expectations and identify degradation sources and prevention methods.

The 2016 round of testing completes the lifetime analysis of the modules from the Trinidad solar array and provides insight into the characteristics of the degradation process that any PV array around the world might experience. Even though modern solar modules have benefited from advances in technology and in materials that can result in better and longer lasting modules, accurate portrayals of the aging process of PV modules can be very useful to enable further technical advances and accurate analyses of the economics of solar PV power generation.

Project Objective

The purpose of this Master's degree project is to analyze the patterns in the causes and effects of power degradation in field-aged solar PV modules. This thesis includes:

- Completing testing and analysis of the performance of the 192 individual solar modules (188 from the original 1990 testing and four newer modules that were

used as replacements when necessary during the life of the array) that made up the 9.2 $kW_{nominal}$ PV array at the Telonicher Marine Lab

- Comparing results of all four testing cycles covering the 25.5-year lifetime of the array in regards to the current, voltage, and power output as well as the other key parameters used in solar module analyses
- Assessing the causes and effects of physical and chemical degradation
- Assessing the effect of bypass diodes on performance in older modules

Background

The Humboldt State University (HSU) Telonicher Marine Lab "Schatz Solar Hydrogen Project" began in 1989 and was led by a group with the same name as the project, now known as the Schatz Energy Research Center (SERC), with aid from Teledyne Brown Engineering. Figure 4 shows an image of a school tour soon after the construction of the energy generation system was completed. As shown in the schematic Figure 5, the energy generation set-up included a solar photovoltaic (PV) array, an electrolyzer, and a hydrogen fuel cell. The oxygen tank in this schematic was replaced early on in the project with an air-hydrogen fuel cell due to the hazard of storing and handling the oxygen gas (Chamberlin, 2016). These components worked together to power an air compressor in the attempt to operate the facility with 100% off-grid renewable energy.

Figure 4: Telonicher Marine Lab, including the solar array and a building that housed the electrolyzer, fuel cell, control system, and other system components (Reis et al., 2002)

The solar array was originally constructed as a 24 V_{DC} system with 12 subarrays of 16 modules each (8 series pairs), but in 2005 the wiring was reconfigured in the attempt to eliminate a portion of the mismatch loss among the modules. This new configuration lasted the rest of the project's life and consisted of six subarrays operating at 48 V_{DC} with maximum power point trackers (Lehman et al., 2011).

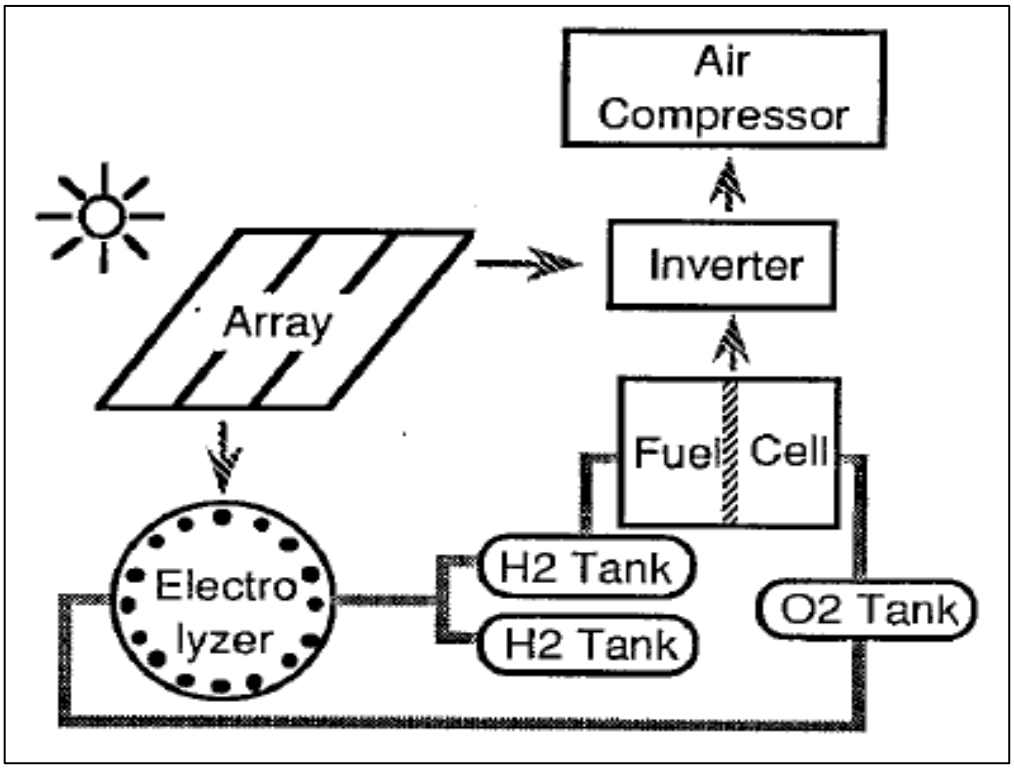

Figure 5: Schematic of the original energy generation system at the Telonicher Marine Lab (Lehman and Chamberlin, 1992)

There was not an economic or energy-value side to the scope of the project. Had it been grid-tied, the offset of greenhouse gas (GHG) and the value of the electricity could have been more closely and accurately evaluated based on data from the utility. Unfortunately, between issues with the electrolyzer, the hydrogen fuel cell, and the air compressor, the system as a whole operated for 43,273 hours, or roughly 5 years, of the 25.5-year project (Chamberlin, 2016). However, this project provided invaluable knowledge and learning opportunities pertaining to the operation of electrolyzers and hydrogen fuel cells in off-grid applications.

Luckily, the focus of this thesis is based up the operation and aging process of the solar PV modules, which were functional for the entire lifespan of the project even though they had a manufacturer's warranty of only 10 years. Of the original 192 ARCO M75 mono-crystalline silicon (c-Si) solar electric modules, 188 survived the whole 25.5 years. These modules were originally rated at 48 W_p under standard testing conditions (STC) (1000 W/m^2, 25°C), which was used as the basis for the nameplate 9.2 kW capacity of the total array, and 46.4 W_p at normal operating cell temperature conditions (NOCT) (1000W/m^2, 47°C).

The IV curve, or the relationship between the current and the voltage in the module, is the primary tool for assessing the performance of the ARCO modules of this array. Solar modules are often tested and analyzed at STC and NOCT. Both of these methods normalize the solar insolation to 1000 W/m^2 and the air-mass ratio (AM) to 1.5, but they differ in the temperature of the module, as STC tests use 25°C and NOCT tests use 50°C (Lighting Global, 2012). The AM quantifies the decrease of energy in sunlight that is available, due to air and dust particles in Earth's atmosphere, based on the light's path length to Earth's surface. An AM of 1.0 occurs at solar noon when the sun is directly overhead, and an AM of 2.0 appears when the sun is 60° from the sun's position at solar noon, also known as the zenith angle (Honsberg and Bowden, 2017 and Solar Energy International, 2013). For consistency, this report utilizes the specific version of NOCT adopted by Zoellick (1990) in the initial round of testing: an insolation of 1000 W/m^2 (tests performed with at least 800 W/m^2), a 1.5 AM, and a module temperature of 47°C.

Table 1 highlights the original manufacturer provided STC specifications of the modules in 1989, Figure 6 shows the STC and NOCT IV curves from the ARCO M75 brochure, and Figure 7 shows what the modules looked like when they were new. Siemens Solar Industries acquired ARCO Solar in 1990. So for the purposes of this report, ARCO and Siemens are synonymous. The four modules that were used as the replacements for the original ARCO M75 modules that had to be removed due to failures were Siemens c-Si SM50-H modules that were rated at 50 W_p (Reis et al., 2002). The first module failure happened early in the project when a passing truck kicked up a rock that cracked the module's glass face. The other three replacements were due to various performance and wiring issues.

These newer Siemens modules came with 25-year warranties, a major improvement from the 10-year warranties of the ARCO modules. Both types of modules are designed the same way, as the ARCO M75 and Siemens SM50-H are each comprised of 33 mono-crystalline silicon cells in series (Specification sheets for these modules are presented in Appendix A in Figure A - 1 to Figure A - 3). A comparison of the aging process between the older original and newer replacement modules is included later in this report.

Table 1: ARCO M75 solar electric module specifications (ARCO, 1989)

Electrical Characteristics (STC = 1000 W/m^2, 25°C)	**ARCO M75 Model**
Rated Power, Watts	48
Typical Open-Circuit Voltage, Volts	19.8
Typical Short-Circuit Current, Amps	3.35
Voltage at Typical Load, Volts	15.9
Current at Typical Load, Amps	3.02
Number of Cell in Series	33
Max Short-Circuit Current at 1000 W/m^2 and 47°C, Amps	3.72
Open-Circuit Voltage at 0°C, Volts	22

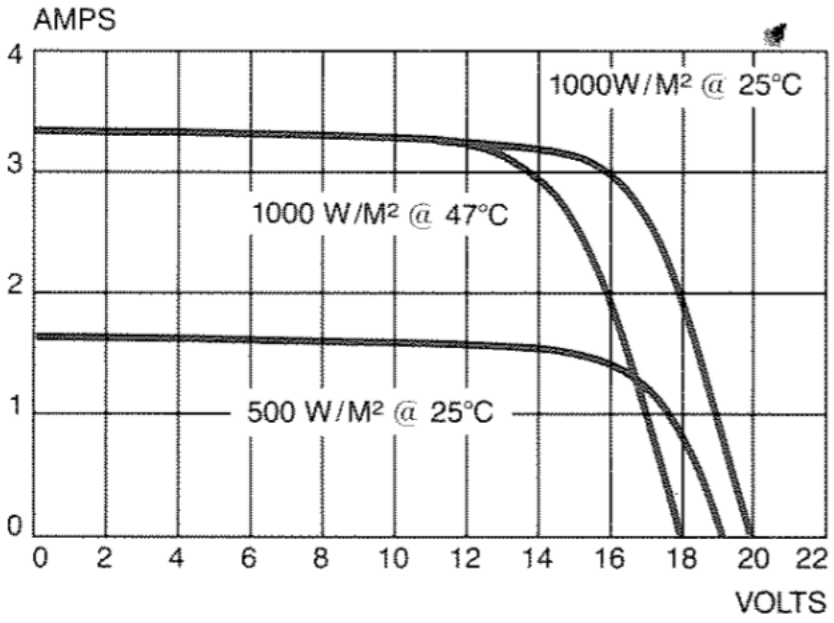

Figure 6: IV curve of the M75 ARCO modules used in the Schatz Solar Hydrogen Project solar array as presented in the original specifications sheet (Siemens Solar Industries, 1990)

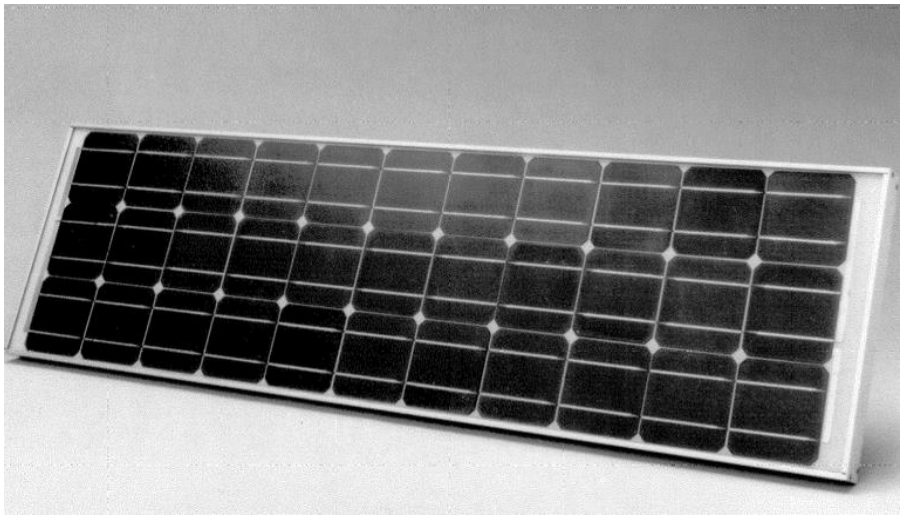

Figure 7: New ARCO M75 solar electric module (Siemens Solar Industries, 1990)

These ARCO M75 modules came equipped with a laminate, also known as an encapsulant, of ethylene vinyl acetate (EVA) around the solar cells and their associated circuits for increased moisture resistance, ultraviolet (UV) stability, and electrical isolation. They also used a strong, low-iron tempered glass glazing for its superior light transmission, and their backsheets were made of a tough, multi-layered polymer that is resistant to abrasion, punctures and tears. Lastly, each module has two Motorola bypass diodes, one in the positive junction port and one in the negative junction port. Figure 8 shows a bypass diode installed in the junction box and in a close-up photo after it has been removed. Bypass diodes are used to reduce potential losses of power resulting from partial shading (Siemens Solar Industries, 1990). The total project cost of roughly $6/W and was paid for through a $275,000 donation from Dr. Louis Schatz (Chamberlin, 2016), but the ARCO modules themselves cost $230.40/each, or about $4.80/W in 1989.

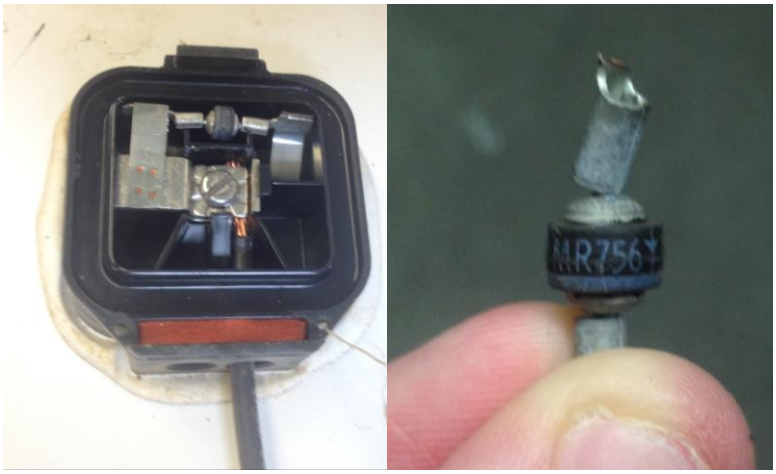

Figure 8: Bypass diode in one of the module junction ports and then after removal (2016)

Tests and analyses were performed on the individual ARCO modules during the construction of the array in 1990 and again in 2001 and 2010. This report is the fourth round of testing and effectively completes the life-cycle assessment (LCA) of the 25.5-year old, now decommissioned, solar array. An outline of the procedures and results of the three previous rounds of testing are in the sections below.

Original Testing (1990 and preliminary data collection)

The Zoellick (1990) report had multiple objectives, but the principal goal was the analysis of the solar modules that were going to make up the HSU Telonicher Marine Lab array. This included developing a testing procedure, choosing and assembling testing equipment, standardizing the results, and comparing the power generation results to the nameplate rating of the modules. The testing procedure, testing equipment, and

formatting of the results were replicated as closely as possible by all the subsequent testing cycles for these PV modules.

Zoellick chose to base his testing procedure and analysis on the American Society for Testing and Materials (ASTM), as its standards are accepted both domestically and internationally. Additionally, the decision was made to analyze the modules using NOCT conditions, instead of the STC that the modules' nameplate ratings used, because the modules typically operated closer to the 47°C of NOCT than the 25°C of the STC. The testing hardware included a curve tracer with a capacitive load connected to a computer interactive data acquisition system, a type-E thermocouple to measure the module temperature, and an Eppley Precision Pyranometer Model PSP to measure incident irradiation with a resolution less than 1 W/m^2. A schematic of his testing setup is reproduced in Figure 9. The tests involved use of a capacitive load, and the capacitor was discharged before each test. A current shunt resistor was used to measure the module current, and a voltage divider was used to measure the module voltage. Each test only took about three seconds to trace the IV curve.

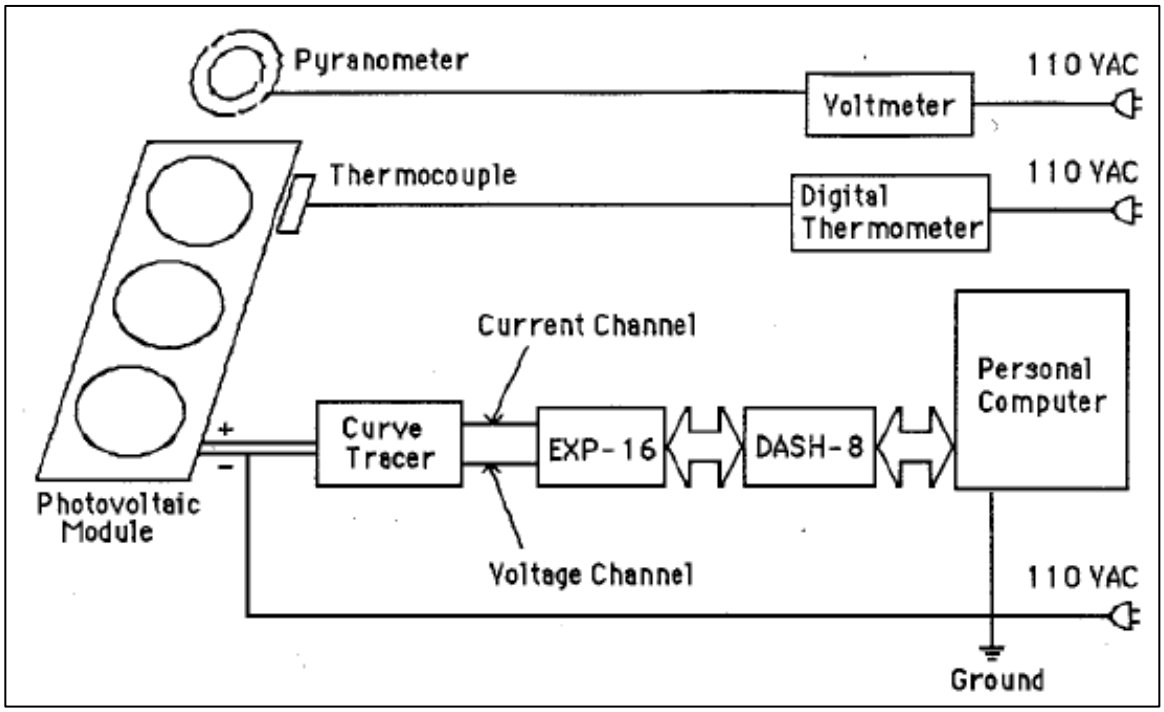

Figure 9: Original round of testing setup (Zoellick, 1990)

Zoellick performed the tests on all 192 ARCO M75 modules at steady state conditions on the HSU campus between June 8, 1990 and July 24, 1990 within two hours of solar noon. To minimize errors resulting from spectral reddening or surface reflection, he attempted to test the modules as close to direct normal to the sun as possible by using an adjustable rack. This goal was not achieved for all his tests, but they all were conducted with the sun-to-module angle of 30° or less from direct normal. Zoellick's testing condition ranges for temperature were 36.7 - 63°C and 861 - 1086 W/m^2 for solar insolation (Zoellick, 1990), which is consistent with the current Lighting Global (2012) testing specifications.

Nonlinear regression was used to determine the IV curve parameters for a lumped parameter equivalent circuit model based on a Schottky diode model applied to the module electrical schematic in Figure 10. In this image, E is the solar insolation, I_L is the light induced cell current, I_c is the cell current, and V_c is the cell voltage. Equation 1 describes this model. The variable describing the degree of the IV curve knee curvature, Ekt, concerns the number of electron-hole pair recombinations, and I_L is essentially equal to the short circuit current (I_{sc}) due to a negligible reverse current and sufficiently large parallel resistance (R_p) (Zoellick, 1990). The best-fit IV curve model was also programmed to clean the data by eliminating any voltage-current pairs that changed by 0.01 A or less, turning 300 data points into 100 points. As the modules aged, this cutoff grew so as to not discard too much of the data.

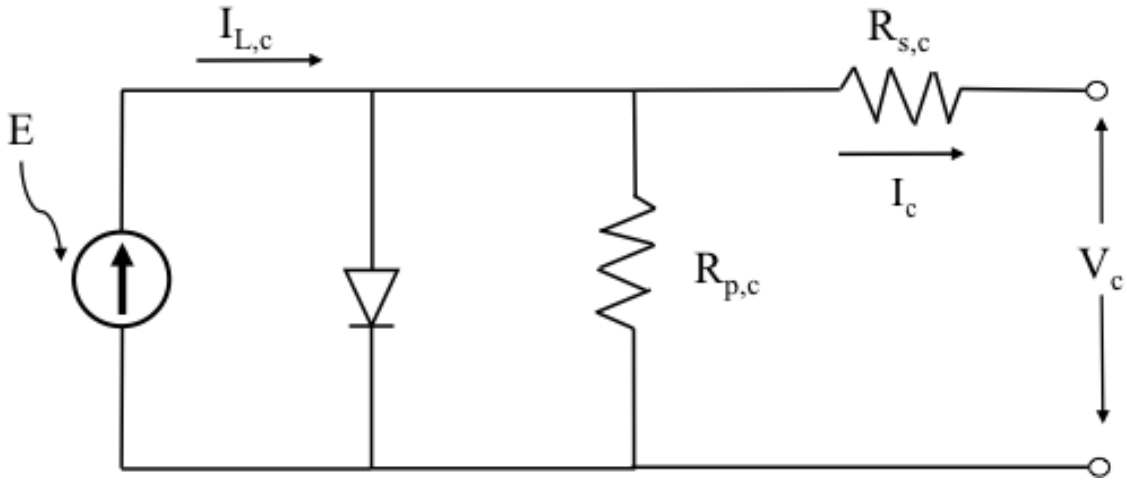

Figure 10: Solar cell equivalent circuit based on an image from Zoellick (1990)

$$I = I_L - \left[\frac{I_L - \frac{V_{oc}}{R_p}}{\exp(ekt * V_{oc}) - 1}\right] * \left[\exp\left(ekt * (V + R_s * I)\right) - 1\right] - \left[\frac{V + R_s * I}{R_p}\right] \quad (1)$$

where

$ekt = \frac{q}{n * k * T}$ [V^{-1}]

I = module current; initial guess [A]

V = module voltage [V]

I_L = light induced module current [A]

V_{oc} = open circuit module voltage [V]

R_s = module series resistance [Ω]

R_p = module parallel resistance [Ω]

q = electronic charge [coulomb]

n = ideality factor per cell [unitless]

k = Boltzmann's constant [Joule/K]

T = temperature [K]

To assess the separate effects of module temperature and incident irradiation on individual module performance, Zoellick tested three random modules from the array and varied one of these primary factors while holding the other constant during the tests. This isolated the effects of each, showing how either module temperature or solar insolation or a combination affects the module's power production. The insolation and module temperature ranges were kept between 800 W/m^2 and 1000 W/m^2 and 35°C and 55°C, respectively, which are purposely close to the NOCT testing conditions. The temperature

study was achieved by keeping modules in the shade before testing with a constant insolation, and the incident irradiation was varied when needed by changing the module tilt with the rack. The results of these tests showed that I_L and V_{oc} were the two primary module parameters that were significantly affected by insolation and module temperature.

The limiting current, I_L, had a positive linear relationship with the insolation on the module, and the open circuit voltage, V_{oc}, had a negative linear relationship with the module temperature. The variation of V_{oc} was determined to be dependent on both temperature and insolation (where I_L was solely responsive to insolation), so Zoellick (1990) used a multiple linear regression analysis, shown in NOCT format in Equation 2, to prove that V_{oc} also relied on insolation at the 5% significance level. Table 2 highlights the correction factor findings from this analysis, and the respective signs with the correction factors indicate V_{oc} decreases with temperature and increases with insolation.

$$V_{oc_{NOCT}} = V_{oc_{raw}} - \Phi * (47°C - T) + \omega * \left(1000\ {}^{W}/_{m^2} - G\right) \quad (2)$$

where:

$V_{oc_{NOCT}}$ = NOCT-corrected open circuit module voltage [V]

$V_{oc_{raw}}$ = field-measured open circuit module voltage [V]

T = field-measured module temperature [°C]

G = field-measured solar insolation [W/m^2]

Φ = open circuit voltage temperature correction factor [V/°C]

ω = open circuit voltage irradiance correction factor [$V/(W/m^2)$]

Table 2: Open circuit voltage correction factors (Zoellick, 1990)

Correction Factor, variable	**95% Confidence Level [units]**
Open circuit voltage temperature, Φ	-0.60291 ± 0.000534 [V/°C]
Open circuit voltage irradiance, ω	0.0009296 ± 0.0000511 [V/(W/m^2)]

Since the sample modules were tested with the previously stated limits (800-1000 W/m^2 and 35-55°C), Zoellick notes that these correction factors for V_{oc} are only applicable in those testing ranges. These correction factors for the ARCO M75 modules were used in every round of testing, including Zoellick's, even though every cycle performed some tests in conditions that created usable data (based on the original assertion that stated that tests must be done in clear sky conditions with an AM of 1.5 and insolation above 800 W/m^2) but fell outside of those narrowed ranges from the sensitivity analysis.

This introduces a source of error in the analyses performed throughout the lifetime of these solar modules. As seen in the table, the correction factor for the effect of insolation on the V_{oc} is small, but the factor for the module temperature is large enough to possibly create a noticeable change in module performance. Therefore, a module temperature analysis was conducted on a subset of seven modules in this 2016 round of testing to determine how applicable the original correction factor from Zoellick (1990) remains after 25.5 years of field-exposure for these particular modules. A similar analysis was completed on 30 modules in the 2001 round of testing, and it found that the two correction factors were still valid after only 10 years of operation (Reis et al., 2002). The

correction factor analysis from the 2016 testing is outlined and discussed in a later section of this report.

Equations 3 and 4 incorporate the information acquired from Equations 1 and 2 to determine the standardized NOCT voltage (V_{NOCT}) and current (I_{NOCT}) for the approximately 300 voltage-current pairs from each IV test of each module. Equation 3 utilizes the open circuit voltage that has been corrected in terms of insolation and module temperature to manipulate the raw module voltage measurements.

$$V_{NOCT} = V_{raw} * \frac{V_{oc_{NOCT}}}{V_{oc_{raw}}} \quad (3)$$

where:

V_{NOCT} = NOCT-corrected module voltage [V]

V_{raw} = field-measured module voltage [V]

$V_{oc_{NOCT}}$ = NOCT-corrected open circuit module voltage [V]

$V_{oc_{raw}}$ = field-measured open circuit module voltage [V]

Equation 4 can be used to correct either the raw measured current or the best initial guess current (I), the result of Equation 1, into comparable and reproducible NOCT data. Simply multiplying the current (I or I_{raw}) by the comparison of the NOCT insolation (1000 W/m^2) and the measured insolation, as I_L showed no dependence on temperature at the 5% significance level, produces a NOCT-corrected current for analysis.

$$I_{NOCT} = I_{raw} * \frac{1000\ {}^{W}/_{m^2}}{G} \quad (4)$$

where:

I_{NOCT} = module NOCT-corrected current [A]

I_{raw} = field-measured module current; or first guess current from Equation 1 [A]

G = field-measured solar insolation [W/m^2]

Zoellick (1990) used the module IV curve parameters (I_L, V_{oc}, R_s, R_p, and ekt) and I_{mp}, V_{mp}, and P_{max} at NOCT conditions to analyze module performance. The module and average cell efficiencies were determined with Equation 5 in STC format, along with the fill factor (FF) and P_{max}, to compare to the STC nameplate ratings of these modules.

$$\eta = \frac{P_{max}}{A*G} \quad (5)$$

where:

η = efficiency [unitless]

P_{max} = maximum module power [W]

A = planar surface area [m^2] (See Figure A - 1 in Appendix A)

G = total irradiance [W/m^2]

The FF in Equation 6 is the percentage that the measured IV curve maximum power is of the ideal IV curve maximum power, where an ideal IV curve is a rectangle

connecting the V_{oc} and I_{sc}, with R_s equal to zero and R_p equal to infinity. The higher the FF, the more ideal the IV curve is in terms of PV module performance (Jacobson, 2016).

$$FF = \frac{P_{max}}{V_{oc} * I_{sc}} \quad (6)$$

where:

FF = fill factor [unitless]

P_{max} = maximum module power [W]

V_{oc} = open circuit module voltage [V]

I_{sc} = short circuit module current [A]

Table 3 highlights the average NOCT results of the array from 1990, and Table 4 provides a summary of the STC criteria. These data are used as the point of comparison for all subsequent testing, and they are included as the original test results in the lifetime assessment of the individual solar modules. With the average tested STC P_{max} of 43.705 W and the ARCO nameplate STC rating for P_{max} of 48 W, Zoellick expressed, based on a 99% confidence interval, that the modules did not meet their nameplate ratings. Surprisingly, almost 20% of the modules tested at less than 90% their nameplate power rating. Previous contemporary research suggested that new photovoltaic modules often performed 10% lower than their manufacturer nameplate ratings with regards to power generation (Jennings, 1987, Russell and Bergman, 1985). The Literature Review portion of this thesis delves further into the research on the possible causes of this shortcoming.

Table 3: 1990 results for NOCT testing at 47°C (Zoellick, 1990)

Parameter	**95% Confidence Interval [units]**
I_L	3.30 ± 0.006 [A]
V_{oc}	18.19 ± 0.019 [V]
R_s	0.346 ± 0.017 [Ω]
R_p	171.036 ± 9.422 [Ω]
ekt	0.708 ± 0.017 [1/V]
P_{max}	39.872 ± 0.120 [W]
V_{mp}	13.860 ± 0.034 [V]
I_{mp}	2.877 ± 0.004 [A]

Table 4: 1990 results for STC testing at 25°C (Zoellick, 1990)

Parameter	**95% Confidence Interval [units]**
P_{max}	43.705 ± 0.123 [W]
η_c (cell)	11.471 ± 0.032 [%]
η_M (module)	10.235 ± 0.029 [%]
FF	0.679 ± 0.002 [unitless]

The narrow confidence intervals from Zoellick's precise measurements and analysis for most of the parameters indicate that the modules tested in 1990 were generating power to the best of their abilities, meaning the manufacturer ratings were most likely overestimations.

After testing all the 192 ARCO M75 modules, Zoellick (1990) concluded that, based on the IV curves, module 124 (where Zoellick labeled the modules 1-192, for easier identification in future analyses, in the order that he tested them without any correlation to their manufacturer serial numbers) had the highest maximum power performance, module 031 produced the median power output among the modules, and module 161 had the lowest maximum power. Figure 11 shows the comparison between the IV curves of these three modules and the ARCO M75 nameplate IV curve at the same testing conditions. At 47°C and 1000 W/m^2, Zoellick (1990) found that the array power output, made up of the sum of the individual module P_{max} values, came to 7,655 W. This is 14% less than the rated array output of 8,900 W, and at the NOCT conditions this production equates to a sunlight-to-electricity efficiency of 9.9% for the total array.

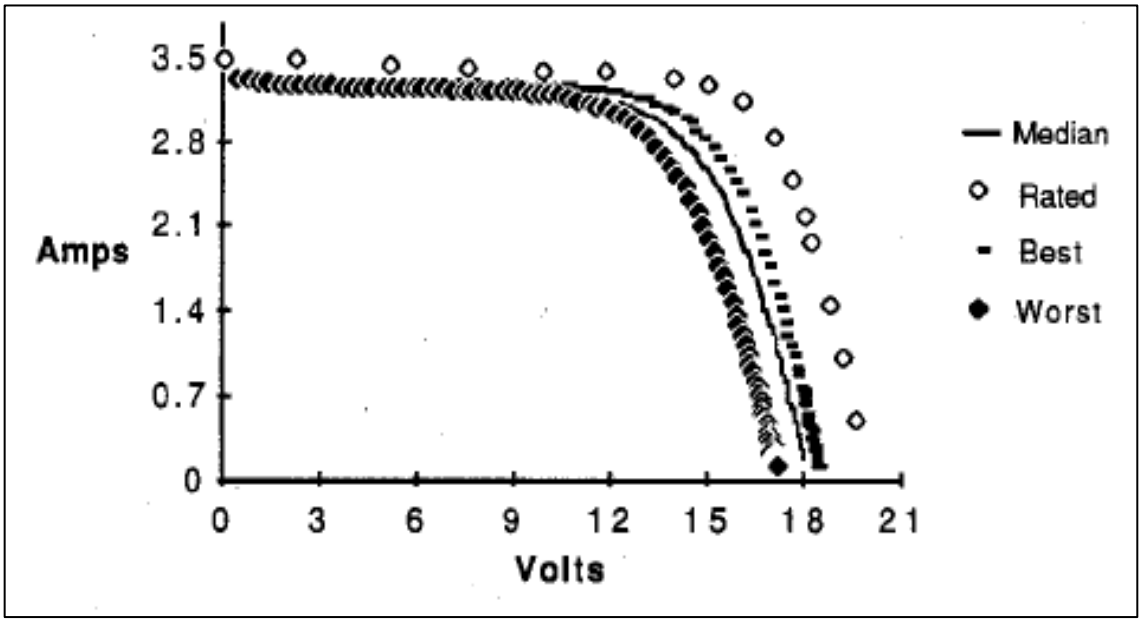

Figure 11: Here are the best, median, and worst IV curves from 1990 versus the manufacturer nameplate rating IV curve (Zoellick, 1990). The worst curve is already showing signs of a second hump at low voltages, a feature present in all of the IV curves from 2016 that will be discussed later in this report.

After construction was completed, preliminary tests were conducted on the entire energy system from 1990-1995, and the results were published in six periodical reports. The fourth report, published in September 1994, focused on the PV array. Jacobson et al. (1994) discovered that the efficiency of the entire array on a typical day averaged around 8.0% and rarely reached above 8.5%. This was partially attributed to the fact that the span of a day covers a range of insolation and module temperature conditions, and there was shading in the mornings and evenings that adversely affected the daily production and efficiency average. Also, the electrolyzer ran at a higher voltage that caused the subarrays to operate further from their maximum power points. Models had predicted that after four years of operation the PV efficiency would drop from 9.9% to 9.0%, but tests performed on a sample subarray found that the average efficiency had dropped to 8.0%, which is an additional 11% drop from the model prediction (Jacobson et al., 1994).

The next analysis on the PV array at the Telonicher Marine Lab was performed on every individual solar module, whereas the preliminary studies were based on the total array, and was conducted in 2001 after 11 years of operation. The summaries and results of this round of testing and the subsequent round of testing completed in 2011, after 20 years of operation, are detailed in the following section.

Subsequent Complete Testing (2001 and 2010)

Reis et al. (2002) headlined the analysis of the modules after 11 years of field exposure, and Lehman et al. (2011) repeated the analysis after 20 years of field exposure. Of the original 192 modules, 191 of them survived the first 11 years of operations. Two

more modules had to be replaced between 2001-2010, and the fourth and final replacement module was added between 2010-2016.

The 2001 and 2010 rounds of testing analyzed each module without removing them from the array, so the modules were tested at a 30° tilt instead of direct normal to the sun as was done in the 1990 testing. These subsequent rounds of testing compared the key results to the Zoellick (1990) NOCT findings, instead of the over-estimated and optimistic manufacturer-advertised specifications, that included a maximum power (P_{max}) of 39.87 W, a short-circuit current (I_{sc}) of 3.30 A, and an open-circuit voltage (V_{oc}) of 18.20 V. Abiding by the NOCT test methods, the tests in 2001 and 2010 were performed twice per module within two hours of solar noon, when the sun and insolation were at their highest, with a module temperature range between 26.5°C to 62.5°C and a solar insolation that was always above 800 W/m^2. All tests used an Eppley PSP pyranometer to measure the insolation in the plane of the module (Reis et al., 2002, Lehman et al., 2011).

The 2001 testing differed from the 1990 testing in that Reis et al. (2002) tested the modules in the plane of the array, while Zoellick (1990) tested them on a portable frame. Moreover, newer equipment was used to perform the data acquisition in 2001. Reis et al. (2002) collected IV curves using a "LabVIEW^{TM} 5.0-based program on a PowerComputing PowerCenter 150 computer with a National Instruments PCI-MIO-16XE-50 data acquisition board installed" and used an Omega CO1-T fast response type-T thermocouple to record the module temperature. Figure 12 shows the appearance and growth of module physical degradation over the first two decades of operation, and

Table 5 summarizes the results and relative changes in the three key results for each decade of operation individually, as well as together, for a then-up-to-date account of the performance abilities of the solar modules.

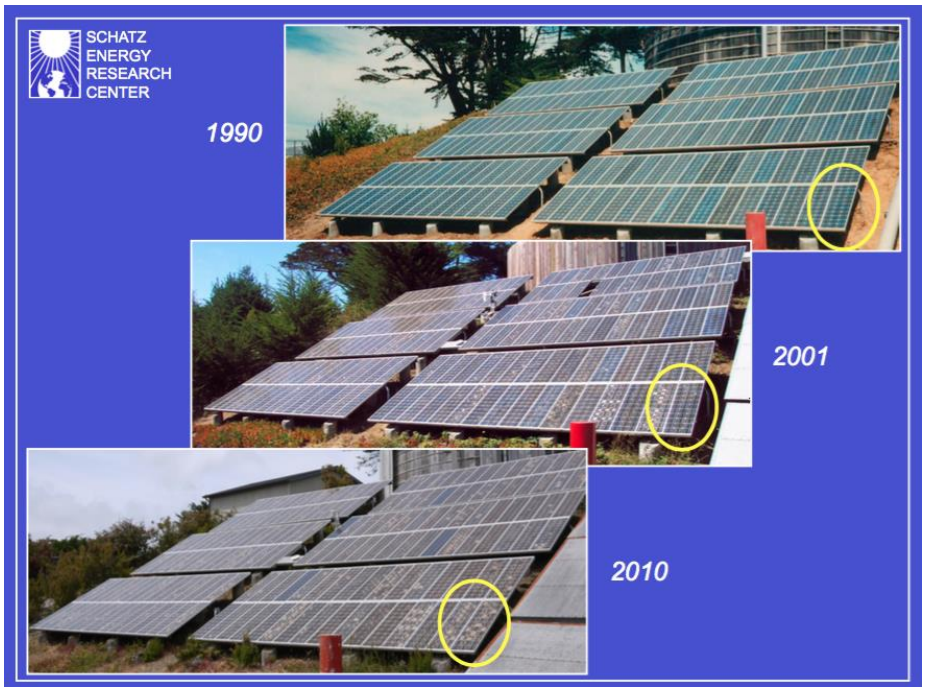

Figure 12: Time-lapse photos of the array highlighting degradation and hot spots (Lehman et al., 2011)

The 2001 and 2010 testing cycles witnessed the same signs of module degradation, which included discoloration and browning of the EVA encapsulant over most of the cells in the modules, delamination of the EVA encapsulant at the silicon cell-EVA interface, and extreme browning of the EVA above individual cells, most likely caused by localized hot spots (Reis et al., 2002, Lehman et al., 2011).

Table 5: 20-year analysis of the key NOCT results of the analysis

Parameter	**Year**	**P_{max} (W)**	**I_{sc} (A)**	**V_{oc} (V)**
Original Rating		46.4	3.72	
Mean	1990	39.87	3.30	18.20
	2001	38.13	3.15	18.15
	2010	33.43	2.86	18.04
% Change	1990 v. 2001	-4.36%	-4.44%	-0.27%
	2001 v. 2010	-12.3%	-9.13%	-0.61%
	1990 v. 2010	-16.2%	-13.2%	-0.89%

Later in this report, additional statistical and graphical comparisons are performed using the 2016 testing cycle to create a full summary of the lifetime changes of these modules. But first, there were a few observations in the past rounds of testing that are worth noting. As it can be seen in Table 5, there were much larger changes in P_{max} and I_{sc} measurements than the in V_{oc}. This indicates that the majority of the power loss in the modules is due to decreased current producing capability. Reis et al. (2002) noticed that the P_{max} point had shifted further down the IV curve by observing the current and voltage at the maximum power point, I_{mp} and V_{mp}, respectively. The increase in the series resistance (R_s), causing a greater amount of the generated power to be lost as heat, and the decrease in the parallel resistance (R_p), producing an increase in current leakage around the cells, also pointed towards the decrease in the available current and the module performance.

The drop in power production in the second decade of operation was almost three times higher than that in the first decade. As discussed in the literature review of solar module degradation of this report, this degradation trend is in fact the opposite of what should happen theoretically because degradation rates typically level out and normalize to a smaller, linear rate after a few years of field exposure with more rapid degradation rates (Quintana et al., 2002, Meydbray and Dross, 2016). In this case, the first decade had a power loss rate of 0.4%/year, when compared to the Zoellick (1990) results, and the second decade experienced a 1.4%/year degradation rate. Over the first twenty years of the Trinidad array, the average degradation rate came to 0.8%/year, which is slightly higher than the rate of degradation in power production reported in the literature for c-Si modules. (Osterwald et al., 2002, Quintana et al., 2002, Jordan and Kurtz, 2011).

Machida et al. (1997) reported degradation statistics for individual single c-Si PV modules after five years of field exposure with declines in P_{max} of 4.8%, in I_{sc} of 5.3%, and a minimal change in V_{oc}. These findings are similar to the results from the first 11 years of operation with the ARCO M75 modules. Because these ARCO M75 modules were not tested before 11 years of exposure, it is possible, yet unverifiable, that they experienced comparable losses to the Machida et al. (1997) study in the first five project years. This would correlate to a PV power loss phenomena called light induced degradation (LID), which is described further in the Literature Review of this report. Reis et al. (2002) suggested that the slightly lower degradation rates in the Trinidad array relative to those reported in some literature could be attributed to the coastal climate, as the array was located only 150 m inland from the coast. The lower ambient temperatures

and windier weather could result in better performance of the modules, and modules tend to degrade faster at higher ambient and module temperatures (Czanderna and Pern, 1996).

Using the Reis et al. (2002) data, Reis and Coleman (2002) identified four types of IV curves observed after 11 years of field exposure. These four curves, simply named Type 0-3, are shown in Figure 13 to Figure 16. Type 0 curves show very little to no degradation from initial testing, Type 1 curves express a decline in the current generated, Type 2 curves show the bypass diodes beginning to activate, indicating negative bias, and Type 3 IV curves have the largest visible effect from the bypass diodes as the series resistance plummets. Type 3 curves became increasingly prevalent by 2016. The captions of the following graphs indicate the test year that each dataset represents for four different modules that provided samples of all four types of curves just defined, and the "X's" on the curves highlight the maximum power point for that module.

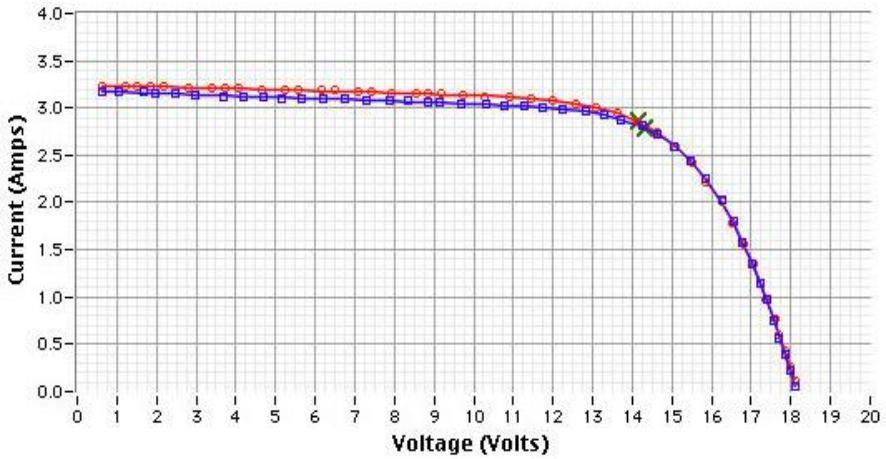

Figure 13: Type 0 IV curve example from 2001 (BLUE) compared to the original 1990 curve (RED) for the same specific module (Reis and Coleman, 2002)

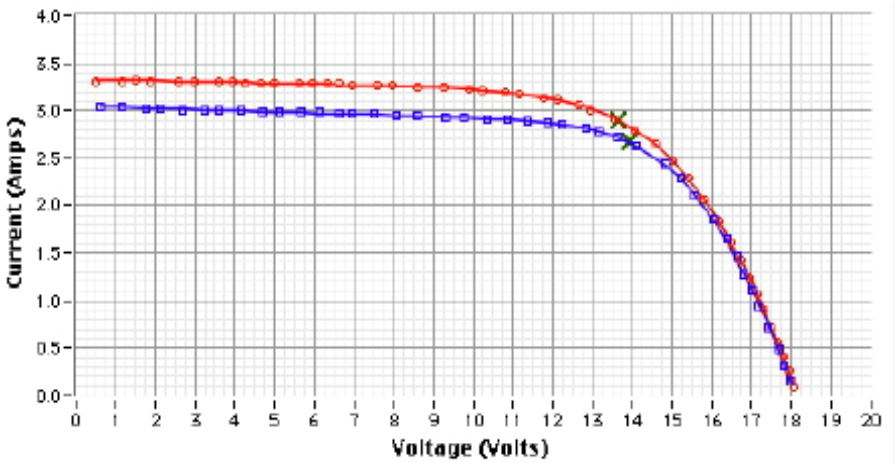

Figure 14: Type 1 IV curve from 2001 (BLUE) compared to the original 1990 curve (RED) for the same specific module (Reis and Coleman, 2002)

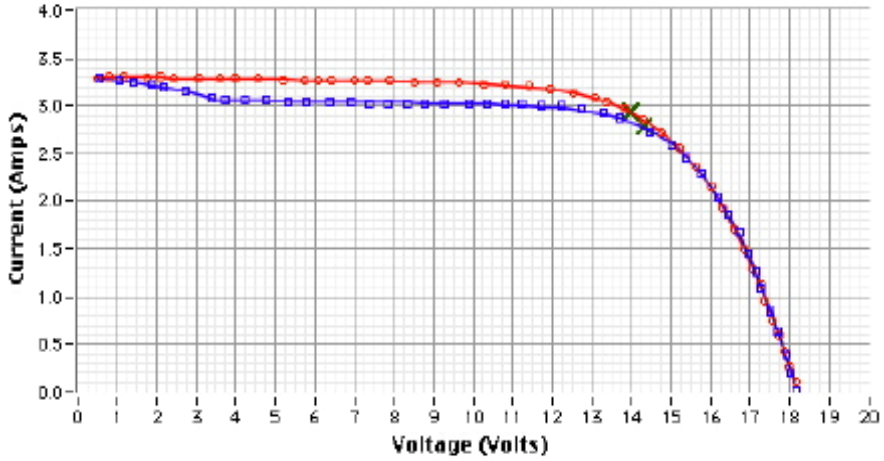

Figure 15: Type 2 IV curve example from 2001 (BLUE) compared to the original 1990 curve (RED) for the same specific module (Reis and Coleman, 2002)

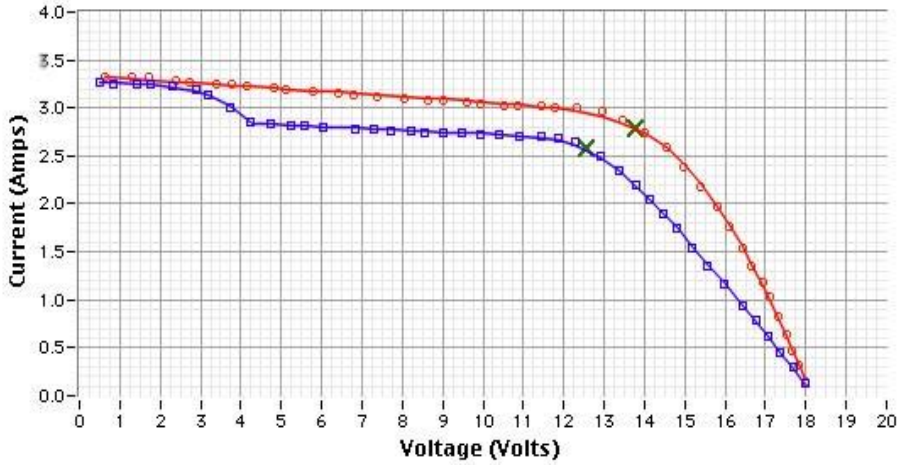

Figure 16: Type 3 IV curve with large knee from 2001 (BLUE) compared to the original 1990 curve (RED) for the same specific module (Reis and Coleman, 2002)

Lehman et al. (2011) concluded from 20 years of data that, as the modules aged, the mean power decreases, the distribution becomes more skewed from normal, and the distribution expands while following the trend of decreasing power. Cumulative distribution curves plotted on normal probability scales were used for analysis in past testing cycles, as shown in Figure 17, and they are utilized in this 2016 study. If the cumulative distribution approximates a straight line in these plots, then the distribution is at least approximately normal. The lower distribution lines indicate a decline in the mean power generation, the steeper slopes mean larger standard deviations, and the less-linear lines have distributions that deviate further from a normal distribution (Lehman at al., 2011).

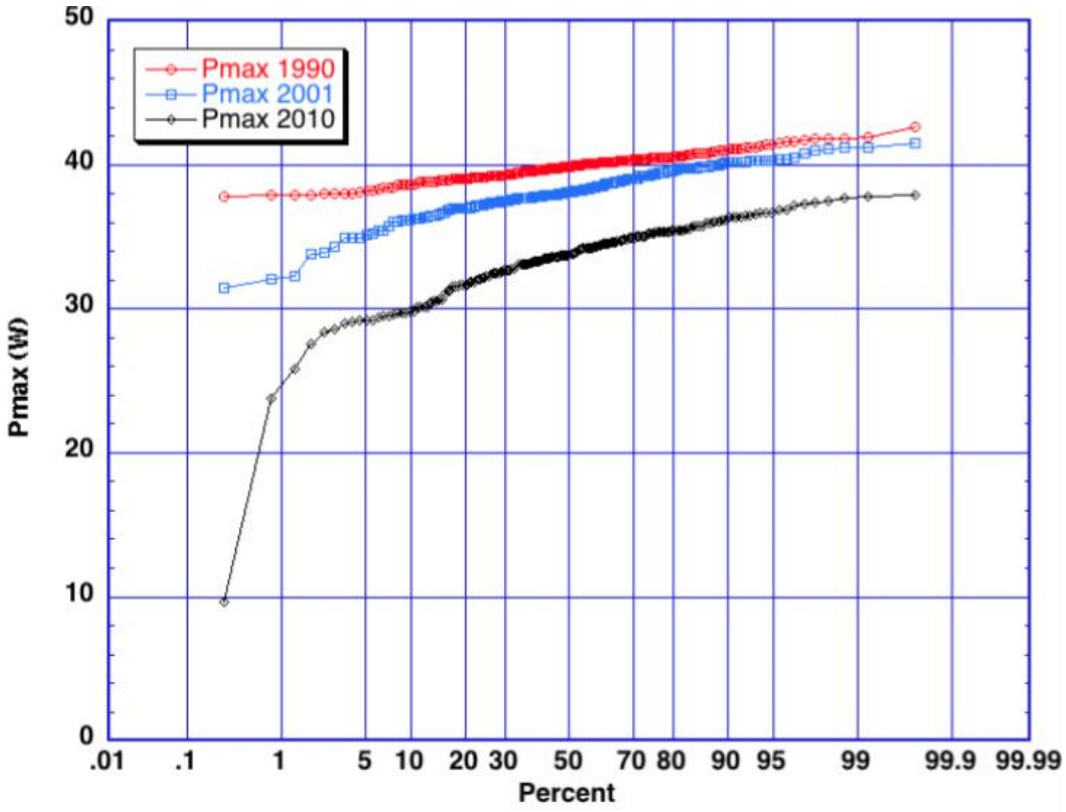

Figure 17: Cumulative probability distribution curves comparing the maximum power for the modules for testing in 1990, 2001, and 2010 plotted on normal probability scales (Lehman et al., 2011)

All rounds of testing–1990, 2001, 2010, and 2016–attempted to test the modules in a consistent manner to accurately depict the power degradation trend over the 25.5-year period. Using a 5-parameter model with a modified version of the non-linear Levenberg-Marquardt algorithm (Reis at al, 2002), IV curves using NOCT are best fit (i.e., minimizing the sum of the squared residuals) to create comparable data and curves. This round of testing (2016) continues this effort and produces a full lifetime account of the effects of 25.5 years of field exposure in a coastal climate on mono-crystalline silicon

PV modules. If past trends continue, the large decline in I_{sc} would be expected to continue to be responsible for whatever loss in P_{max} occurs.

Literature Review

This section includes a broad investigation into the causes that produce PV solar module power generation declines over time, as "identification of the origin of degradation and failure modes and how they affect the photovoltaic modules is necessary to improve the reliability of photovoltaic installations" (Kahoul et al., 2014). A quantitative estimate of this loss of power production over time helps aid the economic evaluation of PV-related projects, as the amount of power produced for a given amount of input solar irradiance is not constant over time. This review focuses on the causes and effects of PV degradation and includes statistical analysis based on past case studies.

Degradation Causes and Effects

Due to the growth of the PV solar industry, there is high demand for early detection of degradation and hidden defects in modules based on visual inspections, current-voltage (IV) curve field measurements of the entire array, thermal evaluations using infrared (IR) imaging, and measurements of the IV and thermal behaviors of selected individual modules from the array (Munoz et al., 2011).

Degradation is typically gradual, baring the instantaneous influence of an object, such as a rock, hitting and cracking the glass encasing the front of the module, and therefore is typically expected in older, field-aged modules. It generally occurs through

either chemical or material processes associated with weathering, thermal stresses, corrosion, or oxidation (Branker et al., 2011). Power performance losses outside of the crystalline cell are typically due to broken solder joints, encapsulant browning, delamination, and interconnection problems (Vazquez and Rey-Stolle, 2008). Figure 18 depicts the layers of a c-Si solar module. The reliability of solar modules is directly linked to the adhesion and cohesion of all the interlayers; loss of adhesion and cohesion is referred to as delamination (Jorgensen and McMahon, 2008).

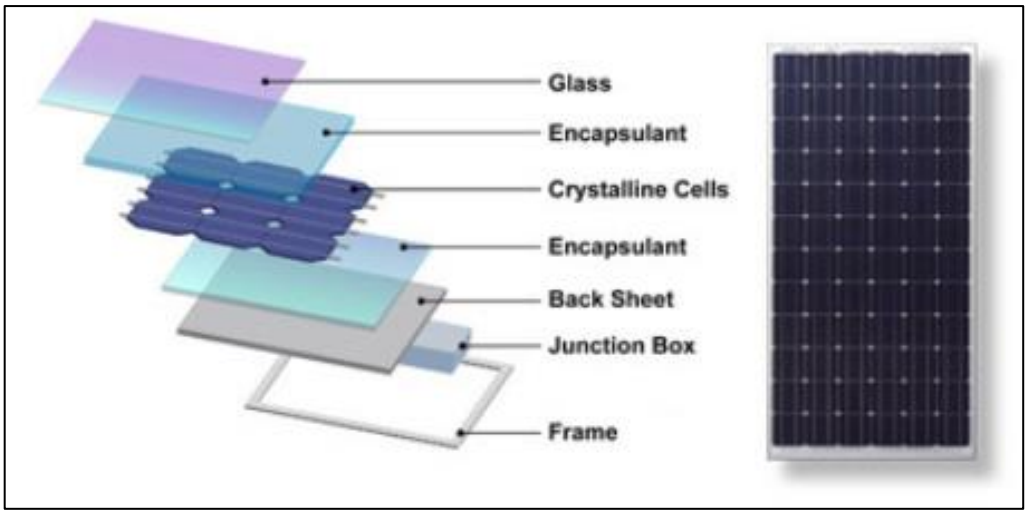

Figure 18: Layers of a c-Si PV module (Meydbray and Dross, 2016)

Ethylene vinyl acetate (EVA) has been used as an encapsulant on PV modules for over 30 years due to its low cost and ability to protect the crystalline cells from the harmful UV rays that accelerate the aging process. There have been great improvements made in the EVA material and the process by which it is applied since the ARCO modules from this project were manufactured. EVA deterioration is prevalent on the front of the module but not on the back (Jorgensen and McMahon, 2008). Adding cerium to

the glass creates an effective barrier to protect the EVA from the UV rays that can expedite the formation of acetic acid, which accelerates the degradation of the polymer in the module (Vazquez and Rey-Stolle, 2008).

Figure 19 shows the various causes of PV module degradation and when they typically occur over a module's productive lifetime, including EVA discoloring, delamination and cracked cells, corrosion, and light induced degradation (LID). The LID effect can occur quickly in the first hours that the module is exposed to sunlight and can create 1-5% loss in the short circuit current (Quintana et al., 2002). Vazquez and Rey-Stolle (2008) concluded that within the first year of field exposure modules show rapid average power degradation of 1-3%, but after that the degradation rate slows to a linear rate of 0.5-1.0%/year. These data and conclusions are considered to represent the expected results of testing modern PV modules. Vazquez and Rey-Stolle (2008) analyzed individual modules that ranged in age from 1-22 years from eight different PV arrays located around the world in various climate settings, including deserts, mountains, and coastal regions. The analysis of the first 11 years of operation of the Trinidad solar project that is the subject of this thesis was even one the arrays in the Vazquez and Rey-Stolle (2008) study.

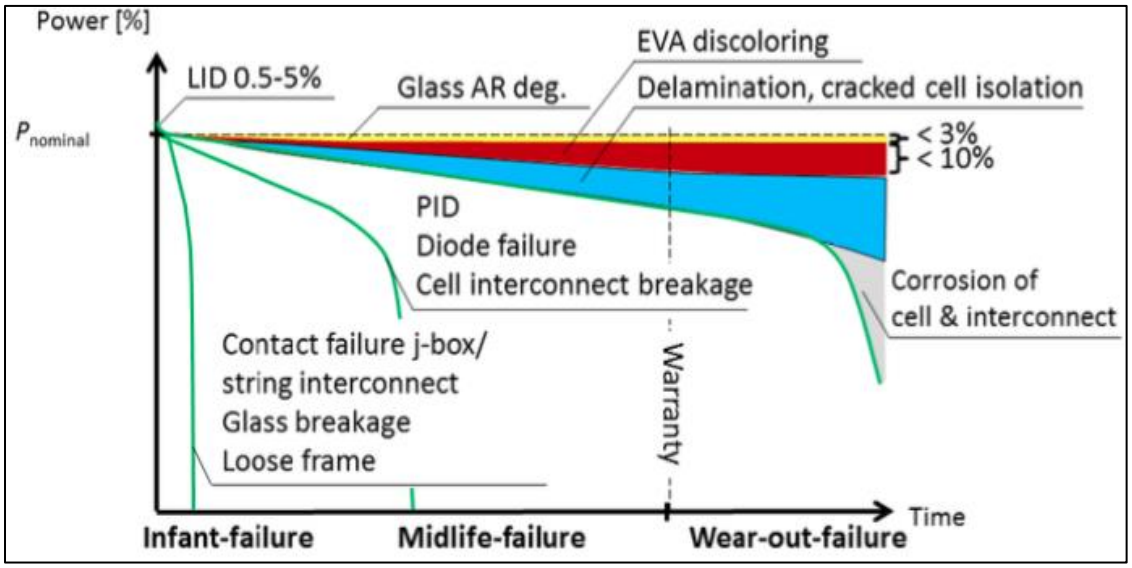

Figure 19: Contributors to performance degradation based on aging/mechanical failures throughout the useful life of the module, where the width of the section represents the percent power output lost from the original power output (Meydbray and Dross, 2016)

Delamination is defined as "the breakdown of the bonds between material layers that constitute a module laminate" (Quintana et al., 2002), and examples of delamination are shown in Figure 20. Hot spots can occur when a cell in a series string of cells is negatively biased (i.e., the voltage drops across the cell instead of increasing), which causes the cell to dissipate power as heat instead of delivering it as electrical power. Prolonged localized heating on a cell can eventually create a permanent open circuit on that cell, leading to a loss in the module's power output abilities. Hot spots, shown with infrared imaging in Figure 21, can be avoided using bypass diodes–discussed later in this report–and strategic solar array design that minimizes dust/snow collection and, most importantly, avoid obstructions that project shadows on the cells of the modules (Molenbroek et al., 1991, Silvestre et al., 2009).

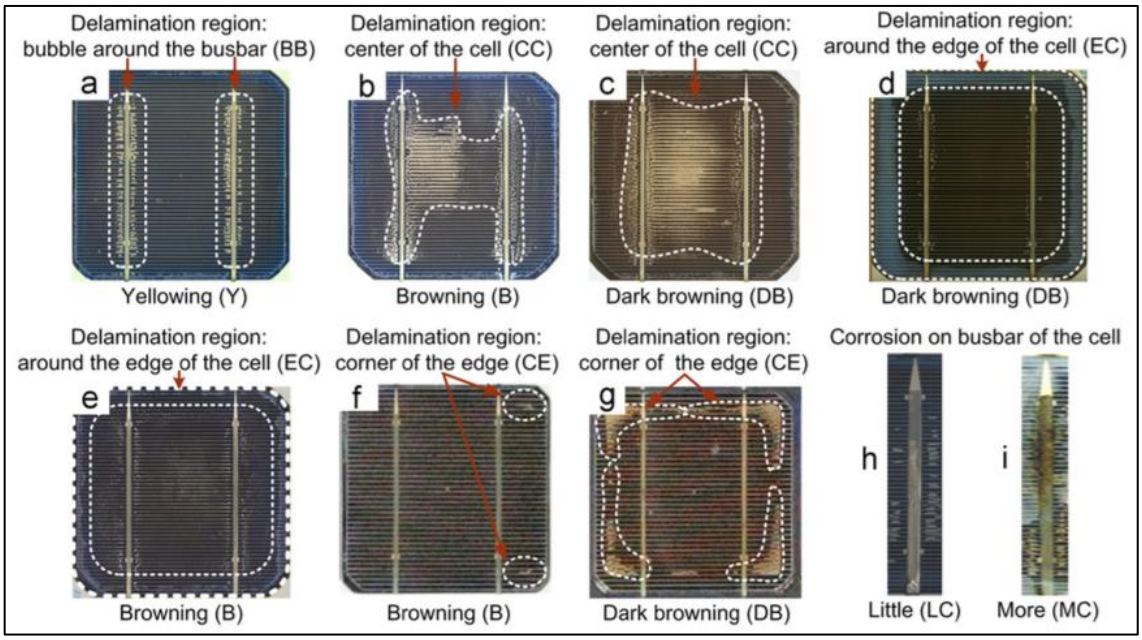

Figure 20: Stages of delamination, including yellowing, browning, and dark browning (Dechthummarong et al., 2010)

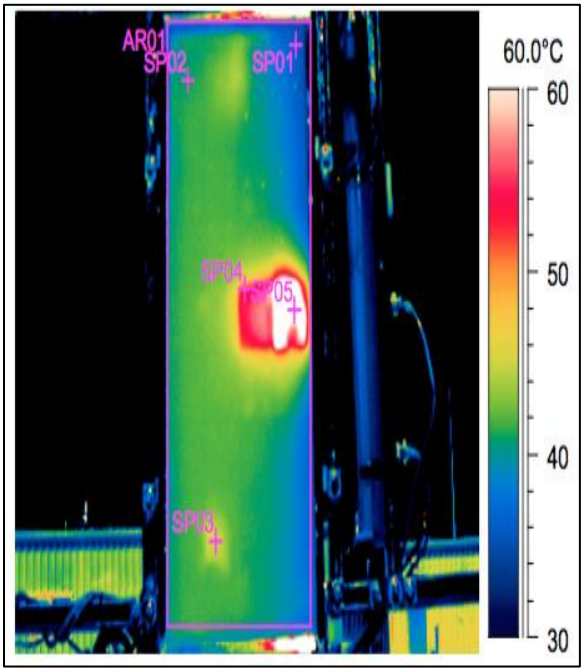

Figure 21: Infrared imaging of a hot spot occurring in a PV module (King et al., 2000)

Figure 22, Figure 23, and Figure 24 show examples of the most prevalent physical signs of degradation–EVA discoloration, delamination, and hot spots, respectively–that were present in the 2001 round of testing after 11 years of field exposure.

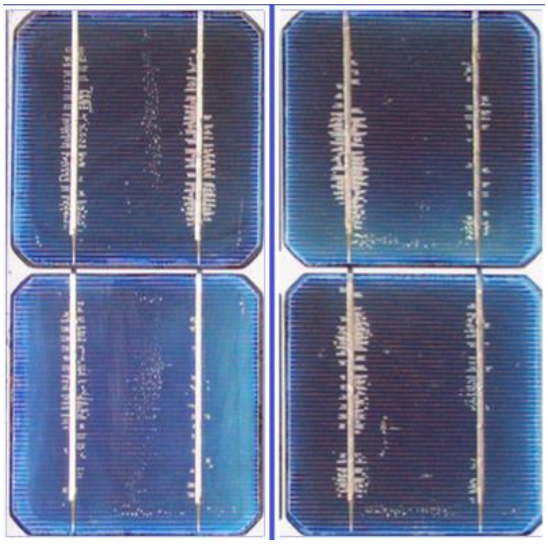

Figure 22: EVA discoloration on a module from the Trinidad array (Reis et al., 2002)

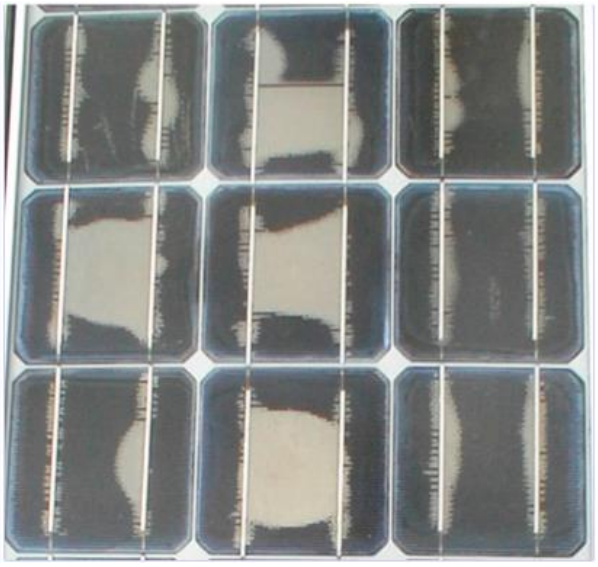

Figure 23: Physical delamination on a module from the Trinidad array (Reis et al., 2002)

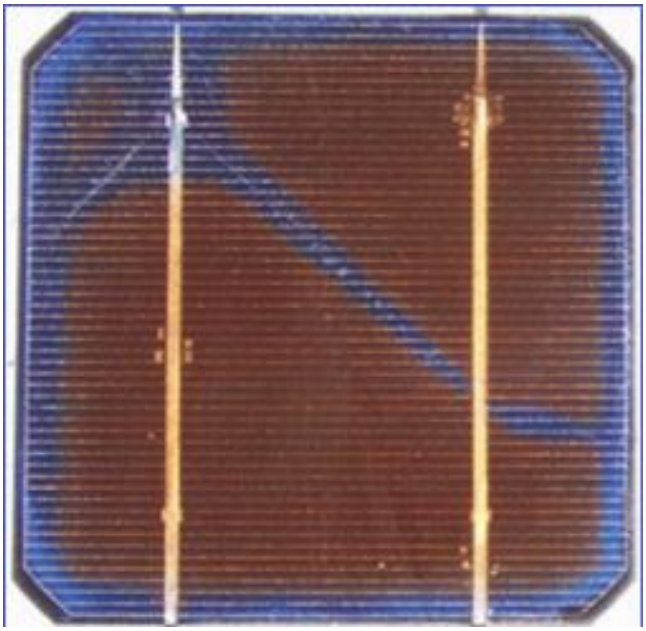

Figure 24: Localized hot spot and EVA browning on an ARCO module from the array (Reis et al., 2002)

The climate and environment at the location of a solar PV array has a large effect on the durability of the productivity of the array. Studies performed on both single and multi-crystalline field-aged modules by Sandia National Laboratories (SNL) and National Renewable Energy Laboratories (NREL) found that higher operating cell temperatures cause accelerated PV performance degradation (Quintana et al., 2002). This is due to the open circuit voltage decreasing as temperature increases while the I_{sc} increases from UV absorption at the top of the silicon surface (Kahoul et al., 2014). Also, high relative humidity in the environment can cause encapsulant delamination through accelerated rusting when the moisture seeps through the seals and gains access to the area that contains the crystalline cells. Dew on the face of the modules collects additional dust, decreasing the module's surface area and therefore access to solar insolation.

Higher velocities of wind can help cool down the modules in particularly hot and humid environments, effectively increasing the efficiency of the cells in the modules (Mekhilef et al., 2012). Mechanical properties are also affected by the weather, as decreases in the productive longevity of a solar module are heavily correlated with delamination (Jorgensen and McMahon, 2008).

Deserts represent the combination of the best average solar resource in the world with poor climate conditions for solar projects. The effect of high operating temperatures and dust on PV modules can counteract the draw of the elevated solar insolation. When operating cell temperatures are above 40°C, modules can lose up to 7% of their STC power generation ratings (Gxashekaa et al., 2004). While it was previously stated that wind could help cool down solar modules to create higher electrical efficiencies, wind in the desert can also increase the dust cover on the surface area of the modules, leading to temporary energy production loss and the long-term possibility of scratched modules.

As it is explored with the case studies later in this report, the reasons for the success and/or failure of a solar project are dependent on local climate, economic, and political atmospheres. Module performance degradation rates range widely and can be influenced by chemical and mechanical reactions. Only increased implementation and further analyses will be able to highlight and effectively address the pertinent causes so that PV solar power can continue its growth in reliability and durability as it competes with other energy generation sources.

Degradation Statistics and Case Studies

This section is used to provide general insight into degradation rates over time, as well as to highlight case studies and results from field experience. Degradation rates are needed to predict power generation for the long term. Modern module manufacturers typically guarantee that their modules will produce at least 80% of the rated maximum power when consistently compared to the original manufacturer ratings in either STC or NOCT conditions over a warranty of 25 years (Swift, 2013).

Jordan and Kurtz (2011) of NREL consider a solar module experiencing a 20% decline in power production to be a failure. This same report found that after testing 2000 different modules and entire arrays, the median and mean degradation rates were 0.5%/year and 0.8%/year, respectively, based on the original rating and testing. For example, a solar module that had lost 10% of its original power production capabilities after 10 years of use would have a degradation rate of 1.0%/year.

A separate study performed on over 200 silicon modules found that 70% of 19–23-year-old field-aged modules had an average annual degradation rate of no more than 0.75% (Skoczek et al., 2008; Branker et al., 2011), which generally agrees with the previous NREL report. However, it must be acknowledged that testing 19–23-year-old modules means that the technology may have advanced a great deal since those modules were produced, and this is evident in the current 2016 degradation benchmark rate of 0.5%/year (Branker et al., 2011, Jordan and Kurtz, 2011). Nevertheless, these degradation rates depend on the sample size and the scatter of the datasets. Osterwald et al. (2002) of NREL tested four different types of commercial c-Si modules using an accelerated solar

weathering program and up to 3.5 years of monthly outdoor testing and found an average degradation rate of 0.7%/year. Data from the LEEE-TISO, CH-Testing Centre for Photovoltaic Modules found that degradation rates for c-Si modules have ranged from 0.7%-9.8% in the first year of exposure to 0.7%- 4.9% in the second year of exposure (Quintana et al., 2002). These ranges have since been narrowed and collectively lowered as solar technology has improved.

Technologies in the solar energy sector after the year 2000 are categorized as significantly more advanced than the technologies available before 2000, essentially creating a split between "old" technology and more currently applicable technology and statistics. In the late 1980's and early 1990's, 10-year old modules were found to have an average degradation rate of 1-2%/year (Quintana et al., 2002). Figure 25 highlights this by showing the reported degradation rates for pre-2000 and post-2000 of long-term field observations of c-Si modules from the four major solar energy regions prior to the year 2000: USA, Europe, Japan, and Australia. The grouping of the post-2000 degradation rates, based on many fewer example case studies due to the data availability for this particular study, appear to be lower than the pre-2000's consistent rate of 0.6%/year. Modules from before 2000 had degradation rates significantly less than the rates of the PV solar array systems as a whole, but there has been an improvement in the stability of the balance-of-system components within the solar engineering field since these case studies from the early 2000's that have brought those respective rates closer together (Jordan and Kurtz, 2011).

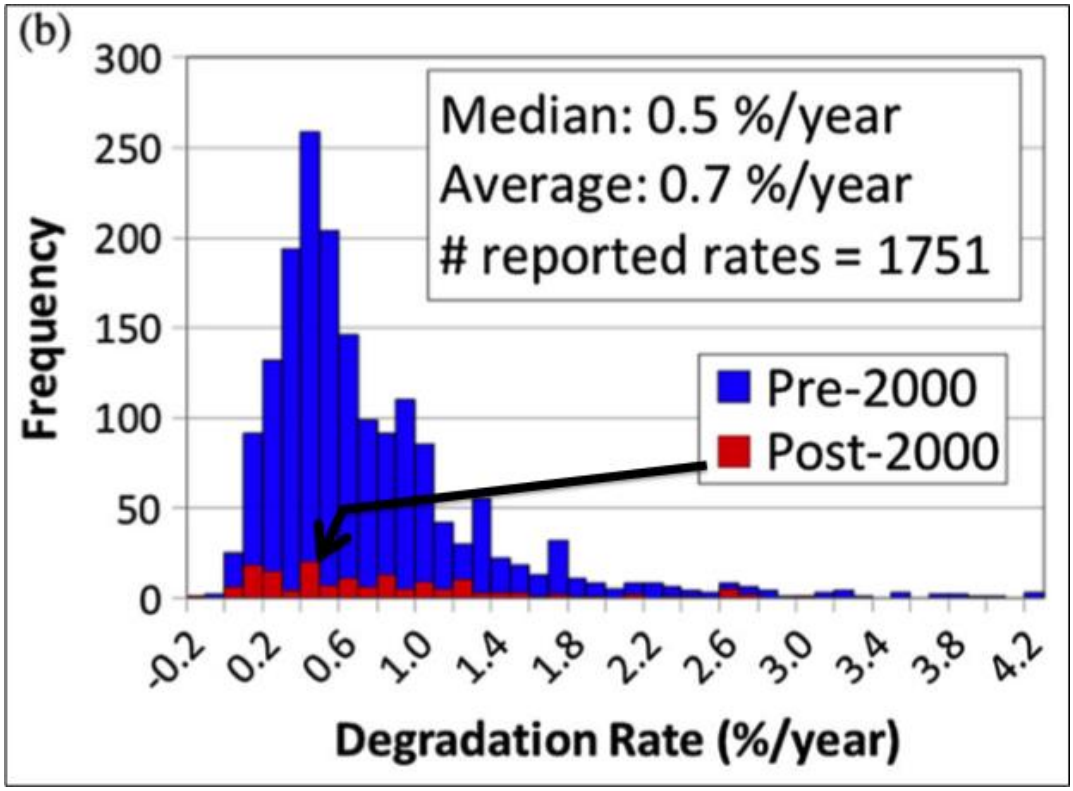

Figure 25: Pre-/Post-2000 degradation data for c-Si modules (Jordan and Kurtz, 2011)

Case Studies.

The following five case studies, noted in Table 6 and detailed further in the proceeding sections, are used here to show examples of both low and high degradation rates, as well as the causes for the associated results.

Table 6: Summary of PV degradation case studies presented in this analysis

Location	Most Important Takeaway
New Delhi, India	Excessive solar insolation and heat can increase power output while also expediting degradation affects.
Thailand	Hot climate and high humidity create accelerated corrosion in PV modules.
Sahara Desert	High operating temperatures, even with ideal solar insolation access, can shorten PV modules' lifespans.
Ispra, Italy	Tests on this 22-year old array show the importance of quality encapsulant material.
Lugano, Switzerland	A 20-year old array produced smaller degradation rates than expected.

New Delhi, India.

This study used sixteen Siemens 75 W modules, which are similar to the modules used in the Trinidad Marine Lab Array, to analyze degradation rates in modules with the consistent excellent solar insolation access that is present in New Delhi. The study stated that, while increased solar radiation can increase a module's short circuit current, maximum power output, and energy conversion efficiency, extended outdoor exposure in such environments, 15 years for this study, can decrease a module's power output by about 20-50% depending on the subarray structure and the location's surrounding climate (Sharma and Tiwari, 2011).

Thailand.

Using the available solar insolation of up to 6.5 kWh/m^2/day, this study analyzed 39 silicon-based modules, originally rated at 47 W and 60 W, over 15 years in a hotter than average (ambient temperature up to 40°C) and extremely humid (90%+ in monsoon

season) environment. The EVA samples from these modules had become opaque from exposure to the elements. Dechthummarong et al. (2010), focused on the creation and existence of physical degradation in solar modules in the Thailand climate, reported "87% of the PV modules had a little corrosion on the busbar, detachment of the backsheet at the corner of the module, and brittle or fracture of seal edge."

Sahara Desert.

This study, performed in the Saharan Desert, found that the cells in the modules degraded by 12% over 11 years of exposure. These modules were very similar to the ARCO M75 modules used in the Trinidad Marine Lab Array project in that they had two bypass diodes in parallel, tempered glass plate, EVA resin, impermeable PV back sheet, and an aluminum frame. At peak air temperatures as high as 63°C in July, average ambient temperatures around 40°C, and an annual average solar insolation above 7 $kWh/m^2/day$, this study provides an excellent case for analyzing solar array performance in a desert setting. With a degradation rate of roughly 1%/year, the analysis concluded that deserts create negative impacts on the performance of PV modules, essentially saying that the higher temperature counteracted the increased insolation and shortened the expected lifespan from 20 years to 11 years (Kahoul et al., 2014).

Ispra, Italy.

The Institute for Environment and Sustainability tested a 20 to 22-year old array in Ispra, Italy, which is one of the oldest arrays to be analyzed for degradation effects. Forty silicon-based modules from six different manufacturers were involved in this study, and their differences revolved around the type of encapsulant (Dunlop and Halton, 2005).

Modules encapsulated with silicone exhibited an average power degradation rate of 0.3%/year based on the original in-lab tests, while modules encapsulated with EVA and a Tedlar aluminum back sheet had a 0.67%/year mean power degradation (Vazquez and Rey-Stolle, 2008). Either way, both types of encapsulants involved had yearly degradation rates well below 1%/year, and the degradation rate for the modules using the silicon encapsulant were as low as 0.25%/year.

Lugano, Switzerland.

The MTBF Project analyzed the performance of a 20-year old 10 kW PV system installed in Lugano, Switzerland. The 252 Arco Solar, ASI 16-2300, c-Si modules had a 10.5% average power degradation from exposure (Realini et al., 2001). While 59% of the modules exhibited a power reduction of less than 10% (<0.5%/year), 35% of the modules displayed a power reduction of 10-20%. The remaining 6% of the modules showed power reduction levels above 20%, or 1%/year of degradation (Vazquez and Rey-Stolle, 2008).

All these case studies derived their conclusions from examining the performance of the PV modules with IV curves, which is the most common method of analysis for this energy generation technology. The next section in this Literature Review describes what aspects of the IV curves are the most crucial to these types of analyses.

IV Curves

In keeping with past research performed on the Telonicher Marine Lab solar array over the last 25.5 years, the current-voltage operational relationship for each module is expressed in the form of an IV curve, exemplified in Figure 26, to determine the

modules' lifetime degradation information by identifying their maximum power output (P_{max}) in 2016 and comparing it to the initial results from 1990. Along with P_{max}, Figure 26 also highlights many of the primary metrics used to analyze the performance of these solar PV modules. These performance parameters include the open circuit voltage (V_{oc}), short circuit current (I_{sc}), series resistance (R_s), parallel resistance (R_p), a lumped parameter describing the degree of knee curvature (ekt), maximum power point voltage (V_{mp}), and maximum power point current (I_{mp}).

V_{oc} is the voltage and I_{sc} (sometimes referred to as I_L, for limiting current) is the current at which there is no current or voltage, respectively; therefore, they are found at the beginning and the end of the IV curve. The current in the module is most affected by the solar insolation, just as the module voltage is most sensitive to the module operating temperature (Jacobson, 2016). R_s, whose inverse is the steep slope of the IV curve to the right of P_{max}, is the product of bulk resistance of the semiconductors and contacts, and the contact resistance between the semiconductor and metal. R_p, as parallel resistance, represents current leakage across the p-n junction diode–where p and n are the two silicon semiconductors in a p-n junction diode of solar modules such as the ARCO M75 models. The inverse of R_p is the slope of the of the IV curve to the left of P_{max} (Zoellick, 1990).

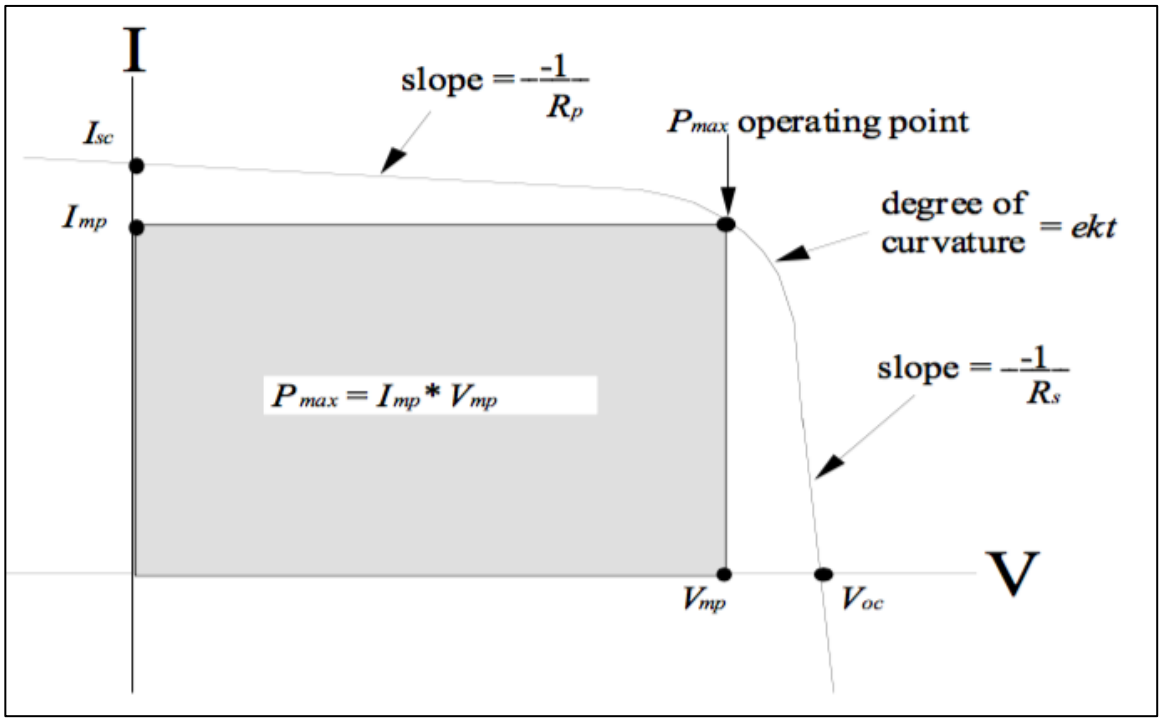

Figure 26: IV curve with all key parameters labeled (Reis et al., 2002)

The equations used to analyze, and the measured correlations between, the parameters described in this section is explored in later portions of this report. This 5-parameter analysis, using the previously defined Equation 1, only involves the second quadrant of a full IV curve analysis. If this project wanted to focus on the on the leakage current experienced in a solar cell with avalanche multiplication, then the first quadrant would also need to be included in the analysis (Pauletto, 1996). Figure 27 shows all four quadrants of a complete IV curve, and quadrant one is the subject of this analysis and is dependent on the module temperature and solar insolation.

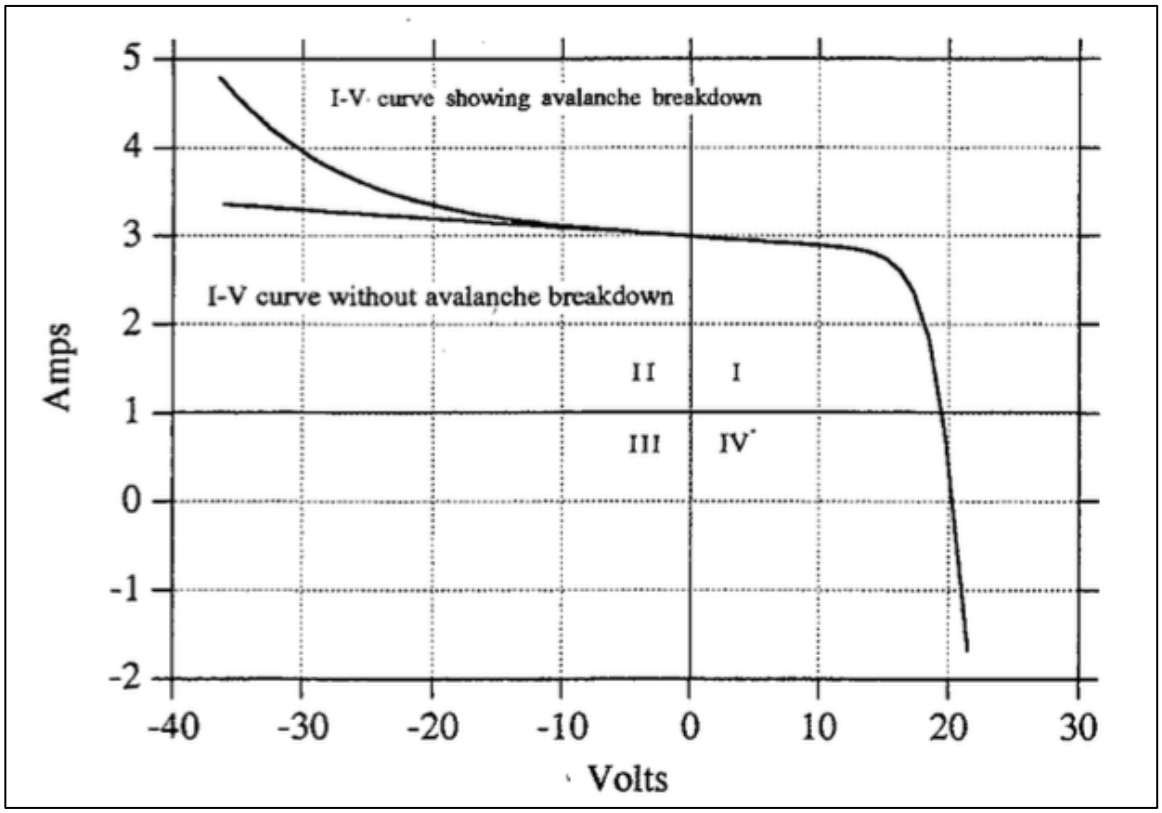

Figure 27: Complete four-quadrant IV curve (Pauletto, 1996)

Bypass Diodes

Losses of power generation in PV arrays typically depend on bypass diodes, inverter voltage limits on the DC side, the layout of the modules, the electrical configuration of the array, and the various types of module degradation (Diaz-Durado et al., 2010). However, as this thesis focuses solely on the PV module and not the array, the bypass diode is the source of power loss that can be quantified. Therefore, the theory of the effect of bypass diodes is explored later in this section, and the measured effect of bypass diodes from a sample of the 188 surviving ARCO modules is covered in the Results and Discussion sections of this report.

As mentioned earlier in this report, bypass diodes can be used to help avoid localized hot spots, caused by shading and unequal electrical currents, from appearing in solar modules. Without a bypass diode, a shaded cell causes the voltage and current to drop in the module, and causes un-shaded cells to operate at a lower current on their associated operation curves. This causes the voltage to fall across the shaded cell, which is referred to as reverse bias, leading to hot spots and dissipated power. Bypass diodes restrict this reverse bias and therefore the power that can be dissipated (Hasyim et al., 1986, Diaz-Durado et al., 2010). The leakage current, covered in the first quadrant of the complete IV curve shown in Figure 27, is a function of the junction voltage and controls these reversing characteristics in the crystalline solar cells (Pauletto, 1996). Figure 28 shows how a bypass diode can be implemented to allow a module to maintain some partial operation when only one cell, or string of cells, is compromised. In this figure, the dotted yellow lines represent current flow. This ability to effectively avoid the damaged or shaded cells reduces power consumption, which can help prolong the module's lifetime (Singh, 2011).

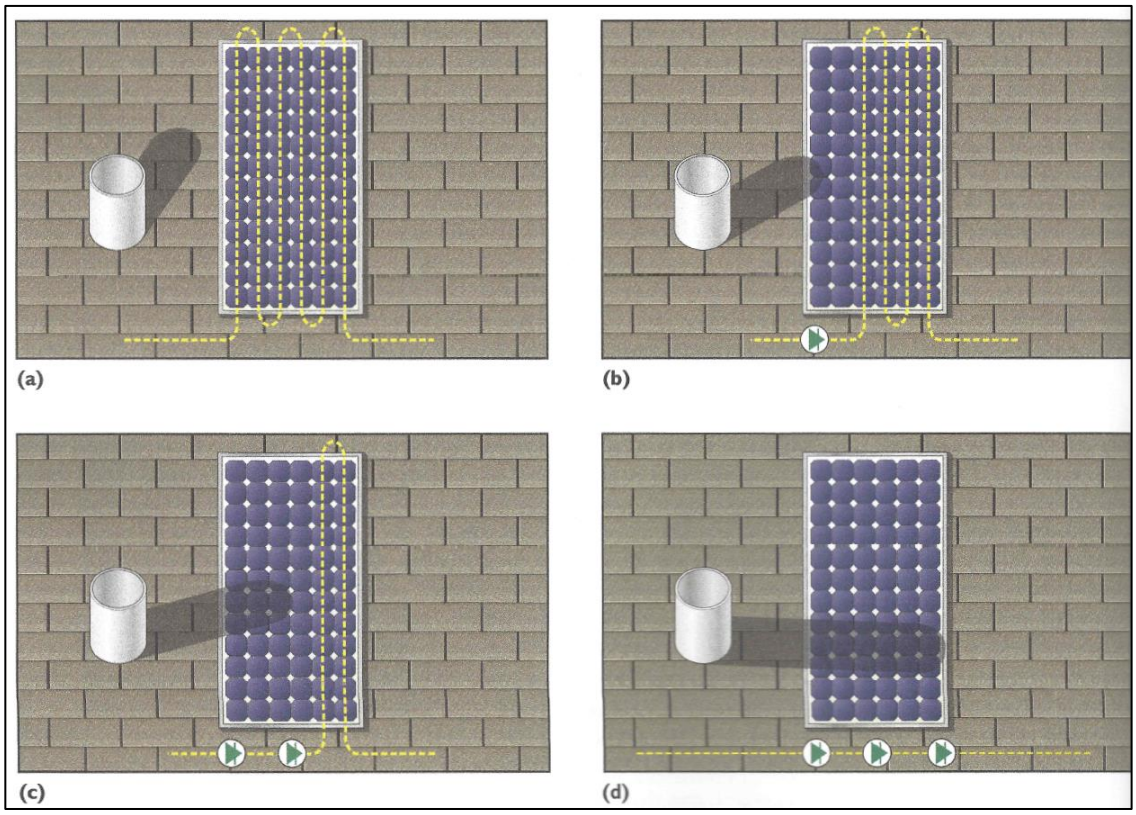

Figure 28: How bypass diodes handle shading (Solar Energy International, 2013)

Hasyim et al. (1986) tested two nominally 24-volt arrays consisting of four and two PV modules with 64 and 72 series-connected cells, respectively, and concluded that bypass diodes did not produce any noticeable benefit in the presence of 10% or less shading on a single cell. However, at 100% shading of one cell, the power generation loss in the array with bypass diodes was $1/20^{th}$ of the loss experienced by the cell in the array without any bypass diodes. Figure 29 and Figure 30 show how including a bypass diode in a solar module can heavily reduce the effect of shading on a single cell. The module represented by the IV curve in Figure 29 has no bypass diodes and therefore loses more generation abilities as the shading increases. Figure 30, which shows the performance of

the module with bypass diodes, hardly loses any generation as the shading of the one cell in the module is increased.

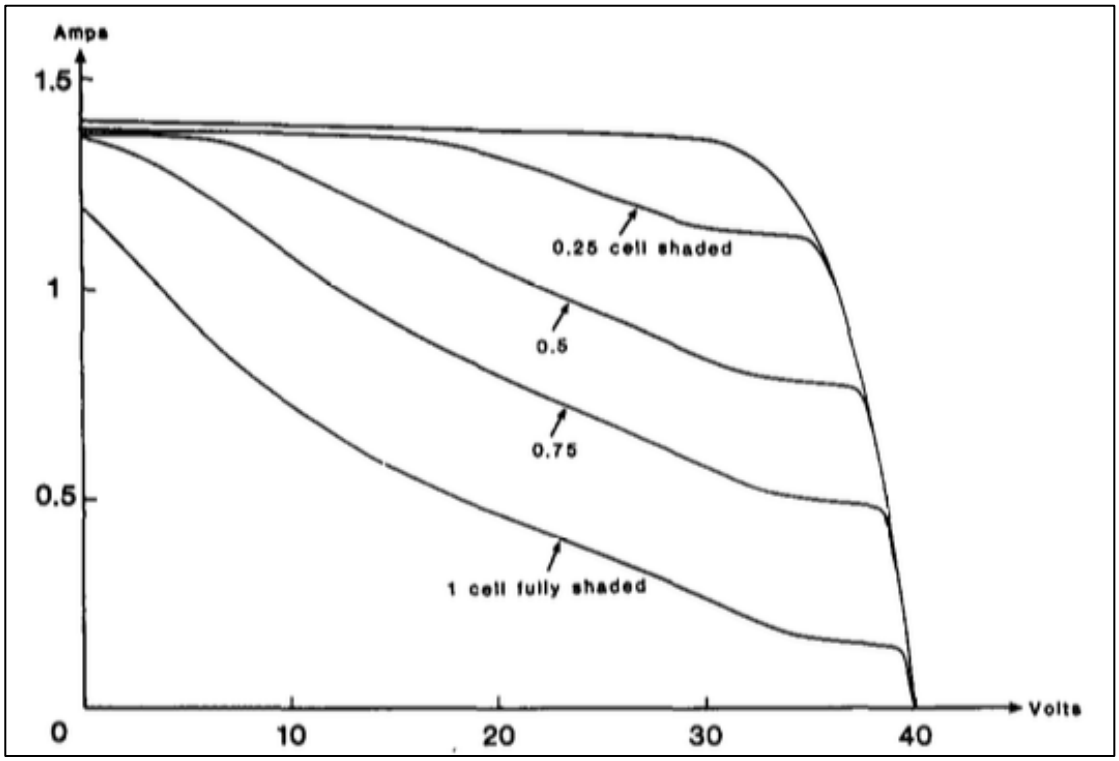

Figure 29: IV curves for a PV module that does not utilize bypass diodes under a range of cell shading conditions (Hasyim et al., 1986)

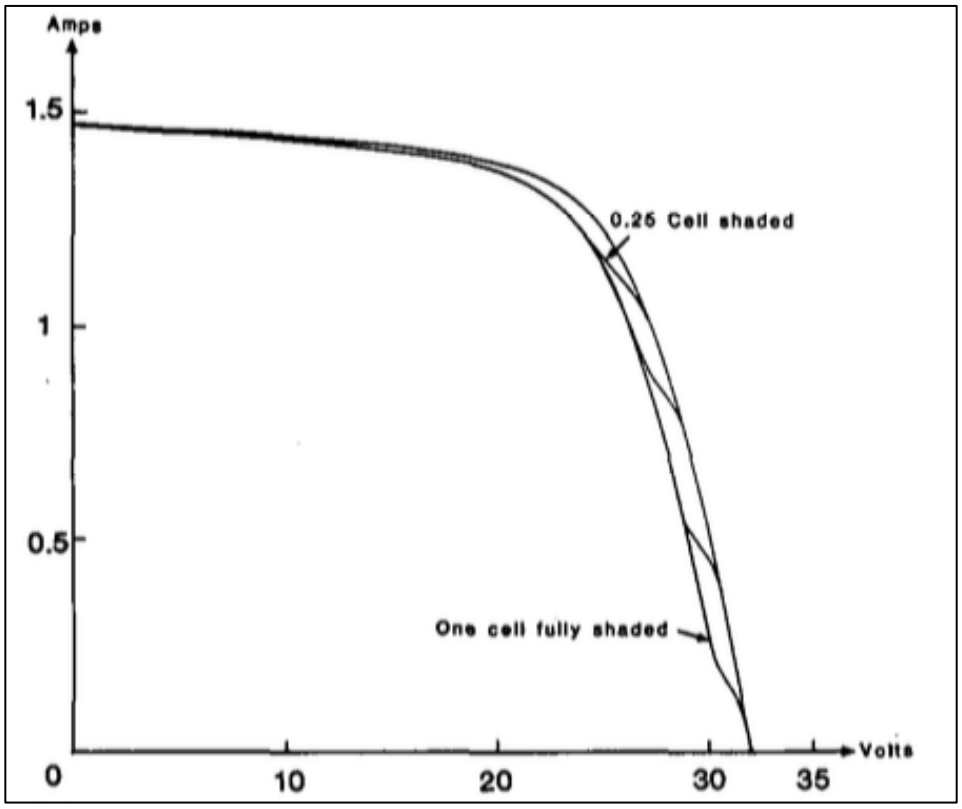

Figure 30: IV curves for a PV module that utilizes bypass diodes to prevent generation losses under a range of cell shading conditions (Hasyim et al., 1986)

The use of bypass diodes also introduces peaks, or knees, in the solar module's IV curve, and as the modules age and more hot spots occur, the momentary influences of the bypass diodes become permanent (Singh, 2011). This involves the current's path consistently directing itself around perceived problem areas (solar cells) that grow in number and size overtime, limiting the module's power output as fewer and fewer cells generate current to create power. This occurrence causes the second knees in the module's IV curve to also grow larger, which is evident for the ARCO M75 modules that are the subject of this Master's project. Figure 31 shows the IV curves from 1990, 2001,

and 2010 for an ARCO module that experienced this type of degradation. The bypass diodes, once a source of over-current protection, became another source of power loss.

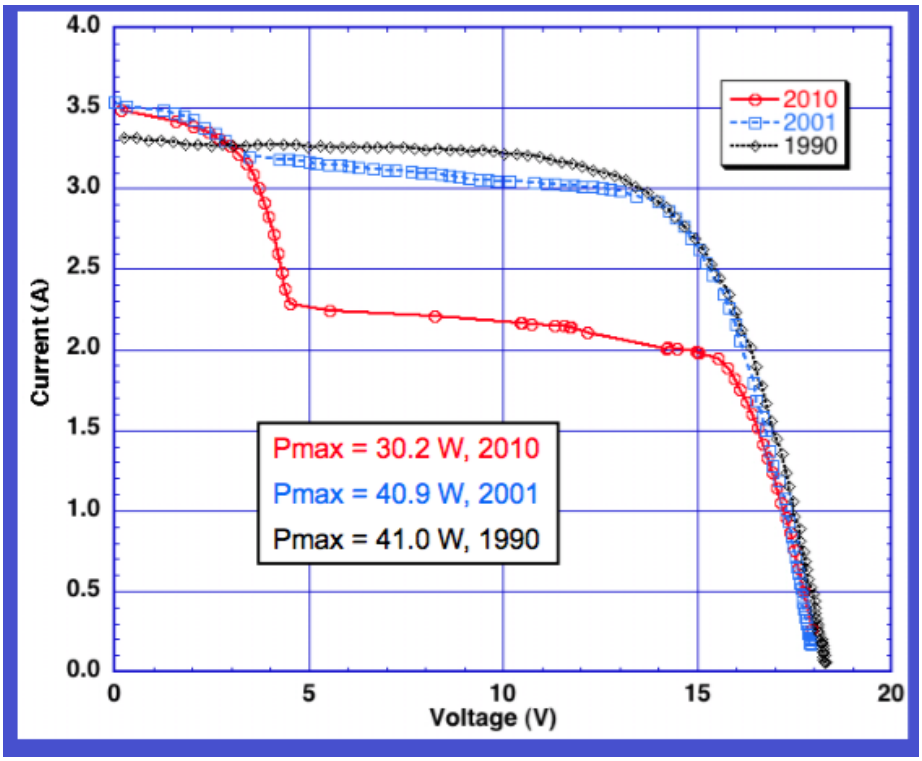

Figure 31: IV curve of ARCO module 184 from the array where the bypass diodes have created a large second knee after 20 years of field exposure (Lehman et al., 2011)

The negative effect of the bypass diodes was already becoming apparent in the 2001 round of analysis, as Reis et al. (2002) noticed that about a third of the modules that experienced the activation of at least one bypass diode during the IV curve testing had a rise in their I_{sc} values when compared to the original 1990 tests. Most of the modules saw the expected decrease in this value, but Figure 32 shows how some modules' I_{sc} increased in a frequency histogram of the 1990 and 2001 cycle results. When one bypass diode is activated, the current bypasses two of the three 11-cell strings based on the design of the

ARCO M75 module circuitry. Therefore, if a single problem-cell is in one of those bypassed strings and is the cell that typically limits the current, the one remaining string would have a cell that would act as the new limit to the current (Reis et al., 2002). This could allow a larger short circuit current, as one string of cells acting alone can produce a smaller voltage than an uninhibited module. Later sections in this report investigate the power loss due to bypass diodes present in the ARCO module after the decommissioning of the Trinidad array.

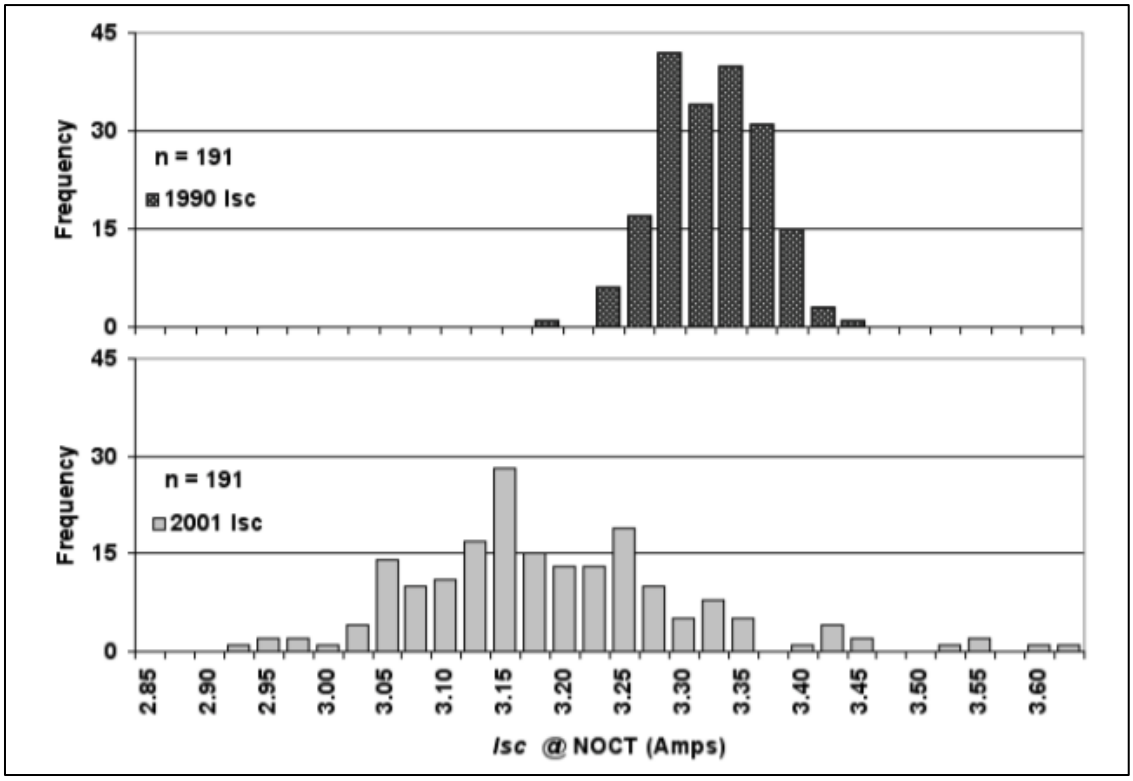

Figure 32: Frequency histogram for the ARCO M75 modules tested in 1990 and 2001 showing their collective drop in average I_{sc} and increased distribution (Reis et at, 2002)

METHODS

This section outlines and highlights the methods used in the collection and the analysis of the data for each of the 192 PV solar modules. This includes methods associated with testing setup, equipment, and procedure. It also includes the equations and software utilized to organize and analyze the data to create comparable results to the previous years of testing. The data in the Results section in this report, following this Methods section, were obtained using these described methods and primarily focus on the power degradation of the modules based on IV curves as exhibited earlier in Figure 26.

PV Module Testing

Reproducibility and consistency are the cornerstones of performing scientific analyses, and, therefore, whenever possible, the procedures and methods of testing the 192 PV modules (188 original ARCO M75 models and four younger Siemens SM50-H models) in this study were performed in similar fashions as the previous rounds of testing in 1990, 2001, and 2010. However, circumstances created situations where some adjustments to the process had to be made. Previously, the analyses were performed on the operating array, which required the testing to take place at the location of the project 150 m off the coast in Trinidad, California. During the current round of testing, the array had been decommissioned and deconstructed in early 2016, and the testing was performed over the following summer. Once decommissioned, the 192 modules were

kept in storage temporarily, and the 2016 testing was performed in the driveway of SERC.

Figure 33 highlights the location of the Telonicher Marine Laboratory in Trinidad and SERC in the city of Arcata. The solar access of these two locations is very similar, and testing a little further off the coast allowed for more testing day opportunities without cloud and fog cover, which is more prevalent closer to the ocean. While there is some tree cover and shade around the SERC building, the tests were all performed within two hours of solar noon just like the previous tests (Lehman et al., 2011, Reis et al., 2002, Zoellick, 1990), and during this timeframe the SERC driveway was free of any shading affects.

Figure 33: Modules were tested at the site of the array in Trinidad, CA in 2001 and 2010 and were tested at the SERC facility in 1990 and 2016. These sites are roughly 13.3 miles apart, as shown on this map. (Google Maps, 2017)

Using past procedures as a guide, the 2016 tests were performed in clear sky conditions with at least 800 W/m^2 of available solar insolation with an AM close to 1.5. Since the data are adjusted to NOCT conditions of 1000 W/m^2 insolation and 47°C module temperature using the same methods that Zoellick (1990) employed, the tests were completed as close to those conditions as possible. The ranges of insolation values and module temperatures in this 2016 round of testing, performed over 17 days of testing from June 22nd to October 19th, were 920-1035 W/m^2 and 37.1-59.5°C (excluding the sensitivity analysis testing that purposely widened the temperature testing range), respectively, which are very similar to the reported ranges in the Reis et al. (2002) study.

Testing close to the specified NOCT conditions reduces the amount of error associated with applying the correction factors to normalize the results. The Lighting Global (2012) IV curve testing procedure states that the insolation must be between 850-1150 W/m^2, the ambient temperature should be 15-35°C, and the AM should be less than 2.0, and all these conditions were met in the 2016 round of testing. While the ambient temperature was not recorded, the NOCT method concerns itself with the module temperature, not the ambient temperature, so keeping the module temperature close to 47°C was important criterion for this analysis.

The physical setup, equipment used, and the procedure for testing these PV solar modules are just as important as the data analysis, and it was necessary to pay meticulous attention to detail to create insightful and reproducible results. All the equipment is described below, but Table 7 highlights the primary output of each unit. All the equipment in this experiment was either bought or already owned by SERC or the Environmental Resources Engineering (ERE) department at HSU. ERE purchased the IV curve tester that came with the PV reference cell. The associated specification sheets for the equipment can be found in Appendix A (Figure A - 4 to Figure A - 9).

Table 7: PV testing equipment

Equipment	**Company; Product**	**Primary Purpose**
Pyranometer	Eppley; PSP	Thermo-based solar insolation
IV Curve Tester	Ingenieurburo Mencke & Tegtmeyer GmbH; Mini-KLA	Produces IV curve and records reference cell data
PV Reference Cell	Ingenieurburo Mencke & Tegtmeyer GmbH; sensor	PV irradiance and temperature

Equipment	Company; Product	Primary Purpose
	Si-01TC-T	
Thermometer	Omega; Omegaette HH303 Type K	Read thermocouple for module temperature
Multimeter	Fluke; 287 True RMS	Read Eppley PSP mV output

The physical setup, shown in Figure 34, includes a metallic frame built by SERC's Mark Rocheleau. This frame also has a frame plate in the plane of the frame where the PV reference cell was attached, and there is a metallic tube attached here that allows the user to adjust the frame and the module to be direct normal to the sun, aptly labeled in the figure as the "Direct Normal Sight Tube." Previous rounds of testing performed their tests at the same angle as the operating array at 30° (Lehman et al., 2011, Reis et al., 2002, Zoellick, 1990), but with the array now decommissioned testing the modules perpendicular to the sun provides the best data closest to the NOCT solar insolation of 1000 W/m^2 and matches the method used in the original 1990 testing.

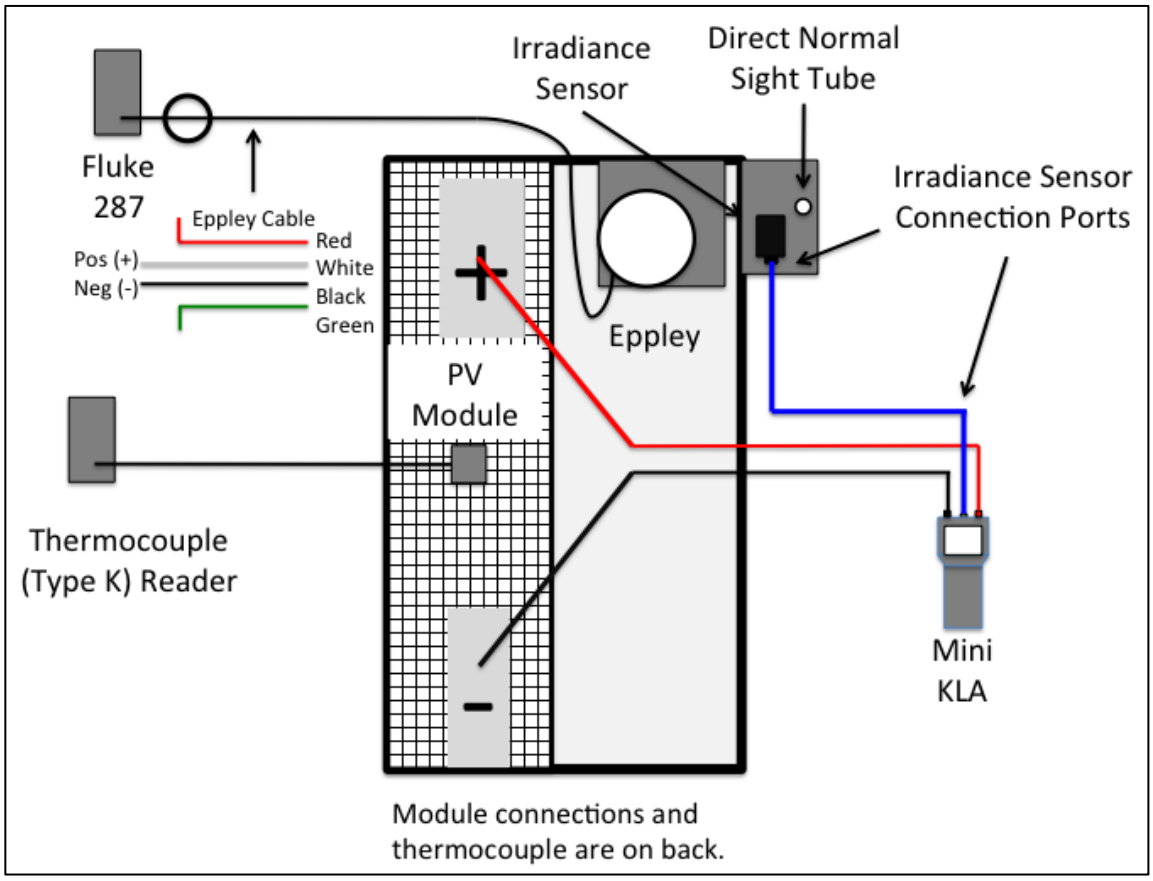

Figure 34: PV module testing schematic

The Mini-KLA PV IV Curve Analyzer (Figure 35), from Ingenieurburo Mencke & Tegtmeyer GmbH, is at the center of this experiment. It can be used to test modules with a V_{oc} as high as 120 V and an I_{sc} as high as 8 A, which is well above the requirements for the ARCO M75 modules. This device can sense the voltage and current capabilities of a module before testing and apply the applicable testing range. For this procedure, the Mini-KLA applied an upper limit of 30 V and 4 A for the V_{oc} and I_{sc}, respectively. The Mini-KLA uses a very simple interface, as there are only two buttons on the device: “Select” and “Change.” The “Change” button is only used to put the Mini-

KLA in sleep mode to extract the data. The Mini-KLA samples up to 500 data pairs of currents and voltages to a create a comprehensive IV curve for each individual module curve, and the internal 1MBit memory can hold up to 100 IV curves at a time before the data need to be cleared (Ingenieurburo Mencke & Tegtmeyer GmbH, 2011). The Mini-KLA receives connecting wires from the positive and negative ports of the module (connected to the module with 4 mm-diameter multi-contact (MC4) connectors), as well as one cable from the irradiance reference sensor, for a total of three input wires (Figure 34).

After each test is complete, the Mini-KLA produces the IV curve on its graphical liquid-crystal display (LCD) screen along with the pertinent data that it has recorded. These data are a combination of the module performance details and the information received from the irradiance reference sensor Si-01TC-T, also made by Ingenieurburo Mencke & Tegtmeyer GmbH. The data include V_{mp}, I_{mp}, P_{max}, V_{oc}, I_{sc}, solar insolation (G), reference cell temperature, and the IV fill factor (FF).

The Mini-KLA advertises 0.4% full-scale range accuracy on its specifications sheet (Appendix A). This means that at the applicable ranges of 30 V, 4 A, 100°C, and 1300 W/m^2, the maximum range of error is ±0.12 V, ±0.016 A, ±0.4°C, and ±5.2 W/m^2 for those respectively categories. The irradiance reference sensor also has associated calibration values for its temperature and insolation readings, which are 10 mV for every degree Kelvin (0°C is 1.235 V) and 1 V for every 1000 W/m^2, respectively (Ingenieurburo Mencke & Tegtmeyer GmbH, 2011). This information is applied in the analysis portion of this report.

Figure 35: Version of the Mini-KLA IV Curve Analyzer with five ports (where the model used in the 2016 testing had only three ports, as indicated in Figure 34) and reference PV cell sensor (Ingenieurburo Mencke & Tegtmeyer GmbH, 2011)

Due to the associated uncertainty with the irradiance reference sensor, additional high quality third-party instruments were used to act as either verification or supplementary data for the solar insolation and module temperature measurements. A newly calibrated Eppley PSP, or Precision Spectral Pyranometer, was used to measure the solar insolation in the plane of the module. Just like the reference cell, it was attached to the testing frame with a frame board fabricated by Mark Rocheleau. As noted in the schematic of Figure 34, the wiring configuration of this Eppley PSP differs from typical color code conventions. In this case, the white wire is the positive lead, the black wire is the negative lead, and the green and red wires are not used. This pyranometer is a thermopile-based insolation measurement instrument, as opposed to a PV-based device

like the Mini-KLA reference cell, and its output signal is in the form of millivolts. Therefore, a Fluke 287 True RMS multimeter is used to read the Eppley mV output with accuracy of 0.025%, or roughly 0.0125 mV while testing over a 50-mV range (Fluke, 2009). The Eppley PSP reports the insolation with a resolution of 1 W/m^2 (The Eppley Laboratory, Inc., 2016). The project-specific Eppley PSP's calibration sheet (Appendix A) states that its sensitivity is 8.78 $\mu V/Wm^{-2}$, which means that a reading on the Fluke 287 of 8.78 mV corresponds to a solar insolation of 1000 W/m^2. This also means that the Fluke 287's accuracy of 0.0125 mV is equivalent to an uncertainty in the insolation value of 1.42 W/m^2. In accordance with the past test procedures, 800 W/m^2, or a 7.024 mV reading from the PSP, is the lowest insolation during which tests can be performed. Also included in the calibration sheet is the PSP's uncertainty of 0.91% at a 95% confidence interval and the advertised 650 Ω resistance at 23°C.

Surface mount thermocouples are often used to measure a PV module's temperature. Due to the mild climate in northern California, a thermocouple with a wide temperature measurement range is not necessary. A type-K surface mount thermocouple, with a wider than necessary operational temperature range of -250°C to 1250°C, was used to measure the temperature of the modules during testing with an accuracy of ±2.2°C or ±0.75% (whichever of the two is greater). This thermocouple is attached to the backsheet of the module with insulation tape, and the Omegaette HH303 thermometer is used to read the type-K thermocouple with a resolution of 0.1°C. This thermometer can record either type K or J thermocouples, and its specification sheet (Appendix A) claims an accuracy of 0.1% of the reading plus an additional 0.7°C (Omega, 2016). The use of

the thermocouple attached directly to the tested module provides a better estimate of the module temperatures than the Mini-KLA reference cell temperature, as each module can be slightly different than the last.

Now that the measurement equipment has been fully described, the step-by-step process of performing the IV curve tests on the solar modules will be described. In order to help the modules reach steady state temperature conditions similar to what would be expected in the field at an operational array, the modules that were being tested on a given day were laid out in the sun. This is done as a first step in the setup process so that IV curve tests can begin soon after the equipment is ready. These modules are then wiped down with a cloth and Windex to eliminate any lingering dust or dirt particles from storage and transportation. Next, the test rack was assembled and equipped with the frame boards that hold the reference sensor and Eppley PSP, as shown in Figure 36. A similar digital image was taken for each of the 192 tested modules to document the physical signs of degradation like delamination, hot spots, and discoloration that appeared over their 25.5 years of field exposure (See Appendix C Figure C - 1 to Figure C - 12). These images can be compared to the image of the new ARCO M75 module in Figure 7 to show the severity of the cell deterioration.

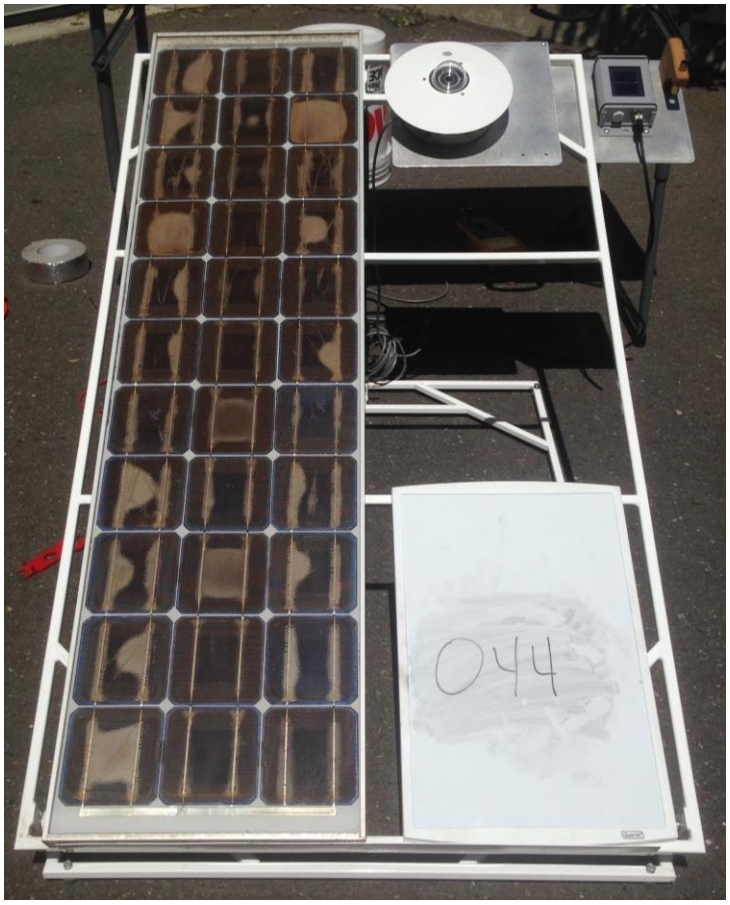

Figure 36: Testing setup with the PV module, test rack, Eppley PSP, and reference cell. The number (044) is used to identify the particular PV module that is being tested.

Once the modules reached steady state temperature, the sensors were appropriately wired to their associated measuring instruments, and, if the sky was still clear of clouds, then the testing was begun. It was important to wait to test until the module temperature had reached steady state, where the temperature was no longer climbing or falling, to get the best results. Also, the direct normal site tube needed constant attention as the sun moved very quickly across the sky, so that the test rack required frequent adjustment to maintain direct normal conditions. The Mini-KLA saves all its data internally, but additional information about the test and the data from the

external sensors must also be recorded. To facilitate documentation of this information, a clipboard-ready data-entry table was created and used (examples as Figure D - 1 and Figure D - 2 in Appendix D). The information included each test's date, module number (001-192), module serial number, test time, module temperature, and the Eppley mV reading. In addition, it was necessary to note the number of visible knees on the Mini-KLA produced IV curve to immediately see the presence of bypass diode issues. Also included was a checkbox to ensure a photo of that module has been taken, the run of that module (each test involved two replicates), the IV curve number (as explained below), and, if necessary, comments about the module or test results. In the effort to identify and address errors in the testing process, two replicate IV curves, or runs (a and b), were performed on each module. As is discussed in the PV Module Analysis section, these runs are averaged to produce a better image of the module's performance abilities. The IV curve number is assigned by the Mini-KLA in the order of the tests until the memory is cleared. Therefore, these numbers are recorded to enable matching the Mini-KLA output file with the other information that was recorded for that IV curve test.

With only two button options, it is very easy to operate the Mini-KLA. Pushing the "Select" button twice maneuvers to the option to start a test. One more push of "Select" begins the test, which only takes 1-3 seconds. During this time, the Eppley reading (via the Fluke 287 multimeter) and the thermocouple reading (via the Omegaette HH303 thermometer) are recorded on the clipboard sheet. This process is repeated for each module, and the Mini-KLA and clipboard data are digitally recorded and saved. When that day's testing is done the modules are put back into storage. The four

replacement Siemens SM50-H modules were tested with the same procedure as the ARCO M75 modules, and their difference in size and nomenclature are addressed in the analysis section of this report.

To represent the relationship between power output and the operating temperature, seven selected modules, including one Siemens module, were tested twice at three different times during a single day to generate IV curves over a range of temperature. Two of the curves were measured at relatively low temperatures, two at close to ambient temperature, and two at a higher temperature that corresponded to the steady state temperature for each module. These seven modules have runs labeled a, b, c, d, e, and f. Other than the process associated with ensuring that the module temperature falls within the appropriate temperature range as described, there is no difference in the testing procedure or data collection process. Outside of this temperature analysis, runs e and f, or the steady state temperature runs, are used for those modules to compare their power degradation compared to past test cycles. Lastly, a small sample of six modules was tested with their bypass diodes removed, shown earlier in Figure 8, to determine if the bypass diodes are now causing more issues than they are solving regarding power generation. This could be true (as investigated in the Results section) because multiple cells may be bypassed by these diodes, which could lead to significant power loss. As with testing of the replacement Siemens modules, the temperature relationship testing, and all the other module tests, the IV curve testing procedure remains the same for consistency's sake.

The next section covers the data collection and organization for activities not discussed above, along with the statistical methods and software used to normalize, organize, and produce the final results that are used to compare the modules' performance over a lifetime of coastal environment exposure.

PV Module Analysis

The primary purpose of this thesis is to complete the 25.5-year analysis of power degradation in the ARCO M75 modules. To carry out this work, the data collected both by the Mini-KLA and by third party instrumentation must be normalized and organized so that the 2016 results can be compared to results from earlier tests. The first step involves recording the clipboard data in an Excel spreadsheet and uploading the Mini-KLA data into its associated software program called MiniLes. MiniLes creates a text file (in .asc form) that reports the raw V_{mp}, I_{mp}, P_{max}, V_{oc}, I_{sc}, G, T, and FF results along with the associated string of current and voltage pairs recorded by the Mini-KLA for each tested module. The Mini-KLA data are uploaded and saved after each day of testing to clear the memory of the device and make room for the next day's testing. MiniLes is only a means to save the data from the Mini-KLA, as it does not normalize the data to NOCT conditions. A coding program written in Scilab, used in the 2010 round of testing, is utilized at this point in the data analysis. Due to progress in technology, the modern software, just like the hardware, is subject to advance past the tools and resources used in earlier stages of the analysis of these solar modules; therefore, the strategy and methods

used to analyze the data may differ even while the equations and normalization procedures remain consistent.

This Scilab code (Appendix B) pulls data from the raw MiniLes and clipboard files and combines their information, including the IV curve data from MiniLes and the module information and third party insolation and module temperature data from the clipboard, to develop for each module test a regression analysis table and a summary table of the pertinent parameters and results, and related standard deviations of the results (Appendix E shows examples of a summary table, as Table E - 1 to Table E - 4, and a regression table, as Table E - 5). The 2016 summary table is used in conjunction with the previous testing cycles' summary tables to create a full depiction of the performance degradation and changes in the parameters of the solar modules, especially with respect to their power generation abilities.

The Scilab code applies Equations 1-4, defined earlier in this report, to normalize the IV curves and data to NOCT conditions through an iterative process. This procedure uses a Gauss-Newton method and least squares to create a best fit for the parameters. The program can produce graphical representations of the observed and predicted IV curves for each module (Figure 37). These curves (examples as Figure E - 1 to Figure E - 4 in Appendix E) can be compared to the original 1990 IV curves to determine the changes in a module's performance.

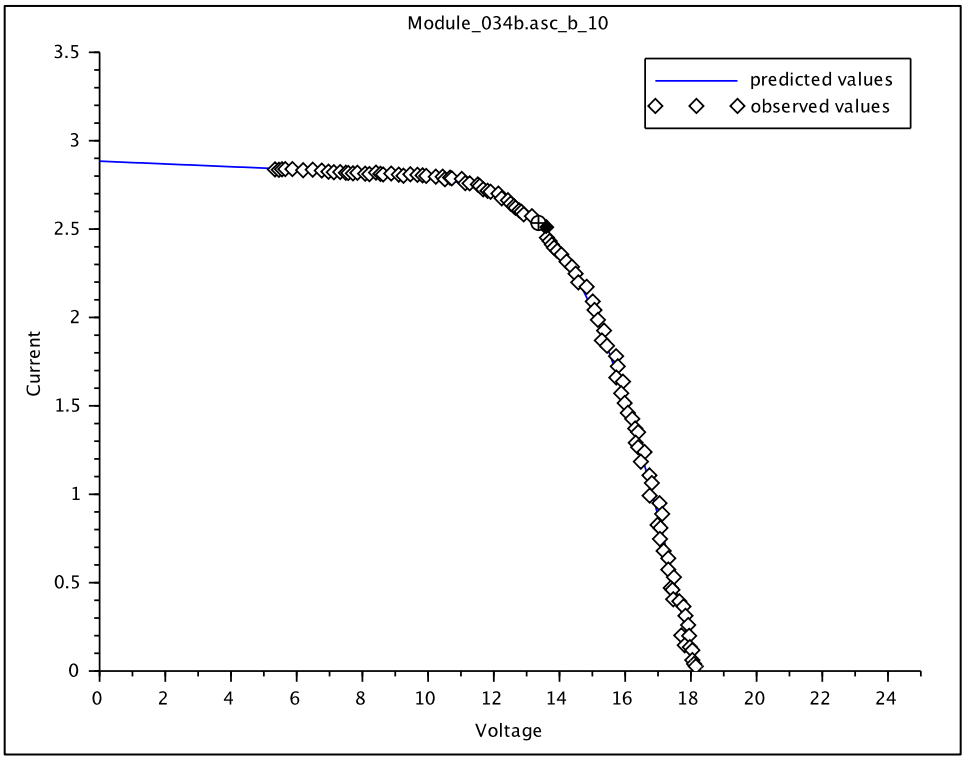

Figure 37: Example of Scilab IV curve in NOCT (Scilab Enterprises, 2016)

Due to the adverse effect of the bypass diodes in many of the modules and the secondary knees in the IV curve that they have created, certain adjustments were made for the power performance results to be comparable to past IV curves. In the code, any current-voltage pair with a voltage below 5 V was clipped from the data, save for a small sample of modules that are used to analyze the quantifiable influence of the bypass diodes. The module temperature and solar irradiance correction factors determined by Zoellick (1990) with multiple linear regression (Equation 2) are used in all the testing cycles for consistency and because they are specific to these exact modules. This 2016 round of analysis investigates and reports the degree to which those correction factors are

still applicable 26 years later, as it is reasonable to assume that the modules may have changed enough to require updated correction factors.

There are other areas outside of the bypass diodes that also require closer attention and small adjustments. One small issue that arose in this round of testing was that for two testing days, June 24th and August 12th, the Mini-KLA file did not input a number in the "comment" space. All other testing days had a number in this area; therefore, a slight change in the code was needed for those two test days. As it can be seen in in Appendix B, line 124 calls for two inputs to account for "comment" and the number following it. For those two days of data without a number after "comment," the second input is removed to avoid an error that prevents the code from executing the analysis procedure.

In addition, lines 231-232 deal with limit constraints for the five key IV curve module parameters: I_{sc}, V_{oc}, ekt, R_s, and R_p. These exist so that the program's iterative process does not vary too far from seemingly reasonable results. Between testing every module twice, the temperature correction verification, and the bypass diode evaluation, 424 IV curve tests were performed, and 151 runs, or 35.6% of the total runs, hit one of the limits. The range of limits for I_{sc} and V_{oc} are set at 2-4 A and 15-25 V, respectively, and no modules reached these limits during the analysis. However, the same cannot be said for the limits pertaining to the other three parameters. Table 8 summarizes the original upper and lower limits for ekt, R_s, and R_p as well as the limits that were ultimately applied.

Table 8: Modeling constraints for key parameters ekt, R_s, and R_p

Parameter (UL and LL refer to the Upper or Lower Limit, respectively)	**Original Limit**	**Final Limit**
ekt (LL)	0.1	0.1
ekt (UL)	2.0	5.5
R_s (LL)	0.05	0.05
R_s (UL)	2.0	4.0
R_p (LL)	50	15
R_p (UL)	1000	3500

Eight IV curve test runs contained data that could not be analyzed adequately by the Scilab software program because their current-voltage relationships differed significantly from the expected curve shape. To address this, an implementation of the analysis algorithm is Excel was used to carry out the necessary analyses. Of these eight runs, four of them came from the two tests on modules 044 and 078, which produced so little power (each under 10 W) that the Scilab code could not interpret their data. The IV curves for the two runs of module 051 produced an unexpected and unusual bump in the high voltage area of the IV curve, and the code could also not interpret that bump from run "a". The first runs (run "a") of modules 023 and 111 produced an r^2 value above 1.0, which is theoretically impossible. Finally, the eighth problematic run occurred with module 118 (run "a") with the bypass diode removed.

Once those eight runs were removed from the primary analysis and the new updated parameter limits were generated, only eight out of the remaining total 416 tests

exceeded a limit. This procedure reduced the percent of tests reaching one of the limits from 35.6% to 1.9%. The eight runs that continued to surpass the limits included seven modules exceeding the R_p upper limit and one module meeting the upper limit of ekt. The tests that resulted in the ekt limit breach and two of the seven that still had issues with the R_p parameter were from the tests with the bypass diodes removed. The final constraint ranges successfully involved the true results for over 98% of the tests, and this provides useful and comparable data for the analysis.

The Excel spreadsheet that is used on the eight modules that had results that could not be managed with the Scilab software performs an iterative process, based on user-defined initial guesses, with the cleaned current-voltage pairs (no pairs below 5 V and pairs with current changes below 0.05 A thrown out) from the Scilab regression file. The end-result is a file containing the same information that the Scilab summary file contains, and therefore the Excel data can be successfully compared to the rest of the results. An example set of results from this Excel spreadsheet is shown in Appendix F in Figure F - 1 and Table F - 1.

This section has outlined how the solar module IV curve data were acquired and then how they were organized for analyses. The following section covers the results from this 2016 round of testing and an examination of the progressive decline of the modules' capabilities over their 25.5-year lifetime in the coastal town of Trinidad, California using the results from the 1990, 2001, and 2010 testing cycles. The majority of the graphs were created in a software package called Kaleidagraph (KaleidaGraph: Graphing and Data Analysis, 2017).

RESULTS

The following section presents the primary findings of this analysis of the performance of the Trinidad PV array modules. Each table and figure is introduced and briefly explained, and the analysis pertaining to the results shown here can be found in the subsequent Discussion section. As noted earlier in this report, the number of modules tested in each cycle (i.e. 1990, 2001, 2010, 2016) varies due to the failure of four modules over time (these modules were replaced with Siemens modules); therefore, the probability curves, histograms, and any other form of results shown in this section unavoidably contain unequal number of modules. Parameter outliers that occurred in now-failed modules are also removed from the following results for comparability.

Equipment Verification

As discussed previously, the Mini-KLA, with its advertised 0.4% full-scale accuracy, came equipped with a PV reference cell with a temperature sensor. However, an Eppley PSP pyranometer was used in the testing for the insolation readings, and a type-K thermocouple was used to measure the module temperature, as detailed in the Methods section. Table 9 shows the comparison between the insolation and temperature recordings from the Mini-KLA and the third-party instruments. The fact that the third-party thermocouple could be attached directly to the module being tested provided more accurate data for the modules' temperatures, and the Eppley PSP is more accurate than

the Mini-KLA. The Mini-KLA consistently reported an insolation 36 W/m^2 higher than the Eppley PSP, or 3.7% more solar energy, and the Mini-KLA temperature sensor under-represented the true module temperature by roughly 4.5°C, or 8.3%. Figure 38 and Figure 39 show the reading comparisons graphically for all the tests performed. The temperature figure has 42 fewer tests, as the temperature sensitivity analysis involved exposing the modules, and not the Mini-KLA reference cell, to adverse conditions. Figure 40 and Figure 41 tell a slightly different story, as they show that the direct relationship of the Eppley PSP and the Mini-KLA reference cell results are generally linear but that there is much less predictability among the temperature readings, respectively. The improved accuracy of the third-party instruments for insolation and module temperature measurements allows the findings presented in this thesis to be more accurate. The Mini-KLA's over estimation of solar insolation would result in tests indicating that the modules generated less power than they did, and the lower module temperatures would lead to incorrect IV curves, calculations, and performance reviews.

Table 9: Comparison of results between Mini-KLA and third-party instruments

	Difference between Eppley and Mini-KLA	**Difference between type-K thermocouple and Mini-KLA**
Average	36.3 W/m^2	4.5 °C
Standard Deviation	9.25 W/m^2	3.4 °C
Average (%)	3.7%	8.3%
Standard Deviation (%)	1.0%	6.4%

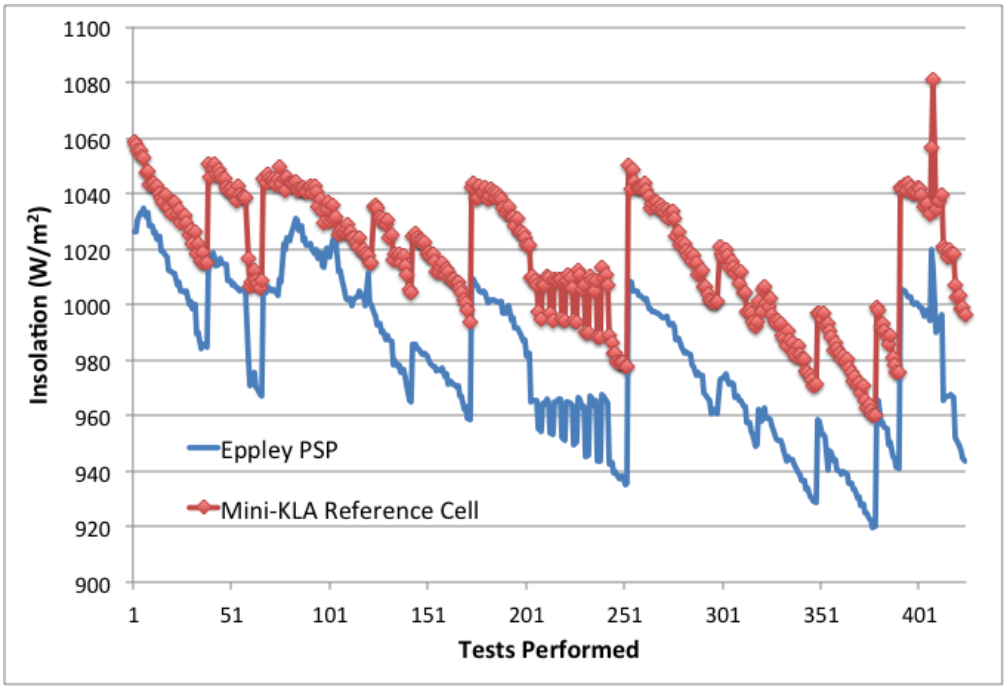

Figure 38: Eppley readings versus the Mini-KLA reference cell insolation output

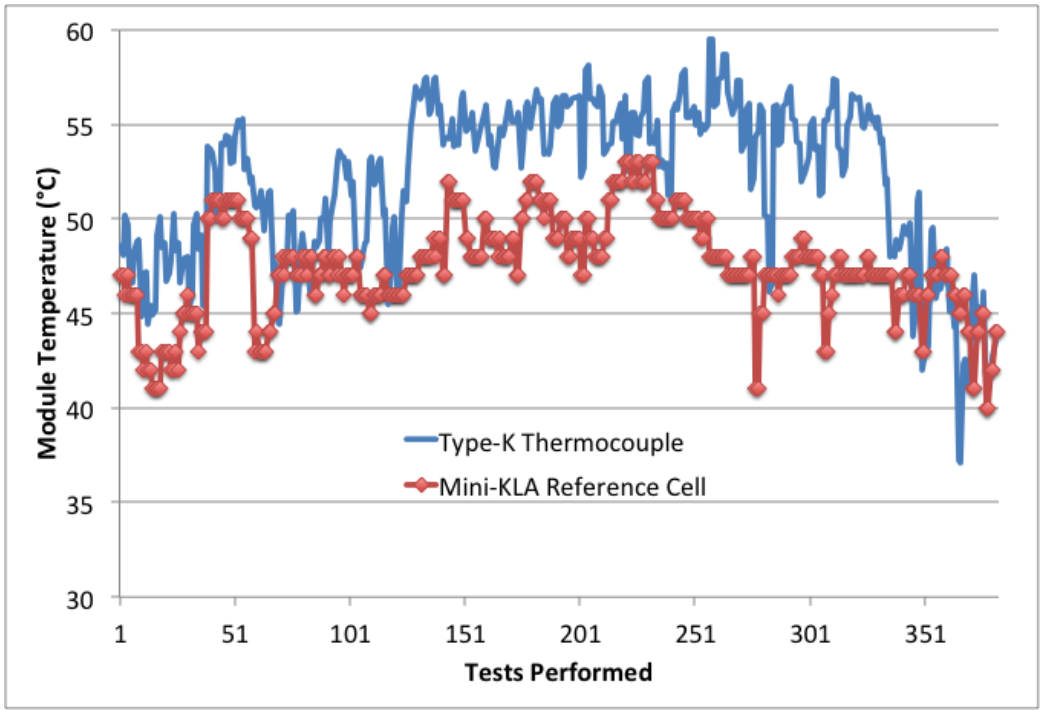

Figure 39: Comparison of thermocouple reading and the Mini-KLA reference cell results

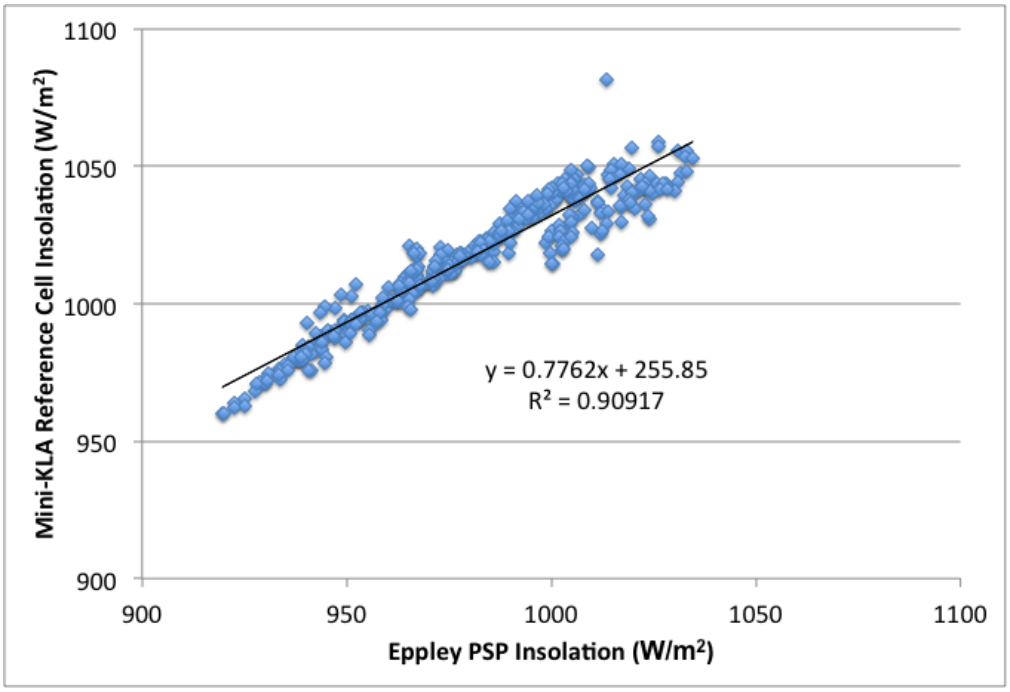

Figure 40: Directly plotting the Eppley PSP and reference cell insolation readings against each other

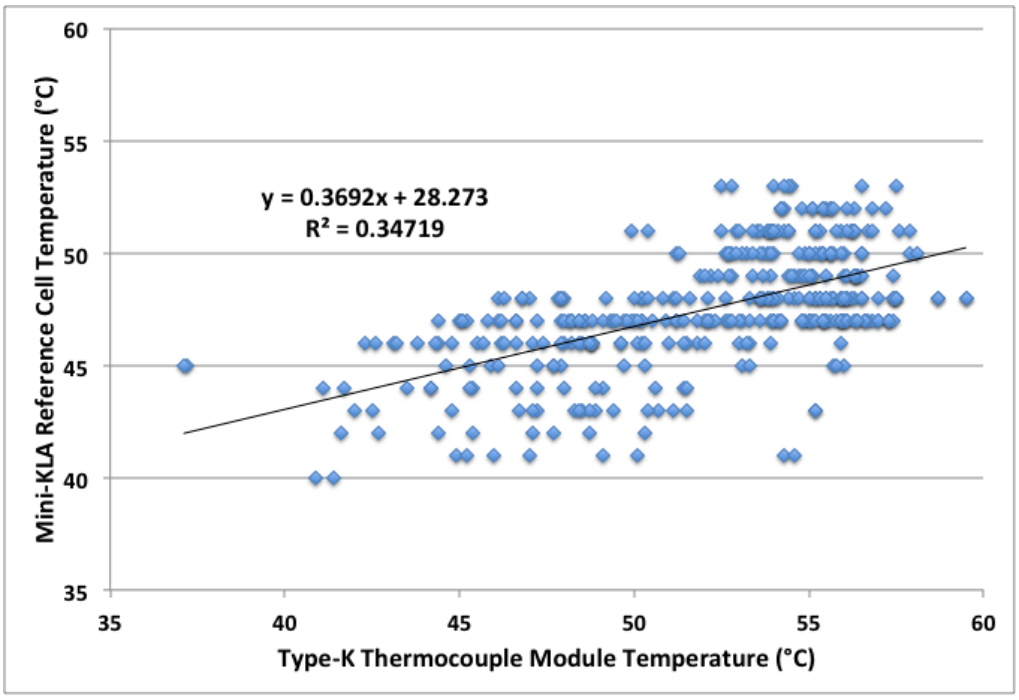

Figure 41: Directly plotting the thermocouple and reference cell temperature readings against each other

Individual Module Maximum Power Output

The most important metric used to compare the 192 ARCO modules over the testing cycles of this project is the maximum power output in NOCT conditions. While many other parameters provide useful insight into the operation and aging of these PV solar modules, such as the fact that the average module NOCT efficiency fell from 10.016% ± 0.063% with a 95% confidence interval in 1990 to 7.915% ± 0.156% with a 95% confidence interval in 2016 using Equation 5, the power output truly represents their remaining viable worth. How these modules degraded and lost their production abilities is the main focus of this thesis, and, therefore, the following two graphics may be the most important results. Figure 42 is a probability curve, or distribution curve, of the P_{max} for the individual modules at NOCT during each of the four testing cycles. As the variability among the modules grows, so does the steepness of the curve's slope and the space between each representative dot. The lower tail of the distributions becomes increasingly long as the modules age. Probability curves for V_{oc}, I_{sc}, V_{mp}, and I_{mp} can be found in Appendix G (Figure G - 1 to Figure G - 4).

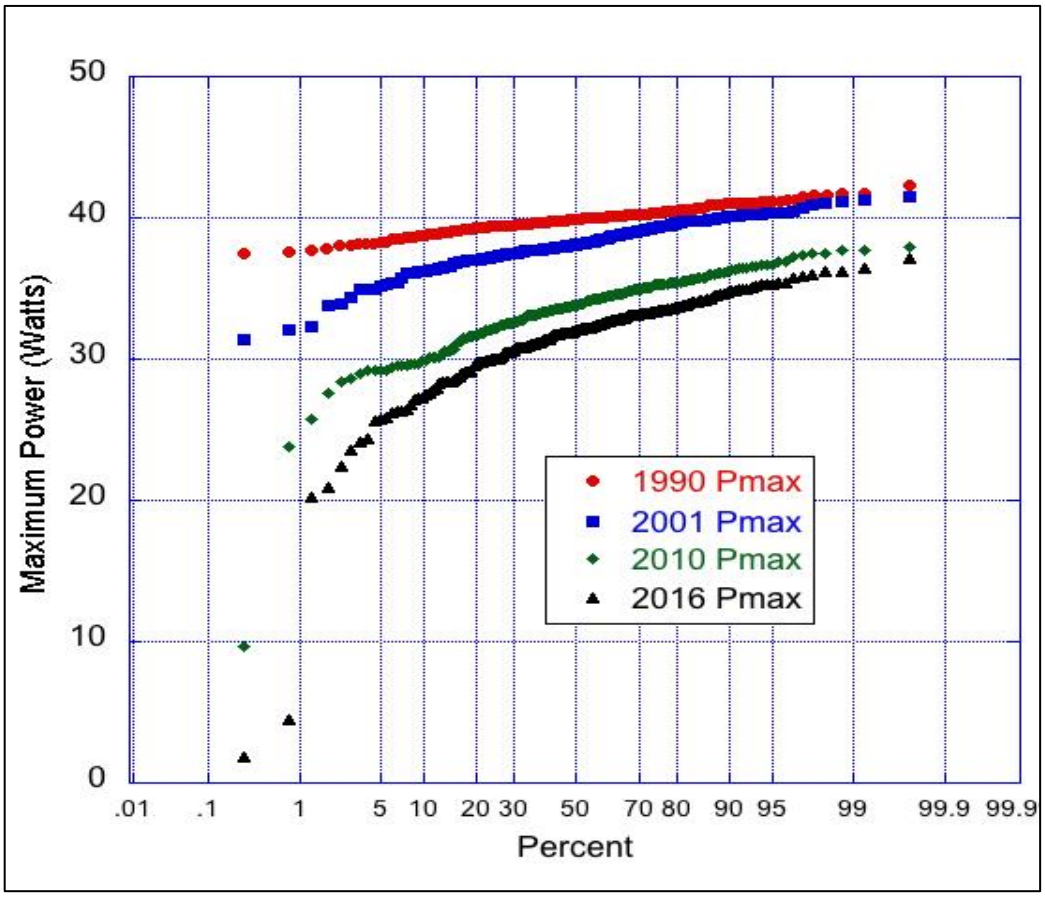

Figure 42: This is a probability distribution curve for the modules' NOCT maximum power showing the drop in the maximum power as the array aged. The steeper slopes indicate a growing variation in the generation abilities among the modules.

Figure 43 expresses the average P_{max} of the modules based on their age, which ranges from zero years old when they were brand new during Zoellick's testing in 1990 to over 25 years old when they were permanently removed from the array in 2016. The accompanying basic linear trend line indicates that, on average, these ARCO modules lost roughly 0.35 W per year of field exposure. Based on Zoellick's original findings with the average P_{max} being equal to 39.87 W, this represents a yearly power degradation rate of 0.82%/year. This is only an estimate, since the degradation experienced by these

modules was not truly linear. Comparing the 2016 average power of 31.25 W after 25.5 years of field exposure to the original average power of 39.87 W in 1990 is consistent with a lifetime degradation rate of 0.85%/year for these ARCO M75 solar modules.

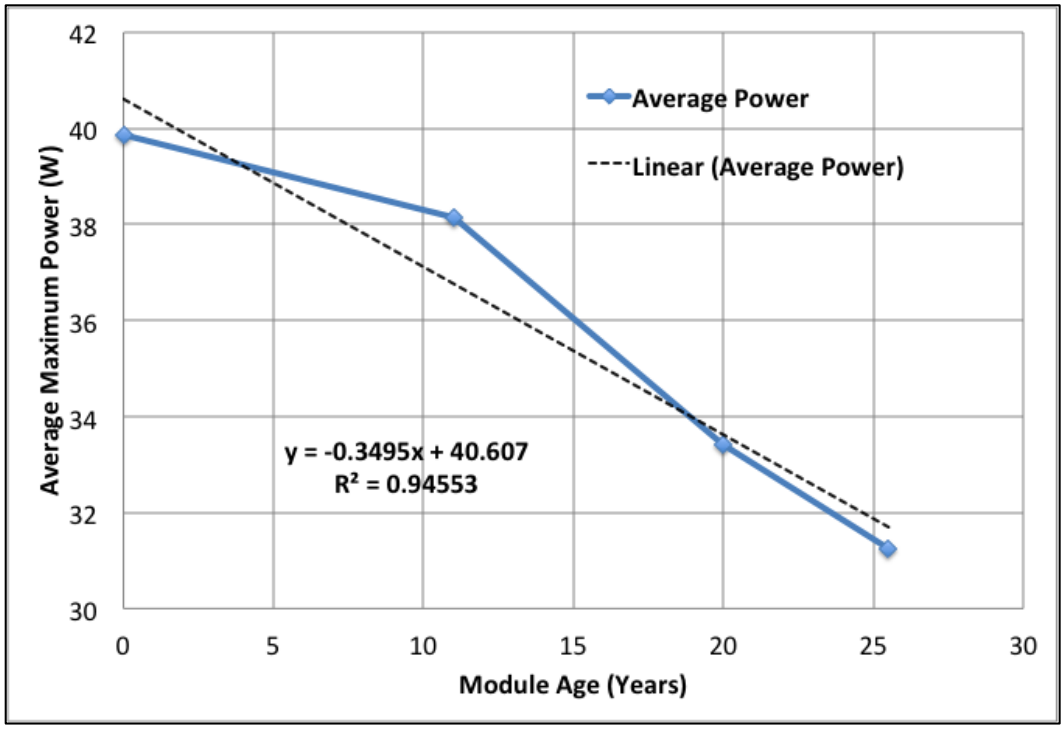

Figure 43: Average module P_{max} based on module age

Table 10 provides summary information for the histogram plots for each test cycle for the averages of the P_{max} and the five key IV curve parameters (I_{sc}, V_{oc}, R_p, ekt, and R_s) that were used to analyze the ARCO modules throughout the lifecycle of this project broken down by testing year. The lower portion of the table compares each of the parameters to the other testing cycle results to develop degradation analyses. The primary results include the 21.6% drop in P_{max} over 25.5 years, the higher drop in I_{sc} than V_{oc} that

lead to this power decline, and the increases in average IV curve related criteria (R_p, ekt, and R_s) as the IV curves physically changed with the modules' performance.

Table 10: Summary of changes in average of P_{max} and the 5-parameters of the IV curve

Year	**P_{max} (W)**	**I_{sc} (A)**	**V_{oc} (V)**	**R_p (Ω)**	**ekt (V^{-1})**	**R_s (Ω)**
1990	39.87	3.30	18.20	171.04	0.71	0.35
2001	38.13	3.15	18.15	95.67	0.89	0.22
2010	33.43	2.86	18.04	80.49	0.85	0.44
2016	31.25	2.77	18.06	96.81	1.54	1.06
'90 v. '01	-4.36%	-4.55%	-0.27%	-44.1%	25.4%	-37.1%
'01 v. '10	-12.3%	-9.21%	-0.61%	-15.9%	-4.49%	100%
'90 v. '10	-16.2%	-13.3%	-0.88%	-52.9%	19.7%	25.7%
'10 v. '16	-6.52%	-3.15%	0.11%	20.3%	81.2%	141%
'90 v. '16	**-21.6%**	**-16.1%**	**-0.77%**	**-43.4%**	**117%**	**203%**

Table 11 summarizes the average degradation rates these modules experienced between testing periods. While there is inconsistent decline in power output from testing cycle to testing cycle, as shown earlier in Figure 43, the lifetime power degradation rate comes to 0.85%/year with a range of rates from 0.4%/year to 1.4%/year. Table 12 summarizes the average and standard deviation of the parameters for each test cycle, with the number of original ARCO modules tested in that cycle noted, as these are the criteria where the parameters experienced the most significant changes throughout the life of the project.

Table 11: Average degradation rates seen throughout the project

Testing Cycle Range	Years in the Field (years)	Average Power Loss (%)	Degradation Rate (%/year)
1990-2001	11	-4.36%	-0.40%/year
2001-2010	9	-12.3%	-1.37%/year
2010-2016	5.5	-6.52%	-1.19%/year
1990-2016	25.5	-21.6%	-0.85%/year

Table 12: Average and standard deviations for important IV curve data

Parameter	Year	ARCO Module Sample Size	Average	Standard Deviation
P_{max} (W)	1990	192	39.87	0.85
P_{max} (W)	2001	191	38.13	1.67
P_{max} (W)	2010	189	33.43	2.93
P_{max} (W)	2016	188	31.25	4.10
I_{sc} (A)	1990	192	3.30	0.04
I_{sc} (A)	2001	191	3.15	0.12
I_{sc} (A)	2010	189	2.86	0.14
I_{sc} (A)	2016	188	2.77	0.25
V_{oc} (V)	1990	192	18.20	0.13
V_{oc} (V)	2001	191	18.15	0.11
V_{oc} (V)	2010	189	18.04	0.26
V_{oc} (V)	2016	188	18.06	0.11

Parameter	Year	ARCO Module Sample Size	Average	Standard Deviation
R_p (Ω)	1990	192	171.04	66.61
R_p (Ω)	2001	191	95.67	55.90
R_p (Ω)	2010	189	80.49	51.05
R_p (Ω)	2016	188	96.81	74.57
ekt (V^{-1})	1990	192	0.71	0.12
ekt (V^{-1})	2001	191	0.89	0.21
ekt (V^{-1})	2010	189	0.85	0.24
ekt (V^{-1})	2016	188	1.54	0.92
R_s (Ω)	1990	192	0.35	0.12
R_s (Ω)	2001	191	0.22	0.24
R_s (Ω)	2010	189	0.44	0.43
R_s (Ω)	2016	188	1.06	0.52

Histograms

The following pages contain color coded histograms for each of the IV curve parameters covered in Table 10 in order of the test cycle, showing how the distribution of the values initially began narrow and then spread out as the modules aged. The precise relationships seen in these histograms are explored in the Discussions section. The P_{max} histogram plots include Figure 44 to Figure 47. The histograms for I_{sc} and V_{oc} are shown in Figure 48 to Figure 51 and in Figure 52 to Figure 55, respectively. The histograms for R_p are given in Figure 56 to Figure 59, for ekt in Figure 60 to Figure 63, and for R_s in Figure 64 to Figure 67. The histograms for V_{mp} and I_{mp} can be found in Appendix G (Figure G - 5 to Figure G - 12). The average V_{mp} stayed relatively the same even as the standard deviation grew, while the average I_{mp} dropped significantly over the lifetime of the project, following the same trends seen with I_{sc} and V_{oc}.

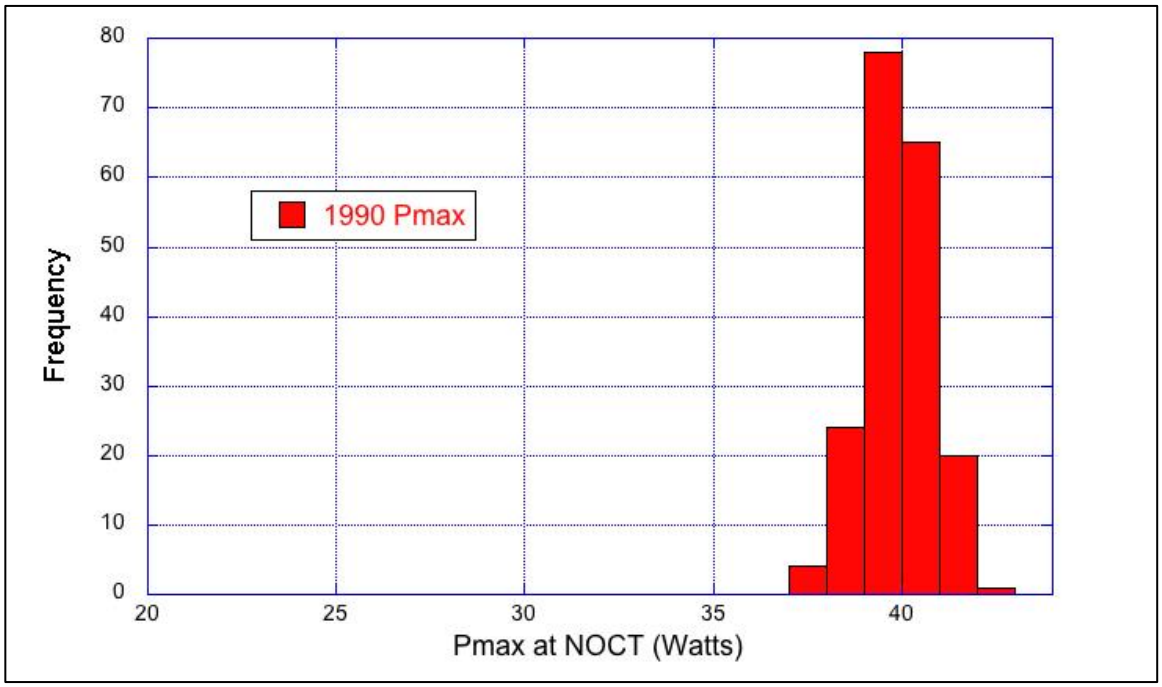

Figure 44: 1990 P_{max} histogram with an initially narrow range

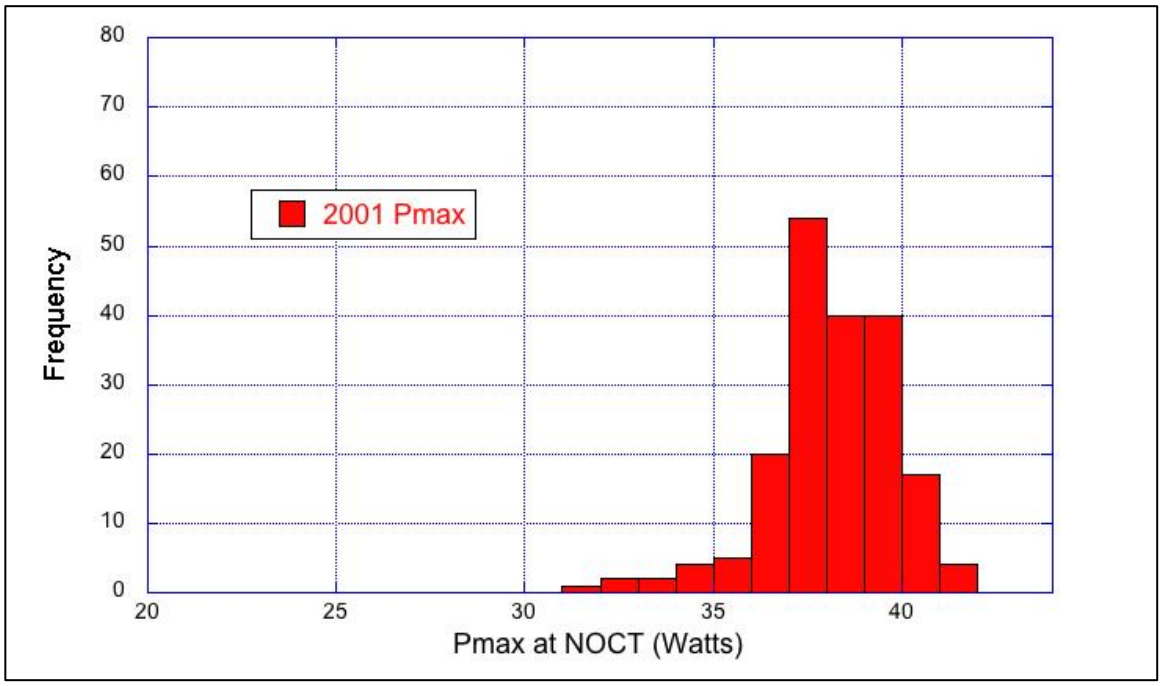

Figure 45: 2001 P_{max} histogram with a widening range after 10 years of field exposure

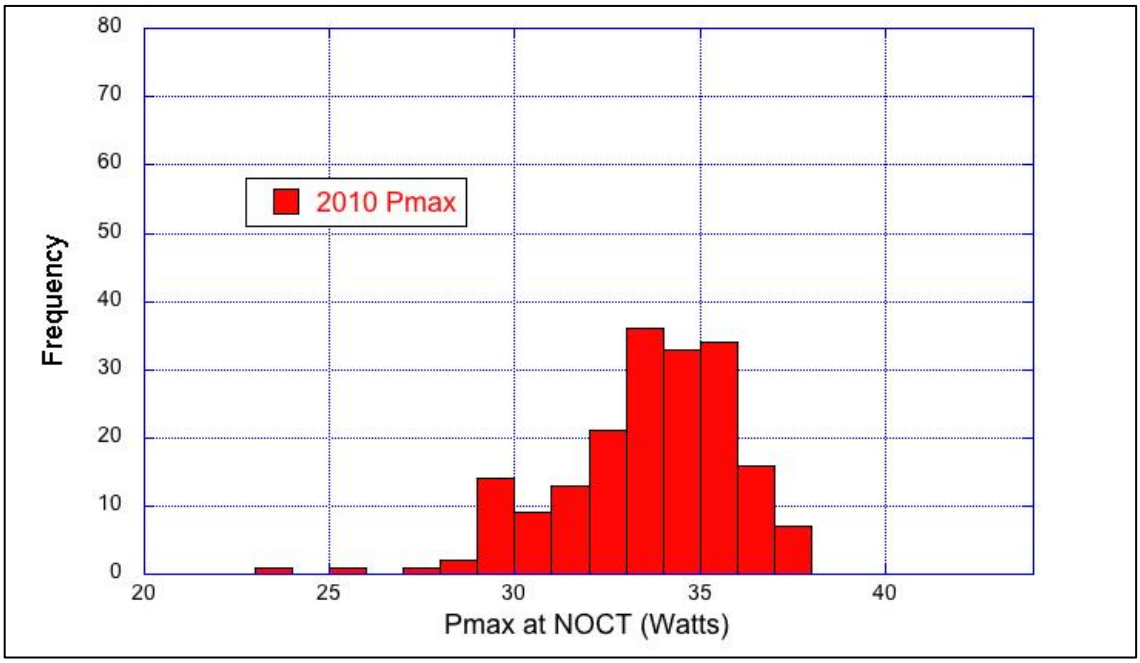

Figure 46: 2010 P_{max} histogram with a lower average after 20 years of field exposure

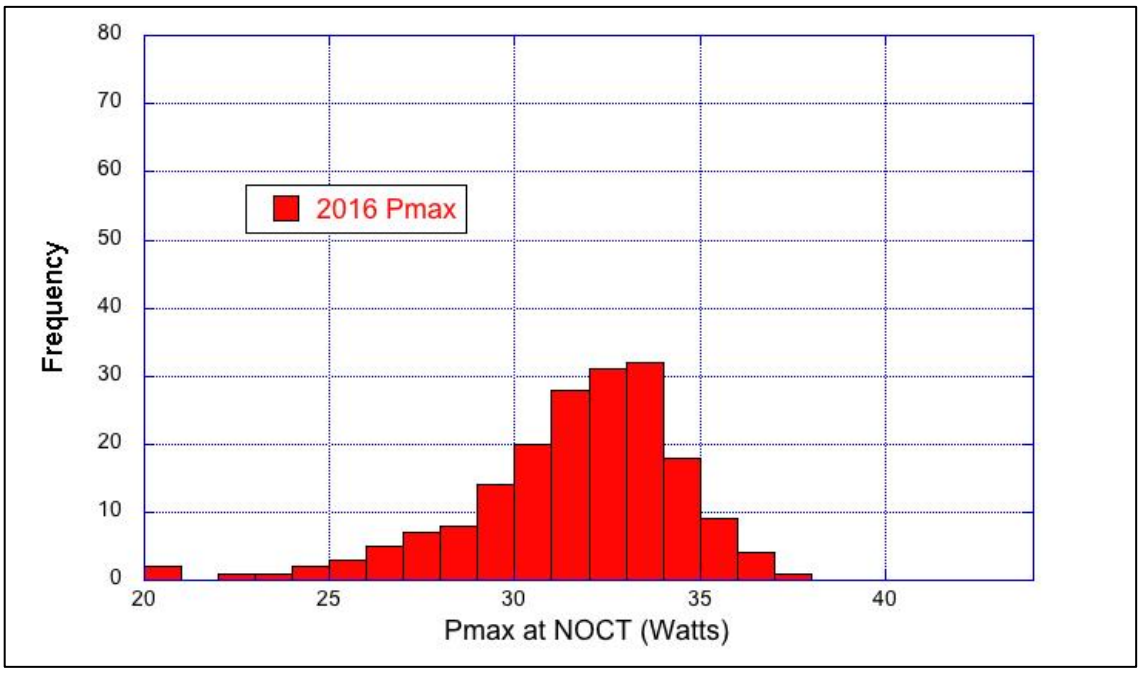

Figure 47: 2016 P_{max} histogram of the modules at the project's completion

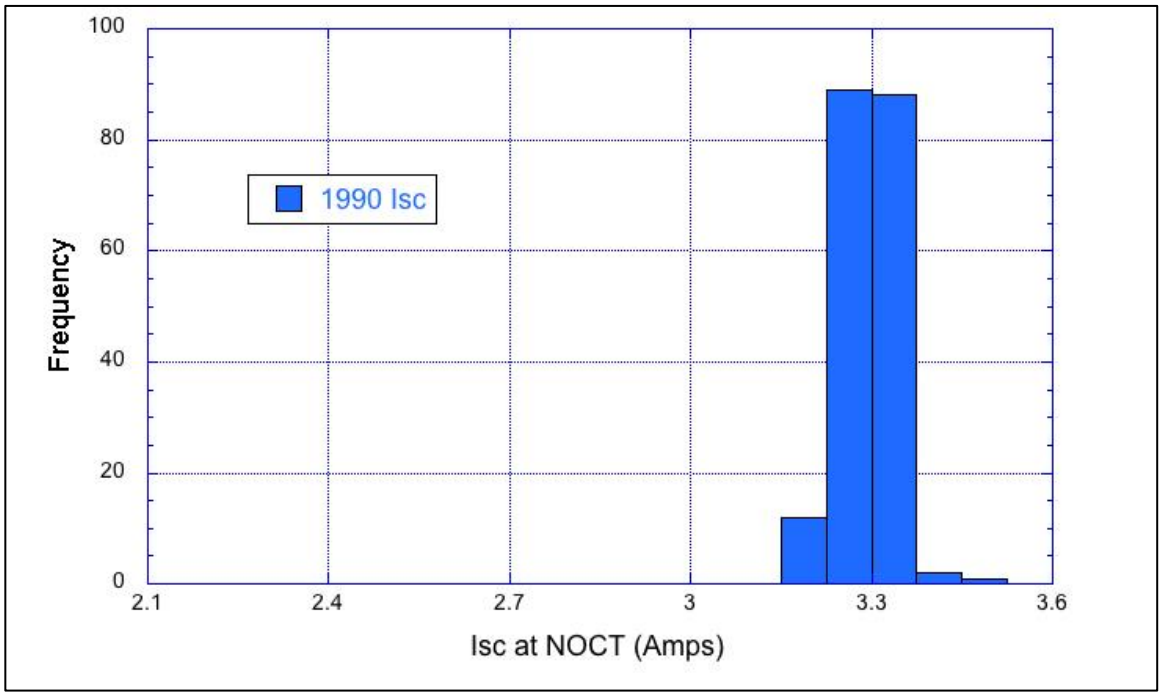

Figure 48: 1990 I_{sc} histogram with narrow range

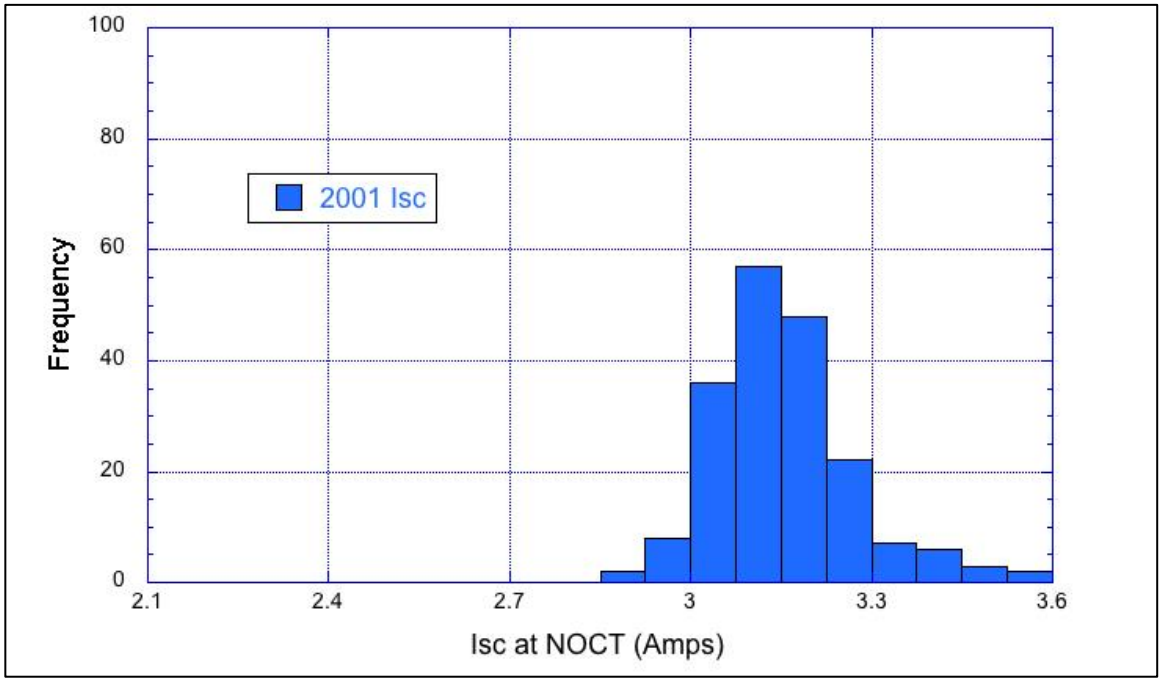

Figure 49: 2001 I_{sc} histogram showing widening range while maintaining similar average

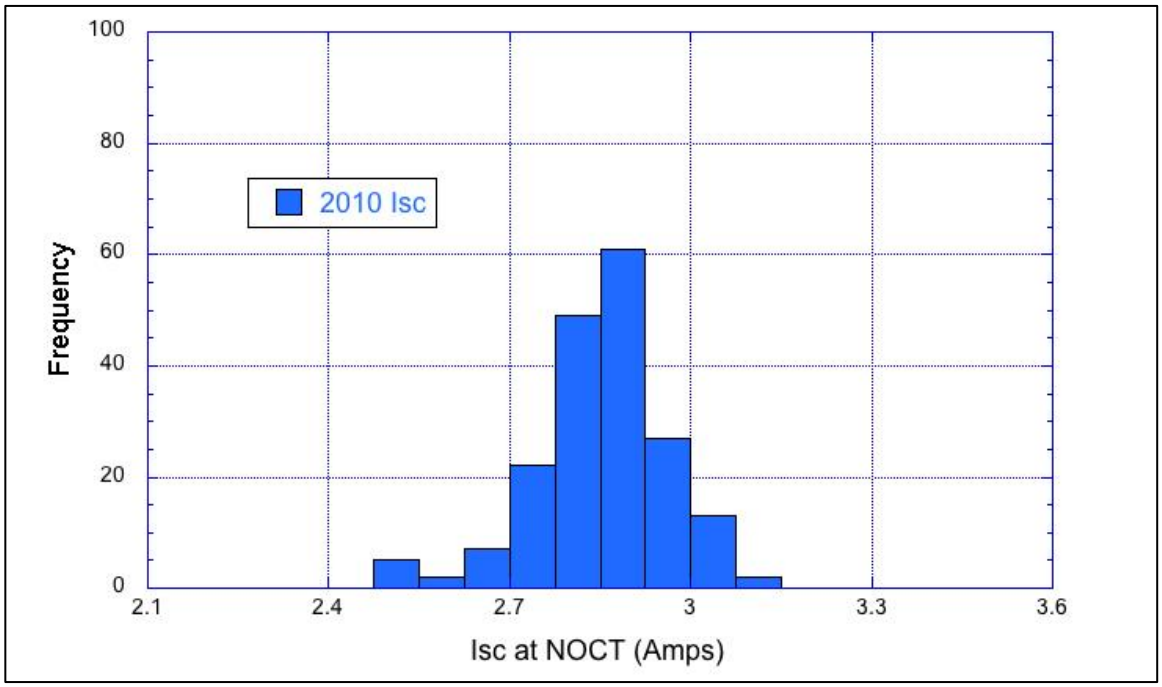

Figure 50: 2010 I_{sc} histogram with decreased average after 20 years

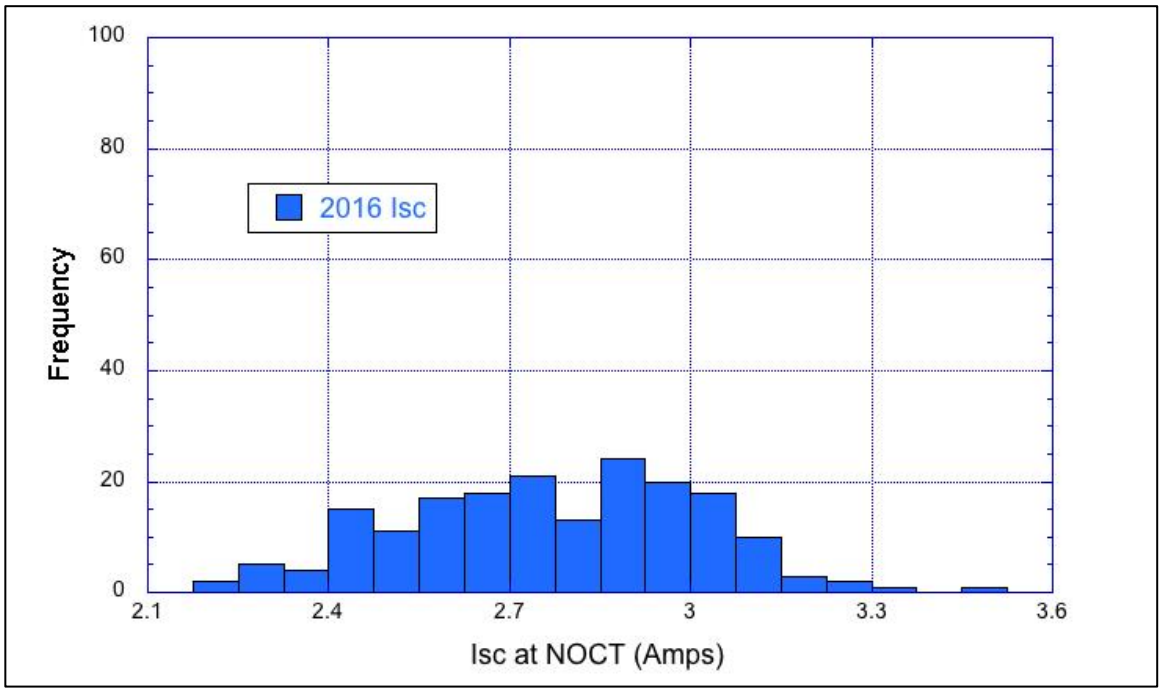

Figure 51: 2016 I_{sc} histogram showing significant spread in the results

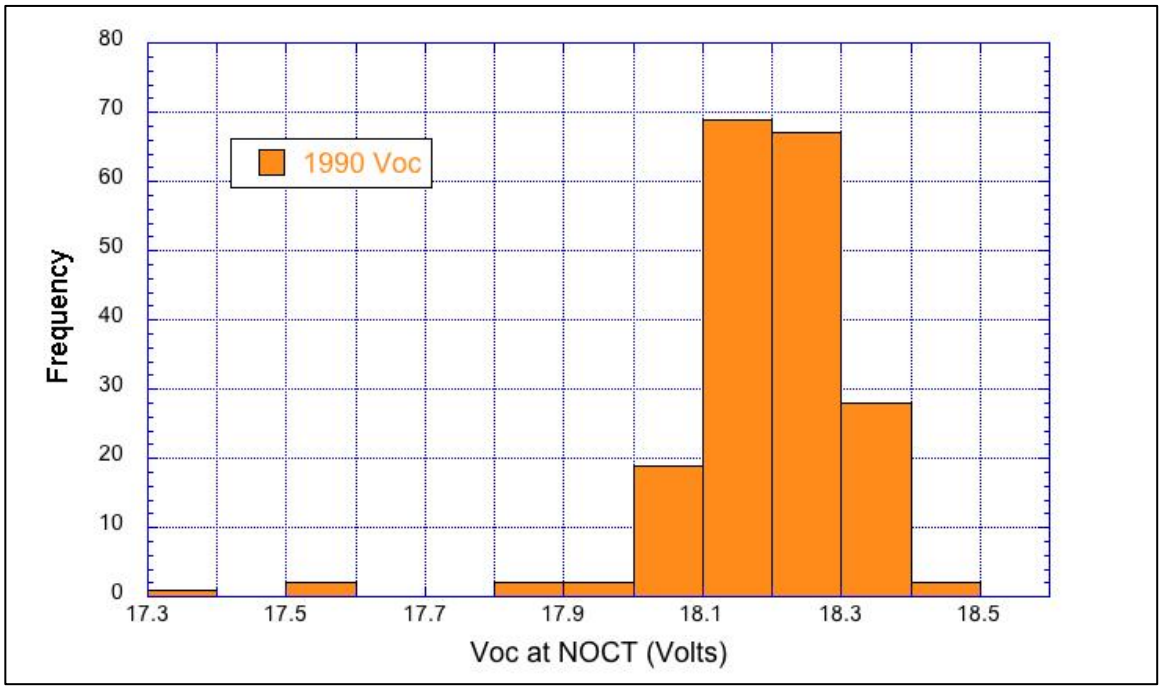

Figure 52: 1990 V_{oc} histogram

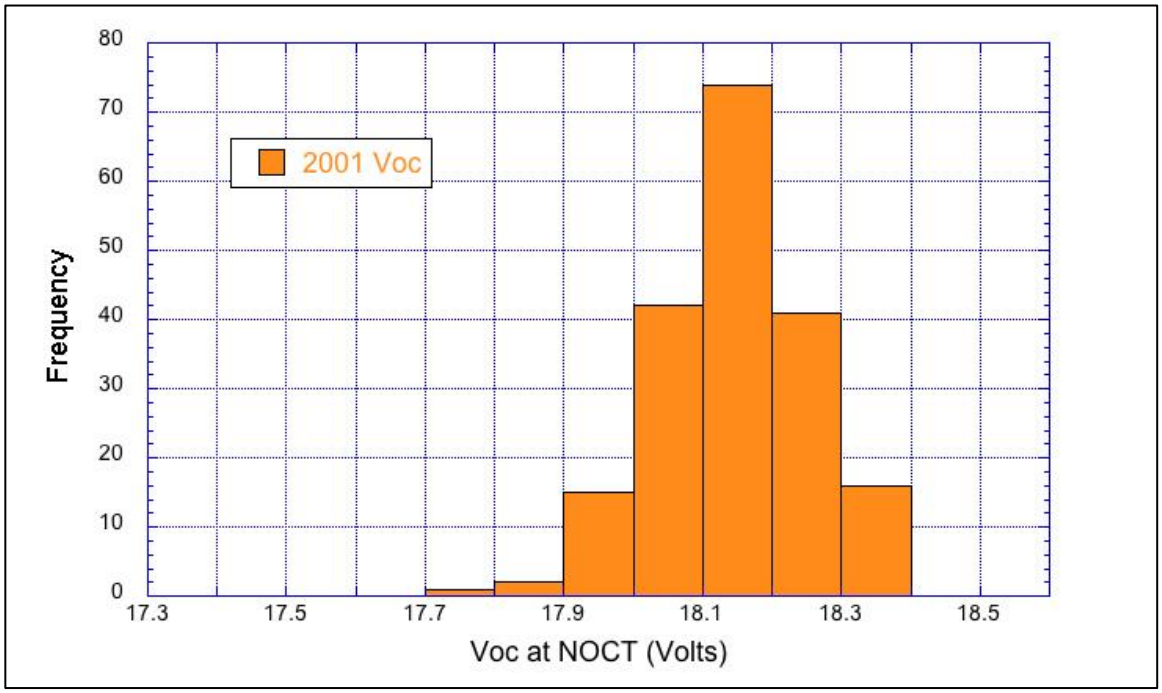

Figure 53: 2001 V_{oc} histogram that shows little change after 10 years

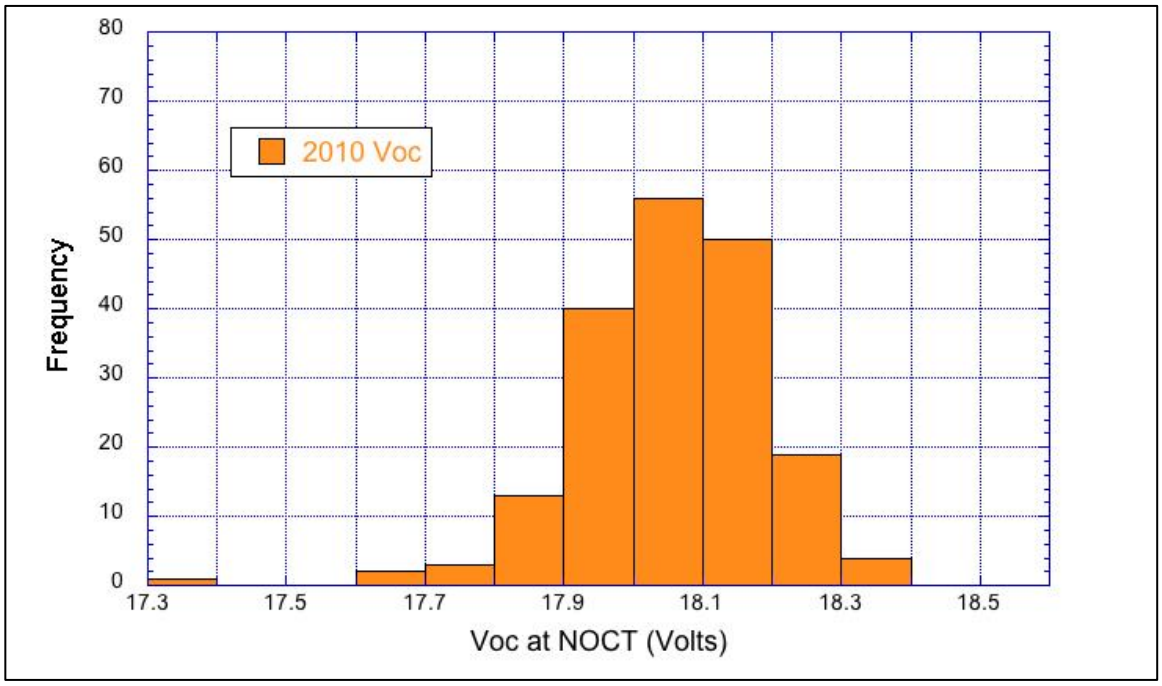

Figure 54: 2010 V_{oc} histogram that is similar to the plot from 1990 and 2001

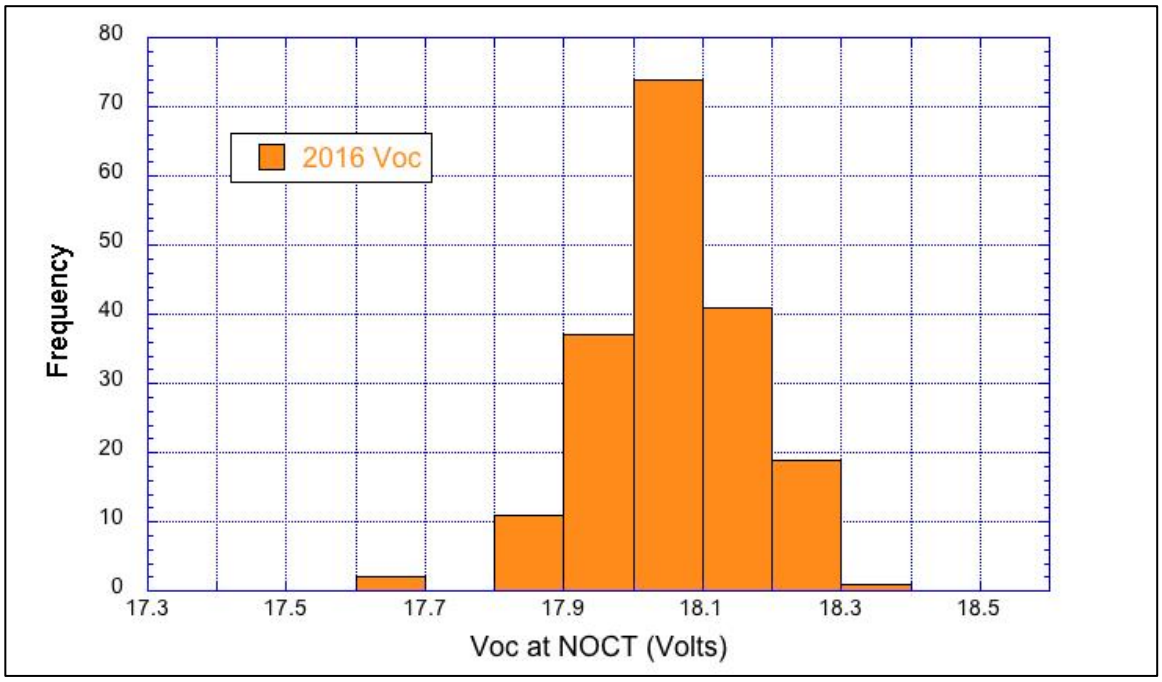

Figure 55: 2016 V_{oc} histogram that hardly changed over 25 years

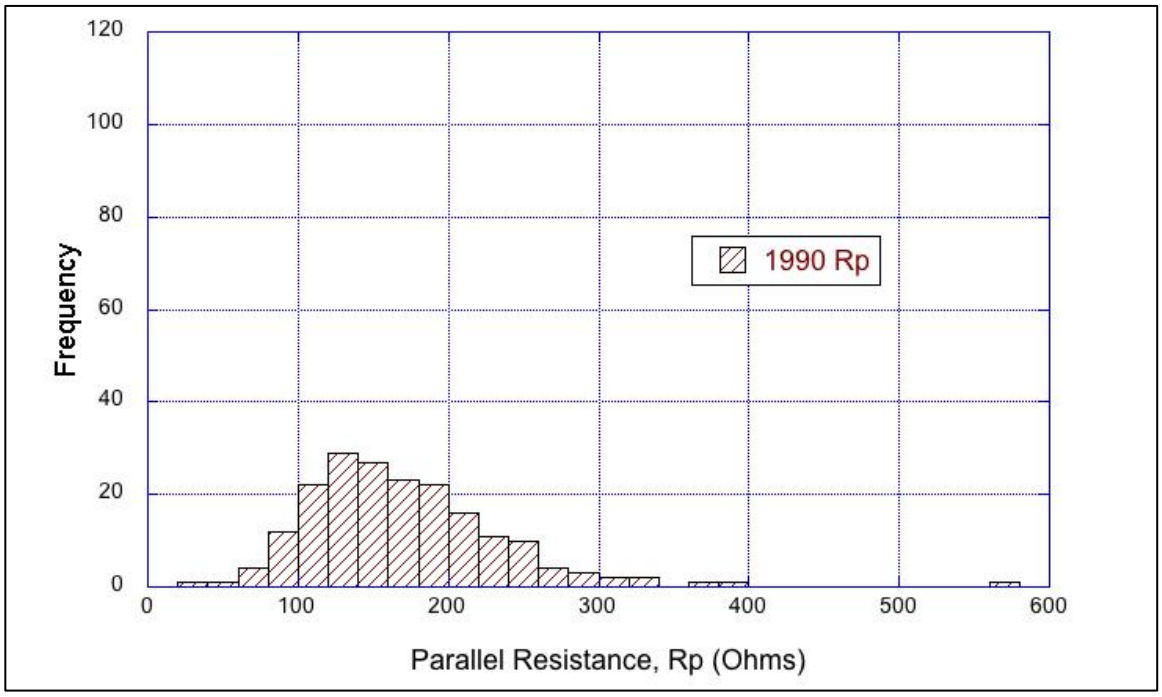

Figure 56: 1990 R_p histogram with relatively wide range at the start of the project

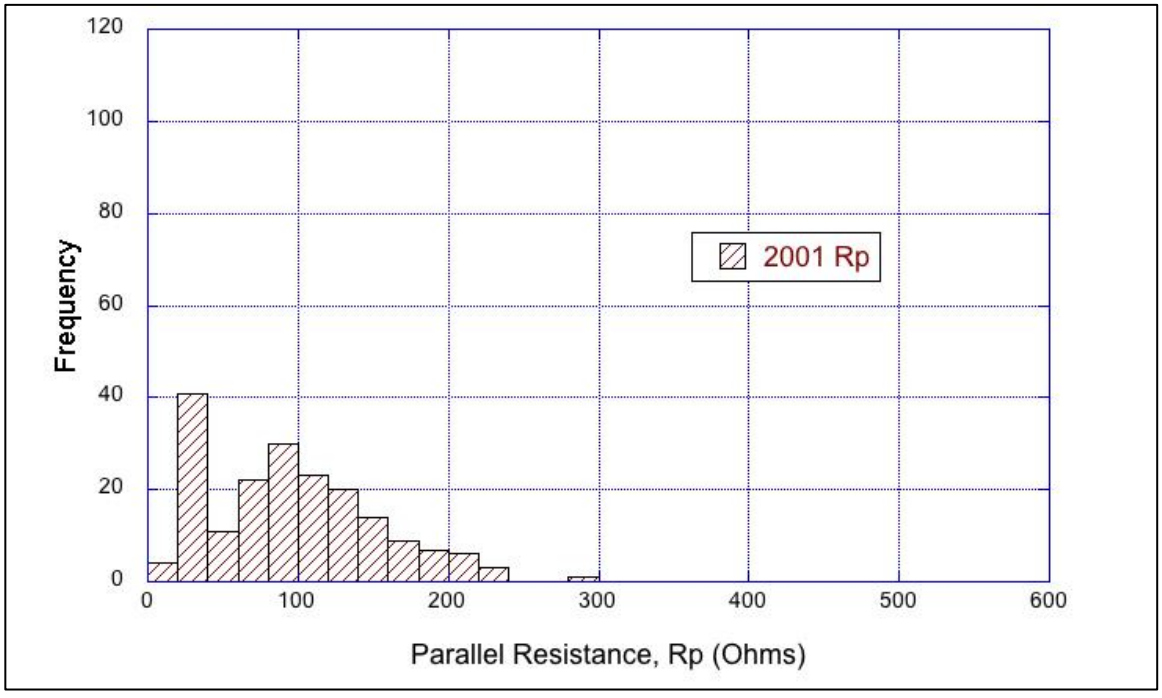

Figure 57: 2001 R_p histogram with collective decrease in the R_p parameter

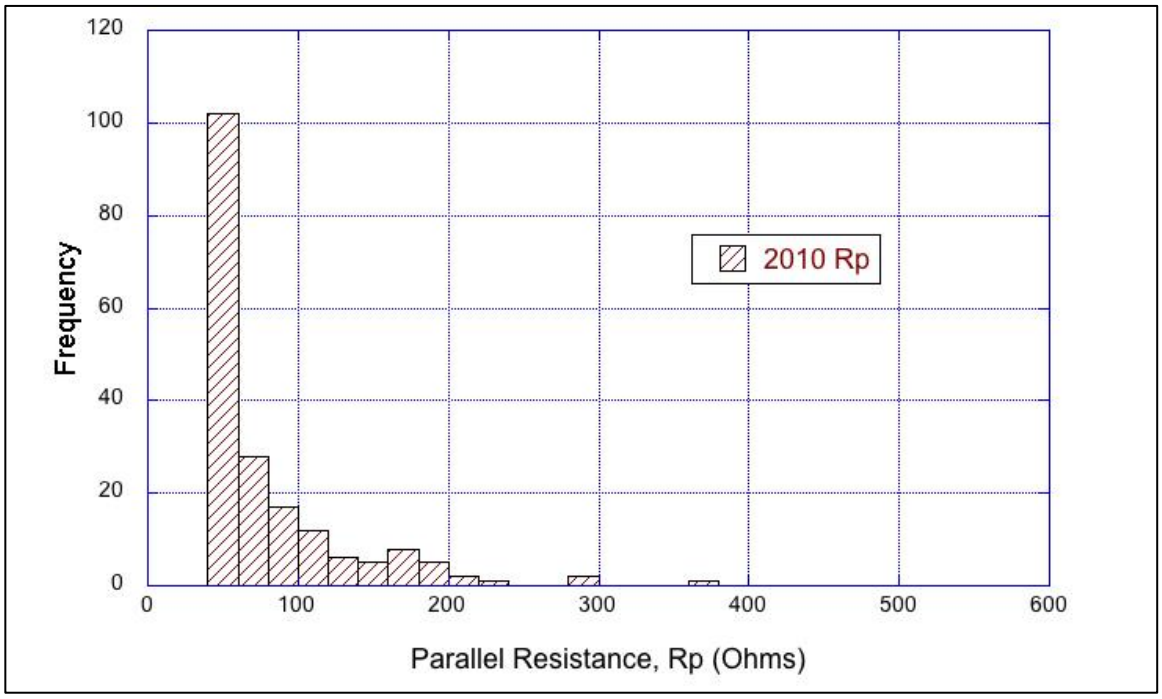

Figure 58: 2010 R_p histogram with large potion hitting the 2010 parameter lower limit

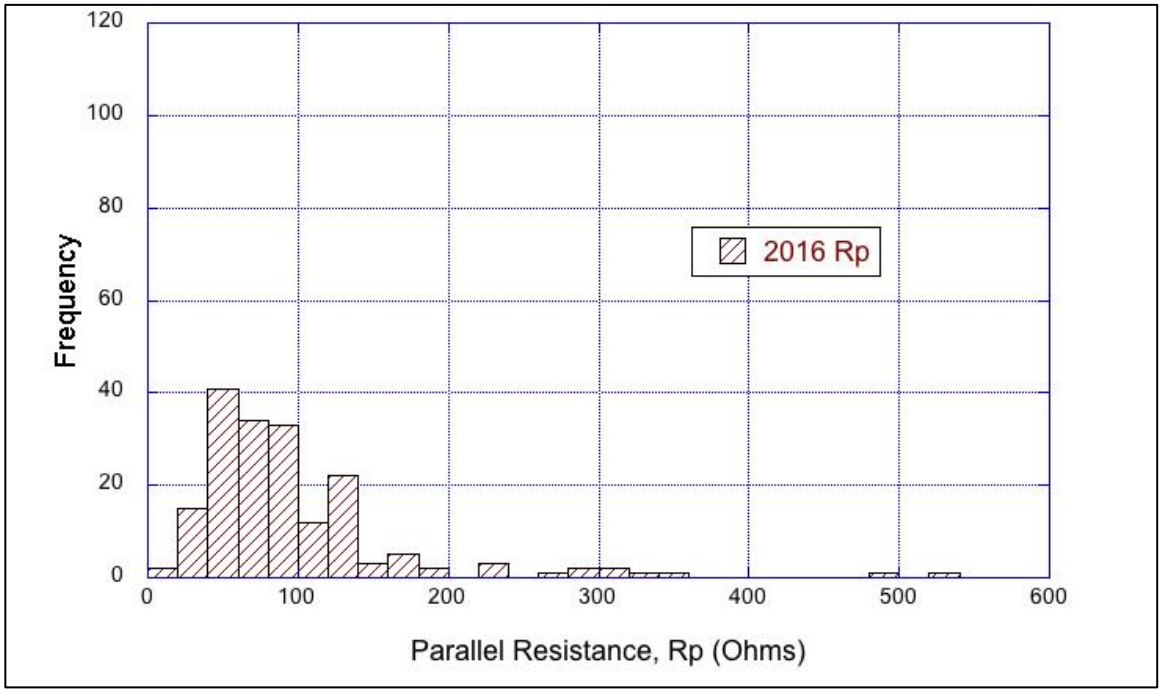

Figure 59: 2016 R_p histogram showing natural spread with widened limits

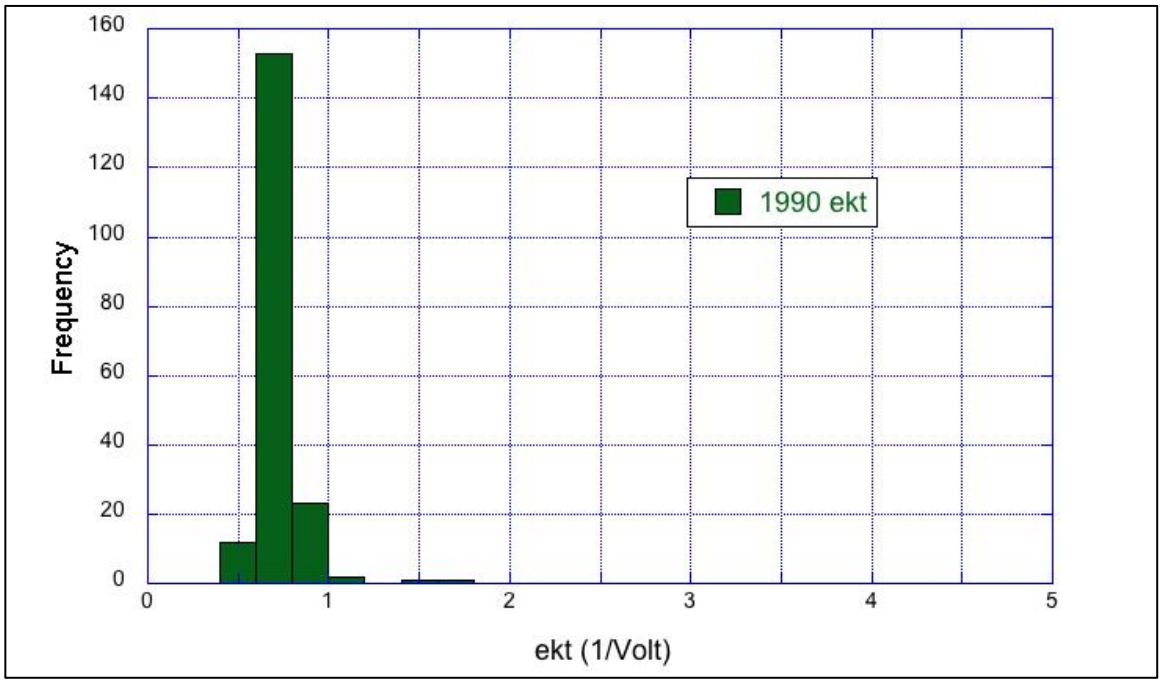

Figure 60: 1990 ekt histogram showing initial consistency with the modules' ekt

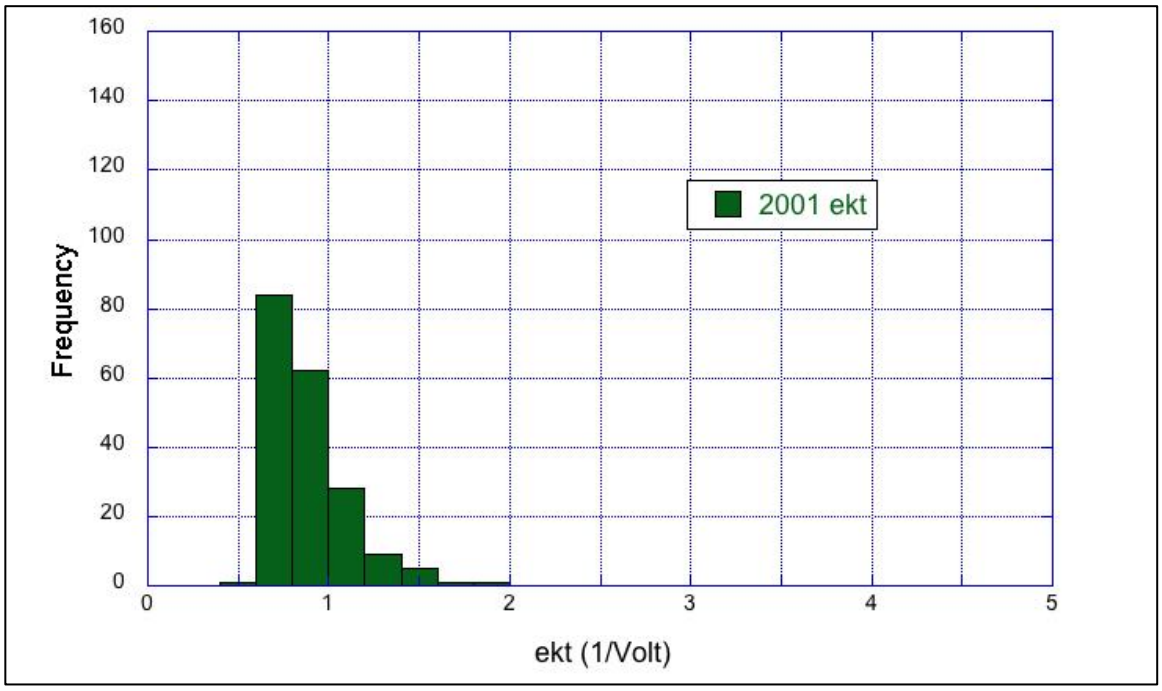

Figure 61: 2001 ekt histogram showing gradual widening of the ekt variation

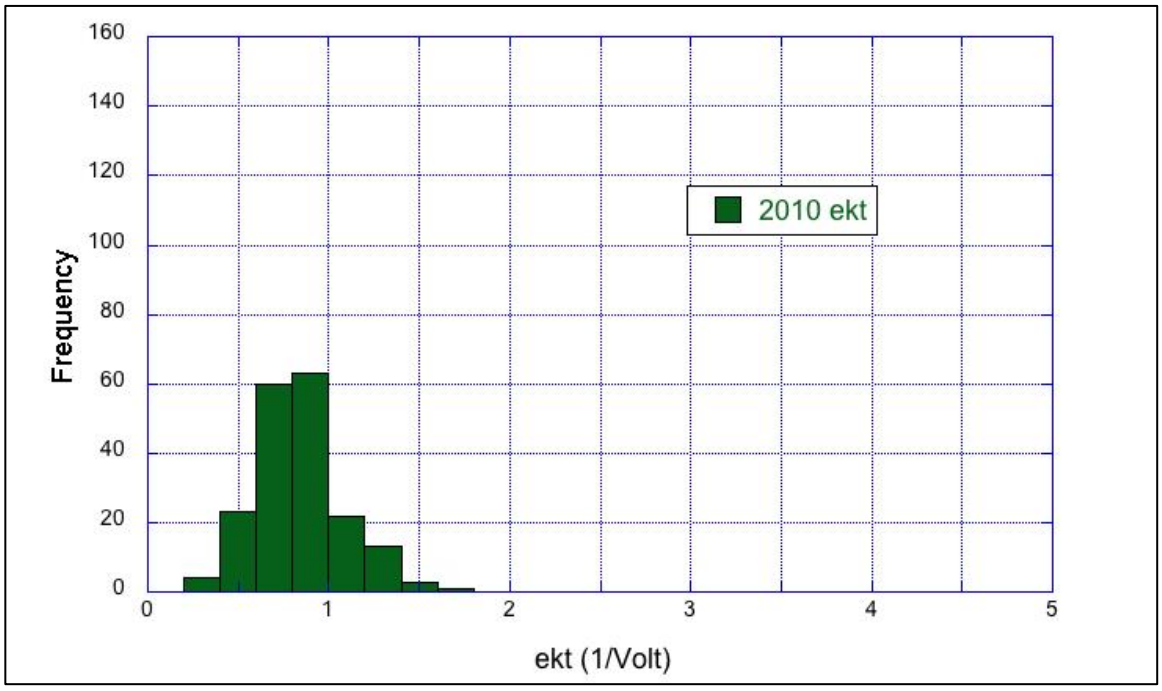

Figure 62: 2010 ekt histogram

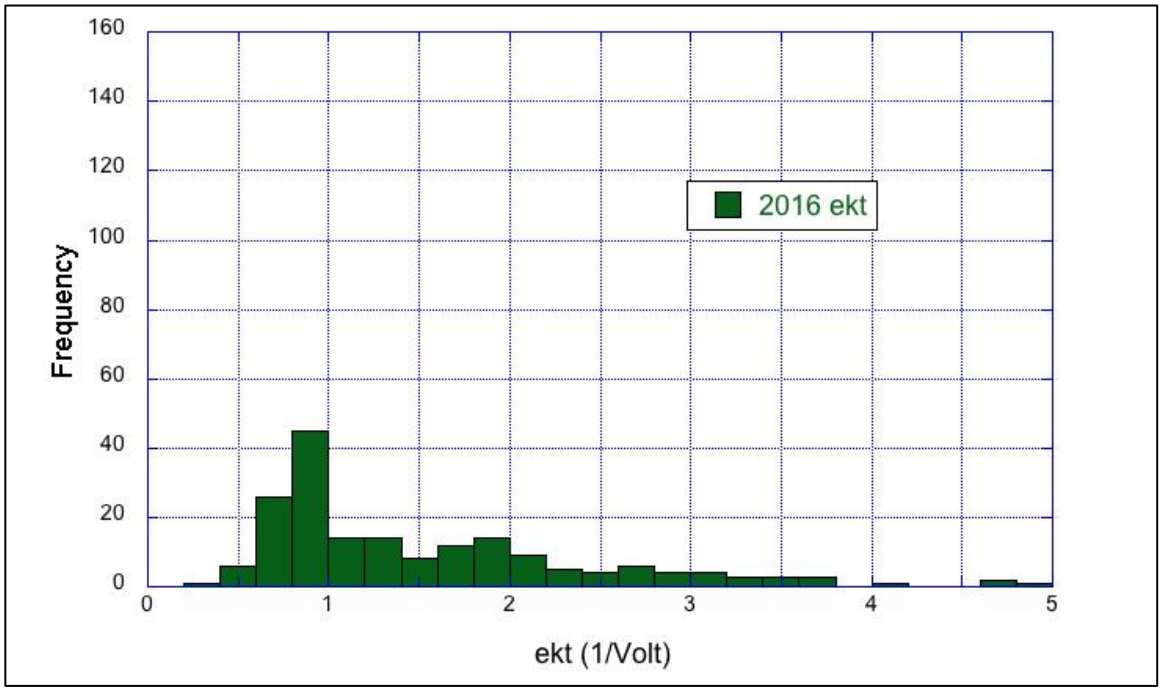

Figure 63: 2016 ekt histogram with large spread after 25 years and with wider limits

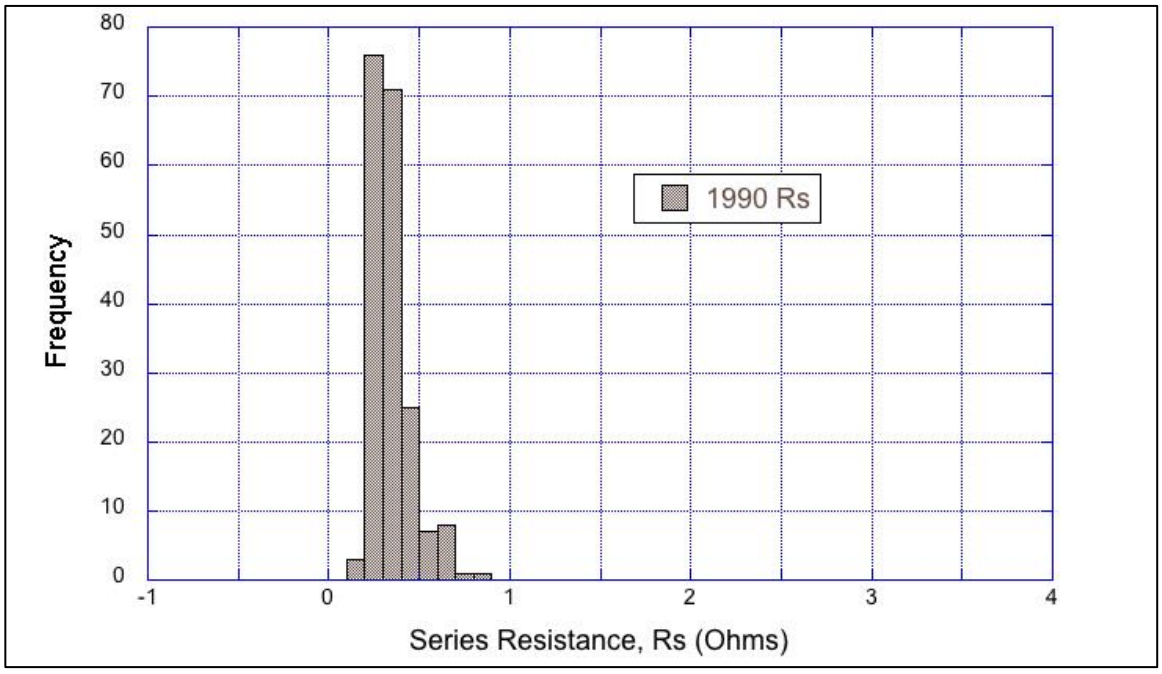

Figure 64: 1990 R_s initial histogram

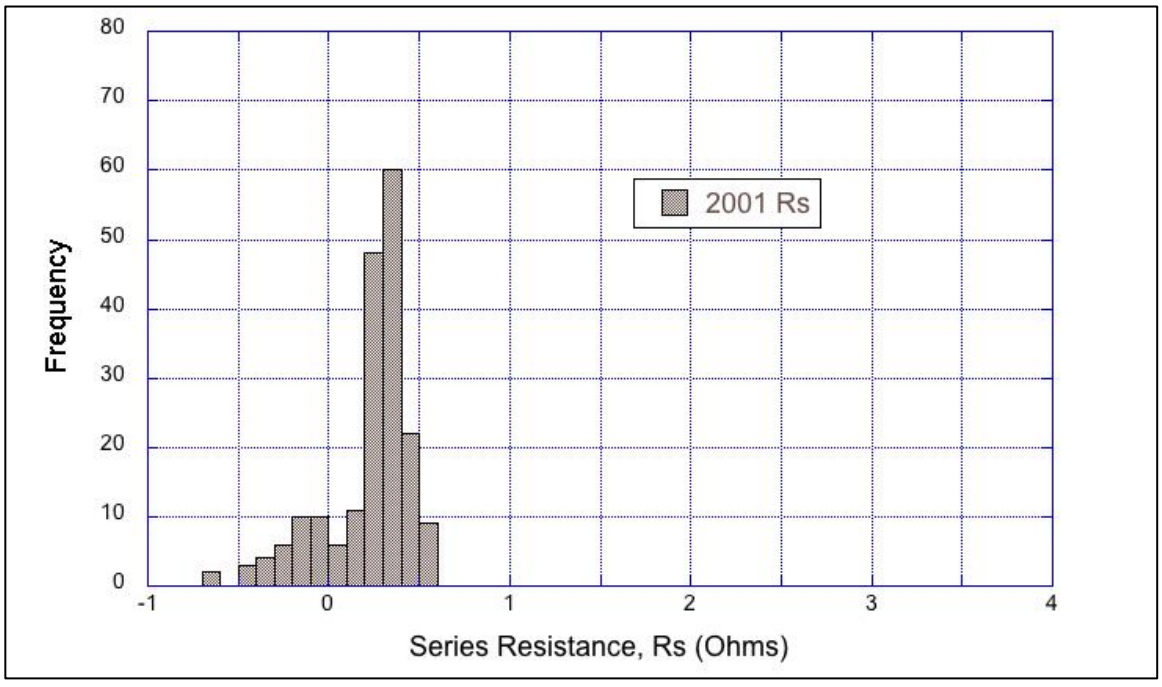

Figure 65: 2001 R_s histogram that shows negative values after 10 years

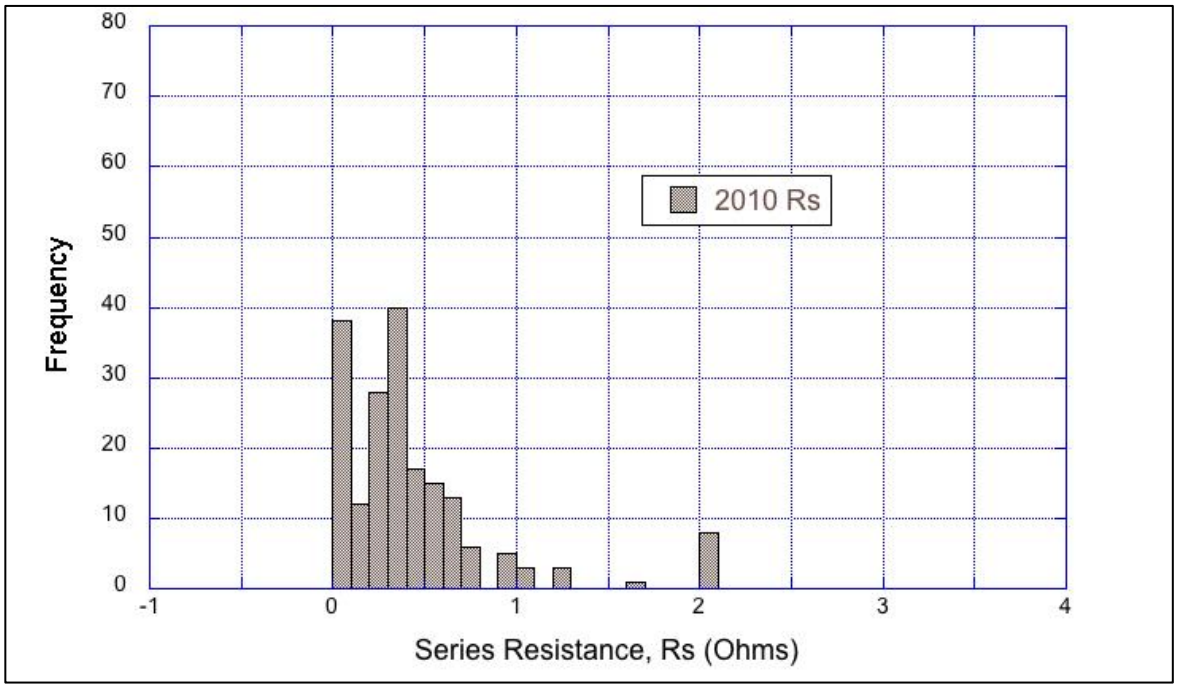

Figure 66: 2010 R_s histogram with a lower limit of zero implemented

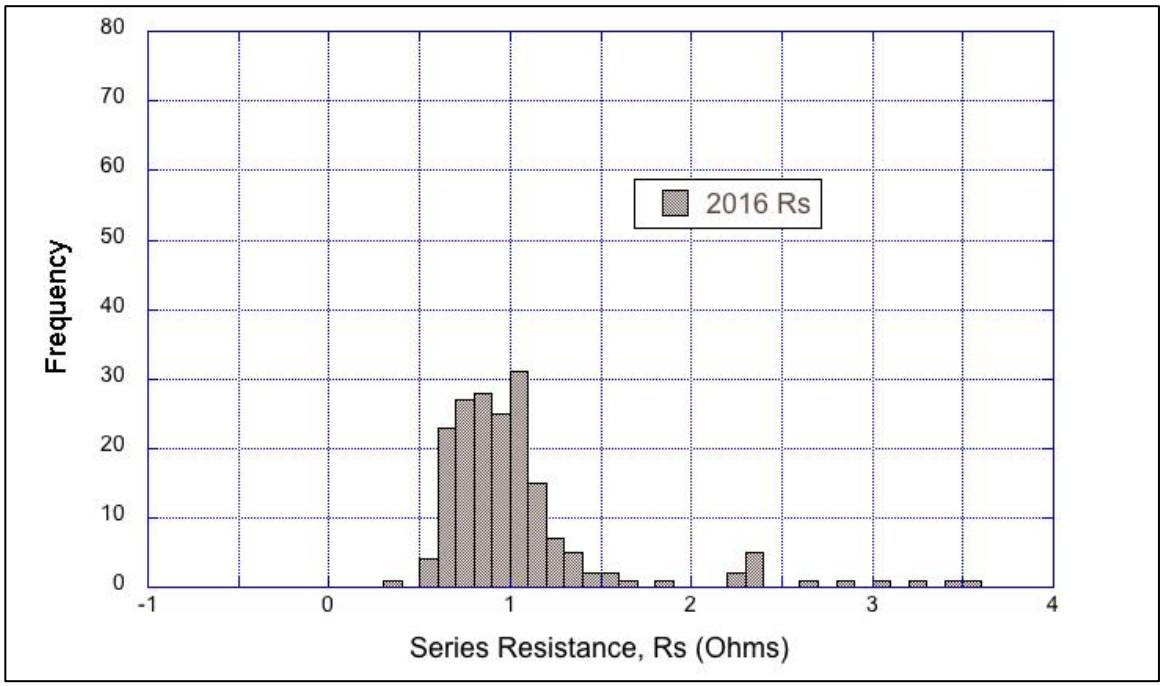

Figure 67: 2016 R_s histogram highlighting a general rise in R_s in last years of the project

IV Curves

IV curves are at the center of this thesis analysis, as all the parameters covered in the previous section are obtained from these curves. This portion of the results section shows a variety of IV curves produced throughout the project, highlighting the smallest and largest changes in performance observed in this sample of solar modules. Figure 68 shows the IV curves from 1990 and 2016 for the module that experienced the smallest decline in performance (i.e., in P_{max}), module 160. Module 160 tested at 40.53 W in 1990, above average, and tested at 37.09 W in 2016, the highest power output among the original modules. This power degradation of only 3.44 W, or 8.5%, is not representative of the typical module.

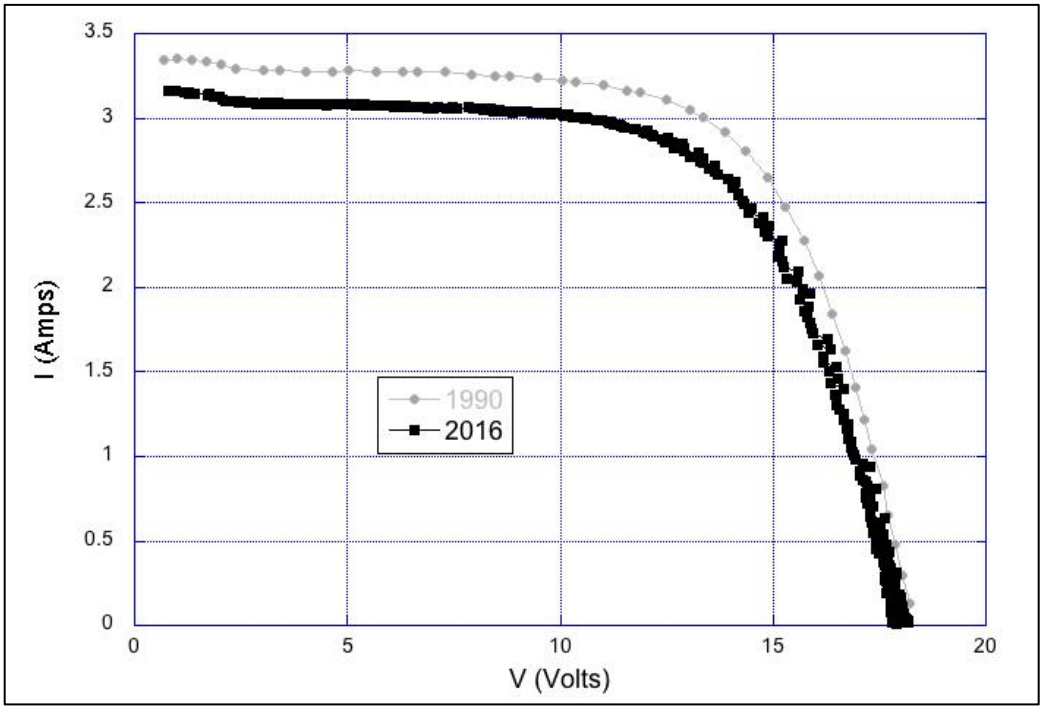

Figure 68: IV curves from 1990 and 2016 for the module 160, which had the smallest decline in power output over the 25-year project

Figure 69 shows the IV curves from 1990 and 2016 of the module that had the largest decline in power output that still produced an IV curve, module 015. There were two modules, module 044 and module 078, that tested at a lower P_{max} than module 015 in 2016, but their current-voltage relationships were so unrecognizable (almost linear, instead of the expected IV curve shape like Figure 68) that they could not be analyzed. Module 015 originally produced 39.18 W in 1990 and only produced 24.40 W in 2016, a drop of 14.78 W, or 37.7%. Note how the slopes of the IV curve flatten out as the performance of the module declines over time. This trend is evident in the progression of the R_p, ekt, and R_s factors in the array average over 25.5 years.

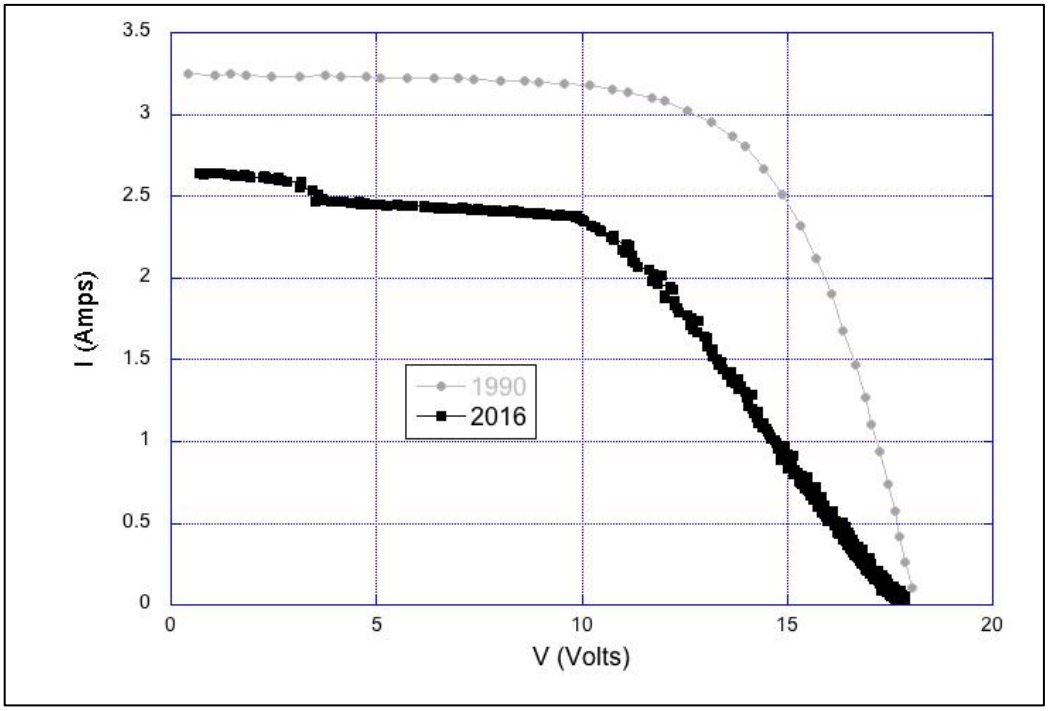

Figure 69: IV curves from 1990 and 2016 for the module 015, which lost the largest power output over 25 years

The replacement modules benefitted from the use of improved materials and manufacturing processes, including improvements to the EVA, that allowed them to age more gracefully than the original ARCO modules. Module 101, which was added to the array between 2001-2010, barely saw a change in its IV curve and performance from 2010 to 2016, as shown in Figure 70. Improved material choices and design in this solar module indicates how improved manufacturing practices can lead to better module performance and durability over their lifetime.

Table 13 summarizes the P_{max} of the four replacement Siemens modules. However, because they were not tested when they were initially installed, the only point of comparison is the nameplate rating of 50 W STC. Figure 71 shows a physical comparison between the newer Siemens module 101 and the best performing ARCO module 160 to highlight the aging process differences, as even the best ACRO module has signs of cell discoloration and delamination.

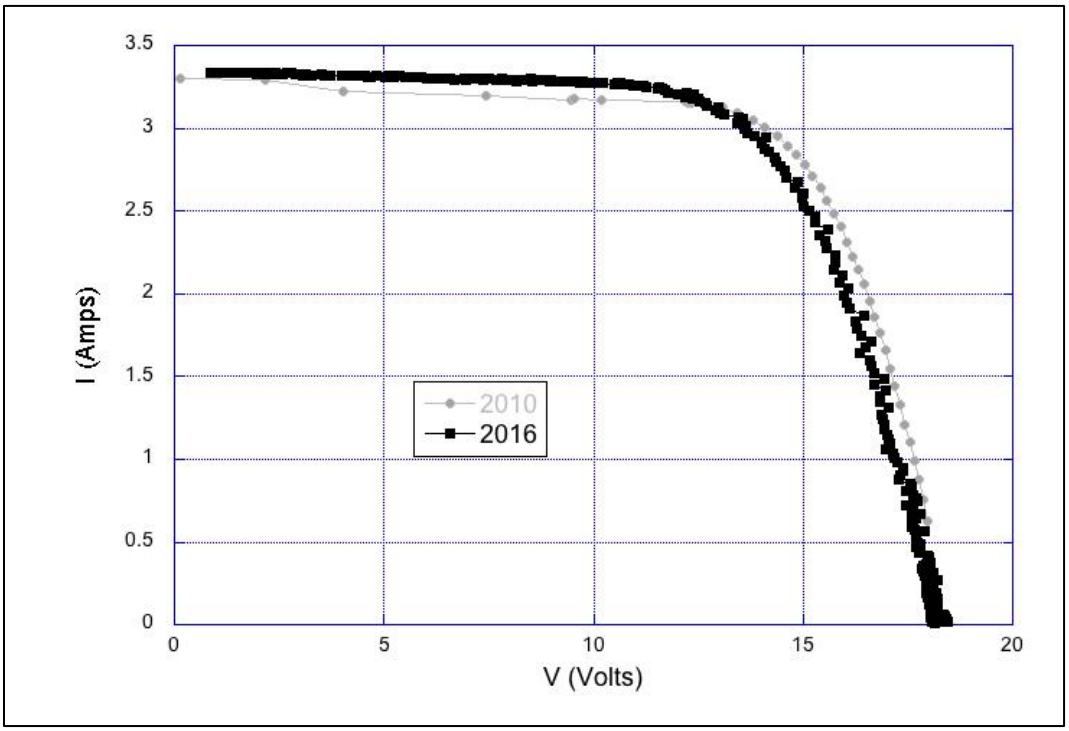

Figure 70: IV curves from 2010 and 2016 for Siemens module 101 with little power loss

Table 13: P_{max} in 2016 for the four Siemens replacement modules of various ages

Siemens Module (estimate of year added)	**2016 Testing P_{max} Results (NOCT)**
035 (circa 2001-2010)	40.60 W
101 (circa 2001-2010)	41.46 W
102 (circa post 2010)	41.27 W
148 (circa 1996)	40.51 W

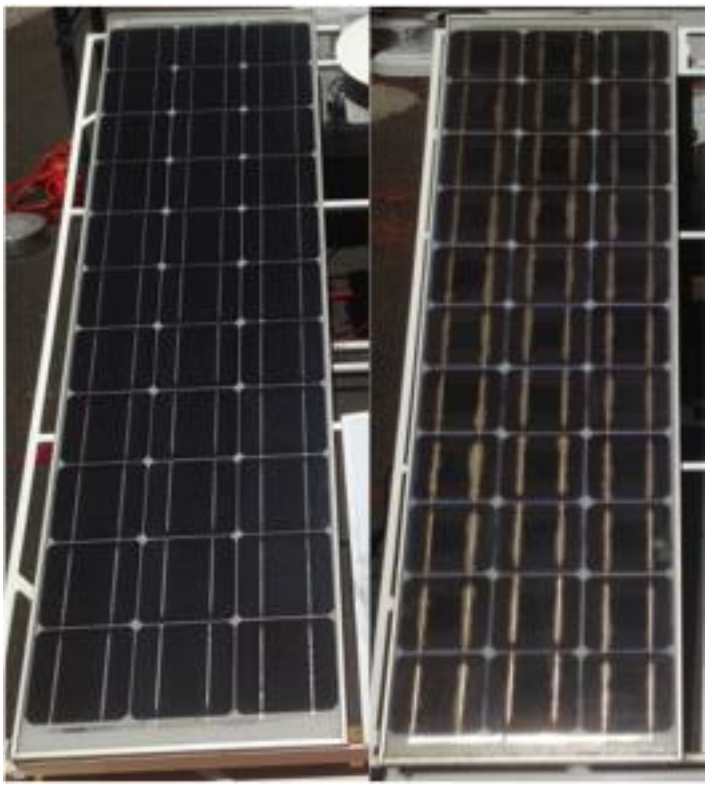

Figure 71: Comparison of Siemens module 101 (left) and ARCO module 160 (right)

Bypass Diode Analysis

Even the best performing module, module 160, shows signs of active bypass diodes creating a second knee in the IV curve. In the 2001, after 11 years of field exposure, there were already 54 modules that were showing signs of active bypass diodes, and in 2016 every single module had some form of a second knee. The Scilab code included a cutoff at 5 V to eliminate the initial false knees in the IV curves created by the activated bypass diodes that would require an 11-parameter analysis. The Scilab graph Figure 72 shows the IV curve with the 5 V cutoff for the first test of module 184.

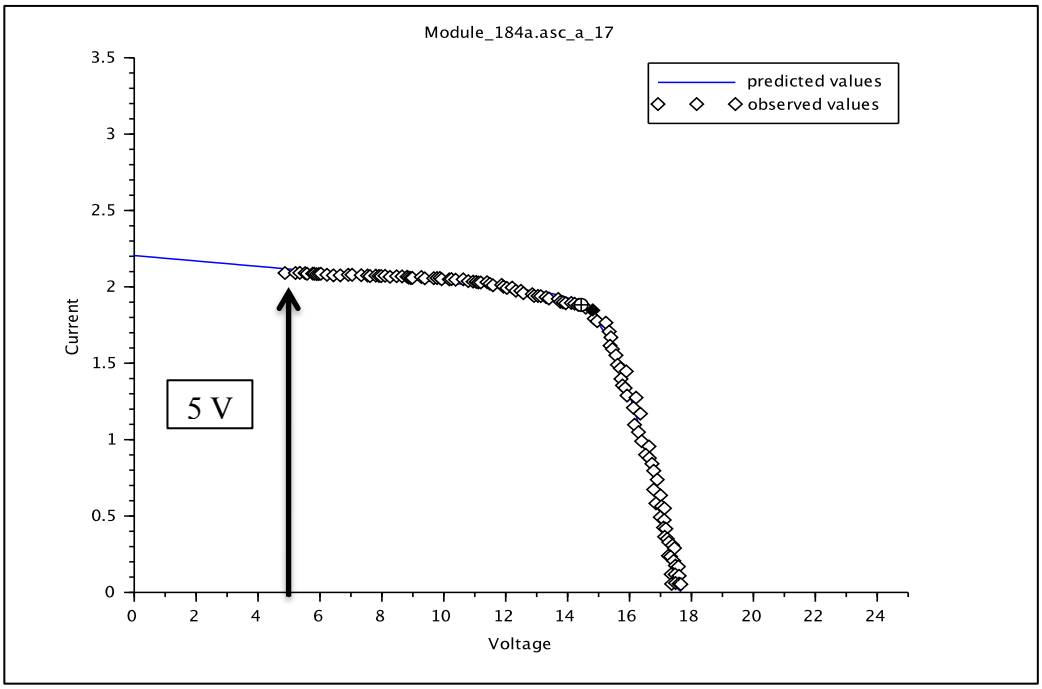

Figure 72: Scilab produced IV curve for module 184

A sample of modules, three that showed significant bypass diode action and three that did not, were re-tested with their bypass diodes removed to determine the effect of the diodes on power production after 26 years. Figure 73 shows the effect of removing the diodes from module 184, the same module shown in Figure 72. Note the 5 V cutoff has been removed to allow for a comparison of the module's true performance. Figure 74 shows the minimal change of removing the diodes from the less affected module 124. In the 2016 testing, module 124 tested at 30.63 W with the diodes and 30.53 W without the diodes (i.e., a decrease of 0.10 W), while module 184 saw an increase in its P_{max} from 27.84 W to 29.12 W (i.e., an increase of 1.28 W) by removing the diodes. The other four IV graphs of the modules included in this extra experiment are in Appendix G (Figure G - 13 to Figure G - 16), and their results are included in the Discussion section.

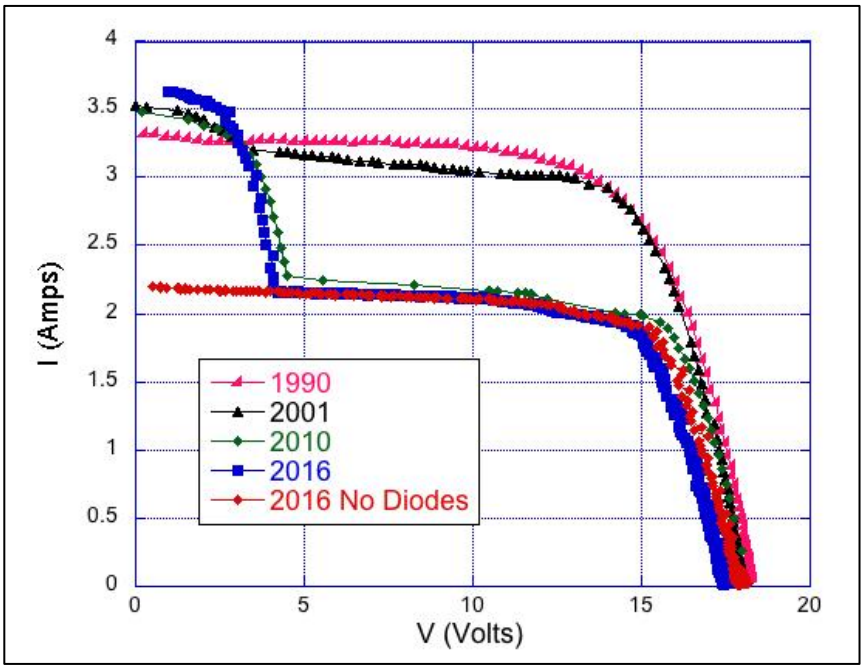

Figure 73: IV curves for module 184 in all testing cycles and then without diodes

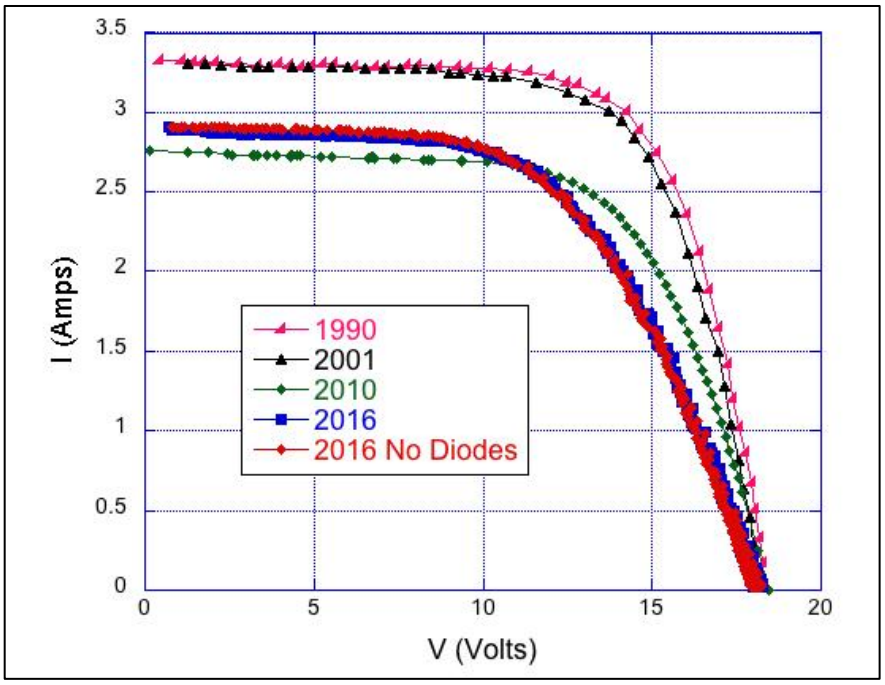

Figure 74: IV curves for module 124 showing small effect of removing diodes

The other two modules that did not have large second knees, modules 028 and 043, experienced an increase in P_{max} without diodes of 0.47 W and 0.21 W, respectively. Comparatively, the other two modules that had large second knees, modules 110 and 118, saw increases in P_{max} of 0.88 W and 0.79 W, respectively. Only module 124 in this sample lost some of its performance abilities with the removal of the bypass diodes and that 0.10 W loss that was small enough to be solely due to measurement error.

Sensitivity Analysis

As covered earlier in this report in the Background section of the Introduction, Jim Zoellick performed sensitivity analyses to quantify the dependence of the modules' V_{oc} on both temperature and solar insolation. This section of the Results goes into detail about similar tests that were performed in the 2016 round of testing in the attempt to investigate any changes in that relationship since Zoellick's initial findings.

Additional tests were performed on seven modules (045, 047, 101 (Siemens replacement), 103, 115, 151, and 164) at cold, warming up, and steady state conditions, as described in the Methods section. This created a temperature relationship profile for the performance of those modules. However, during the testing all of the temperature tests were conducted at insolation values relatively close to 1000 W/m^2, just like all of the other normal tests on the modules. Because of this, these 2016 results are not well suited to check the dependence of V_{oc} on insolation as was done in Zoellick's multiple linear regression analysis detailed in Equation 2. Therefore, this report focuses primarily on the

dependence of module V_{oc} on module temperature. However, since there was some degree of variation in the insolation conditions during testing, the complete multiple linear regression involving both the module temperature and the solar insolation is also reported.

Omitting the insolation-dependent term in Equation 2 and using the thermocouple readings and the raw V_{oc} (not corrected to NOCT), a simple linear regression was conducted between V_{oc} and module temperature (Equation 7):

$$V_{oc} = a + b * T \qquad (7)$$

where:

V_{oc} = open circuit voltage of the module (V)

a = V_{oc} intercept (V) (i.e., the estimated V_{oc} at 0°C)

b = temperature coefficient for V_{oc} (V/°C)

T = module temperature (°C)

This regression was first performed on combined data from all six ARCO modules. Then a regression was performed to estimate a common slope but with a separate intercept for each module. Using the original 1990 sensitivity analysis data, the simple linear regression was performed on V_{oc} versus the module temperature. Finally, the regression of V_{oc} on temperature was also performed for the one Siemens module (101) that was included in the 2016 sensitivity analysis. Figure 75 shows the observed

V_{oc} versus temperature relationships for the 1990 ARCO, 2016 ARCO, and 2016 Siemens testing for the V_{oc} temperature coefficient. Table 14 summarizes the estimated slopes (i.e., the temperature dependence coefficient) from these four linear regression analyses and includes a 95% confidence interval for the slopes.

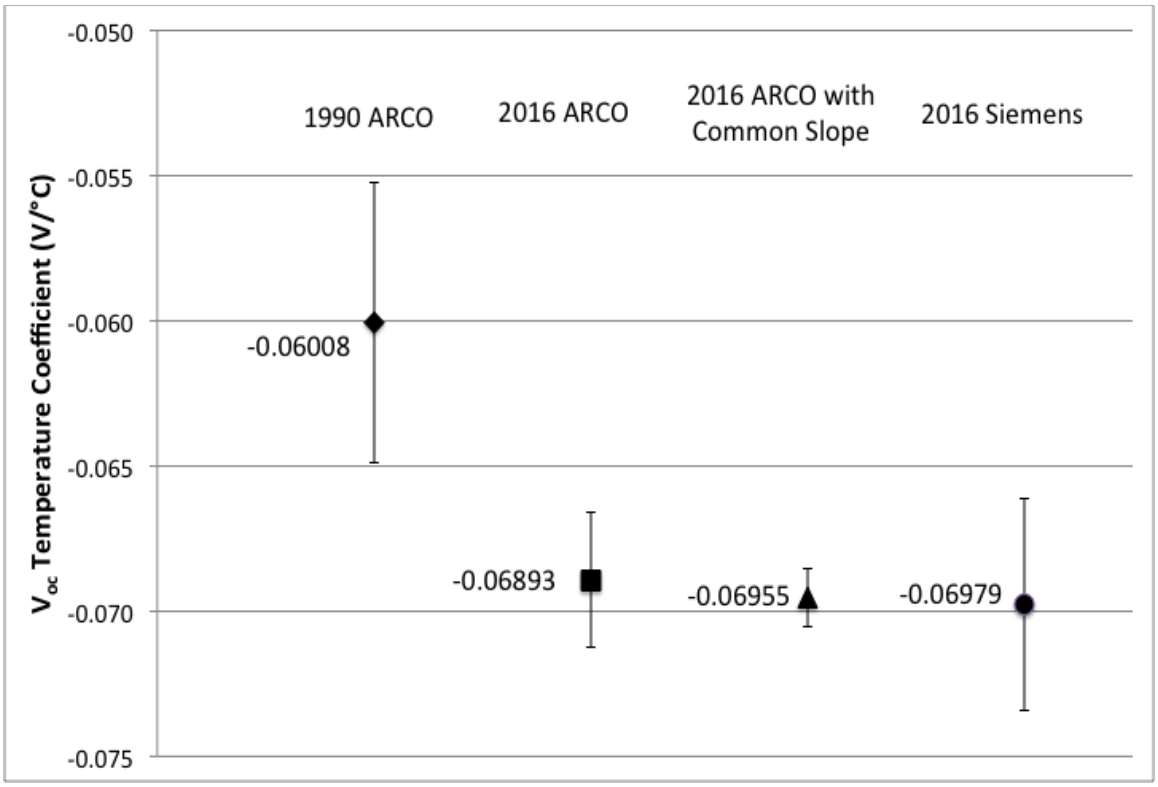

Figure 76 compares the confidence intervals for the estimated temperature sensitivity coefficients in a graphical form. The results of the 2016 round of analysis fall within the associated confidence intervals, but the temperature coefficient for the V_{oc} has changed from roughly -0.06 V/°C to -0.07 V/°C over the 25.5 years of this project, which could consequently result in varying values for the NOCT-adjusted data and in the P_{max} and other calculations.

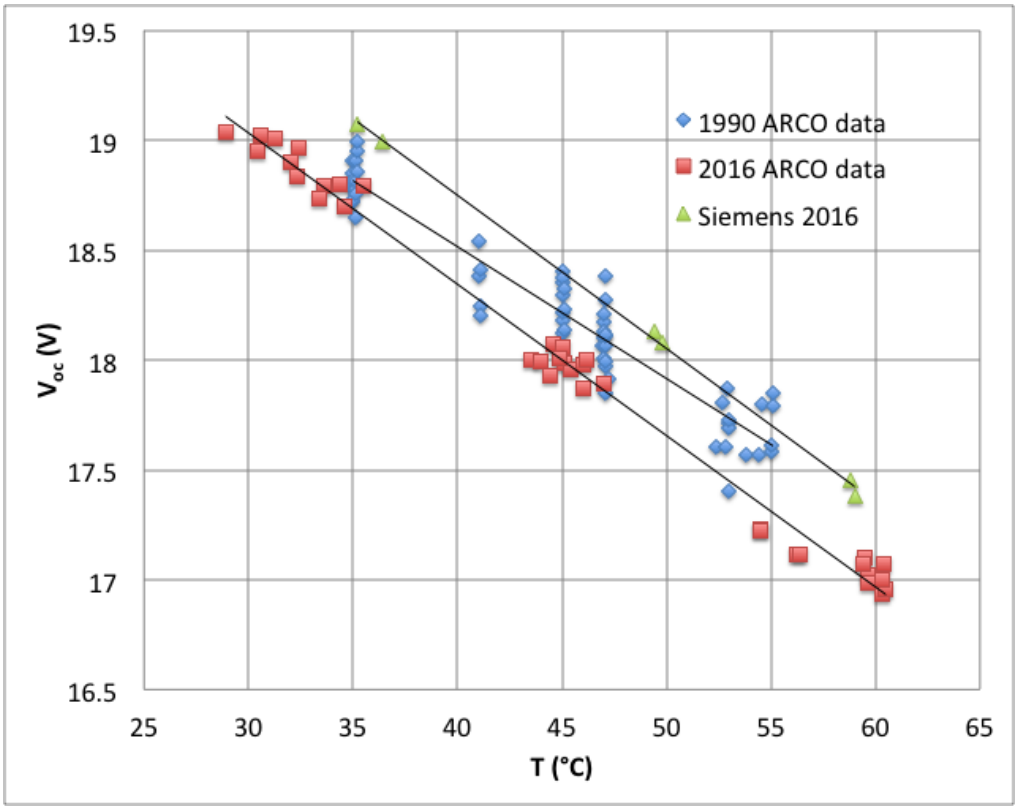

Figure 75: Test information for the temperature sensitivity analysis

Table 14: Temperature linear regression sensitivity analysis results

Temperature Coefficient	**1990 ARCO**	**2016 ARCO**	**2016 ARCO with Common Slope**	**2016 Siemens**
Estimate (V/°C)	-0.06008	-0.06893	-0.06955	-0.06979
Standard Deviation	0.002414	0.001146	0.000482	0.001316
Degrees of Freedom	58	34	29	4
Sample Size (Tests)	60	36	36	6
95% CI Upper Limit	-0.05525	-0.06660	-0.06857	-0.06614
95% CI Lower Limit	-0.06491	-0.07126	-0.07054	-0.07345

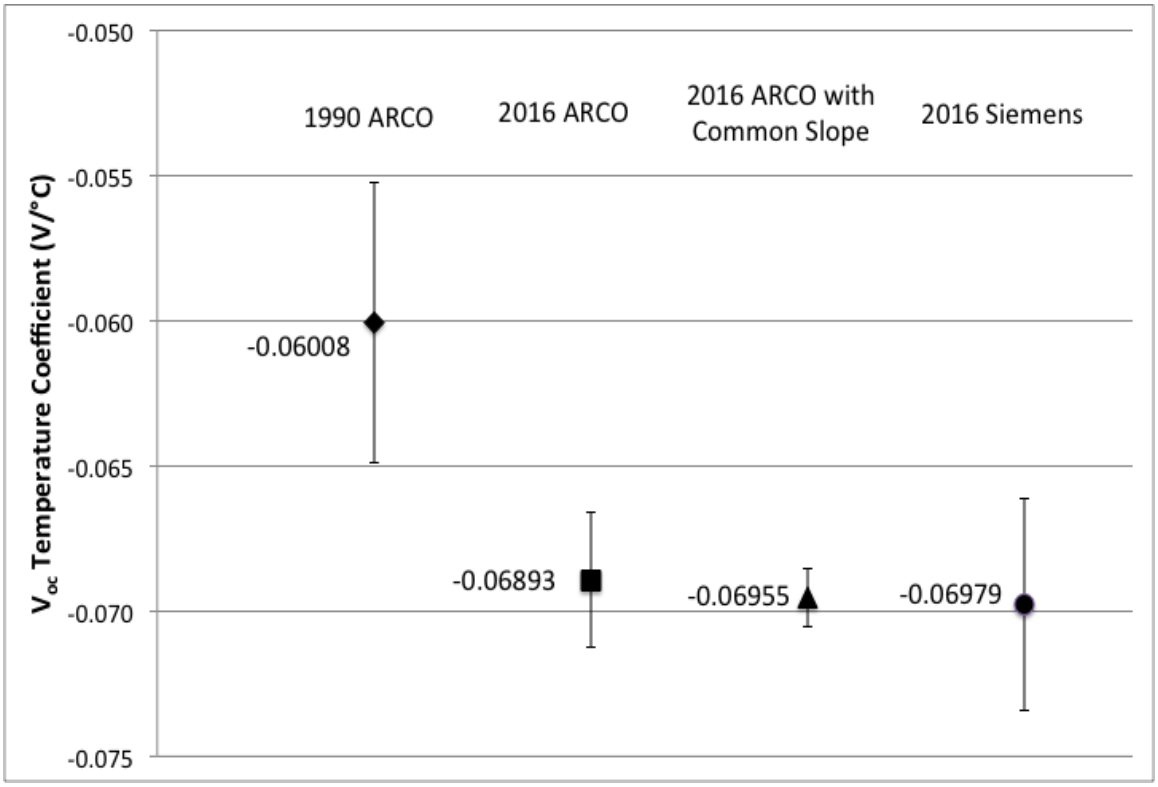

Figure 76: Temperature sensitivity analysis with error bars

While the range of module temperatures in the 2016 testing was sufficient for this sensitivity analysis, the range of insolation values was only 942-967 W/m^2, whereas the module temperature range was 29-61°C. Acknowledging that this narrow range of insolation conditions severely limits the ability to estimate the dependence of V_{oc} on insolation, a multiple linear regression of V_{oc} on temperature and insolation was performed in an attempt to determine if there is a noticeable change in the insolation coefficient for V_{oc}. Table 15 compares the 1990 and 2016 coefficients obtained by this regression. Although the confidence interval for the estimated insolation coefficient from the 2016 data is quite wide, note that the confidence intervals for the 1990 coefficient

does not overlap with the 2016 coefficient, indicating that the insolation coefficient has substantially increased over 25.5 years. Table H - 1 and Table H - 2 in Appendix H contain the complete multiple linear regression tables for the 1990 and 2016 irradiance and module temperature V_{oc} coefficient analyses.

Table 15: 1990 and 2016 V_{oc} coefficients for temperature and irradiance

Correction Factor, variable	**95% Confidence Level [units]**
1990 Open circuit voltage temperature, Φ	-0.060291 ± 0.000534 [V/°C]
1990 Open circuit voltage irradiance, ω	0.0009296 ± 0.0000511 [V/(W/m^2)]
2016 Open circuit voltage temperature, Φ	-0.065381 ± 0.00357 [V/°C]
2016 Open circuit voltage irradiance, ω	0.006211 ± 0.00497 [V/(W/m^2)]

To see the range of effects that these updated module temperature and solar insolation coefficients would have on the current round of analysis on the ARCO modules, the tests that experienced the highest and lowest temperatures and insolation values, exempting the sensitivity analysis runs, were re-run in Scilab with the 2016 coefficients. The module temperature outliers used in this analysis ranged from 37.1°C to 59.5°C, and the highest and lowest raw insolations from the 2016 testing were 919.6 W/m^2 and 1034.6 W/m^2, respectively. For consistency with Zoellick's analysis decisions, the coefficients found for the collective 2016 sensitivity data, not the individual modules with separate intercepts, are used here. However, it became apparent that the method using a common slope with individual intercepts for the module results in slightly more precise estimate. This data points towards less dependency of the V_{oc} on either the solar

insolation or the module temperature. Table 16 summarizes the changes seen both in the V_{oc} and the resulting P_{max}, and it must be noted that the percent changes in the V_{oc} calculations were mirrored into the P_{max} changes. Overall, the coefficients determined for these ARCO M75 modules back in 1990 still apply today, as they may only affect the all-important P_{max} calculations by up to 2.5%, or less than 1 W.

Table 16: Effect of new 2016 V_{oc} coefficients on the extreme 2016 tests

Test Description	**Module Test**	**NOCT V_{oc} (V) with 1990 Coeff.**	**NOCT V_{oc} (V) with 2016 Coeff.**	**NOCT P_{max} (W) with 1990 Coeff.**	**NOCT P_{max} (W) with 2016 Coeff.**	**Change in P_{max} (%)**
Lowest Temperature	184b	17.61	17.49	28.34	28.15	-0.7%
Highest Temperature	105a	18.19	18.40	31.73	32.09	1.1%
Lowest Insolation	127a	18.08	18.51	30.85	31.58	2.4%
Highest Insolation	038b	18.25	18.07	30.96	30.64	-1.0%

DISCUSSION

This section of the report involves a discussion about the concepts and results covered in earlier sections, focusing on quantifying and discussing the 2016 testing results and comparing them to the past rounds of testing on these modules and relevant findings reported in the Literature Review. The primary conclusion is that these modules experienced physical degradation that led to a substantial and roughly linear drop in power output over the 25.5 years of the project. The reasons for this decline in performance are further explored here.

Interpreting the Results

The characteristics of these ARCO M75 modules have clearly changed over the 25.5 years of field exposure that they have endured, as can be seen in the appearance of the typical 2016 IV curves seen in Figure 72, Figure 73, or Figure 74 versus the nameplate IV curve that came with the original specifications shown in Figure 6 and the changes in the P_{max} and the five key IV parameters covered in Table 12.

Table 10, Table 11, and the histograms of P_{max} and the five IV parameters for each test cycle (Figure 44 to Figure 67) present information about the drop in P_{max} and the main contributors to that decline. The 21.6% drop in average P_{max} is almost completely reflected in the 16.1% drop in the average I_{sc} values after 25.5 years. Meanwhile, the V_{oc} did not even fall 1.0% below its original measure. The increased

degradation of the modules' I_{sc} can be attributed to corrosion and delamination within the layers of the modules, especially in relation to the EVA, and, to a lesser degree, performance reductions due to activation of the bypass diodes. With the active bypass diodes, the current is redirected around problematic cells and strings of cells by the diodes, which sometimes increased the I_{sc} in modules such as 184 (Figure 73). However, the average I_{sc} in the array, along with the average I_{mp}, declined throughout the life of the project, which led to the loss of average P_{max}. This is exaggerated by analyzing the modules with a 5-parameter model instead of an 11-parameter model, essentially eliminating the effect of the bypass diodes with the 5 V lower limit with the IV curve. The power produced by PV modules comes directly from the current and voltage in that module, so a drop in either voltage or current is carried through to the power output. With these modules, it was a drop in the current.

While the activation of the bypass diodes has created a second knee in the modules' IV curves, the experimental removal of the diodes proved that these additional knees only hindered the power output by a few Watts at most while providing crucial over-current protection by redirecting excessive current away from potential hot spots on the module. The bypass diode analysis portrayed in Figure 73 and Figure 74 suggest that the effect of removing the diodes is only evident in the IV curves of modules that had significant second knees from active bypass diodes. Even then, the increase in power through the removal of the bypass diodes was limited to less than 2 W. Siemens apparently updated their material and manufacturing practices between 1989 and 1995 when the replacement modules were created, and the problems with physical and

chemical degradation and the inherent drop in I_{sc} and P_{max} that the ARCO modules experienced are not seen in these replacement modules.

The histograms help visualize the growing spread and skew in the measurements of the results for the IV curve parameters that are presented in Table 12. The standard deviation of the P_{max} results almost quintupled throughout the project lifetime; the I_{sc} standard deviation grew to be six times its original value; and, oddly, the V_{oc} standard deviation decreased slightly in the last 5.5 years after growing over the previous 20 years. This response in the V_{oc} of the modules could be due to the permanent effects of the bypass diodes on the current, which may have allowed the voltage to adjust, or it could just be random variation present in the data for the last 5.5 years of the project.

While the V_{oc} and I_{sc} determine where the IV curves start and end, the parameters that influence the shape of the curve between these points on the curve changed even more dramatically—explaining the progressive decline in the modules' fill factors (FF). The slope of the IV curve during higher currents, the reciprocal of R_p, was cut in half over the life of the project. Curiously, the standard deviation of the metric hardly changed. The parameter that controls the degree of curvature in the IV curves, ekt, doubled over the 25.5 years, and its standard deviation grew to eight times its original 1990 value. This substantial growth in the value and standard deviation indicates that the radius of the IV curve changed significantly from its original rectangular shape to a more linear curve across the sample of modules. Lastly, the slope of the portion of the IV curves with lower current and higher voltage, the reciprocal of R_s, tripled over the project while its standard deviation quadrupled. The conclusion from the analysis of these three

IV curve parameters indicates that more changes in the modules' operational characteristics are experienced when the modules were subjected to smaller currents and larger voltages during the IV curve testing process.

Comparison of Results to Literature Review

The three most common types of PV module degradation, cell discoloration, delamination, and hot spots (Vazquez and Rey-Stolle, 2008), were all seen throughout the 188 remaining ARCO modules from the Trinidad array. Every module that spent over 25 years at the project site has changed from a black/blue color to brown, and significant delamination of the EVA layer on at least one entire cell is evident in roughly 82% of the ARCO modules (155 of the original 188) as seen in the collection of photos of each module from 2016 testing. All of the original modules have experienced EVA delamination to some degree. This occurred, as expected, on the front of the modules where UV exposure was at its greatest and not on the back panel of the modules (Jorgensen and McMahon, 2008). These are the main contributors to the degradation of these particular modules that resembled aged modules from similar projects (Figure 20 versus Figure 22, Figure 23, and Figure 24). Hot spots, while prevalent, were not nearly as common as the other two types of degradation witnessed with these modules, indicating that the bypass diodes successfully handled their responsibility of over current protection for much of the project.

The physical degradation appeared gradually over time, as expected, but it is certainly possible, although not provable since the tests were not performed on the modules between 1990 and 2001, that the 4% power loss experienced in the first 11 years of the project could have occurred within the first year of field exposure. This would be consistent with the literature on the light induced degradation (LID) effect that causes modules to lose up to 5% of their power production in the first year of exposure (Quintana et al., 2002, Meydbray and Dross, 2016). The smallest degradation rate seen in the project, 0.4% ± 0.057% per year with a 95% confidence interval, occurred in the first decade of operation, but then, opposite of expectations, the second decade of operation saw an almost tripling in the degradation rate to 1.4% ± 0.195% per year at a 95% confidence interval. While only four data points over 25.5 years cannot truly map the degradation of these modules like yearly tests could have, the last 14.5 years (2001-2016) of the project, as shown in Figure 43, appear to have experienced a relatively linear degradation of power output. This agrees with the literature review that states that the degradation of PV modules tends to level out as the modules get older (Quintana et al., 2002, Vazquez and Rey-Stolle, 2008).

Studies performed on modules manufactured around the same time and of similar design of the ARCO M75 modules resulted in the expected degradation rate range of 0.5%/year-0.8%/year. Considering that the Trinidad ARCO modules were located outside and rarely moved over 25 years in a coastal marine environment, the lifetime average degradation rate of 0.85% ± 0.121% per year with a 95% confidence interval, or 0.35 W per year in power loss, is consistent with the findings in the literature (Osterwald et al.,

2002, Quintana et al., 2002, Jordan and Kurtz, 2011, Branker et al., 2011). Without testing these same modules in a non-coastal environment, it is impossible to conclude how the degradation rate was exactly affected by the coastal conditions, but with only 0.05%/year in additional degradation when compared to published literature on the subject, the performance of these ARCO modules can be considered consistent with the literature review.

The successful operation of the ARCO modules can be further evidenced by the fact that 48% of the modules are still producing at least 80% of their original production capabilities in 2016—and 90% of them still produce over 70% of their initial tests—when their warranties only covered 10 years (Siemens Solar Industries, 1990). Most modern warranties advertise 80% production at the end of the warranty (Meydbray and Dross, 2016, Vazquez and Rey-Stolle, 2008). In 2001, after the warranty-guaranteed years of operation had been surpassed for these modules, 100% of the modules were still producing over 80% of their original performance abilities.

Continuing Trends of Past Rounds of Testing

Overall, the success of producing repeatable and consistent testing procedures from 1990 to 2016 created data in similar analysis categories that made each cycle of testing, and its results, comparable to the other reports. In this manner, each preceding cycle dictated what the next cycle focused on. This allowed the final 2016 report to consider all of the theories and questions posed in 1990, 2001, and 2010. Zoellick's work

in 1990 set the stage for this lifecycle analysis of the modules at the Telonicher Marine Lab PV array over 25 years later. Many of the observations and analyses from the 2001 and 2010 rounds of testing presented trends in the performance of the ARCO modules that continued into the final cycle of testing in 2016. The general trends were an obvious general decline in power production and current paired with the physical deterioration of the modules due to UV field exposure.

Reis et al. (2002) pointed out that the decrease in R_p and increase in R_s would lead to a decrease in the available current for the modules that would create further decline in the P_{max}. This observation held true through the next 14.5 years of the project. As the modules aged, the location of V_{mp} and I_{mp} also continued to work their way down the IV curve, just as Reis et al. (2002) predicted. The 2001, 2010, and 2016 rounds of testing all saw some modules experience an increase in their I_{sc}, while the general trend shown in the histograms involved a decline in I_{sc}. This rise in I_{sc} for individual modules is related to the activation of the bypass diodes affecting the current characteristics within the modules. However, after 25.5 years all the modules experienced a drop in their I_{sc} values relative to the measured values in 1990.

The limits for the IV curve parameters written into the Scilab modeling code to filter out any outliers, or instances of poorly performed tests, in the data became more relevant later in the project, specifically in 2010 and 2016 for R_s, R_p, and ekt that dealt with the changing physical shape of the IV curves. As is shown in the respective histograms, the minimum limit for R_s of 0.050 Ω was violated 36 times in 2010, and the maximum limit for R_p of 50 Ω was reached 90 times in 2010. These limits were

introduced and enforced in the attempt to clean the data of any outliers, but as the modules aged and their parameter ranges grew, the majority of the results fell outside the previously defined boundaries for identifying outliers. If the limits were initially set in 2010 to be wider, then the histograms would more closely reflect the true spread of the data. This is the reason why, in the 2016 round of testing, the limits were heavily expanded to include almost all the results. As stated in the Methods section of this report, only eight limits were exceeded in 2016 given the wide range of limits. Seven of these occurrences were related to the upper limit for R_p of 3500 Ω, essentially infinity for all intents and purposes with this analysis, indicating adverse effects of the initial IV curve slope due to bypass diodes. The remaining incidence was for the upper limit of 3.5 V^{-1} for ekt, which occurred when the diodes were removed from that particular module (118). This resulted in a sharp radius of curvature in the IV curve that can be seen in Appendix G as Figure G - 16. Most of the module tests did not approach these limits, which indicates that most of the modules aged gracefully in terms of performance. However, the same cannot be said for their physical appearance.

Holes in the 2016 Round of Testing

As the 2016 round of testing attempted to mirror the previous rounds of testing in terms of data collection methods and analysis, some issues were not addressed due to time and resource constraints.

At no time were any of the ARCO modules dissected, save for the removal of the bypass diodes in six of the modules for that analysis. Dissection is destructive, but it could contribute to an understanding of the specific processes that occurred that led to physical and/or chemical delamination or deterioration in the respective modules. This could have been useful for the analysis of the degradation that appeared in these modules and the causes for that deterioration. However, the scope of past cycles of testing focused on the performance of the modules in spite of degradation rather than on the causes of the degradation itself. Seeing how these modules physically aged on the UV-facing side helped conclude which modules would test better and when cell browning, EVA delamination, or hot spots occurred. Inspecting the hidden layers of the modules (i.e., soldering joints, layer-to-layer adhesion, etc.) would be a fruitful endeavor to determine what other aspects of degradation arose in over 25 years of field exposure. All the modules are currently in storage and still in possession of HSU/SERC, so that analysis opportunity is still present. However, it may not be an option for very long as the project analysis period has now come to an end.

One missing part of this report is a complete sensitivity analysis for the module temperature and solar insolation effect on the modules' V_{oc} and inherently the P_{max}. While data were collected for a set of modules with a wide range of module temperatures, all of those tests had insolation values in a small window (940-970 W/m^2). Zoellick achieved a better sensitivity analysis in 1990, when he determined the V_{oc} coefficients that then were applied to the modules throughout the rest of the analysis project. His range of insolation values had a wider range because he adjusted the testing rack to

dictate the solar insolation hitting the module rather than orienting the modules direct normal to the sun as was done in the 2016 testing. A complete temperature sensitivity analysis was still performed in 2016, leading to the findings of a -0.01 V/°C change in the effect of module temperature on V_{oc} over 25.5 years. Further studies then proved that this change could only affect the P_{max} results from the most extreme testing conditions by a matter of 2.5% at most, validating Zoellick's findings and assertions from 1990. A multiple linear regression with both module temperature and solar insolation was included in this report, but due to the small insolation window, the results are less useful. Unfortunately, the sunny testing period of the year was lost before this lack of data range was realized. Nonetheless, the analysis based on the available data indicate a possibly negligible effect of insolation on the module V_{oc}.

CONCLUSION

The work done on this research project by the many people involved throughout the years has produced one of the best-analyzed PV solar arrays in the world. Information and knowledge gained from this project can be applied to better manufacture PV modules, specifically mono-crystalline cell modules, and to apply realistic warranties on such products that reflect the true degradation tendencies in field-aged solar modules. The analyses show that the ARCO M75 modules from the Telonicher Marine Lab PV array in Trinidad, California performed consistent with other real projects and modeling programs pertaining to similar PV modules from the early 1990s. This round of testing in 2016 completed study of the now decommissioned array, and the primary results are summarized below:

- The average P_{max} of the remaining 188 ARCO M75 modules declined by 21.6% over 25.5 years of field exposure on the coastal location of the Telonicher Marine Lab solar PV array, which corresponds to an average annual power output decline of 0.85% ± 0.121% per year with a 95% confidence interval.
    - The drop in I_{sc} that almost paralleled the P_{max} drop (16.1% and 21.6%, respectively) as modules aged, partially contributed to by the widespread activation of the modules' bypass diodes, is identified as the primary factor in the power loss experienced by the modules.
    - Conversely, the V_{oc} hardly changed throughout the lifetime of the project, with an average decline of only 0.77%, or 0.14 V.

- Average module NOCT efficiency fell from 10.016% ± 0.063% with a 95% confidence interval in 1990 to 7.915% ± 0.156% from 1990 to 2016
- Considering the possibly degradation-accelerating marine environment, a 0.85%/year degradation rate is consistent with the 0.5-0.8%/year reported in other studies on modules from the late 1980s and early 1990s.
    - After 26 years, 185 of the original 192 ARCO modules successfully produce IV curves. Four were replaced throughout project, and three were successfully tested during the 2016 round of analysis and categorized as failures.
    - Of the 188 original ARCO modules tested in 2016, 47% of them still produce above 80% of original power, and 89% produce over 70% of original power. This maintained power generation outperformed the expected performance, based on the 10-year warranty, as literature suggests that manufacturers often promise 80% of the original performance at the end of the warranty, not 15 years after the warranty expires.
    - Appearance isn't everything, as shown by the ARCO modules that all physically degraded yet maintained their functionality in power output.
- Cell browning, EVA delamination, and hot spots were the most prevalent signs of degradation experienced by these modules; however, based on the 2016 module images in Appendix C (Figure C - 1 to Figure C - 12), there is not a clear correlation between the highest and lowest performing modules and the most and least aesthetically changed module. Module 160 (Figure C - 12 in Appendix C) shows little signs of degradation and is the highest producing module in 2016, but the module

with the smallest power output, module 078 (Figure C - 6 in Appendix C), does not exhibit the largest signs of physical degradation. Modules 103 and 045 (Figure C - 7 and Figure C - 10 in Appendix C) show the most signs of physical degradation, yet they each performed within 1 W of the average power output of the entire array.

- While all bypass diodes became active over the project, the over-current protection and associated extension of the modules' lifetimes is worth the small amount of increased power that occurs with their removal.
- Siemens appears to have fixed many of the issues seen in the ARCO modules, as the replacement Siemens modules have aged much more gracefully (see module 148 in Figure C - 1 in Appendix C).

REFERENCES

ARCO. “Supplement to Installation Guide: Specifications.” 1989.

Bazilian, Morgan, Ijeoma Onyeji, Michael Liebreich, Ian MacGill, Jennifer Chase, Jigar Shah, Dolf Gielen, Doug Arent, Doug Landfear, and Shi Zhengrong. “Re-considering the economics of photovoltaic power.” Renewable Energy: An International Journal (2013): 329-338.

Benbennick, David. “Map of California highlighting Humboldt County.” 2006. <https://commons.wikimedia.org/wiki/File:Map_of_California_highlighting_Humboldt_County.svg>.

Branker, K., M.J.M. Pathak and J. M. Pearce. “A review of solar photovoltaic levelized cost of electricity.” Renewable and Sustainable Energy Reviews (2011): 4470-4482.

Chamberlin, Charles. “Interview with Charles Chamberlin Pertaining to the Funding and Operation of the PV Array at the Trinidad Telonicher Marine Lab with Jake Rada.” October 2016.

Czanderna, A. W. and F. J. Pern. “Encapsulation of PV modules using ethelyne vinyl acetate copolymer as a pottant: A critical review.” Solar Energy Materials and Solar Cells (1996): 101-181.

Dechthummarong, C., B. Wiengmoon, D. Chenvidhya, C. Jivacate and K. Kirtikara. “Physical deterioration of encapsulation and electrical insulation properties of PV modules after long-term operation in Thailand.” Solar Energy Materials and Solar Cells (2010): 1437-1440.

Díaz-Dorado, E., A. Suarez-Garcia, C. Carrillo and J. Cidras. "Influence of the shadows in photovoltaic systems with different configurations of bypass diodes." International Symposium on Power Electronics, Electrical Drives, Automation and Motion (2010).

Dunlop, Ewan D. and David Halton. “The Performance of Crystalline Silicon Photovoltaic Solar Modules after 22 Years of Continuous Outdoor Exposure.” Progress in Photovoltaics: Reasearch and Applications (2005): 53-64.

Fluke. “Fluke 287 FlukeView Forms Combo Kit.” 2009.

Google Maps. 2017. January 2017 <https://www.google.com/maps/@40.8454209,-124.053224,12z>.

Gxasheka, A. R., E. E. van Dyk and E. L. Meyer. "Evaluation of performance parameters of PV modules deployed outdoors." Renewable Energy (2004): 611-620.

Hasyim, E. Suryanto, S. R. Wenham and M. A. Green. "Shadow Tolerance of Modules Incorporating Integral Bypass Diode Solar Cells." Solar Cells (1986): 109-122.

Honsberg, Christiana and Stuart Bowden. "Air Mass." 2017 <http://www.pveducation.org/pvcdrom/2-properties-sunlight/air-mass>.

Humboldt State University Foundation. "Purchase Order of M75 ARCO Solar Electric Modules." Arcata, 10 October 1989.

Ingenieurburo Mencke & Tegtmeyer GmbH. "Mini-KLA PV I-V Curve Analyser." 2011.

Jacobson, Arne. "Photovoltaic Module Performance." 2016.

Jacobson, Arne, Gian Pauletto, Charles Chamberlin, Mark Rocheleau and Peter Lehman. "Research Issues In Photovoltaic Electrolysis." Humboldt State University. Arcata: Schatz Energy Research Center, 1994.

Jennings, C. "Outdoor Versus Rated Photovoltaic Module Performance." 19th IEEE Photovoltaic Specialists' Conf., New Orleans, LA (1987): 1257-1260.

Jordan, D. C. and S. R. Kurtz. "Photovoltaic Degradation Rates—an Analytical Review." Progress in Photovoltaics: Reasearch and Applications (2011).

Jorgensen, G. J. and T. J. McMahon. "Accelerated and Outdoor Aging Effects on Photovoltaic Module Interfacial Adhesion Properties." Progress in Photovoltaics: Reasearch and Applications (2008): 519-527.

Kahoul, Nabil, Mourad Houabes and Mohammed Sadok. "Assessing the early degradation of photovoltaic modules performance in the Saharan region." Energy Conversion and Management (2014): 320-326.

KaleidaGraph. "Graphing and Data Analysis. Version 3.5 for Windows." Synergy Software, 2457 Perkiomen Ave., Reading, PA 19606-2049. www.Synergy.com. Accessed 2017.

King, D. L., M. A Quintana, J. A. Kratochvil, D. E. Ellibee and B. R. Hansen. "Photovoltaic Module Performance and Durability Following Long-Term Field Exposure." Albuquerque: Sandia National Laboratories, 2000.

Lehman, Peter A. and Charles E. Chamberlin. “Operating Experience With A Photovoltaic-Hydrogen-Fuel Cell Energy System.” Solar Hydrogen Energy Systems Symposium at the ASME Winter Annual Meeting. Anaheim: Humboldt State University, 1992.

Lehman, Peter, Charles Chamberlin, Marc Marshall and Mark Rocheleau. “Comparison of PV Module Performance Before and After 11 and 20 Years of Field Exposure.” Seattle: 37th IEEE PVSC, 2011.

Lighting Global. “Quality Assurance Protocals 3.0.” 2012.

Machida, Kyoichi, Takeo Yamazaki and Tatsuo Hirasawa. “Secular degradation of crystalline photovoltaic modules.” Solar Energy Materials and Solar Cell (1997): 149-153.

Mekhilef, S., R. Saidur and M. Kamalisarvestani. “Effect of dust, humidity and air velocity on efficiency of photovoltaic cells.” Renewable and Sustainable Energy Reviews (2012): 2920-2925.

Meydbray, Jenya and Frederic Dross. “PV Module Reliability Scorecard Report 2016.” 2016.

Molenbroek, E., D. W. Waddington and K. A. Emery. “Hot Spot Susceptibility and Testing of PV Modules.” National Renewable Energy Laboratories, 1991.

Munoz, M. A., M. C. Alonso-Garcia, N. Vela and F. Chenlo. “Early degradation of silicon PV modules and guaranty conditions.” Solar Energy (2011): 2264-2274.

Omega. “Revised Thermocouple Reference Tables: Type K.” 2016.

Osterwald, C. R., A. Aderberg, S. Rummel and L. Ottoson. “Degradation Analysis of Weathered Crystalline-Silicon PV Modules.” 29th IEEE PV Specialists Conference. New Orleans: NREL, 2002.

Pauletto, Gian. “Power Loss in the Photovoltaic Array Elecrolyzer System of the Schatz Solar Hydrogen Project.” Senior Project. Humboldt State University, 1996.

Peters, Michael, Tobias Schmidt, David Wiederkeh and Malte Schneider. "Shedding light on solar technologies—A techno-economic assessment and its policy implications." Energy Policy (2011): 6422-9439.

Quintana, M. A., D. L. King, T. J. McMahon and C. R. Osterwald. “Commonly Observed Degradation in Field-Aged Photovoltaic Modules.” NREL and SNL. 2002.

Realini, A., E. Bura, N. Cereghetti, D. Chianese and S. Rezzonico. “Study of a 20-Year Old PV Plant (MTBF Project).” University of Applied Sciences of Southern Switzerland (SUPSI), 2001.

Reis, A. M., N. T. Coleman, M. W. Marshall, P. A. Lehman and C. E. Chamberlin. “Comparison of PV Module Performance Before and After 11-Years of Field Exposure.” 29th IEEE Photovoltaics Specialists Conference. New Orleans: IEEE, 2002.

Reis, Antonio and Nate Coleman. “Updated Report on Comparison of PV Module performance before and after 11-Years of Field Exposure.” Arcata, 2002.

Russell, M.C. and D.A. Bergman. “Photovoltaic Flat-Plate Array and Insolation Measurements.” Proc. Photovoltaics and Insolation Measurements Workshop, Vail, CO. Golden, CO: Solar Energy Research Institute, 1985.

Scilab Enterprises. "SciLab." Scilab Enterprises, 2016.

Sharma, Rakhi and G. N. Tiwari. “Technical performance evaluation of stand-alone photovoltaic array for outdoor field conditions of New Delhi.” Applied Energy (2011): 644-652.

Siemens Solar Industries. “M75 High efficiency solar electric module.” 1990.

Silvestre, S., A. Boronat and A. Chouder. “Study of bypass diodes configuration on PV modules.” Applied Energy (2009): 1632-1640.

Singh, Priyanka O. “Modeling of photovoltaic arrays under shading patterns with reconfigurable switching and bypass diodes.” Theses and Dissertations. Toledo: The University of Toledo, 2011.

Skoczek, Artur, Tony Sample and Ewan D. Dunlop. “The Results of Performance Measurements of Field-aged Crystalline Silicon Photovoltaic Modules.” Progress in Photovoltaics: Reasearch and Applications (2008): 227-240.

Solar Energy International. “Solar Electric Handbook: Photovoltaic Fundamentals and Applications.” Vol. 2nd. Pearson Learning Solutions, 2013.

Swift, Kenton D. “A comparison of the cost and financial returns for solar photovoltaic systems installed by businesses in different locations across the United States.” Renewable Energy: An International Journal (2013): 137-143.

The Eppley Laboratory, Inc. “Precision Spectral Pyranometer Model PSP Specifications.” Newport, 2016.

U.S. Bureau of Labor Statistics. “CPI Inflation Calculator.” 2017 <https://data.bls.gov/cgi-bin/cpicalc.pl?cost1=4.80&year1=1989&year2=2016>.

Vazquez, Manuel and Ignacio Rey-Stolle. “Photovoltaic Module Reliability Model Based on Field Degradation Studies.” Progress in Photovoltaics: Reasearch and Applications (2008): 419-433.

Wohlgemuth, J. H., D. W. Cunningham, A. M. Nguyen and J. Miller. “Long Term Reliabiltiy of OV Modules.” BP Solar International, 2006.

Zhang, Peng, Wenyuan Li, Sherwin Li, Yang Wang and Weidong Xiao. "Reliability assessment of photovoltaic power systems: Review of current status and future perspectives." Applied Energy (2013): 822-833.

Zoellick, J. I. “Testing and matching photovoltaic modules to maximize solar electric array performance.” Senior Project. Humboldt State University. Arcata, 1990.

Appendix A: Instrument Specifications Sheets

This Appendix contains the specification sheets for the equipment and instruments used in the data collection for this project (Figure A - 1 to Figure A - 9). This covers the solar modules, Mini-KLA PV IV Curve Tracer, Eppley PSP, Fluke 287 True RMS Multimeter, Omegaette HH303 Type K Thermometer, and Type K thermocouple.

SUPPLEMENT TO INSTALLATION GUIDE 233-701500-20 MAY, 1989

SPECIFICATIONS

	MODEL M55	MODEL M58	MODEL M75	MODEL M78	MODEL M65	MODEL M68	MODEL M25
ELECTRICAL CHARACTERISTICS:							
Rated Power, Watts	53 Wp	48 Wp	48 Wp	40 Wp	43 Wp	37 Wp	22 Wp
Open Circuit Voltage, Typical	21.7	21.6	19.8	19.5	18.0	18.0	18.0
Short Circuit Current, Typical	3.35	3.2	3.35	3.0	3.32	3.0	1.68
Voltage at Load, Typical	17.4	17.3	15.9	15.7	14.6	14.5	14.5
Amperage at Load, Typical	3.05	2.78	3.02	2.55	2.95	2.56	1.52

NOTE: All electrical specifications are at Standard Test Conditions of: 1000 W/m^2, 25°C cell temperature and solar spectral irradiance per ASTM E 892.

PHYSICAL CHARACTERISTICS:							
No. Cells in Series	36	36	33	33	30	30	30
Cell Size	4.05" (102.9 mm) Sq.						1/2 of 4.05" cell
Module - Length:	50.9" (1293 mm)		48" (1219 mm)		42.6" (1083 mm)		22.4" (569 mm)
- Width:	13" (330 mm)						
- Depth:	1.4" (36 mm)						
Weight	12.6 lb. (5.7 kg.)		11.6 lb. (5.2 kg.)		10.5 lb. (4.8 kg.)		5.6 lb. (2.5 kg.)
Mounting Holes:							
Across Length of Module:	49.8" (1265 mm)		46.9" (1191 mm)		41.5" (1054 mm)		21.3" (541 mm)
Inner Set:			25.3" (643 mm)				None
Across the Width of Module:				11.3" (287 mm)			
Diameter:				0.26" (6.6 mm)			
Wiring Provisions:			2 Junction Covers for 14 to 8 AWG wire				18 AWG, 2 cond. cable attached
SYSTEM DESIGN INFORMATION:							
Max Short Circuit Current at 1000 W/m^2 & 47°C	3.72	3.53	3.72	3.30	3.68	3.31	1.86
Open Circuit Voltage at 0°C	24V	24V	22V	22V	20V	20V	20V
Maximum System Open Circuit Voltage	600V						20V
Factory Installed Bypass Diodes	Yes	Yes	Yes	Yes	Yes	Yes	No
Maximum Number Series Modules	25	25	27	27	30	30	1

233-701500-41, REV. 2

103

Figure A - 1: ARCO M75 specifications sheet

M75 High efficiency solar electric module

FEATURES

Large, high efficiency single crystal solar cells provide the highest light to energy conversion efficiency available from Siemens.

Cells are textured and have an anti-reflection coating.

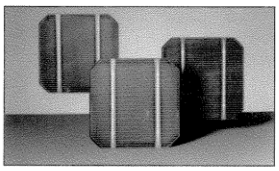

Multiple redundant contacts provide a high degree of fault tolerance and circuit reliability.

Cells within a module are electrically-matched for increased efficiency.

Circuit is laminated between layers of ethylene vinyl acetate (EVA) for moisture resistance, UV stability and electrical isolation.

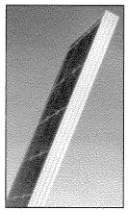

Low iron tempered glass front for strength and superior light transmission.

Rugged anodized aluminum frame is designed for exceptional strength.

Side rails with multiple mounting holes for easy installation.

Tough, multi-layered polymer backsheet is used for environmental protection, resistance to abrasion, tears and punctures.

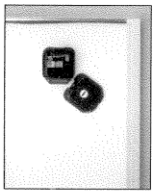

Two junction covers with lids are designed for easy field wiring, safety and environmental protection.

Wired-in bypass diodes reduce potential loss of power from partial array shading.

SPECIFICATIONS

Rated Power	48 Watts
Current (typical at load)	3.02 Amps
Voltage (typical at load)	15.9 Volts
Short Circuit Current (typical)	3.4 Amps
Open Circuit Voltage (typical)	19.8 Volts

Power specifications are at standard test conditions of: 1000 W/M² solar irradiance, 25°C cell temperature and solar spectral irradiance per ASTM E892

Weight	11.6 lb/5.2 kg

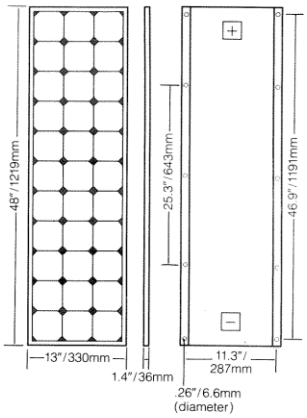

CHARACTERISTICS

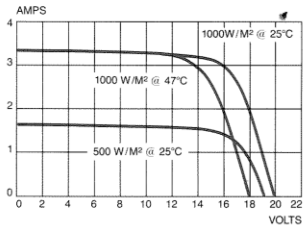

The IV curve (current vs. voltage) above demonstrates typical power response to various light levels at 25°C and a 47°C cell temperature.

- Minimum power upon final factory inspection is within 10% of rated power.
- Module leakage current of less than 50μA at 3000 VDC.
- Normal operating cell temperature (NOCT) as defined by ASTM E 1036 is 42°C +/−2°C.
- Laboratory tested for wide range of operating conditions (−40°C to 90°C, 0 to 85% humidity).
- Passes Salt Fog Test per Mil-Standard 810.
- Passes complete environmental requirements of JPL Specification No. 5101-61 (Block V).
- External grounding screw for electrical safety.
- Ground continuity of less than 1 ohm for all metallic surfaces.
- Ten-year limited warranty on power output.*
- UL Listed. (Per UL 1703).

Charts are for estimating purposes only. Specifications subject to change without notice.

*Complete warranty and installation information is included in the module package or is available from Siemens or your Siemens Solar dealer prior to purchase.

Siemens Solar Industries
P.O. Box 6032, Camarillo, CA 93011
Telephone: (805) 482-6800 FAX: (805) 388-6395

Figure A - 2: Siemens M75 module brochure

Intelligent module design

- All cells are electrically matched to assure the greatest power output possible.
- Ultra-clear tempered glass provides excellent light transmission and protects from wind, hail, and impact.
- Torsion and corrosion-resistant anodized aluminum module frame ensures dependable performance, even through harsh weather conditions and in marine environments.
- Built-in bypass diodes (12V configuration) help system performance during partial shading.

High quality

- Every module is subject to final factory review, inspection, and testing to assure compliance with electrical, mechanical, and visual criteria.
- 33 PowerMax® single-crystalline solar cells deliver excellent performance even in reduced light or poor weather conditions.
- Cell surfaces are treated with the Texture Optimized Pyramidal Surface (TOPS™) process to generate more energy from available light.
- Fault tolerant multi-redundant contacts on front and back of each cell provide superior reliability.
- Solar cells are laminated between a multi-layered polymer backsheet and layers of ethylene vinyl acetate (EVA) for environmental protection, moisture resistance, and electrical isolation.
- Durable back sheet provides the module underside with protection from scratching, cuts, breakage, and most environmental conditions.
- Laboratory tested and certified for a wide range of operating conditions.
- Ground continuity of less than 1 ohm for all metallic surfaces.
- Manufactured in ISO 9001 certified facilities to exacting Siemens quality standards.

Easy installation

- Standard ProCharger™-S terminal enclosures are designed for trouble-free wiring and environmental protection. (Modified versions are also available, e.g. as SM50-HJ with the special ProCharger™-CR junction box.)
- Lightweight aluminum frame and pre-drilled mounting holes for easy installation.
- Modules may be wired together in series or parallel to attain required power levels.

Performance warranty

- 25 Year limited warranty on power output.

Further information on solar products, systems, principles, and applications is available in the Siemens Solar product catalog.

Siemens modules are recyclable.

Solar module SM50-H

Electrical parameters		
Maximum power rating P_{max}	[W_p][1]	50
Rated current I_{MPP}	[A]	3.15
Rated voltage V_{MPP}	[V]	15.9
Short circuit current I_{SC}	[A]	3.35
Open circuit voltage V_{OC}	[V]	19.8
Thermal parameters		
NOCT[2]	[°C]	45±2
Temp. coefficient: short-circuit current		1.2 mA / °C
Temp. coefficient: open-circuit voltage		-.077 V / °C
Qualification test parameters[4]		
Temperature cycling range	[°C]	-40 to +85
Humidity freeze, Damp heat	[%RH]	85
Maximum system voltage	[V]	600 (1000 V per ISPRA)
Wind Loading PSF	[N/m²]	50 [2400]
Maximum distortion[3]	[°]	1.2
Hailstone impact Inches	[mm]	1.0 [25]
MPH	[m/s]	52 [v=23]
Weight Pounds	[kg]	11.5 [5.2]

1) W_p (Watt peak) = Peak power (Mimimum W_p = 45 Watts)
Air Mass AM = 1.5
Irradiance E = 1000 W/m²
Cell temperature T_C = 25 °C

2) Normal Operating Cell Temperature at:
Irradiance E = 800 W/m²
Ambient temperature T_U = 20 °C
Wind speed v_W = 1 m/s

3) Diagonal lifting of the module plane

4) Per EIC 1215 test requirements

5) 12 Volt configuration

Voltage-current characteristic[5]

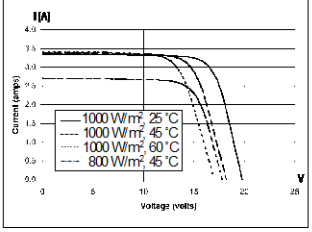

Module dimensions

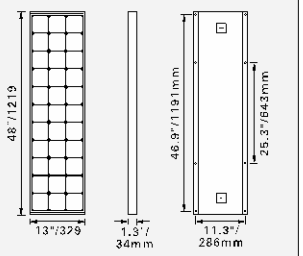

Hole diameter 0.26 inch (6.6 mm)
Mounting hole dimensions are center to center

ProCharger™-S Junction-box
Maximum cable diameter: 4 mm²
Type of protection: IP54

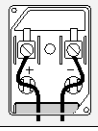

Your address for photovoltaics from Siemens Solar

Status 3/98 – Subject to modification.

Siemens Solar GmbH
A joint venture of
Siemens AG and Bayernwerk AG
Postfach 46 07 05
D-80915 München
Germany

Siemens Solar Industries
P.O. Box 6032
Camarillo, CA 93011, U.S.A.
Tel: 805-482-6800
Fax: 805-388-6395
Web site: www.siemenssolar.com
E-mail: sunpower@solarpv.com

Printed in U.S.A.

Siemens Showa Solar Pte. Ltd.
Blk. 164 Kallang Way
#05-14/15 Kolam Ayer Industrial Park
Singapore 349248
Tel: 65-842-3886
Fax: 65-842-3887

Order No. 619816 Rev. C

Figure A - 3: Replacement Siemens SM50-H specifications sheet

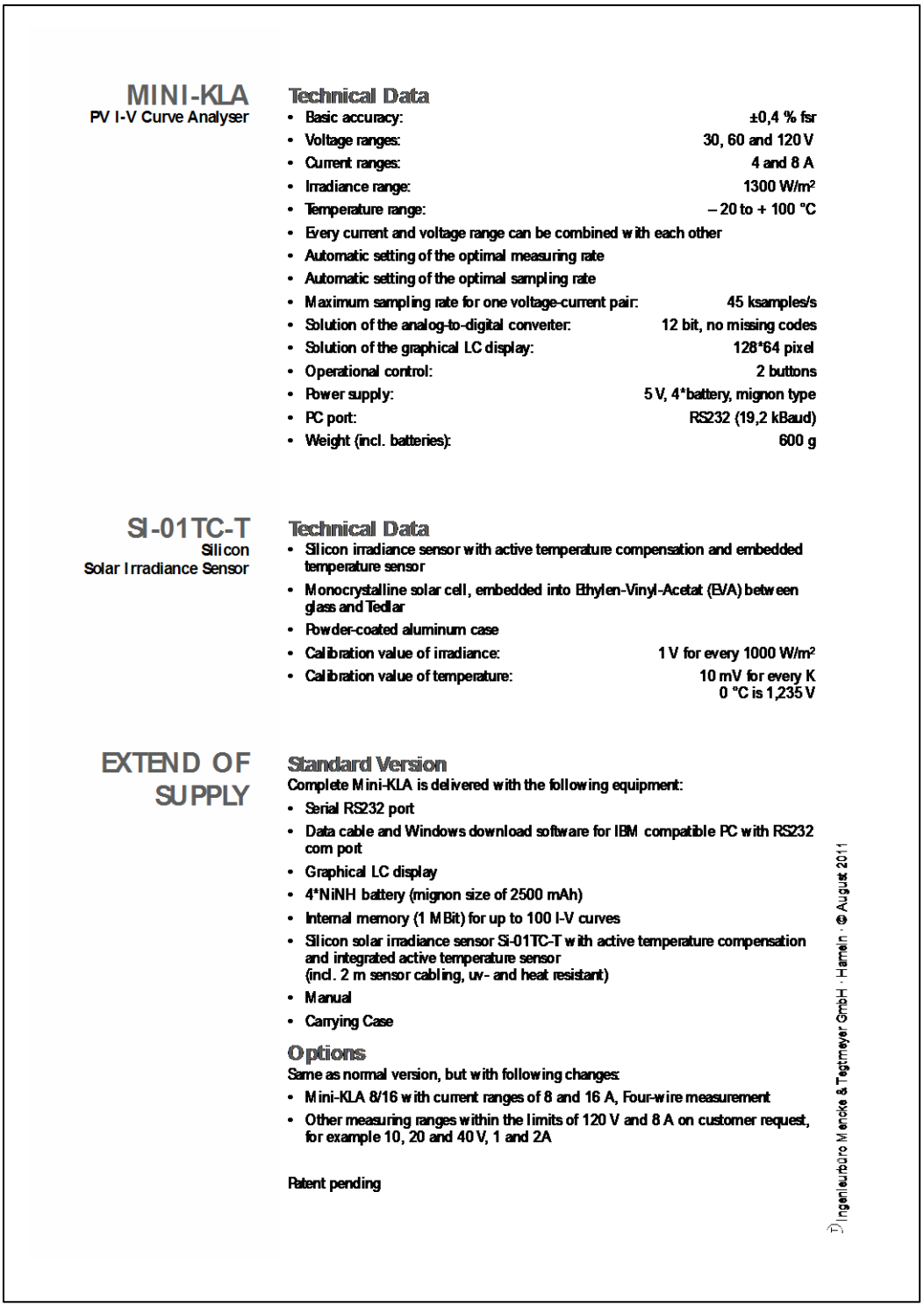

MINI-KLA
PV I-V Curve Analyser

Technical Data

- Basic accuracy: ±0,4 % fsr
- Voltage ranges: 30, 60 and 120 V
- Current ranges: 4 and 8 A
- Irradiance range: 1300 W/m²
- Temperature range: – 20 to + 100 °C
- Every current and voltage range can be combined with each other
- Automatic setting of the optimal measuring rate
- Automatic setting of the optimal sampling rate
- Maximum sampling rate for one voltage-current pair: 45 ksamples/s
- Solution of the analog-to-digital converter: 12 bit, no missing codes
- Solution of the graphical LC display: 128*64 pixel
- Operational control: 2 buttons
- Power supply: 5 V, 4*battery, mignon type
- PC port: RS232 (19,2 kBaud)
- Weight (incl. batteries): 600 g

SI-01TC-T
Silicon
Solar Irradiance Sensor

Technical Data

- Silicon irradiance sensor with active temperature compensation and embedded temperature sensor
- Monocrystalline solar cell, embedded into Ethylen-Vinyl-Acetat (EVA) between glass and Tedlar
- Powder-coated aluminum case
- Calibration value of irradiance: 1 V for every 1000 W/m²
- Calibration value of temperature: 10 mV for every K
0 °C is 1,235 V

EXTEND OF SUPPLY

Standard Version

Complete Mini-KLA is delivered with the following equipment:

- Serial RS232 port
- Data cable and Windows download software for IBM compatible PC with RS232 com port
- Graphical LC display
- 4*NiNH battery (mignon size of 2500 mAh)
- Internal memory (1 MBit) for up to 100 I-V curves
- Silicon solar irradiance sensor Si-01TC-T with active temperature compensation and integrated active temperature sensor
(incl. 2 m sensor cabling, uv- and heat resistant)
- Manual
- Carrying Case

Options

Same as normal version, but with following changes:

- Mini-KLA 8/16 with current ranges of 8 and 16 A, Four-wire measurement
- Other measuring ranges within the limits of 120 V and 8 A on customer request, for example 10, 20 and 40 V, 1 and 2A

Patent pending

Figure A - 4: Mini-KLA PV IV Curve Analyser specifications sheet

Model PSP Specifications

There are two generally accepted Classification Systems used for Pyranometers. ISO classifies pyranometers as a "Secondary Standards", "First Class" or "Second Class" while WMO uses "High Quality", "Good Quality" and "Moderate Quality".

The Precision Spectral Pyranometer, Model PSP is classified as a ISO Secondary Standard or WMO High Quality Pyranometer.

- Classification: ISO Secondary Standard Pyranometer / WMO High Class
- Response Time (95%): 10-15 seconds
- Zero Offset to 200 Wm^{-2} net radiant loss to sky: 4-6 Wm^{-2}
- Zero Offset to 5° C/hr change in ambient temperature: 1-2 Wm^{-2}
- Resolution: < 1 Wm^{-2}
- Non-Stability: <0.5% / yr (typical)
- Non-Linearity: ±0.5% from 0-2800 Wm^{-2}
- Directional Response: < 10 Wm^{-2}
- Spectral Selectivity: 1%
- Temperature Response: ±1%
- Tilt Response: < 0.5%
- Achievable Uncertainty (Hourly): 1-2 %
- Achievable Uncertainty (Daily): 1-2 %
- Suitable Application: Working Standard or Network Measurements

Figure A - 5: Eppley PSP specifications sheet

EPLAB

THE EPPLEY LABORATORY, INC.

12 Sheffield Avenue, PO Box 419, Newport, Rhode Island USA 02840
Phone: 401.847.1020 Fax: 401.847.1031 Email: info@eppleylab.com

Calibration Certificate

Instrument:	Precision Spectral Pyranometer, Model PSP, Serial Number 25913F3
Procedure:	This pyranometer was compared in Eppley's Integrating Hemisphere according to procedures described in ***ISO 9847 Section 5.3.1*** and Technical Procedure, TP01 of The Eppley Laboratory, Inc.'s Quality Assurance Manual on Calibrations.
Transfer Standard:	Eppley Standard Precision Pyranometer, Model SPP, Serial Number 37501F3
Results:	**Sensitivity: S = 8.78 μV / Wm^{-2}** Uncertainty: U_{95} = ±0.91% (95% confidence level, k=2) Resistance: 650 Ω at 23°C
	Date of Test: April 22, 2016
Traceability:	This calibration is traceable to the World Radiation Reference (WRR) through comparisons with Eppley's AHF standard self-calibrating cavity pyrheliometers which participated in the Eleventh International Pyrheliometric Comparisons (IPC XI) at Davos, Switzerland in September-October 2010. Unless otherwise stated in the remarks section below or on the Sales Order, the results of this calibration are "AS FOUND / AS LEFT".
Due Date:	Eppley recommends a minimum calibration cycle of five (5) years but encourages annual calibrations for highest measurement accuracy.
Customer:	Shatz Energy Research Center – Humboldt State University Arcata, CA
Signatures:	In Charge of Test: Debra L. Dority Reviewed by: Thomas D Kirk
Eppley SO:	64699
Date of Certificate:	April 22, 2016
Remarks:	Sensitivity before Repainting Element = 8.32 μV / Wm^{-2}

End of Report

Figure A - 6: Calibration sheet for the specific Eppley PSP used in this project

FLUKE®

Ordering information

Fluke-287/FVF True-rms Logging Multimeter Combo Kit with TrendCapture

287 specifications

Function	Range and resolution	Basic accuracy
DC volts	50.000 mV,500.00 mV, 5.0000 V, 50.000 V, 500.00 V, 1000.0V	0.025 %
AC volts		0.4 % (true-rms)
DC current	500.00 µA, 5000.0 µA, 50.000 mA, 400.00 mA, 5.0000 A, 10.000 A	0.06 %
AC current		0.6%(true-rms)
Temperature (excluding probe)	-200.0 °C to 1350.0 °C (-328.0 °F to 2462.0 °F)	1.0 %
Resistance	500.00 Ω, 5.0000 kΩ, 50.000 kΩ, 500.00 kΩ, 5.0000 MΩ, 50.00 MΩ, 500.0 MΩ	0.05 %
Capacitance	1.000 nF,10.00 nF 100.0 nF, 1.000 µF, 10.00 µF, 100.0 µF, 1000 µF, 10.00 mF, 100.00 mF	1.0 %
Frequency	99.999 Hz, 999.99 Hz, 9.9999 kHz, 99.999 kHz, 999.99 kHz	0.005 % + 5

Fluke. *Keeping your world up and running.*®

Fluke Corporation
PO Box 9090, Everett, WA 98206 U.S.A.

Fluke Europe B.V.
PO Box 1186, 5602 BD
Eindhoven, The Netherlands

For more information call:
In the U.S.A. (800) 443-5853 or
Fax (425) 446-5116
In Europe/M-East/Africa +31 (0) 40 2675 200 or
Fax +31 (0) 40 2675 222
In Canada (800)-36-FLUKE or
Fax (905) 890-6866
From other countries +1 (425) 446-5500 or
Fax +1 (425) 446-5116
Web access: http://www.fluke.com

Figure A - 7: Fluke 287 Multimeter specifications sheet

Mini Thermometers

HH300 Series
Starts at
$89

1 YEAR WARRANTY · NIST · CE
Standard
No Points

POCKET PAL™

HH308, $89. HH303, $119.

Choice of USB or RS232 Interface.

- **Wide Measurement Range: -200 to 1370°C (-328 to 2498°F)**
- **Auto Ranging**
- **Auto Power-Off**
- **Dual Input and Dual Display**
- **REL Function**
- **Hold Function**
- **Min/Max Function**
- **Resolution 0.1°C/0.1°F up to 599.9°C/999.9°F**

The HH300 Series are low cost digital thermometers, small enough to fit in your pocket. They are available in Type K or Type J/K input models with standard features such as min/max reading, reading hold, and both are °C to °F switchable. Their temperature range is from -200 to 1370°C (-328 to 2498°F). The HH303 also offers a software and USB or RS232 interface cable option that allows a PC to read the data.

Specifications

Range:
Type K: -200 to 1370°C (-328 to 2498°F)
Type J: -200 to 760°C (-328 to 1400°F)
Accuracy:
HH303: 0.1% rdg + 0.7°C (1.4°F)
HH308: 0.3% rdg + 1°C (2°F)
Input Protection: 60 Vdc or 24 Vrms AC maximum
Battery: 9V (included), MN 1604
Battery Life: 120 hour (with alkaline)
Operating Range: 0 to 40°C (32 to 104°F) <80% RH
Storage Range: -10 to 60°C (14 to 140°F) <80% RH
Dimensions:
HH303: 184 H x 64 W x 30 mm D (7.5 x 2.5 x 1.2")
HH308: 164 H x 54 W x 34 mm D (6.5 x 2.1 x 1.3")
Weight: Approx 200 g (7 oz)

Free Thermocouple Included!
These models include a free 1 m (40") Type K insulated beaded wire thermocouple with subminiature connector and wire spool caddy (1 per channel). **Order a Spare! Model No. SC-GG-K-30-36, $15.**

AVAILABLE FOR FAST DELIVERY!

To Order *(Specify Model Number)*

Model No.	Price	Description
HH308	$89	Type K handheld 0.1°C/F thermometer
HH303	119	Type J/K handheld 0.1°C/F thermometer
HH310-SW	50	Software and RS232 interface cable for HH303
HH300-SW-USB*	50	Software driver and USB interface cable for HH303
HH300-ADAPTER	18	AC adaptor for HH303
HH300-CABLE	18	Spare RS232 interface cable for HH303
HH300-CABLE-USB	18	Spare USB interface cable for HH303
CAL-3-HH	75	NIST-traceable calibration, with points

** Requires **HH310-SW***
Comes complete with beaded wire Type K thermocouple (one per input), 9V battery, operator's manual and NIST certificate (no points).
Ordering Example: HH308,** dual input Type K thermocouple thermometer, **$89.

Figure A - 8: Omegaette HH303 Type-K Thermometer specifications

MAXIMUM TEMPERATURE RANGE
Thermocouple Grade
– 328 to 2282°F
– 200 to 1250°C
Extension Grade
32 to 392°F
0 to 200°C
LIMITS OF ERROR
(whichever is greater)
Standard: 2.2°C or 0.75% Above 0°C
2.2°C or 2.0% Below 0°C
Special: 1.1°C or 0.4%
COMMENTS, BARE WIRE ENVIRONMENT:
Clean Oxidizing and Inert; Limited Use in Vacuum or Reducing; Wide Temperature Range; Most Popular Calibration
TEMPERATURE IN DEGREES °C
REFERENCE JUNCTION AT 0°C

°C
Nickel-Chromium
vs.
Nickel-Aluminum

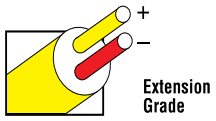

OMEGA

Revised Thermocouple Reference Tables

IEC color code

ANSI color code

TYPE K

Reference Tables
N.I.S.T. Monograph 175
Revised to ITS-90

Thermoelectric Voltage in Millivolts

°C	-10	-9	-8	-7	-6	-5	-4	-3	-2	-1	0	°C
-260	-6.458	-6.457	-6.456	-6.455	-6.453	-6.452	-6.450	-6.448	-6.446	-6.444	-6.441	-260
-250	-6.441	-6.438	-6.435	-6.432	-6.429	-6.425	-6.421	-6.417	-6.413	-6.408	-6.404	-250
-240	-6.404	-6.399	-6.393	-6.388	-6.382	-6.377	-6.370	-6.364	-6.358	-6.351	-6.344	-240
-230	-6.344	-6.337	-6.329	-6.322	-6.314	-6.306	-6.297	-6.289	-6.280	-6.271	-6.262	-230
-220	-6.262	-6.252	-6.243	-6.233	-6.223	-6.213	-6.202	-6.192	-6.181	-6.170	-6.158	-220
-210	-6.158	-6.147	-6.135	-6.123	-6.111	-6.099	-6.087	-6.074	-6.061	-6.048	-6.035	-210
-200	-6.035	-6.021	-6.007	-5.994	-5.980	-5.965	-5.951	-5.936	-5.922	-5.907	-5.891	-200
-190	-5.891	-5.876	-5.861	-5.845	-5.829	-5.813	-5.797	-5.780	-5.763	-5.747	-5.730	-190
-180	-5.730	-5.713	-5.695	-5.678	-5.660	-5.642	-5.624	-5.606	-5.588	-5.569	-5.550	-180
-170	-5.550	-5.531	-5.512	-5.493	-5.474	-5.454	-5.435	-5.415	-5.395	-5.374	-5.354	-170
-160	-5.354	-5.333	-5.313	-5.292	-5.271	-5.250	-5.228	-5.207	-5.185	-5.163	-5.141	-160
-150	-5.141	-5.119	-5.097	-5.074	-5.052	-5.029	-5.006	-4.983	-4.960	-4.936	-4.913	-150
-140	-4.913	-4.889	-4.865	-4.841	-4.817	-4.793	-4.768	-4.744	-4.719	-4.694	-4.669	-140
-130	-4.669	-4.644	-4.618	-4.593	-4.567	-4.542	-4.516	-4.490	-4.463	-4.437	-4.411	-130
-120	-4.411	-4.384	-4.357	-4.330	-4.303	-4.276	-4.249	-4.221	-4.194	-4.166	-4.138	-120
-110	-4.138	-4.110	-4.082	-4.054	-4.025	-3.997	-3.968	-3.939	-3.911	-3.882	-3.852	-110
-100	-3.852	-3.823	-3.794	-3.764	-3.734	-3.705	-3.675	-3.645	-3.614	-3.584	-3.554	-100
-90	-3.554	-3.523	-3.492	-3.462	-3.431	-3.400	-3.368	-3.337	-3.306	-3.274	-3.243	-90
-80	-3.243	-3.211	-3.179	-3.147	-3.115	-3.083	-3.050	-3.018	-2.986	-2.953	-2.920	-80
-70	-2.920	-2.887	-2.854	-2.821	-2.788	-2.755	-2.721	-2.688	-2.654	-2.620	-2.587	-70
-60	-2.587	-2.553	-2.519	-2.485	-2.450	-2.416	-2.382	-2.347	-2.312	-2.278	-2.243	-60
-50	-2.243	-2.208	-2.173	-2.138	-2.103	-2.067	-2.032	-1.996	-1.961	-1.925	-1.889	-50
-40	-1.889	-1.854	-1.818	-1.782	-1.745	-1.709	-1.673	-1.637	-1.600	-1.564	-1.527	-40
-30	-1.527	-1.490	-1.453	-1.417	-1.380	-1.343	-1.305	-1.268	-1.231	-1.194	-1.156	-30
-20	-1.156	-1.119	-1.081	-1.043	-1.006	-0.968	-0.930	-0.892	-0.854	-0.816	-0.778	-20
-10	-0.778	-0.739	-0.701	-0.663	-0.624	-0.586	-0.547	-0.508	-0.470	-0.431	-0.392	-10
0	-0.392	-0.353	-0.314	-0.275	-0.236	-0.197	-0.157	-0.118	-0.079	-0.039	0.000	0
0	0.000	0.039	0.079	0.119	0.158	0.198	0.238	0.277	0.317	0.357	0.397	0
10	0.397	0.437	0.477	0.517	0.557	0.597	0.637	0.677	0.718	0.758	0.798	10
20	0.798	0.838	0.879	0.919	0.960	1.000	1.041	1.081	1.122	1.163	1.203	20
30	1.203	1.244	1.285	1.326	1.366	1.407	1.448	1.489	1.530	1.571	1.612	30
40	1.612	1.653	1.694	1.735	1.776	1.817	1.858	1.899	1.941	1.982	2.023	40
50	2.023	2.064	2.106	2.147	2.188	2.230	2.271	2.312	2.354	2.395	2.436	50
60	2.436	2.478	2.519	2.561	2.602	2.644	2.685	2.727	2.768	2.810	2.851	60
70	2.851	2.893	2.934	2.976	3.017	3.059	3.100	3.142	3.184	3.225	3.267	70
80	3.267	3.308	3.350	3.391	3.433	3.474	3.516	3.557	3.599	3.640	3.682	80
90	3.682	3.723	3.765	3.806	3.848	3.889	3.931	3.972	4.013	4.055	4.096	90

°C	0	1	2	3	4	5	6	7	8	9	10	°C
250	10.153	10.194	10.235	10.276	10.316	10.357	10.398	10.439	10.480	10.520	10.561	250
260	10.561	10.602	10.643	10.684	10.725	10.766	10.807	10.848	10.889	10.930	10.971	260
270	10.971	11.012	11.053	11.094	11.135	11.176	11.217	11.259	11.300	11.341	11.382	270
280	11.382	11.423	11.465	11.506	11.547	11.588	11.630	11.671	11.712	11.753	11.795	280
290	11.795	11.836	11.877	11.919	11.960	12.001	12.043	12.084	12.126	12.167	12.209	290
300	12.209	12.250	12.291	12.333	12.374	12.416	12.457	12.499	12.540	12.582	12.624	300
310	12.624	12.665	12.707	12.748	12.790	12.831	12.873	12.915	12.956	12.998	13.040	310
320	13.040	13.081	13.123	13.165	13.206	13.248	13.290	13.331	13.373	13.415	13.457	320
330	13.457	13.498	13.540	13.582	13.624	13.665	13.707	13.749	13.791	13.833	13.874	330
340	13.874	13.916	13.958	14.000	14.042	14.084	14.126	14.167	14.209	14.251	14.293	340
350	14.293	14.335	14.377	14.419	14.461	14.503	14.545	14.587	14.629	14.671	14.713	350
360	14.713	14.755	14.797	14.839	14.881	14.923	14.965	15.007	15.049	15.091	15.133	360
370	15.133	15.175	15.217	15.259	15.301	15.343	15.385	15.427	15.469	15.511	15.554	370
380	15.554	15.596	15.638	15.680	15.722	15.764	15.806	15.849	15.891	15.933	15.975	380
390	15.975	16.017	16.059	16.102	16.144	16.186	16.228	16.270	16.313	16.355	16.397	390
400	16.397	16.439	16.482	16.524	16.566	16.608	16.651	16.693	16.735	16.778	16.820	400
410	16.820	16.862	16.904	16.947	16.989	17.031	17.074	17.116	17.158	17.201	17.243	410
420	17.243	17.285	17.328	17.370	17.413	17.455	17.497	17.540	17.582	17.624	17.667	420
430	17.667	17.709	17.752	17.794	17.837	17.879	17.921	17.964	18.006	18.049	18.091	430
440	18.091	18.134	18.176	18.218	18.261	18.303	18.346	18.388	18.431	18.473	18.516	440
450	18.516	18.558	18.601	18.643	18.686	18.728	18.771	18.813	18.856	18.898	18.941	450
460	18.941	18.983	19.026	19.068	19.111	19.154	19.196	19.239	19.281	19.324	19.366	460
470	19.366	19.409	19.451	19.494	19.537	19.579	19.622	19.664	19.707	19.750	19.792	470
480	19.792	19.835	19.877	19.920	19.962	20.005	20.048	20.090	20.133	20.175	20.218	480
490	20.218	20.261	20.303	20.346	20.389	20.431	20.474	20.516	20.559	20.602	20.644	490
500	20.644	20.687	20.730	20.772	20.815	20.857	20.900	20.943	20.985	21.028	21.071	500
510	21.071	21.113	21.156	21.199	21.241	21.284	21.326	21.369	21.412	21.454	21.497	510
520	21.497	21.540	21.582	21.625	21.668	21.710	21.753	21.796	21.838	21.881	21.924	520
530	21.924	21.966	22.009	22.052	22.094	22.137	22.179	22.222	22.265	22.307	22.350	530
540	22.350	22.393	22.435	22.478	22.521	22.563	22.606	22.649	22.691	22.734	22.776	540
550	22.776	22.819	22.862	22.904	22.947	22.990	23.032	23.075	23.117	23.160	23.203	550
560	23.203	23.245	23.288	23.331	23.373	23.416	23.458	23.501	23.544	23.586	23.629	560
570	23.629	23.671	23.714	23.757	23.799	23.842	23.884	23.927	23.970	24.012	24.055	570
580	24.055	24.097	24.140	24.182	24.225	24.267	24.310	24.353	24.395	24.438	24.480	580
590	24.480	24.523	24.565	24.608	24.650	24.693	24.735	24.778	24.820	24.863	24.905	590
600	24.905	24.948	24.990	25.033	25.075	25.118	25.160	25.203	25.245	25.288	25.330	600
610	25.330	25.373	25.415	25.458	25.500	25.543	25.585	25.627	25.670	25.712	25.755	610
620	25.755	25.797	25.840	25.882	25.924	25.967	26.009	26.052	26.094	26.136	26.179	620
630	26.179	26.221	26.263	26.306	26.348	26.390	26.433	26.475	26.517	26.560	26.602	630
640	26.602	26.644	26.687	26.729	26.771	26.814	26.856	26.898	26.940	26.983	27.025	640

Figure A - 9: Type-K thermocouple specifications sheet

Appendix B: Scilab Code

This Appendix contains the code from Scilab that was used to collect, organize, and calculate the data used in the Results section, and create the summary files, regression analyses, and IV curves for each test. The code below includes the adjusted constraints used in the 2016 testing in line 231-232, and lines that begin with "//" are comments. As noted in the body of this report, not all the Mini-KLA files were identical, so this example of the code includes "txt 2" and a second "%s" on line 124 to account for the comment number present in most of the file (excluding test from June 24th and August 12th). Another important aspect in this code is the V_{oc} sensitivity equation that factors in the effects of module temperature and solar insolation on a module's V_{oc}.

```
//---- Using only data with raw voltages above 5 V ---------------------------------------------

 //---- 5 parameter single module tests with filtered data and output to file-------------------------

 //-----------------------------start pv5 function----------------
 function amps=pv5(vv, b)

   //pv5 function
   //compute and return PV module current in Amps at operating voltage v
   //5 parameter model of a PV module
   //v=PV module voltage (Volt)
   //iL=short circuit current (Amp)
   iL=b(1);
   //voc=open circuit voltage (Volt)
   voc=b(2);
   //ekt = q/(n*k*t) (1/Volt)
   ekt=b(3);
   //q = Electron charge (Coulomb)
   //n = Ideality factor per cell (unitless)
   //k = Boltzmann's constant (Joule/K)
   //T = Temperature (K)
   //rs=series resistance (Ohm)
   rs=b(4);
   //rp=parallel resistance (Ohm)
   rp=b(5);
```

```
 //tol = tolerance criterion for Newton's Method
 tol=0.00001;
 //disp([iL,voc,ekt,rs,rp])

 // simplify later equations
 i0=(iL-voc/rp)/(exp(ekt*voc) - 1);

 [row,col]=size(vv);
 for i=1:row
  v=vv(i)

  //calulate initial guess using 3 parameter version of model
  i1=iL-i0*(exp(ekt*v) -1);
  di=(iL-i0*(exp(ekt*(v+rs*i1))-1)-(v+rs*i1)/rp) - i1;
  count=0;
  maxcount=20;


  while (abs(di)>tol)
   count=count+1;
   if(count>maxcount) then
    disp("exceded maximum iterations",[i,v,i1,di,iL,voc,ekt,rs,rp])
    amps=0;
   end
   i2=i1+tol;
   di2=(iL-i0*(exp(ekt*(v+rs*i2))-1)-(v+rs*i2)/rp) - i2;
   //disp([i1,di,tol,di2])
   i1=i1-di*tol/(di2-di);

   //calculate revised discrepancy in function at new i1
   di=(iL-i0*(exp(ekt*(v+rs*i1))-1)-(v+rs*i1)/rp) - i1;
   //disp([v,i1,di])
  end

  amps(i)=i1;
 end
endfunction
//------------------------------end pv5 function-------------------

//------------------------------start resid function---------------
function e=resid(b, pv_v, pv_i)
 pv_i_pred=pv5(pv_v,b);
 e=pv_i_pred - pv_i;
endfunction
//------------------------------end resid function---------------

p=5;  //number of parameters
name=["iL","voc","ekt","rs","rp"];
//tmp_path='/Users/charles/Desktop/Temp File/';
tmp_path='/Users/jakerada/Desktop/Temp File/';
cd(tmp_path);
```

```
//open data file for input
filename="Temporary Clipboard Data.txt";
fd_r=mopen(filename,"r");
if(fd_r==-1)
  error("cannot open file for reading")
end

//open data file for regression output
fileout="pv5_regr_results_2016.txt";
fd_w=mopen(fileout,"w");
if(fd_w==-1)
  error("cannot open file for writing")
end

//open data file for summary output
fileout2="pv5_summary_results_2016.txt";
fd_ww=mopen(fileout2,"w");
if(fd_ww==-1)
  error("cannot open file for writing")
end
//write headers to summary file
mfprintf(fd_ww,'%s %s %s %s  %s %s %s %s %s %s  %s  %s %s %s  %s %s %s %s %s %s %s %s %s %s %s %s %s %s %s %s %s\n',"Date", "Panel_Number", "Serial_Number_(SN)", "Module_Brand", "File_Name", "Test_Time", "Panel_Temperature", "Eppley_Insol(W/m2)", "Knees", "Run_a_or_b", "Curve_no", "m", "Se", "r2", "Pmax", "Vmax", "Imax", "Isc_obs", "VOC_obs", "iL", "voc", "ekt", "rs", "rp", "sd_iL", "sd_voc", "sd_ekt", "sd_rs", "sd_rp")

num_read=1;
k=0;
while(num_read>0)
  k=k+1;
  //read data in from "Temporary Clipboard Data.txt"
  [num_read,date_txt,panel,serial,maker,filename,time,temp,Eppley,knee,run,curve]=mfscanf(fd_r,"%s %i %i %s %s %s %f %f %s %s %s");

  // Eppley calibration equation
  insol=Eppley/8.78e-3

  mprintf('\n%s %s %s %s %s %s %s',date_txt,maker,filename,time,knee,run,curve);
  mprintf('\n%i %i %f %f %f',panel,serial,temp,Eppley,insol);

  if(num_read>0)

    //open module data file for input
    fd_rr=mopen(filename,"r");
    if(fd_rr==-1)
      error("cannot open file for reading")
    end

    [num_read,txt1,txt2,txt3,txt4,txt5,date_txt2,time2,ampm]=mfscanf(fd_rr,"%s %s %s %s %s %s %s %s");
    //disp([date_txt2,time2,ampm]);
```

```
    [num_read,txt1,txt2]=mfscanf(fd_rr,"%s %s"); //test dates 6/24 and 8/12 didn't have numbers in the
mini-KLA "comment:" so only txt1 and one %s for those two days...the rest have txt2 and a second %s here
    //disp([txt1]);

[num_read,txt1,txt2,txt3,txt4,txt5,txt6,txt7,txt8,txt9,txt10,txt11,txt12,txt13,txt14,txt15,txt16]=mfscanf(fd_rr
,"%s %s %s %s %s  %s %s %s %s %s  %s %s %s %s %s  %s");

    //disp([txt1,txt2,txt3,txt4,txt5,txt6,txt7,txt8,txt9,txt10,txt11,txt12,txt13,txt14,txt15,txt16]);
    mfprintf(fd_w,'\n\n%s %s',date_txt,time)
    [num_read,vmpp0,impp0,pmpp0,voc0,isc0,insol2,temp2,ff0]=mfscanf(fd_rr,"%f %f %f %f %f %f %f
%f %f");
    mfprintf(fd_w,'\n%f  %f  %f  %f',insol,insol2,temp,temp2);
    mprintf('\n%f  %f  %f  %f  %f  %f  %f  %f',vmpp0,impp0,pmpp0,voc0,isc0,insol2,temp2,ff0);
    //skip blank line and header line
    [num_read,txt1,txt2]=mfscanf(fd_rr,"%s %s");
    [num_read,txt1,txt2]=mfscanf(fd_rr,"%s %s");

    i=0;
    while (num_read>0)
      i=i+1;
      [num_read,xx(i),yy(i)]=mfscanf(fd_rr,"%f %f");
      if(num_read>0)
        //disp([xx(i),yy(i)]);
      end
    end

    mclose(fd_rr); //close module data file

    m=i-1 //number of data points

     //filter the data
    dv=0.05;
    di=0.05;

 // find the starting point for voltages above 5.0V
    for i=1:m
      if(xx(i)<5.0)
        k0=i;
      end
    end
    k0=k0+1

    pv_v_raw(1)=xx(k0);
    pv_i_raw(1)=yy(k0);
    kk=1;
    //mprintf('\n\n%i  %f %f',kk,pv_v_raw(kk),pv_i_raw(kk))

    for i=k0:m
       if(xx(i)-pv_v_raw(kk)>dv)
         kk=kk+1;
         pv_v_raw(kk)=xx(i);
         pv_i_raw(kk)=yy(i);
```

```
    //mprintf('\n%i  %f %f',kk,pv_v_raw(kk),pv_i_raw(kk))
   else
    if(abs(yy(i)-pv_i_raw(kk))>di)
     kk=kk+1;
     pv_v_raw(kk)=xx(i);
     pv_i_raw(kk)=yy(i);
     //mprintf('\n%i  %f %f',kk,pv_v_raw(kk),pv_i_raw(kk))
    end
   end
end
m=kk

 //correct data for insolation and temperature
mod_in_series=1;
voc_raw=pv_v_raw(m);
voc_noct=voc_raw-0.060291*mod_in_series*(47 - temp) + 0.0009296*mod_in_series*(1000-insol);
//-0.06538 and 0.006211 for 2016 Voc coefficients
pv_v=zeros(m,1);
pv_i=zeros(m,1);
for i=1:m
  pv_i(i)=pv_i_raw(i)/insol*1000;
  pv_v(i)=pv_v_raw(i)*voc_noct/voc_raw;
  //mprintf('\n%f  %f  %f  %f',pv_v_raw(i),pv_i_raw(i),pv_v(i),pv_i(i))
end
//[rowi,coli]=size(pv_i);
//[rowv,colv]=size(pv_v);
//mprintf('\n%i  %i  %i',m,rowv,rowi)

//find observed Pmax, Vmax, and Imax
Pmax_obs=-1;
Vmax_obs=-1;
Imax_obs=-1;
for i=1:m
  pp=pv_v(i)*pv_i(i);
  if(pp>Pmax_obs)
    Pmax_obs=pp;
    Vmax_obs=pv_v(i);
    Imax_obs=pv_i(i);
  end
end

//initial parameter guess
//iL=24.55;
iL=pv_i(1);

isc_obs=pv_i(1);
voc_obs=pv_v(m);

//voc=36;
voc=pv_v(m);
ekt=0.7;
rs=.4;
```

```
rp=60;
b0=[iL;voc;ekt;rs;rp];
//disp(b0)
//e=resid(b0,pv_v,pv_i)
//[row,col]=size(e)
//disp([e])

bLL=[2;15;0.1;0.05;15];
bUL=[4;25;5.5;4;3500];
//call leastsq function
[min_ssr,b_opt,grad_opt]=leastsq(list(resid,pv_v,pv_i),"b",bLL,bUL,b0);
//disp(b_opt)

//compute Se & r2
Se=sqrt(min_ssr/(m-p));
Se2=Se^2;

mfprintf(fd_w,'\npanel number, serial number, run, & curve %i  %i  %s  %s',panel,serial,run,curve)

mfprintf(fd_w,'\nsample_size %i',m)
format('v',4);
mfprintf(fd_w,'\nstandard_error(Amps) %f',Se)

pv_i_pred=pv5(pv_v,b_opt);
mean_pred_i=mean(pv_i_pred);
mean_obs_i=mean(pv_i);
explained=sum((pv_i_pred-mean_obs_i).^2);
mean_obs_i=mean(pv_i);
total=sum((pv_i-mean_obs_i).^2);
r2=explained/total;
format('v',4);
mfprintf(fd_w,'\nr2 %f',r2)

vv=linspace(0,b_opt(2),100)';
pv_i_plot=pv5(vv,b_opt);

//find predicted Pmax, Vmax, and Imax
Pmax_pr=-1;
Vmax_pr=-1;
Imax_pr=-1;
for i=1:100
  pp=vv(i)*pv_i_plot(i);
  if(pp>Pmax_pr)
    Pmax_pr=pp;
    Vmax_pr=vv(i);
    Imax_pr=pv_i_plot(i);
  end
end
mfprintf(fd_w,'\nObserved_and_Predicted_Pmax %f  %f',Pmax_obs,Pmax_pr)
mfprintf(fd_w,'\nObserved_and_Predicted_Vmax %f  %f',Vmax_obs,Vmax_pr)
mfprintf(fd_w,'\nObserved_and_Predicted_Imax %f  %f',Imax_obs,Imax_pr)
```

```
    //plot the observed and the predicted curves
    clf(k)
    scf(k)
    plot2d(vv,pv_i_plot,style=2,rect=[0,0,25,3.5]);
    plot2d(pv_v,pv_i,style=-5,rect=[0,0,25,3.5]);
    plot2d(Vmax_pr,Imax_pr,style=-3,rect=[0,0,25,3.5]);
    plot2d(Vmax_obs,Imax_obs,style=-4,rect=[0,0,25,3.5]);
    legend(["predicted values","observed values"]);
    plot_title=filename+"_"+run+"_"+curve
    xtitle( plot_title,"Voltage","Current");
    //plotname="plot_"+serial+"_"+string(run)+"_"+panel+"_"+string(mon)+"-"+string(day)+"-
"+string(10)+".jpg";
    //xs2jpg(k,plotname);
    //*****************************************

    J=numderivative(resid,b_opt);
    JT=J.';
    JTJ=JT*J;
    JTJinv=inv(JTJ);
    cov_matrix=Se2*JTJinv;
    sd2=diag(cov_matrix);
    sd=sqrt(sd2);

    //mprintf('\n%i %f %f %f %f %f %f %f %f %f %f %f', sa, b_opt(1), b_opt(2), b_opt(3),
b_opt(4), b_opt(5), sd(1), sd(2), sd(3), sd(4), sd(5), Se)

    mfprintf(fd_w,'\n\n%s %s %s %s %s %s %s
\n','name','coef','SD','t','p','LL','UL')
    conf_level=0.95;
    plevel=(1-conf_level)/2;
    t=cdft("T",m-p,1-plevel,plevel);
    LL=b_opt-t*sd;
    UL=b_opt+t*sd;
    for i=1:p
      tval=b_opt(i)/sd(i);
      [pv,qv]=cdft("PQ",1-tval,m-p);
      pval=pv;
      mfprintf(fd_w,'%s %f %f %f %e %f %f \n',name(i),b_opt(i),sd(i),tval,pval,LL(i),UL(i))
    end

     //write to summary file
     mfprintf(fd_ww,'%s %i %i %s %s %s %f %f %s %s %s %i %f %f %f %f %f %f %f %f
%f %f %f %f %e %e %e %e %e \n',date_txt,panel,serial,maker,filename, time, temp,
insol,knee,run,curve, m, Se, r2, Pmax_obs, Vmax_obs, Imax_obs, isc_obs, voc_obs, b_opt(1), b_opt(2),
b_opt(3), b_opt(4), b_opt(5), sd(1), sd(2), sd(3), sd(4), sd(5))

    for i=1:p
      for j=1:p
        cor(i,j)=cov_matrix(i,j)/(sd(i)*sd(j));
      end
    end
    format('v',7);cor;
```

```
    mfprintf(fd_w,'\n\n Correlation_Matrix_for_Parameter_Estimates')
    for i=1:p
      mfprintf(fd_w,'\n%s  %f  %f  %f  %f  %f \n',name(i),cor(i,1),cor(i,2),cor(i,3),cor(i,4),cor(i,5))
    end

    pv_i_pred=pv5(pv_v,b_opt);
    e=resid(b_opt,pv_v,pv_i);

    mfprintf(fd_w,'\n\n%s    %s     %s       %s          %s',
"i","Obs_V(Volts)","Obs_I(Amps)","Pred_I","Residual")
    for i=1:m
      mfprintf(fd_w,'\n%i  %f  %f  %f  %f',i,pv_v(i),pv_i(i),pv_i_pred(i),e(i))
    end
    mfprintf(fd_w,'\n\n%s'," ")

  else
    mclose(fd_r); //close file name list
  end //end if statement
  num_read=1;

end  //end "while" for file name list loop

mclose(fd_w); //close regression results output data file
mclose(fd_ww); //close summary results output data file
```

Appendix C: Photos of Modules

This Appendix has a sample of the photos taken of each module during testing. As there are 192 modules, there are 192 images. The complete collection of these pictures will accompany the submission of this thesis in a digital form, but they are not all included in this Appendix. The sample of images shown here envelope the range of physical degradation experienced and witnessed in the modules over 26 years. When a picture is of a module younger than that, the caption details the age of the module. The first image (Figure C - 1) is of one of the four Siemens replacement modules, which aged much better, and the rest (Figure C - 2 to Figure C - 12) are of ARCO M75 modules.

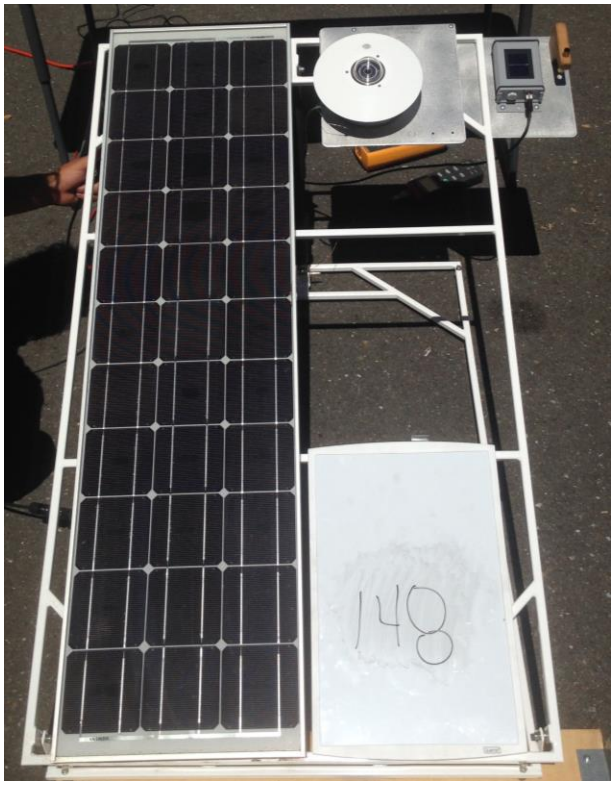

Figure C - 1: First Siemens replacement (module 148), roughly 19 years old in 2016

These next few images show the original ARCO modules that aged the most gracefully after over 25 years of field exposure. Module 054 (Figure C - 2) shows very little evidence of physical degradation besides a little browning of the cells, which was the most common degradation seen in these ARCO modules. Module 132 (Figure C - 3) also aged relatively well but with complete cell browning.

Figure C - 2: Module 054 aged much better than the average ARCO M75 module

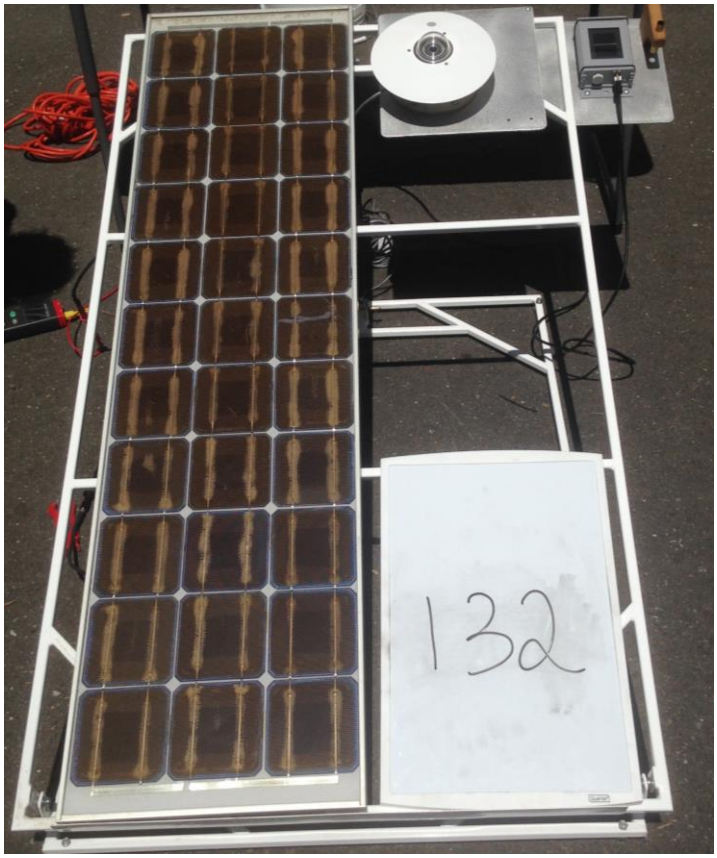

Figure C - 3: Module 132 shows complete cell browning of the module with out other types of degradation present

The next collection of pictures shows the worst modules in terms of performance, but they do not particular portray the worst looking modules. Module 015 (Figure C - 4) produced the worst IV curve, of the modules that produced IV curves, in 2016 and generated only 24 W. Module 161 (Figure C - 5) was the worst performing module in 1990, and in 2016 it generated slightly below the average power output. Module 078 (Figure C - 6), generating only 1.8 W with an essentially linear IV curve, was the worst module to survive 25.5 years of field exposure.

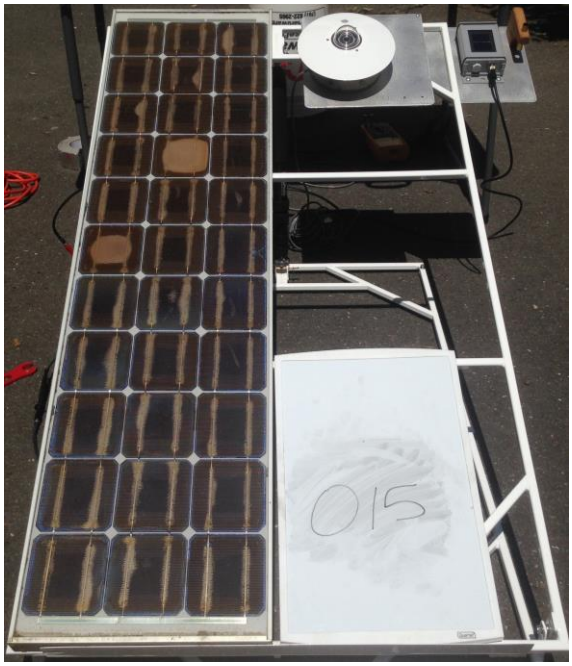

Figure C - 4: Module 015 produced the worst recognizable IV curve in 2016

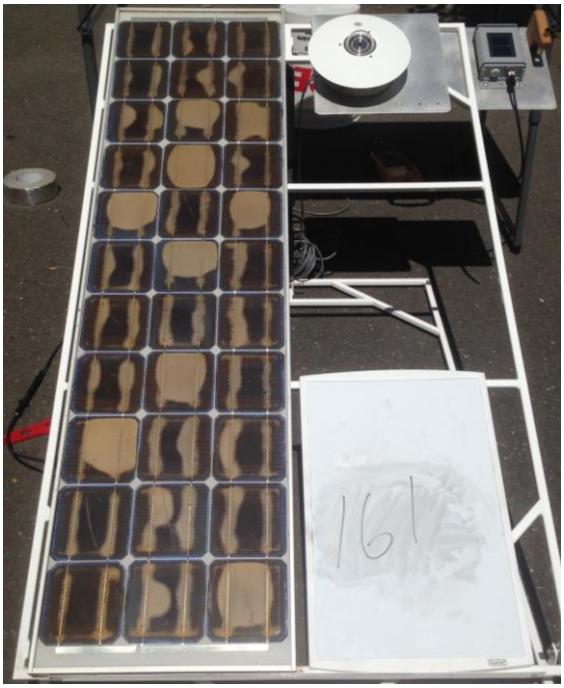

Figure C - 5: Module 161 was the lowest performer in 1990 but was average in 2016

Figure C - 6: While it did not physically age dramatically, module 078 had the lowest power production of all the modules tested in 2016 (1.8 W) — possibly due to bypass diodes or the almost completely delaminated cell in the center string

While the previous pictures showed the poorest performing modules, this next set shows the modules that experienced the worst physical degradation, such delamination and hot spots. The delamination between the EVA and the cells was the second most common degradation of these modules, behind cell browning, and hot spots were the third most common sighting. Hot spots were less common than the other two degradation types in this array. Module 103 (Figure C - 7) shows the highest count of delaminated cells found on one module, and module 059 (Figure C - 8) adequately highlights the stages of cell delamination, as the process starts in the current-carrying strings and then grows together to create a square or circle of delamination that takes up the entire cell.

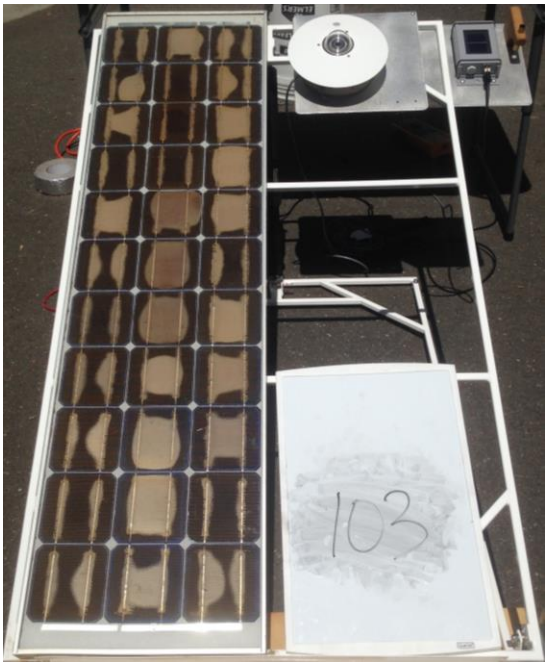

Figure C - 7: Module 103 shows the largest presence of delamination in the data set

Figure C - 8: Module 059 exhibiting the stages of the delamination process

Module 026 shows a more typical example of the hot spots that occurred in the ARCO modules (5th cell from the bottom on the furthest string to the right in Figure C - 9), while module 045 (Figure C - 10) shows to largest and worst instance of hot spots from this array. As reported in the body of this thesis, the hot spots occur due to elevated current in the cell that creates a local thermal increased that burns the crystalline cell.

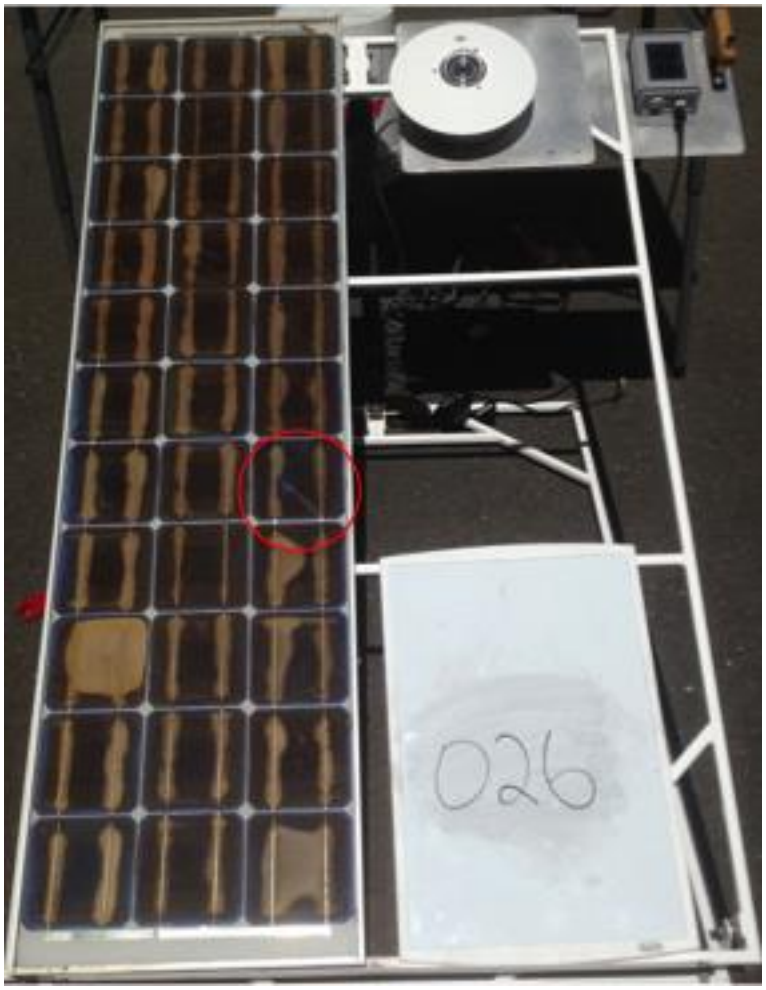

Figure C - 9: Module 026 with a basic example of hot spots seen in this array

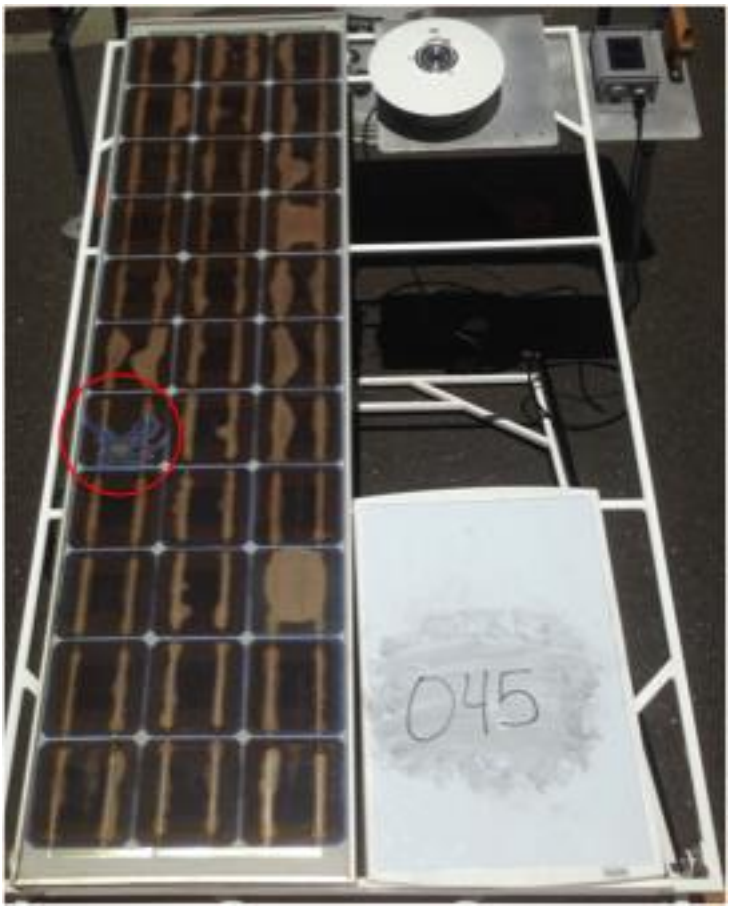

Figure C - 10: Module 045 experienced the worst hot spot seen in the array

These last module images are of the highest testing modules. Module 124 (Figure C - 11) was the most productive module in the original 1990 testing, but by 2016 its performance was close to the average of the array. Module 160 (Figure C - 12), generating about 37 W in 2016, had the highest output of any module from this project, and its lack of physical degradation supports the results. However, this comparison is not as applicable to the worst modules because the lowest performers, modules 078 and 044 (Figure 36), look much better than others, such as modules 045 or 103, shown earlier.

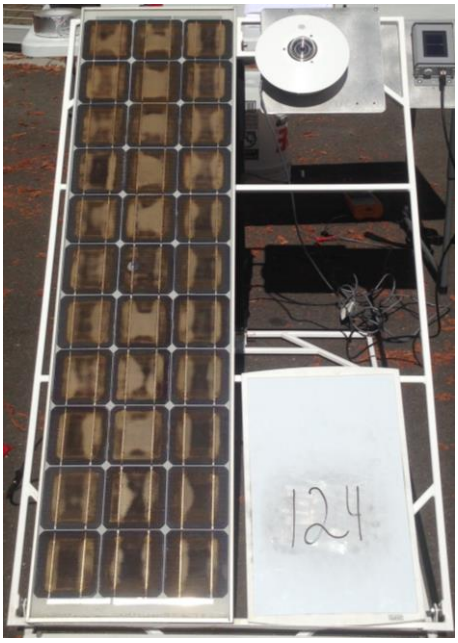

Figure C - 11: Module 124, with the highest module output in 1990, was average in 2016

Figure C - 12: Module 160 is the highest performing module in 2016 (37 W)

Appendix D: Clipboard Recording

This Appendix shows a brief example of the data recorded externally of the Mini-KLA, which includes the date, module number (1-192), manufacturer-assigned serial number, test time, module temperature reading from the thermocouple reader, insolation reading from the Eppley PSP (in millivolts), the number of knees perceived in the initial Mini-KLA graphical display of the IV curve, verification that a photo of the module was taken, the run on that specific module (a, b, c, d, e, f), the curve number assigned by the Mini-KLA, and finally any comments about the module or explanations why certain curve numbers were thrown out. Figure D - 1 shows an example of this clipboard data from July 26, 2016, and Figure D - 2 shows the recordings from August 3, 2016. This information was recorded for every test during all 17 days of testing, but all of those will not be included in entirety in this Appendix due to the similarity in their appearance. For the Scilab code, additional columns were created to identify the module brand (ARCO or Siemens) and the filename for the output of the code for each respective module test (i.e., "Module167b.asc"), and the comments and photo check columns were unnecessary for the code and were removed.

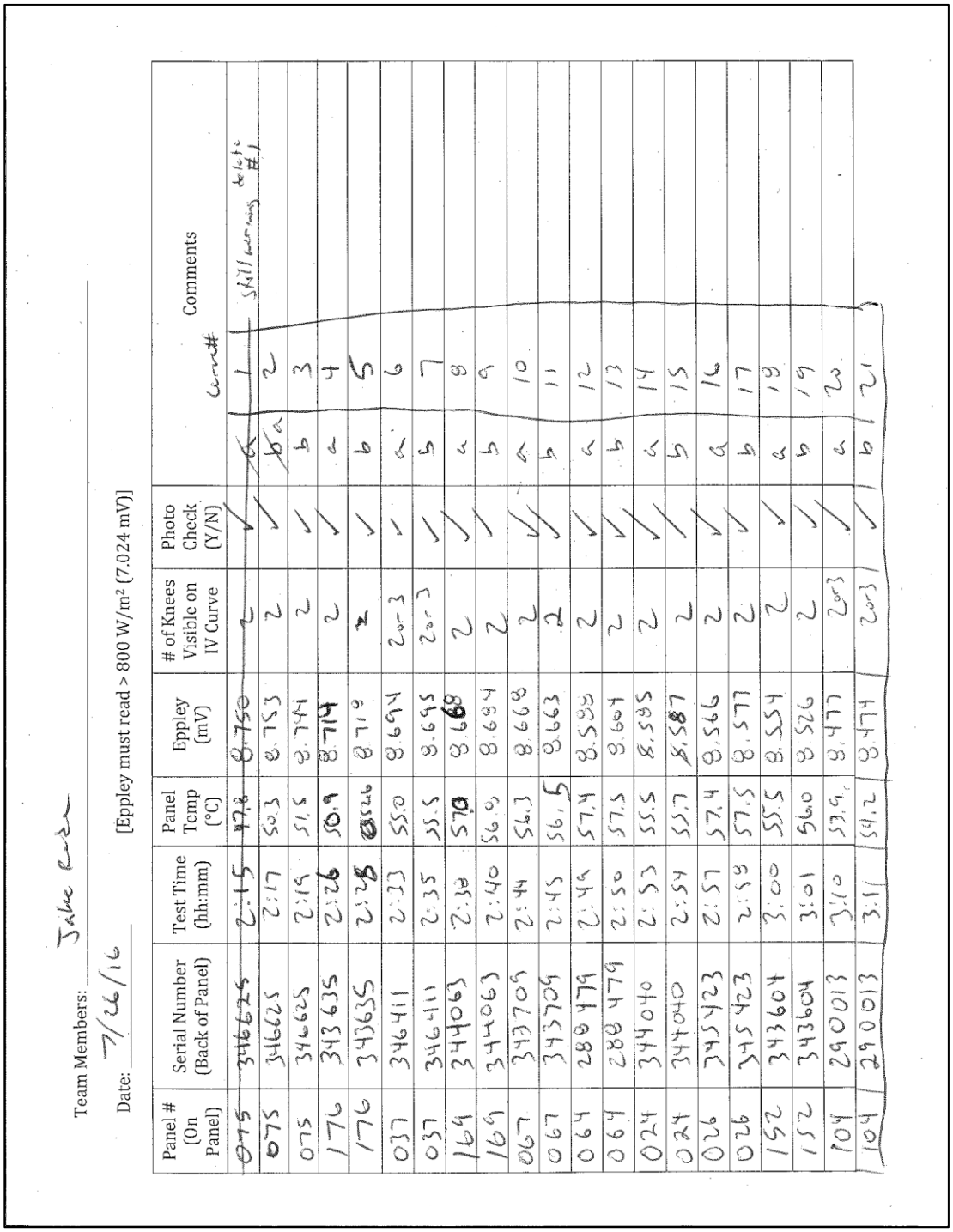

Team Members: Jake Cox

Date: 7/26/16

[Eppley must read > 800 W/m² (7.024 mV)]

Panel # (On Panel)	Serial Number (Back of Panel)	Test Time (hh:mm)	Panel Temp (°C)	Eppley (mV)	# of Knees Visible on IV Curve	Photo Check (Y/N)	Comments: curve#	Comments
~~075~~	~~346625~~	~~2:15~~	~~47.8~~	~~8.750~~	~~2~~	✓	~~1~~	~~Skill issues delete #1~~
075	346625	2:17	50.3	8.753	2	✓	2	
075	346625	2:19	51.5	8.744	2	✓	3	
176	343635	2:26	50.9	8.714	2	✓	4	
176	343635	2:28	52.6	8.719	2	✓	5	
037	346411	2:33	55.0	8.694	2or3	✓	6	
037	346411	2:35	55.5	8.695	2or3	✓	7	
169	344093	2:38	57.0	8.669	2	✓	8	
169	344093	2:40	56.6	8.694	2	✓	9	
067	343709	2:44	54.1	8.668	2	✓	10	
067	343709	2:45	56.5	8.663	2	✓	11	
064	289479	2:48	57.4	8.585	2	✓	12	
064	289479	2:50	57.5	8.604	2	✓	13	
024	344040	2:53	55.5	8.585	2	✓	14	
024	344040	2:54	57.7	8.587	2	✓	15	
026	345423	2:57	57.4	8.546	2	✓	16	
026	345423	2:58	57.5	8.577	2	✓	17	
152	343604	3:00	55.5	8.554	2	✓	18	
152	343604	3:01	56.0	8.526	2	✓	19	
104	290013	3:10	53.9	8.477	2or3	✓	20	
104	290013	3:11	54.2	8.474	2or3	✓	21	

Figure D - 1: Example image from July 26, 2016 of the clipboard data taken externally of the Mini-KLA, complete with comments explaining why the first test was discarded

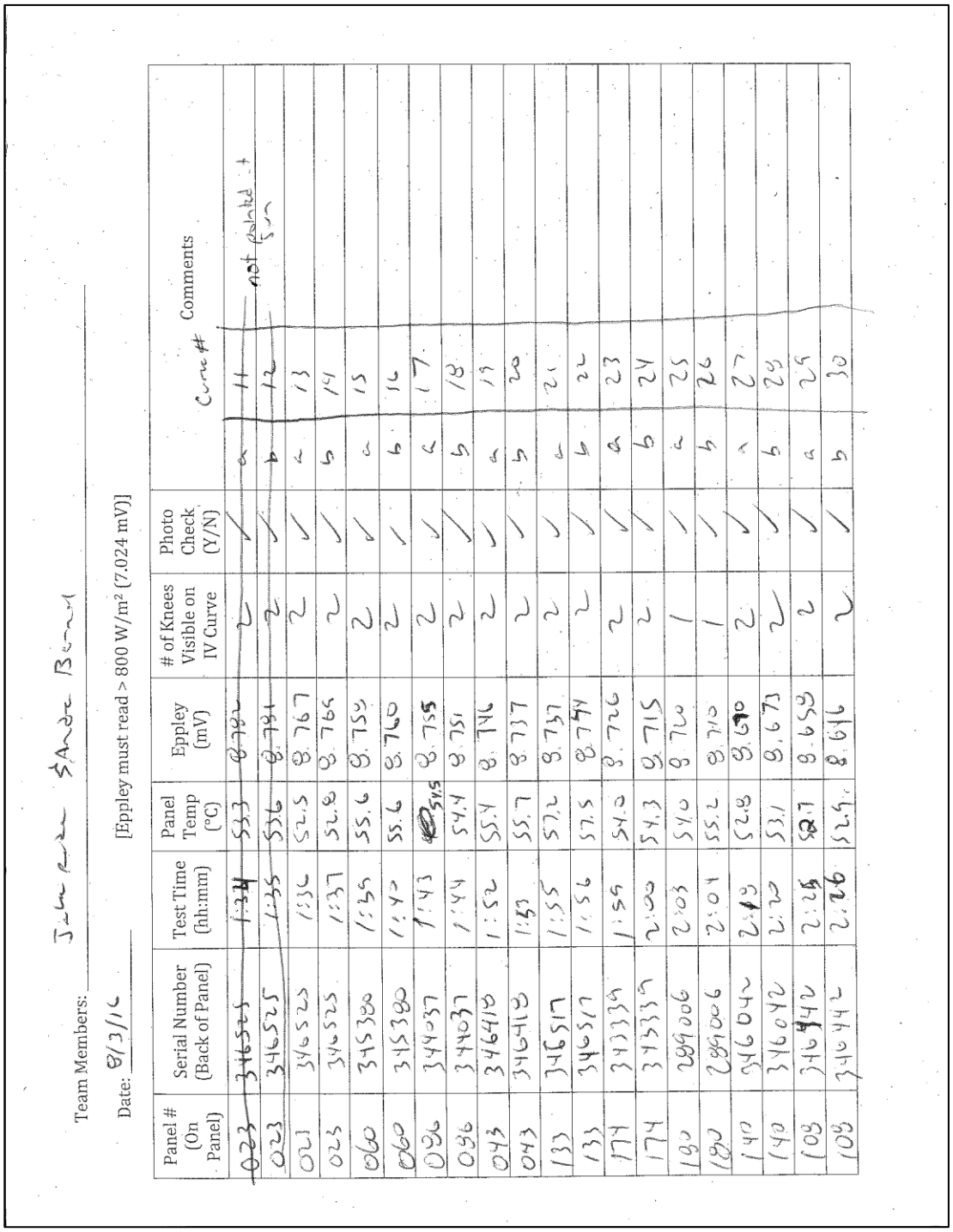

Team Members: Jim and Sandy Bean

Date: 8/3/16 [Eppley must read > 800 W/m² (7.024 mV)]

Panel # (On Panel)	Serial Number (Back of Panel)	Test Time (hh:mm)	Panel Temp (°C)	Eppley (mV)	# of Knees Visible on IV Curve	Photo Check (Y/N)	Curve #	Comments
023	346525	1:34	53.3	8.792	2	✓	11	not packed +
023	346525	1:35	53.6	8.791	2	✓	12	Sun
021	346523	1:36	52.5	8.767	2	✓	13	
023	346525	1:37	52.8	8.764	2	✓	14	
020	345380	1:39	55.6	8.755	2	✓	15	
020	345380	1:40	55.6	8.760	2	✓	16	
026	344037	1:43	56.5	8.755	2	✓	17	
026	344037	1:44	54.4	8.751	2	✓	18	
043	346418	1:52	55.7	8.746	2	✓	19	
043	346418	1:53	55.7	8.737	2	✓	20	
133	346517	1:55	57.2	8.737	2	✓	21	
133	346517	1:56	57.5	8.734	2	✓	22	
174	343334	1:59	54.2	8.726	2	✓	23	
174	343336	2:00	54.3	8.715	2	✓	24	
190	296006	2:03	54.0	8.710	1	✓	25	
190	296006	2:04	55.2	8.710	1	✓	26	
140	346042	2:09	52.8	8.690	2	✓	27	
140	346042	2:10	53.1	8.673	2	✓	28	
109	346442	2:25	53.7	8.659	2	✓	29	
109	346442	2:26	52.9	8.616	2	✓	30	

Figure D - 2: Example image from August 3, 2016 of the clipboard data taken externally of the Mini-KLA, complete with reasons why the first two tests needed to be deleted

Appendix E: Scilab Code Output

The output from the Scilab code came in three forms, a summary file for all of the module tests inputted for that day of testing, a regression file for every inputted test, and an IV curve for each of the tests.

The summary file reproduced the information from the clipboard data in Appendix D, and added to it the number of iterations the code ran (m), standard error, the r-squared value showing the finally degree of accuracy, P_{max}, V_{mp}, I_{mp}, I_{sc}_obs, and V_{oc}_obs. The P_{max} here is what was used to compare the loss of power in the modules to the previous testing cycles' results. The I_{sc}_obs and V_{oc}_obs were the initial guesses that the code used when analyzing the data. Following this data came the five IV curve parameters (I_L, V_{oc}, ekt, R_s, and R_p) and the standard deviations associated with the calculations for those five parameters. The I_L and V_{oc} presented here represent the I_{sc} and V_{oc} used to compare the modules, as opposed to the initial guesses mentioned earlier. Because this summary file was not designed to fit into a typical Word document, an example summary file for Modules 026, 037, and 064 from July 26th, 2016 (both runs "a" and "b") are shown in Table E - 1 to Table E - 4. Keep in mind that this data came in one continuous form from Scilab. The updated 2016 parameter limits are also present in these tables.

Table E - 1: Part one of four tables showing the Scilab summary file output

Module	**Run**	**m**	**Se**	**r^2**
026	a	118	0.043679	0.997423
026	b	111	0.040004	0.996516
037	a	119	0.067807	0.993919
037	b	118	0.066084	0.995157
064	a	110	0.053845	0.995551
064	b	113	0.056034	0.994849

Table E - 2: Part two of four tables showing the Scilab summary file output

Module	**Run**	**P_{max}**	**V_{mp}**	**I_{mp}**	**I_{sc}_obs**	**V_{oc}_obs**
026	a	28.561305	13.287475	2.149491	2.417421	18.125385
026	b	29.611183	13.806764	2.144687	2.438684	18.101049
037	a	26.803258	11.892069	2.253877	2.857792	18.156934
037	b	26.826024	11.137517	2.408618	2.858473	18.194273
064	a	31.03949	14.805775	2.096445	2.403152	18.174155
064	b	31.114295	14.826449	2.098567	2.398683	18.112789

Table E - 3: Part three of four tables showing the Scilab summary file output

Module	Run	I_L	V_{oc}	ekt	R_s	R_p
026	a	2.611363	18.020661	1.361325	1.208173	39.319926
026	b	2.529459	18.084558	2.014995	1.347732	60.00524
037	a	2.937872	18.425255	0.509536	1.715115	636.083014
037	b	3.108383	18.20764	0.191437	0.073918	3500
064	a	2.676599	18.119044	3.633782	1.099772	29.670829
064	b	2.667242	18.112507	3.200149	1.067996	30.062536

Table E - 4: Part four of four tables showing the Scilab summary file output

Module	Run	sd_I_L	sd_V_{oc}	sd_ekt	sd_R_s	sd_R_p
026	a	4.53E-02	1.85E-02	1.75E-01	7.45E-02	5.87E+00
026	b	3.52E-02	1.91E-02	2.02E-01	4.49E-02	1.01E+01
037	a	5.81E-01	5.79E-02	2.66E-01	3.48E-01	2.50E+04
037	b	2.52E-01	4.65E-02	1.71E-01	9.16E-01	1.11E+06
064	a	3.87E-02	2.12E-02	8.15E-01	6.31E-02	2.59E+00
064	b	4.09E-02	2.34E-02	6.49E-01	6.59E-02	2.86E+00

The regression file shows the iteration process that the Scilab code goes through to determine the correct values of the variables needed to analyze the modules' performance (five IV curve parameters). Many of these are also reported in the summary file, as the earlier examples showed. Table E - 5 exhibits these iterations for the "b" run of module 064, which was a part of the example summary files. The "i" here is the same

as “m” in the summary tables. The observed voltages and currents help find the predicted currents, and the residuals, or difference between the prediction and the new solution, are minimized until a satisfactory current-voltage relationship is determined.

Table E - 5: Iteration process of Scilab code produced by the regression file

i	Obs_V(Volts)	Obs_I(Amps)	Pred_I	Residual
1	5.346048	2.398683	2.352829	-0.045853
2	5.580795	2.398683	2.34822	-0.050463
3	5.671664	2.38654	2.346435	-0.040104
4	5.754961	2.384499	2.344799	-0.039699
5	5.81554	2.383478	2.34361	-0.039868
6	6.216777	2.389601	2.335731	-0.05387
7	6.322791	2.38256	2.333649	-0.048911
8	6.549965	2.38256	2.329188	-0.053372
9	6.708986	2.378478	2.326065	-0.052413
10	6.777138	2.373376	2.324727	-0.048649
11	6.966449	2.370416	2.321009	-0.049407
12	7.072464	2.362355	2.318927	-0.043428
13	7.292065	2.360314	2.314615	-0.045699
14	7.428369	2.352252	2.311938	-0.040314
15	7.746412	2.343068	2.305693	-0.037375
16	7.844854	2.326945	2.303759	-0.023185
17	7.988731	2.324904	2.300934	-0.02397

i	Obs_V(Volts)	Obs_I(Amps)	Pred_I	Residual
18	8.102318	2.313781	2.298703	-0.015078
19	8.291629	2.30674	2.294986	-0.011754
20	8.496085	2.308781	2.29097	-0.01781
21	8.57181	2.291535	2.289483	-0.002052
22	8.639961	2.286535	2.288145	0.00161
23	8.806556	2.287555	2.284873	-0.002682
24	9.026157	2.275412	2.28056	0.005148
25	9.359345	2.273371	2.274016	0.000645
26	9.419925	2.256227	2.272826	0.016598
27	9.472932	2.251125	2.271784	0.020659
28	9.647098	2.256227	2.268363	0.012135
29	9.881741	2.248166	2.263752	0.015586
30	10.078624	2.242043	2.259881	0.017838
31	10.320943	2.237043	2.255115	0.018072
32	10.517826	2.2299	2.251239	0.02134
33	10.752572	2.219797	2.246612	0.026815
34	10.919167	2.205715	2.24331	0.037595
35	10.972174	2.210715	2.242261	0.031546
36	11.282645	2.204694	2.236091	0.031397
37	11.335652	2.192551	2.235033	0.042482
38	11.388659	2.197653	2.233972	0.036319
39	11.471956	2.184489	2.232302	0.047812

i	Obs_V(Volts)	Obs_I(Amps)	Pred_I	Residual
40	11.585543	2.183469	2.230013	0.046544
41	11.721847	2.18653	2.227248	0.040718
42	11.774854	2.18653	2.226166	0.039635
43	12.153476	2.182448	2.218269	0.03582
44	12.289781	2.169284	2.215322	0.046038
45	12.38065	2.169284	2.213314	0.044029
46	12.653258	2.170305	2.206991	0.036686
47	12.978874	2.158162	2.198515	0.040354
48	13.21362	2.153161	2.191347	0.038186
49	13.281772	2.148059	2.189023	0.040964
50	13.349924	2.1451	2.186562	0.041463
51	13.516518	2.149079	2.179852	0.030773
52	13.766305	2.147141	2.1673	0.02016
53	13.849603	2.137956	2.16223	0.024273
54	13.978334	2.133977	2.153271	0.019294
55	14.160073	2.137956	2.137749	-0.000207
56	14.402392	2.132956	2.110186	-0.02277
57	14.629565	2.123874	2.074896	-0.048979
58	14.826449	2.098567	2.034962	-0.063605
59	15.04605	2.061218	1.978318	-0.082901
60	15.01576	1.995501	1.986947	-0.008554
61	15.091485	1.976316	1.964865	-0.011451

i	Obs_V(Volts)	Obs_I(Amps)	Pred_I	Residual
62	15.144492	1.935906	1.94839	0.012483
63	15.242934	1.914681	1.91552	0.000839
64	15.35652	1.877332	1.873888	-0.003444
65	15.394383	1.824779	1.859125	0.034346
66	15.462535	1.808656	1.831437	0.022781
67	15.545832	1.756102	1.795668	0.039565
68	15.636701	1.733856	1.754264	0.020408
69	15.697281	1.71161	1.725309	0.013699
70	15.856302	1.691405	1.644329	-0.047076
71	16.045614	1.642934	1.539053	-0.103881
72	16.007751	1.569155	1.560842	-0.008312
73	16.015324	1.51456	1.556513	0.041952
74	16.303078	1.471089	1.3819	-0.089188
75	16.166773	1.413535	1.466992	0.053457
76	16.242498	1.39231	1.420225	0.027915
77	16.409091	1.375166	1.312978	-0.062188
78	16.507533	1.319551	1.246979	-0.072573
79	16.386374	1.251895	1.32794	0.076046
80	16.719562	1.233731	1.098836	-0.134895
81	16.522678	1.182198	1.236662	0.054464
82	16.674127	1.163013	1.131231	-0.031782
83	16.62112	1.095255	1.168588	0.073333

i	Obs_V(Volts)	Obs_I(Amps)	Pred_I	Residual
84	16.727134	1.078111	1.093404	0.015293
85	16.893729	1.018517	0.971631	-0.046886
86	16.871011	0.956881	0.988483	0.031602
87	16.969453	0.940656	0.914923	-0.025733
88	17.075467	0.895246	0.834213	-0.061033
89	17.105756	0.831569	0.810883	-0.020687
90	17.211772	0.813405	0.728327	-0.085078
91	17.083039	0.742688	0.828391	0.085704
92	17.295069	0.728503	0.662528	-0.065975
93	17.348076	0.673909	0.62025	-0.053659
94	17.453987	0.617376	0.534873	-0.082503
95	17.151192	0.55972	0.77567	0.21595
96	17.310214	0.550638	0.65048	0.099842
97	17.506994	0.534515	0.491712	-0.042803
98	17.597864	0.497166	0.417084	-0.080082
99	17.393511	0.440531	0.583768	0.143237
100	17.476704	0.429408	0.51641	0.087002
101	17.643297	0.423387	0.379482	-0.043905
102	17.628153	0.359711	0.392037	0.032326
103	17.794746	0.321341	0.25282	-0.068521
104	17.862898	0.302157	0.195193	-0.106963
105	17.597864	0.24246	0.417084	0.174624

i	Obs_V(Volts)	Obs_I(Amps)	Pred_I	Residual
106	17.923479	0.248583	0.14366	-0.104923
107	17.696306	0.193989	0.335377	0.141389
108	17.900762	0.19603	0.163018	-0.033011
109	17.741739	0.139394	0.297376	0.157982
110	17.878044	0.138374	0.182336	0.043963
111	17.976486	0.126332	0.098338	-0.027994
112	18.037065	0.085922	0.046287	-0.039635
113	18.112789	0.042451	-0.019147	-0.061597

The final output from the Scilab code is an IV curve for each test. Figure E - 1 to Figure E - 4 show the graphs created for both tests on modules 026 and 064, the same modules used as examples previously in this Appendix, as examples of the IV curves from the code. Note that these show the 5 V cutoff that eliminates the second knee caused by the bypass diodes that existed in all of the modules in the 2016 testing, and the darker dot in these curves represents the maximum power point.

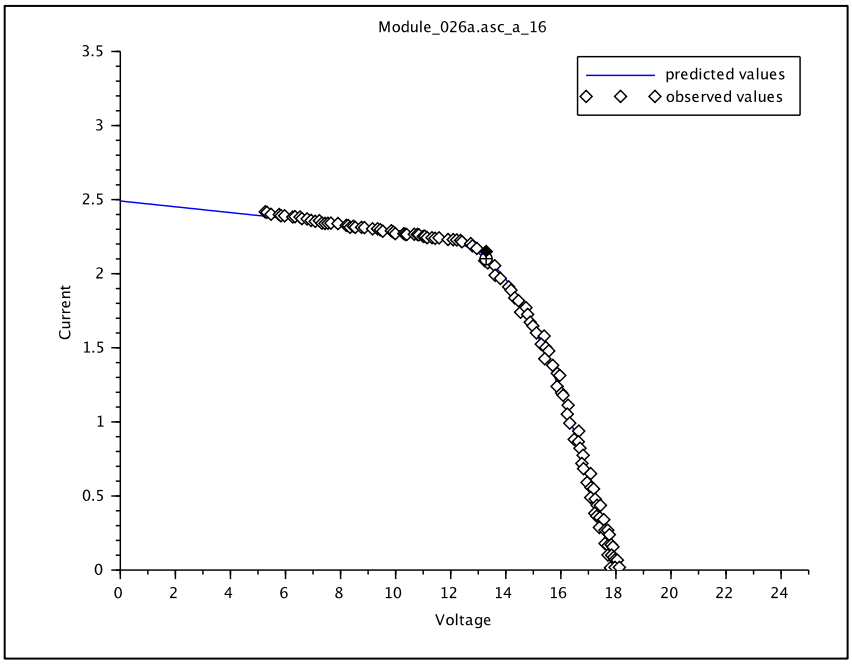

Figure E - 1: Scilab curve for test "a" of module 026

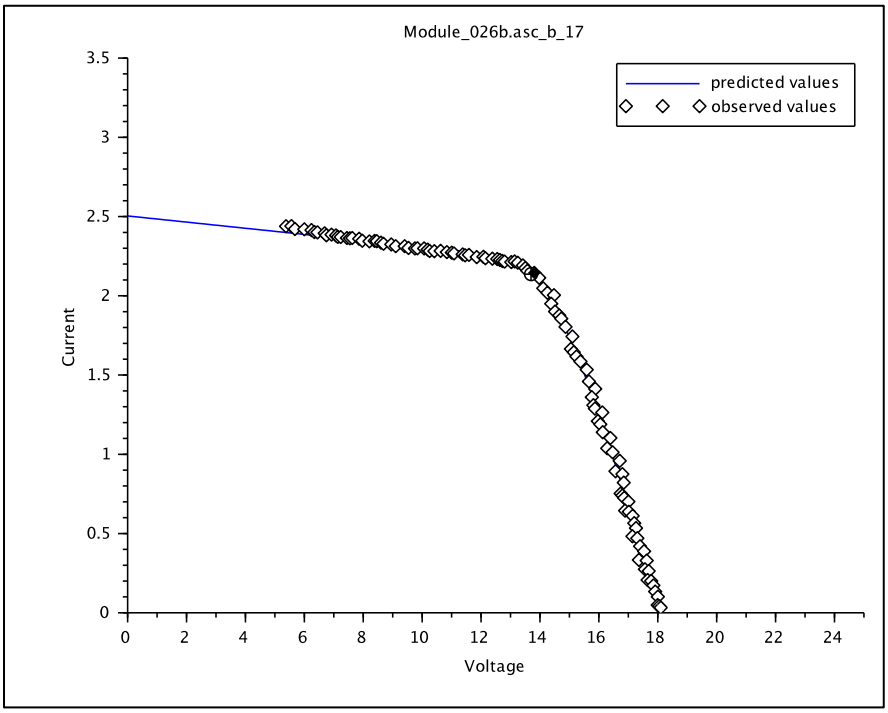

Figure E - 2: Scilab IV curve for test "b" of module 026

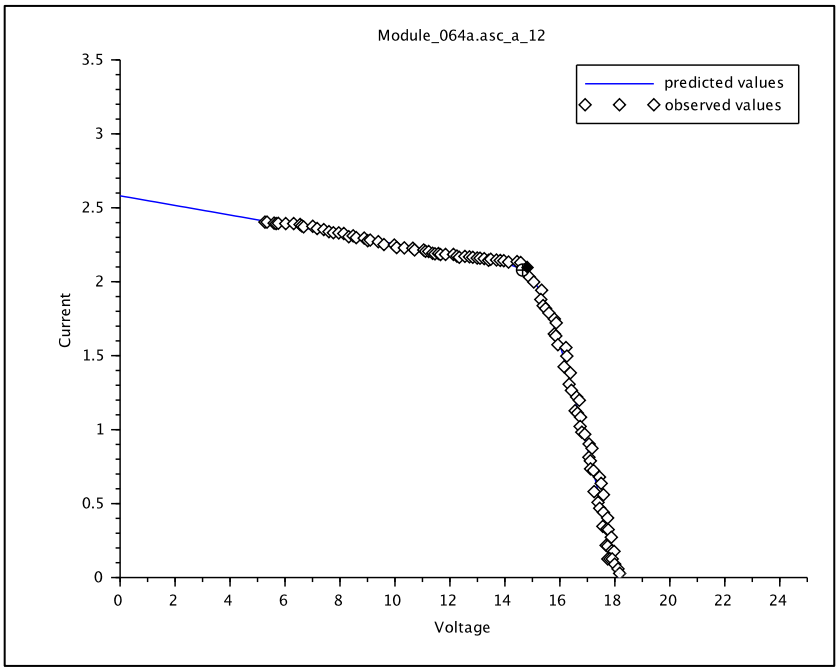

Figure E - 3: Scilab IV curve for test "a" of module 064

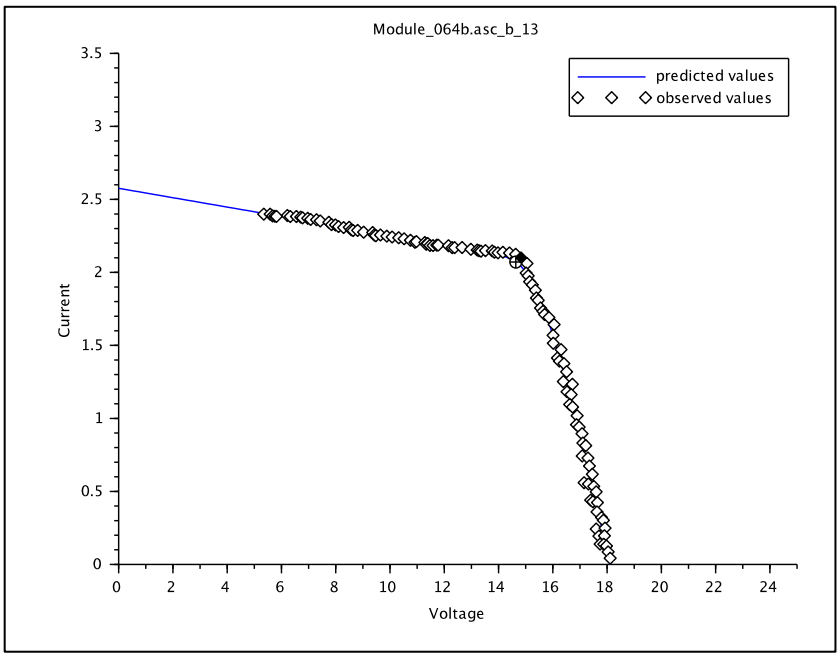

Figure E - 4: Scilab IV curve for test "b" of module 064

Appendix F: Excel Analysis For Pooly Performing

The Scilab code produced such poor IV curves for five modules (seven tests, not including the one bad test of module 118 without its diodes) throughout the 2016 testing (tests 023a, 044a&b, 051a, 078a&b, and 111a) that an Excel model was created to attempt to retrieve better data for the analysis of those modules. The "Solver" tool in Excel is used to adjust the five IV curve parameters to minimize the residuals, or differences, between the current-voltage data from the regression file and the Excel model's new estimations. As an example of this spreadsheet analysis, Table F - 1 and Figure F - 1 are the two primary results from this Excel model for test "a" on module 023. The model is a five-parameter model and, therefore, only models the main IV curve, not the second knee that is present in the curve below 5 V. This is done to match the way the Scilab code approached the IV curve modeling. Table F - 1 shows the results of the Excel model after the Solver has minimized the residuals, complete with parameter estimates, the standard deviations, the t-value (estimate divided by the standard deviation), and the upper (UL) and lower (LL) limits based on a 95% confidence interval. Figure F - 1 shows the IV curve that the model produces, highlighting how accurate it is. The R-squared value, where 1.0 is perfect, is also used in this model to confirm the accuracy, and for this test that value is 0.9904. The rest of this IV curve Excel model for this test, as well as the other seven tests, will be digitally submitted with this paper.

Table F - 1: IV curve parameter results from Excel model for module 023

Parameter	Estimate	St Dev	t = est/SD	LL 95%	UL 95%
I_L (A)	2.464263443	0.031776393	77.55	2.402	2.527
V_{oc} (V)	17.98242447	0.170024117	105.76	17.647	18.318
ekT (1/V)	2.626641276	0.475413317	5.52	1.688	3.565
R_s (Ohm)	2.320528198	0.148687329	15.61	2.027	2.614
R_p (Ohm)	149.1094855	51.69903866	2.88	47	251.160

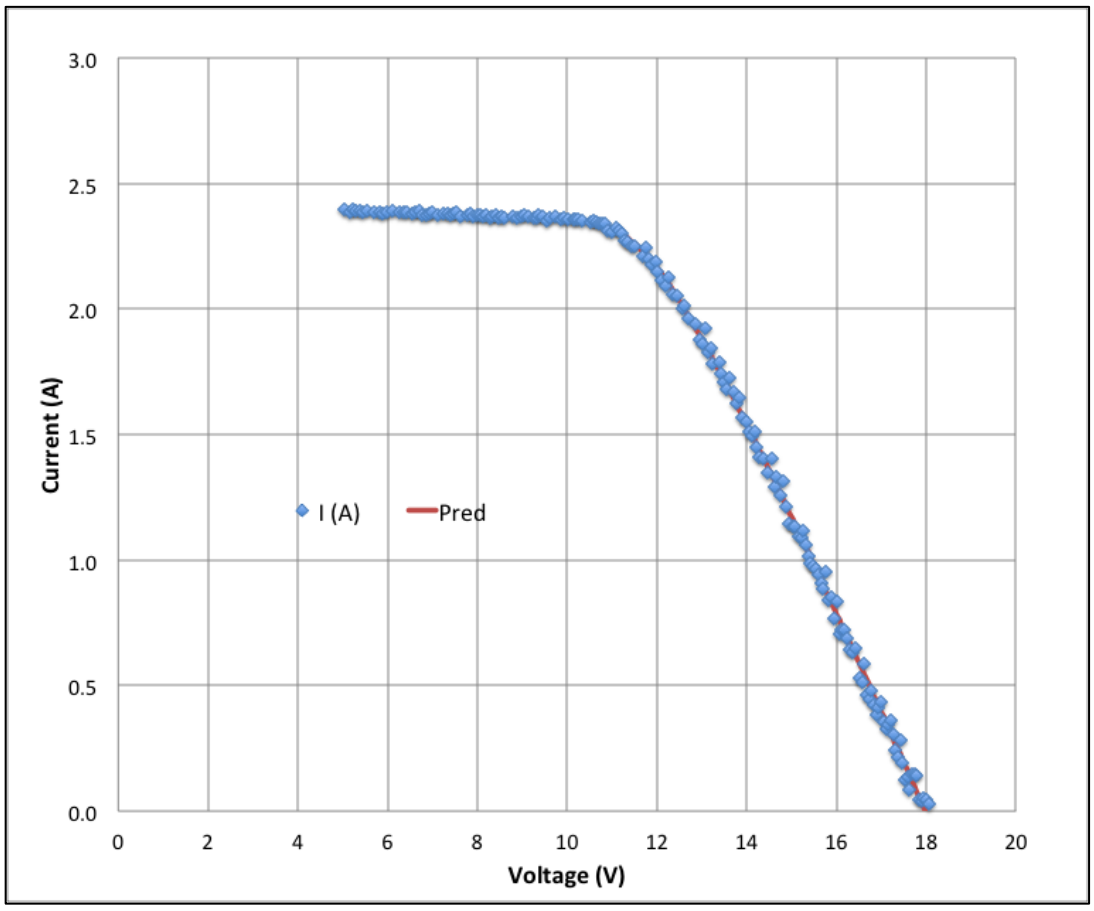

Figure F - 1: Excel-modeled IV curve for module 023a that Scilab couldn't model

Appendix G: Extra Figures For Results

This section contains additional graphs that were created for analysis but were not pertinent to the focus of the thesis (Figure G - 1 to Figure G - 16). These first graphs are probability curves for V_{oc} (Figure G - 1), I_{sc} (Figure G - 2), V_{mp} (Figure G - 3), and I_{mp} (Figure G - 4) over the course of the project. The voltages hardly changed, while the current in the modules saw much more dramatic changes over time.

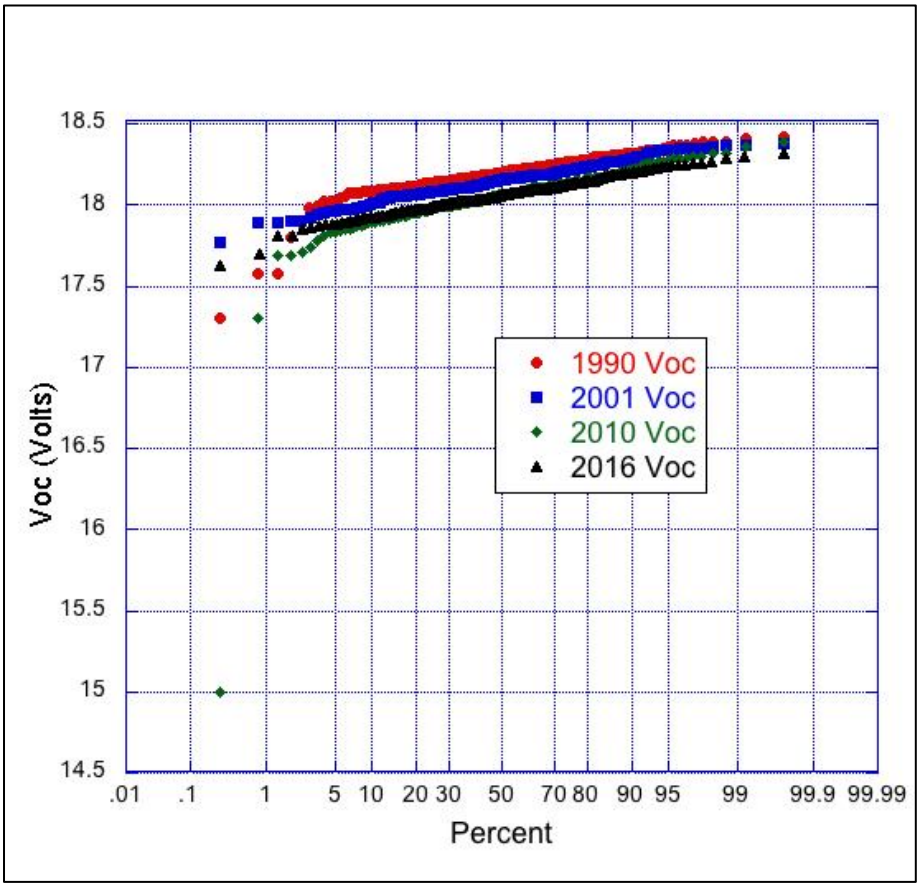

Figure G - 1: Probability distribution curves for V_{oc} from all four testing cycles

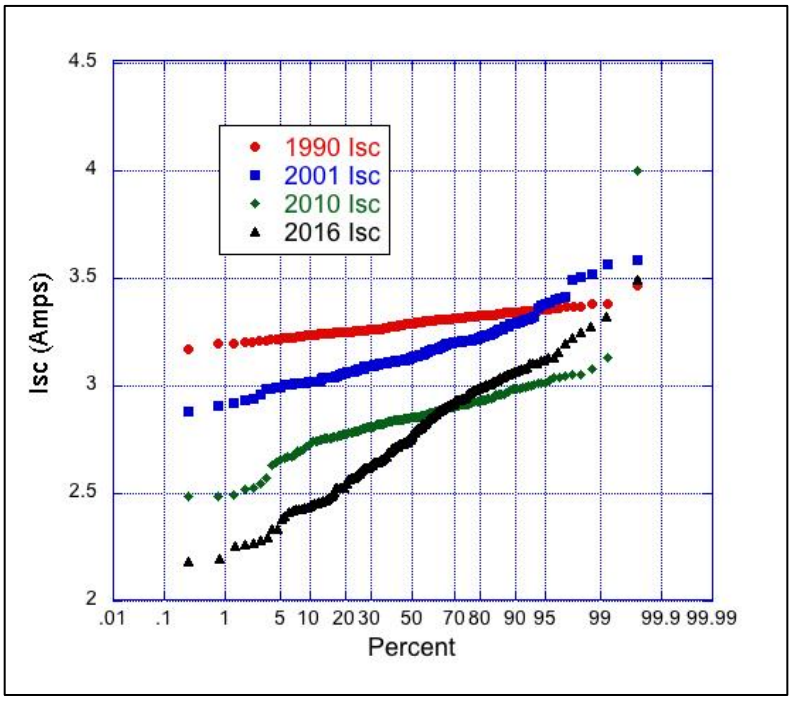

Figure G - 2: Probability distribution curves for I_{sc} from all four testing cycles

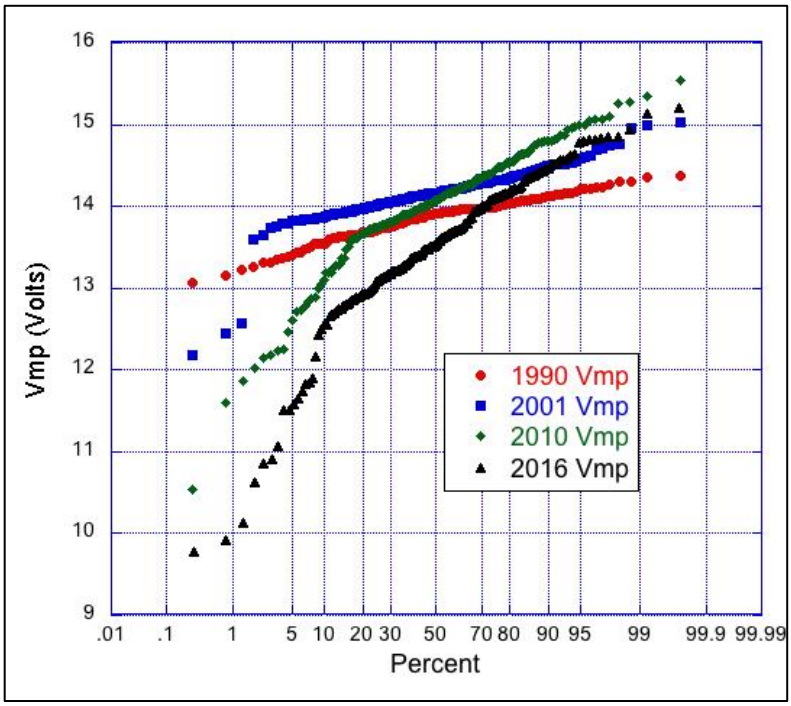

Figure G - 3: Probability distribution curves for V_{mp} from all four testing cycles

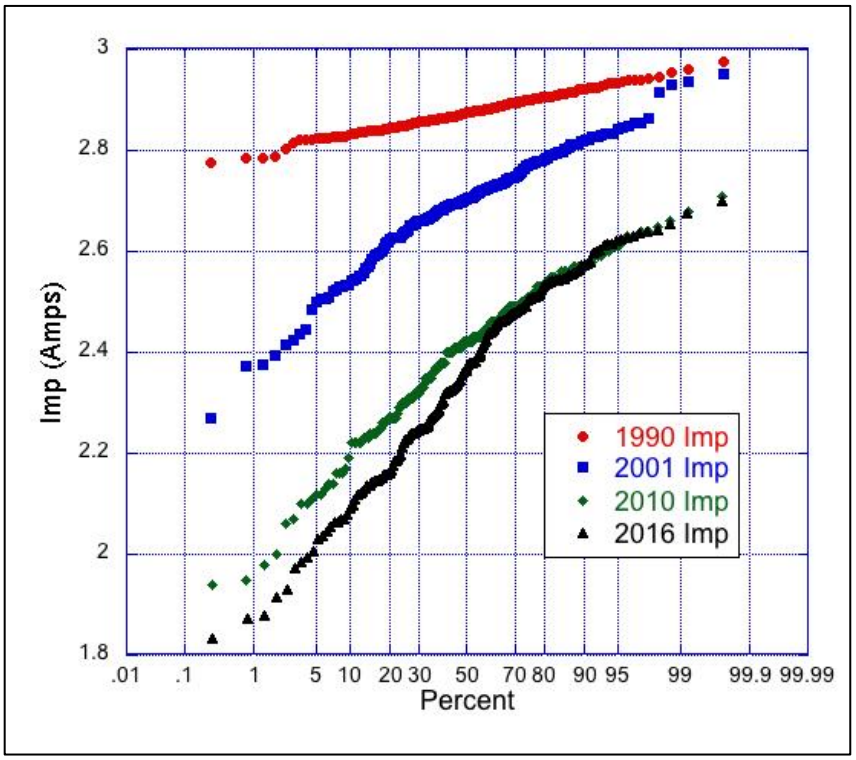

Figure G - 4: Probability distribution curves for I_{mp} from all four testing cycles

These next graphs are histograms for V_{mp} (Figure G - 5 to Figure G - 8) and I_{mp} (Figure G - 9 to Figure G - 12) for the modules from each test cycle, and their trends are similar to those seen in the report with V_{oc} and I_{sc}, respectively. The four sets of IV curves following the histograms are for the other four of the six modules with removed bypass diodes that were not included in the body of the report. The two included in the report (module 184 as Figure 73 and module 124 as Figure 74) showed the largest and smallest effects of the removal of the diodes, and these graphs (Figure G - 13 to Figure G - 16) show the effects between those two extremes witnessed in this small module sample.

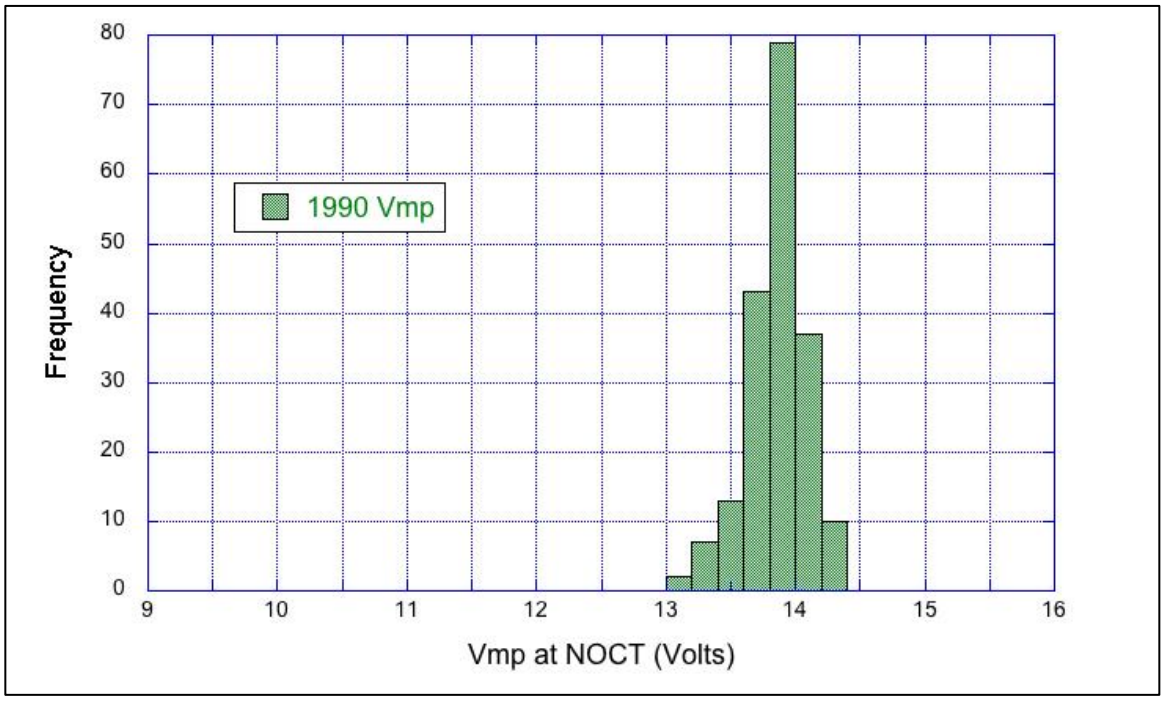

Figure G - 5: 1990 V_{mp} histogram

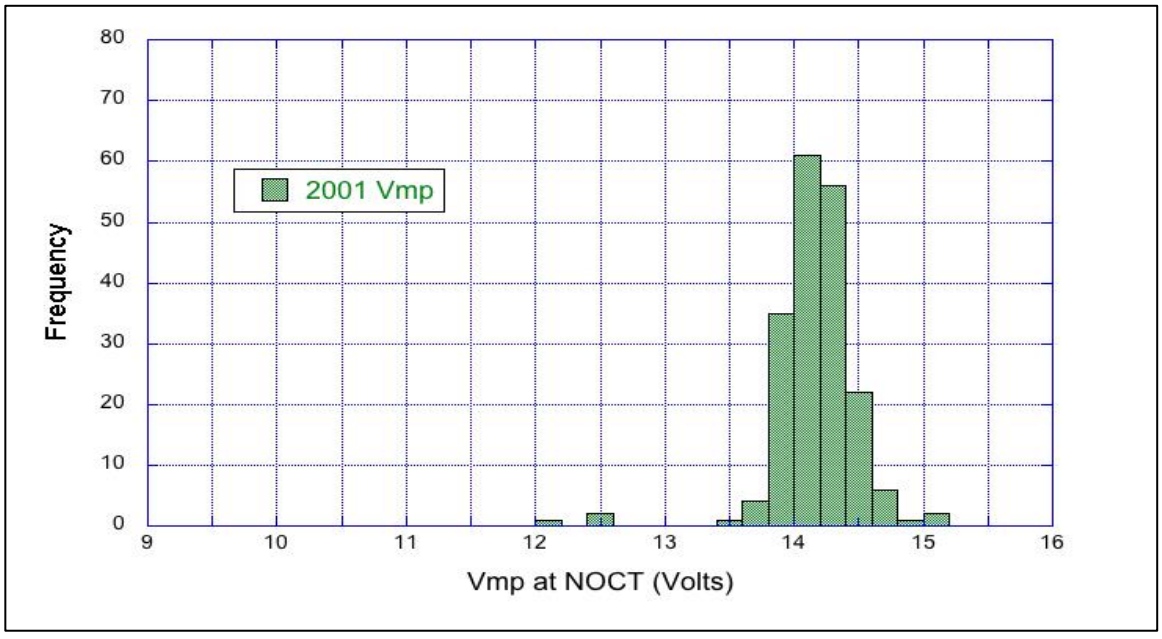

Figure G - 6: 2001 V_{mp} histogram with slightly larger spread

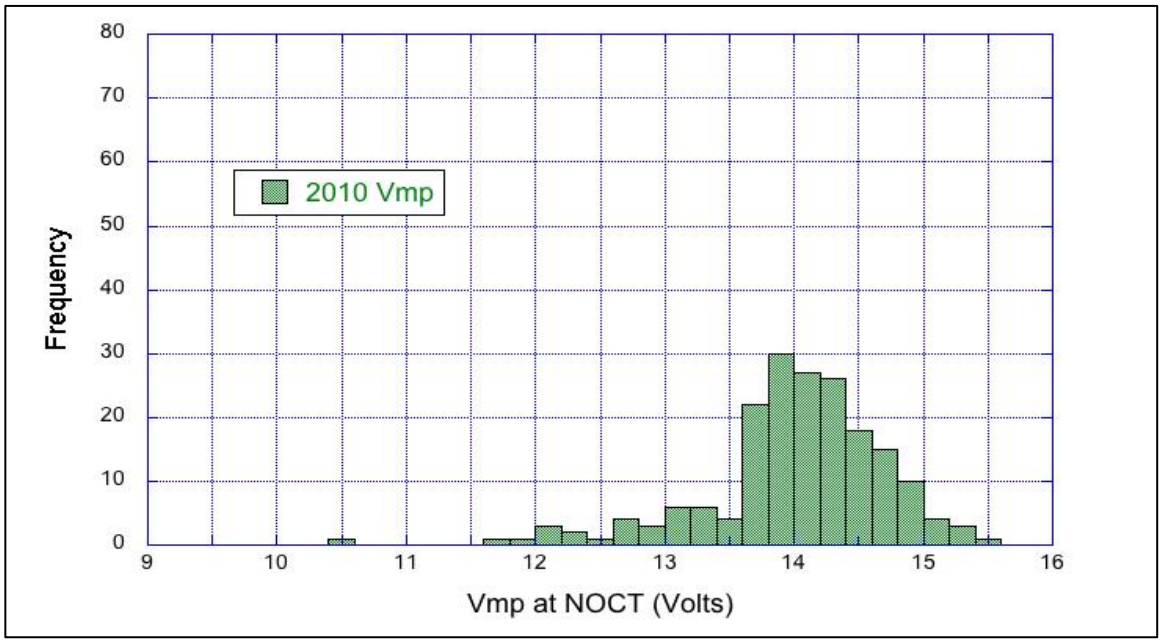

Figure G - 7: 2010 V_{mp} histogram with growing variability

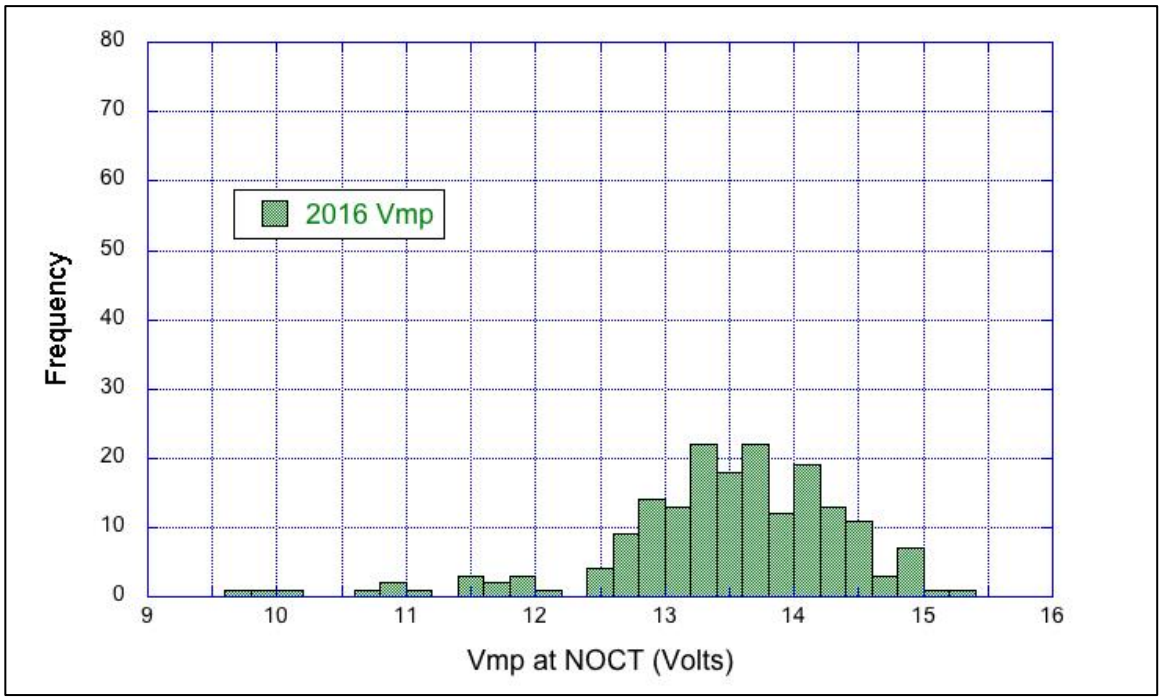

Figure G - 8: 2016 V_{mp} histogram with largest variability

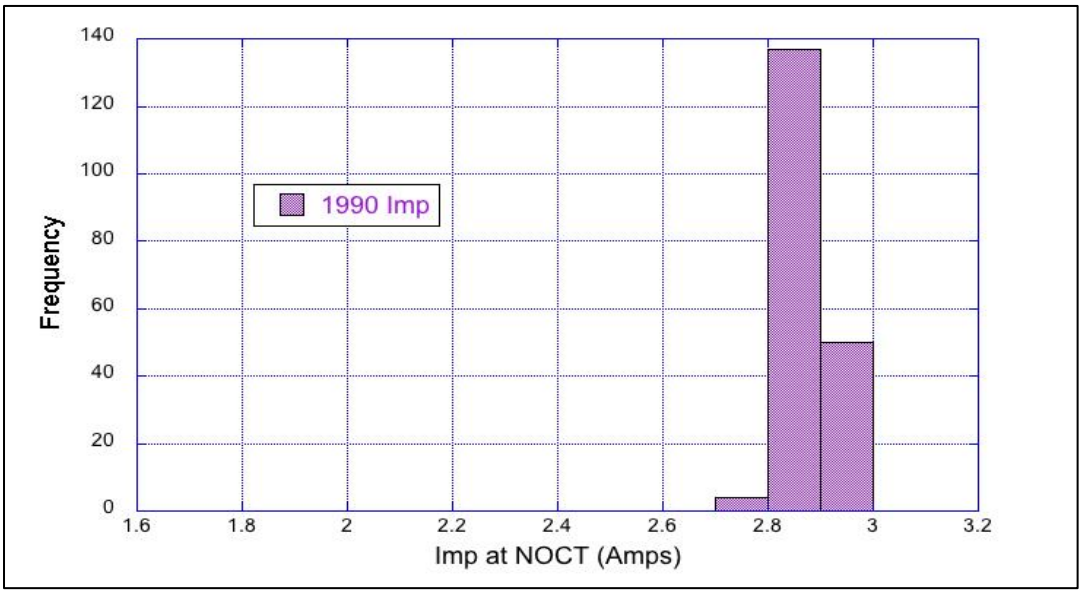

Figure G - 9: 1990 I_{mp} histogram

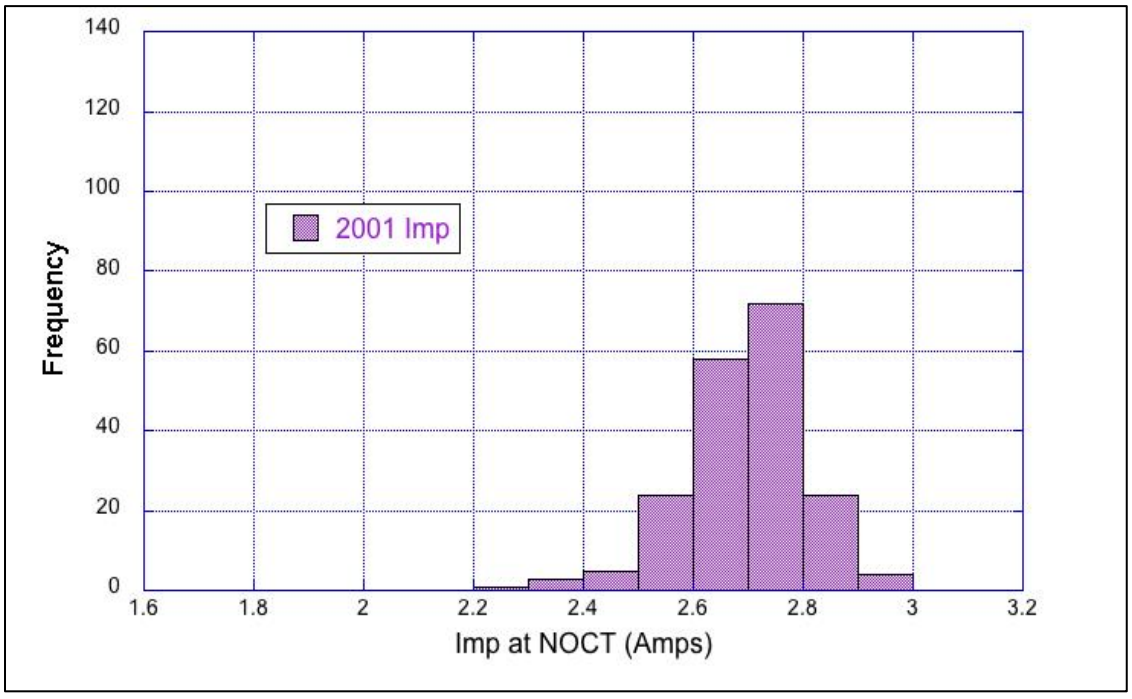

Figure G - 10: 2001 I_{mp} histogram starting to spread out

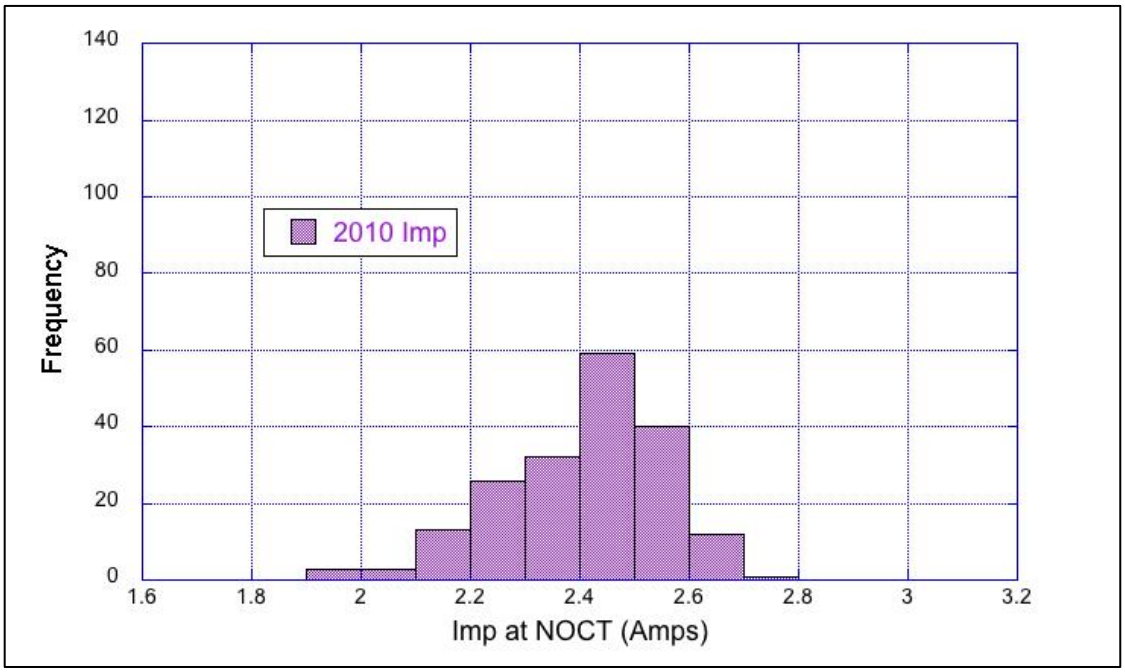

Figure G - 11: 2010 I_{mp} histogram with larger spread

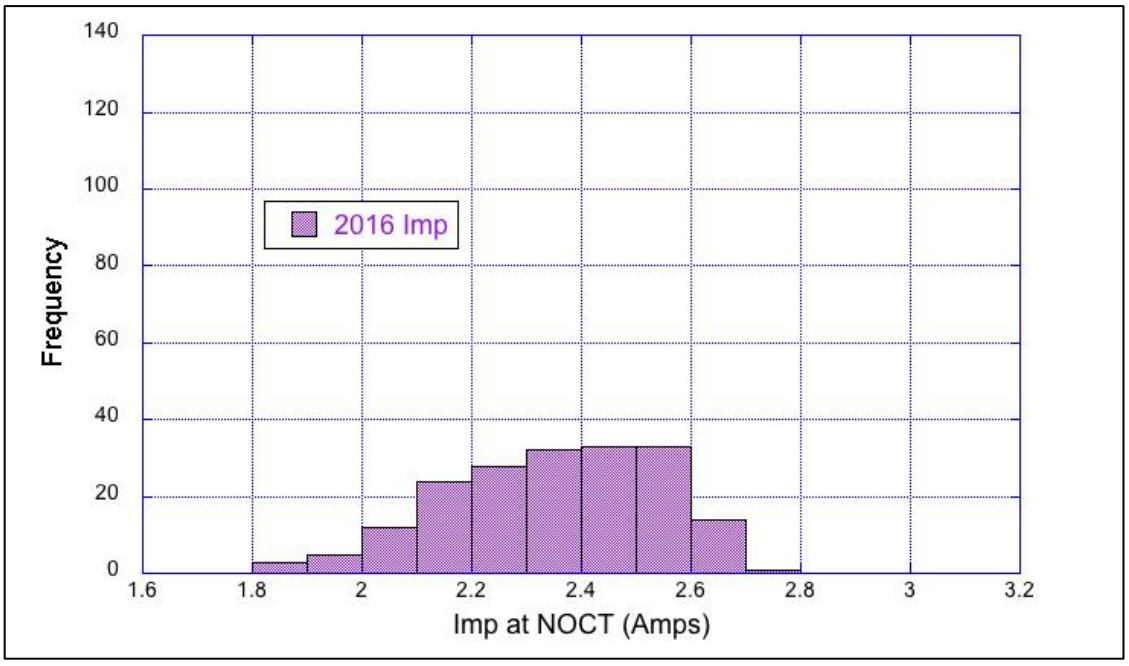

Figure G - 12: 2016 I_{mp} histogram showing collective drop after 26 years

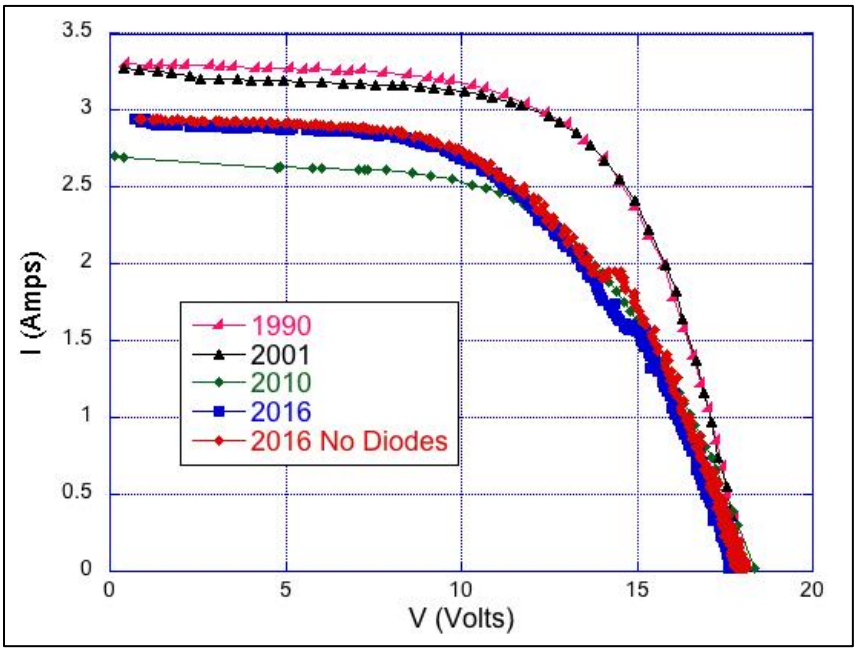

Figure G - 13: Module 028 IV curves from all four cycles and without bypass diodes

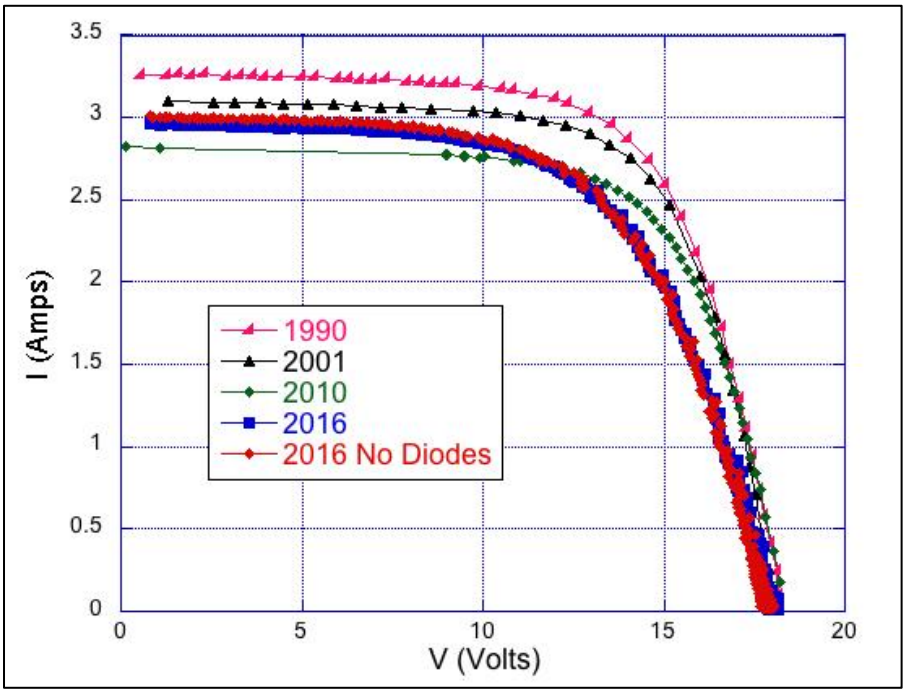

Figure G - 14: Module 043 IV curves from all four cycles and without bypass diodes

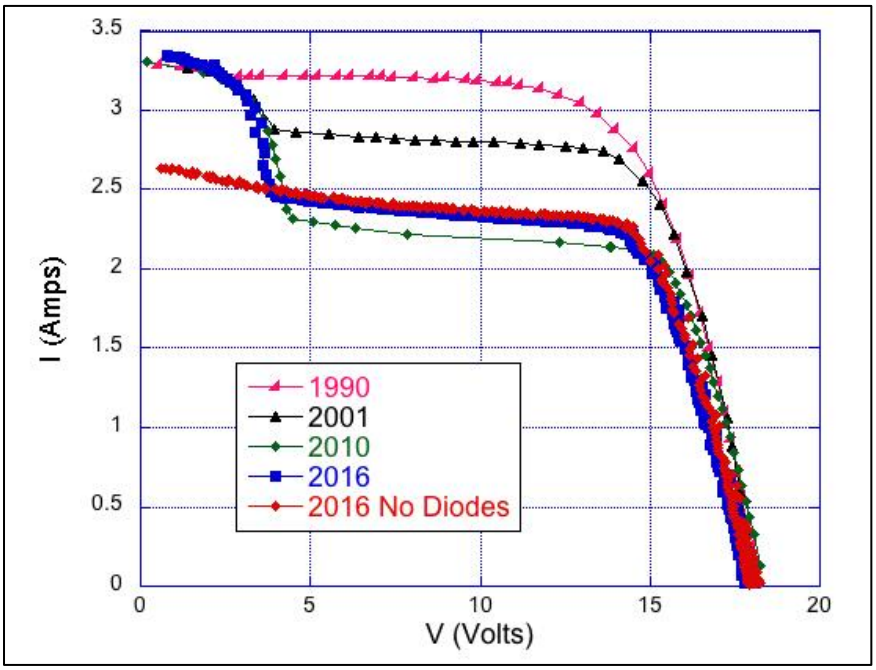

Figure G - 15: Module 110 IV curves from all four cycles and without bypass diodes

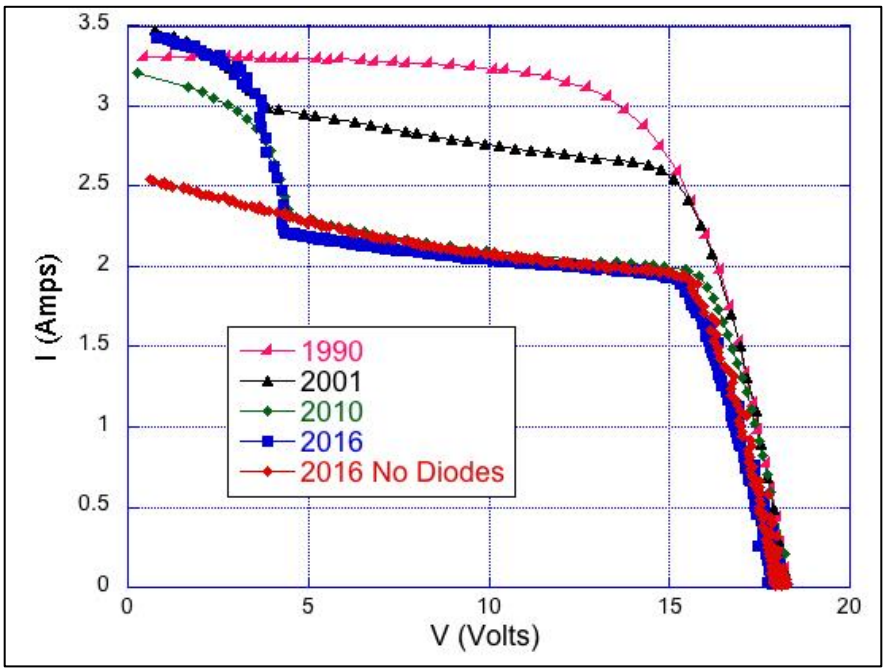

Figure G - 16: Module 118 IV curves from all four cycles and without bypass diodes

Appendix H: Regression Tables for Sensitivity Analysis

The report included a comparison of the correction coefficients of the solar insolation and module temperature for V_{oc} from the 1990 data to the 2016 results in Table 15. Table H - 1 shows the complete multiple linear regression analysis from the 1990 data, and Table H - 2 shows the same for the 2016 testing cycle. The 1990 multiple linear regression model had an r^2 value of 0.9383 and a standard error of 0.109 V. The 2016 model r^2 value was 0.9922, and its standard error was calculated to be 0.0687 V.

Table H - 1: 1990 V_{oc} multiple linear regression results

Variable	Estimate	Standard Error	95% CI LL	95% CI UL
Intercept (V)	18.2	0.03	18.14	18.25
T-47°C (V/K)	-0.0603	0.0021	-0.0644	-0.0562
Insol - 1000W/m2 (V/(W/m2))	0.00093	0.000198	0.000534	0.001326

Table H - 2: 2016 V_{oc} multiple linear regression results

Variable	Estimate	Standard Error	95% CI LL	95% CI UL
Intercept (V)	18.1	0.1007	18.32	17.91
T-47°C (V/K)	-0.0654	0.0018	-0.0618	-0.0690
Insol - 1000W/m^2 (V/(W/m^2))	0.00621	0.0024	0.0112	0.001244